Precision Autonomous Underwater Navigation

by

Brian Steven Bingham

Submitted to the Department of Mechanical Engineering
in partial fulfillment of the requirements for the degree of

Doctor of Philosophy

at the

MASSACHUSETTS INSTITUTE OF TECHNOLOGY

May 2003

Author .....
Department of Mechanical Engineering
April 2, 2003

Certified by .....
Warren P. Seering
Professor, Department of Mechanical Engineering
Thesis Supervisor

Certified by .....
David A. Mindell
Associate Professor, Program in Science, Technology and Society
Thesis Supervisor

Certified by .....
Dana R. Yoerger
Associate Scientist, Woods Hole Oceanographic Institution
Thesis Supervisor

Accepted by .....
Ain A. Sonin
Chairman, Departmental Graduate Committee

Precision Autonomous Underwater Navigation

by

Brian Steven Bingham

Submitted to the Department of Mechanical Engineering
on April 2, 2003, in partial fulfillment of the
requirements for the degree of
Doctor of Philosophy

Abstract

Deep-sea archaeology, an emerging application of autonomous underwater vehicle (AUV) technology, requires precise navigation and guidance. As science requirements and engineering capabilities converge, navigating in the sensor-limited ocean remains a fundamental challenge. Despite the logistical cost, the standards of archaeological survey necessitate using fixed acoustic transponders - an instrumented navigation environment. This thesis focuses on the problems particular to operating precisely within such an environment by developing a design method and a navigation algorithm.

Responsible documentation, through remote sensing images, distinguishes archaeology from salvage, and fine-resolution imaging demands precision navigation. This thesis presents a design process for making component and algorithm level tradeoffs to achieve system-level performance satisfying the archaeological standard. A specification connects the functional requirements of archaeological survey with the design parameters of precision navigation. Tools based on estimation fundamentals - the Cramér-Rao lower bound and the extended Kalman filter - predict the system-level precision of candidate designs. Non-dimensional performance metrics generalize the analysis results. Analyzing a variety of factors and levels articulates the key tradeoffs: sensor selection, acoustic beacon configuration, algorithm selection, etc. The abstract analysis is made concrete by designing a survey and navigation system for an expedition to image the USS Monitor.

Hypothesis grid (Hgrid) is both a representation of the sensed environment and an algorithm for building the representation. Range observations measuring the line-of-sight distance between two acoustic transducers are subject to multipath errors and spurious returns. The quality of this measurement is dependent on the location of the estimator. Hgrids characterize the measurement quality by generating *a priori* association probabilities - the belief that subsequent measurements will correspond to the direct-path, a multipath, or an outlier - as a function of the estimated location. The algorithm has three main components: the mixed-density sensor model using Gaussian and uniform probability distributions, the measurement classification and multipath model identification using expectation-maximization (EM), and the grid-based spatial representation. Application to data from an autonomous benthic explorer (ABE) dive illustrates the algorithm and shows the feasibility of the approach.

Thesis Supervisor: Warren P. Seering
Title: Professor, Department of Mechanical Engineering

Acknowledgments

I've imagined writing this section many times over the last few years. It is both the easiest and hardest portion of wrapping up my stint as a graduate student. It is easy because I have been blessed with great opportunities, advisors, family and friends, but hard because I know it is impossible convey how fortunate I've been and give thanks to the wonderful people who have deliberately and indirectly supported me over the last five years.

My advisors, the thesis committee, have provided guidance, insight, and unbelievable opportunities. What I've learned about doing research and tackling new problems I owe to Warren Seering. Professor Seering's subtle advice through the many stages of graduate school, his unselfish dedication of time and energy, and his incisive ability to navigate new terrain with aplomb are an inspiration. I've known for a long time that I will spend a career trying to emulate his model of education and research. David Mindell has successfully 'blown my mind' as he's done with many of his students and introduced me to what has to be the most exciting research field I could ever imagine. David's unique ability to cut new veins through any topic has made the complex aspects of research seems simple. Dana Yoerger completed the committee with an unbelievable knowledge about engineering underwater robots. I have to thank Dana for his great feedback along the way, sharing some wonderful data along with colorful stories of its collection, and commuting from Woods Hole to MIT.

Hopefully my family knows how important they've been in this long process, but I can't say thank you enough. John and Mary Bingham, my grandparents, have supported education for two generations of Binghams. Despite the occasional confusion of having a son and brother that is 'still in school', my parents and my sister provided just the right mix of encouragement and questioning to keep me moving.

To me MIT is not a place, but a collection of enthused and capable individuals. The institution is not the buildings; it is the relationships. I'm certain my great fortune in finding wonderful friends and colleagues at MIT is unique. There simply cannot be that many such individuals. One such person is Dr. Brendan Foley, who introduced me to this world of underwater research. I've learned so much from working with him, and I look forward to continuing our careers together. Along with Brendan, Alex Makarenko gave valuable comments on the original draft of this document. Alex and Fred Bourgault provided time-saving snippets of LaTeX(the only way to write a thesis). I have to thank the MIT trained critics for help preparing my defense presentation: Eric, Mads, Tim, John, and Megan. I owe Joel Gendron and Megan Galbraith a thank you for the illustrations and graphical tutorials. Harry Truman, a fellow Missourian, got some great advice when coming to Washington, "Harry, don't you go to the Senate with an inferiority complex. You sit there about 6 months, and you wonder how you got there. And after that you wonder how the rest of them got there". Well I'm still wondering how I got here.

I'd also like to thank Joe Apicella and my friends from New England Outdoor Center in Carratunk, Maine. My days on the river the past three summers have given me the needed perspective to return to Cambridge refreshed and enthused. It truly is a great thing we do.

This research could not have happened without the support from the NOAA office of Ocean Exploration, NSF, and MIT Sea Grant, and the AUV Lab. Chryssostomos Chryssostomidis' generosity in providing resources, opportunities, and space is greatly appreciated, and the men of the AUV Lab, Rob, Sam, Jim, and Joe, have been wonderful to work with.

Finally, the real people who make things happen at MIT are the administrators. Leslie, Joan, ReRe, Lori, Maggie, and May make any day at MIT a little brighter and graduate school a little smoother.

Thank You All,
b.

Contents

Chapter 1

Introduction

> We shall not cease from exploration
> And the end of all our exploring
> Will be to arrive where we started
> And know the place for the first time.
> - T. S. Eliot[1]

Engineering technology and archaeological science converge in deep-sea exploration. Answering questions about the ancient past challenges current capabilities; the ability to precisely, autonomously navigate is the distinctive characteristic of deep-ocean survey systems for archaeology. This thesis is about navigation, specifically precision autonomous navigation for deep-sea archaeology. The approach is based on engineering fundamentals of design, estimation, and control; the solution is novel because of the distinct requirements of deep-sea archaeology site-survey; and the results increase the capabilities of current autonomous underwater vehicle (AUV) systems.

Navigation is a fundamental technology, and navigation of an AUV presents a unique challenge in two dimensions: the limitations of underwater sensors and the demands of autonomous survey. The propagation properties of sea-water challenge perception. Terrestrial navigation techniques requiring electromagnetic signals (GPS, LORAN, etc.) are ineffective. Sound propogates relatively well in seawater making navigation reliant on acoustic means that present unique design and operation challenges. An AUV is a signal processing unit where estimation and control converge. Algorithms link the sensor signals with internal models and external actuation. Concepts from controls, estimation (probabilistic inference), and stochastic processes yield new algorithms for increasing the performance and capabilities of AUV navigation. The second distinct dimension of AUV navigation is autonomy. Engineering a system capable of localization and guidance without a human operator is a basic problem for robotics. Probabilistic navigation for mobile robots provides methods and representations that must be adapted to the unique aspects of underwater operation. This thesis draws on these engineering fundamentals to develop new methods for precise autonomous navigation in the deep-ocean.

[1] T. S. Eliot, *Four Quartets* (London: Faber and Faber, 1944).

Archaeology in the deep-sea presents a novel and important application, focusing engineering development on functional requirements that are both distinct and representative. The required precision and the spatial extent of a typical site differs by as least an order of magnitude compared with large scale survey missions such as resource prospecting, navy operations, and oceanographic investigations[2]. Precision survey is also representative of burgeoning applications demanding fine resolution imaging: industrial deep-ocean operations are increasingly remotely operated or autonomous, requiring new levels of precision; new military scenarios demand autonomy and precision; and continued oceanographic discoveries make use of such emerging capabilities. This dissertation focuses on deep-sea archaeology with an eye towards unforeseen applications.

The methods of this thesis advance the design of navigation systems in general and the operation of precision positioning in particular. As AUV technology evolves and the applications expand, vehicle capabilities are clustering around important missions. New applications demand making the engineering design decisions in a quantitative way. This dissertation proposes a design method, focusing on precision, to aid in making future tradeoffs. The unique aspects of archaeological sites and autonomous operation demand developing new methods of navigation. This thesis proposes a new method, the *hypothesis grid*, for characterizing the sensed environment, enabling precision navigation, and expanding the capabilties of autonomous systems.

This work is concerned with advancing the precision of underwater navigation. Precision is indicative of the ability to build fine-resolution images and maps. This work develops a conception of underwater navigation for deep-sea archaeology based on the precise localization and autonomous operation. The problem is distinct because of the requirements for precision in archaeology; the problem is challenging because of the sensor limitations in the underwater environment; the problem is fundamental because navigation is critical to the operation of any autonomous robot; and the problem is important because it facilitates not only the work of deep-sea archaeology, but a set of anticipated applications with requirements for precision navigation and applications not yet anticipated.

1.1 Approach

This thesis tells two stories. One focuses on the methods of design for precision navigation systems, the other on the development of hypothesis grids for performing precision site-surveys. Both contribute to bridging the gap between the requirements scientific investigations and the technical capabilities. Figure 1-1 illustrates the overall goal. An AUV is operating within a discrete envrionment. The lines making the rectangular box represent the boundaries of the survey environment (100m on each side). The two beacons are shown in the corners of the box and the AUV, surveying over the bottom, interacts with these beacons to determine its relative position. The design question considers how to assemble and operate the navigation system of such a vehicle to operate within this environment. The colored grid, shown in two-dimensions and with the AUV in the same plane, represents a hypothesis grid. The colors map to the characterisics of the acoustic

[2]Experiments on ocean basin scales use acoustic transmissions traveling 1000's of kilometers; this work focuses on sites that that span 10's - 100's of meters.

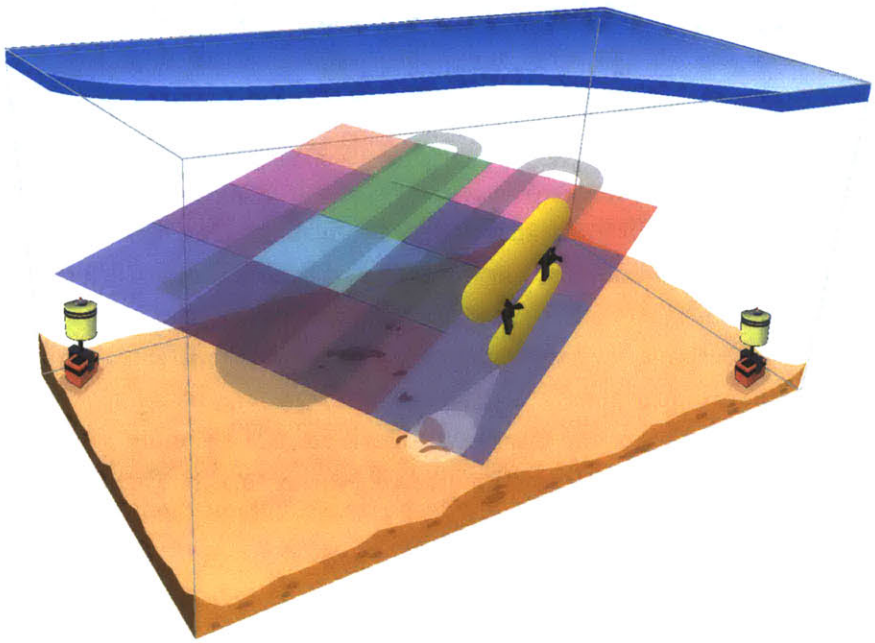

Figure 1-1: Illustration of an AUV surveying a discrete environment represented using a hypothesis grid.

beacons within the environment, increasing the localization precision and enabling the vehicle to reason about its environment with new information.

Engineering design is conceived as a process of making tradeoffs, of balancing performance and cost. The qualitative aspects of this process are important and undeniable. Rather than offer a particular design implementation, a point in the design space, to be accepted or rejected, this report presents a general method treating the quantitative system aspects. Using this method to articulate the design tradeoffs critical to precision and autonomy delivers an understanding of the design space. The mission goals, environment, and platform characterize underwater investigations. Mapping these missions first to a specification for navigation precision and then to sensor components and software algorithms is accomplished through the application of estimation techniques as design tools: the Cramér Rao lower bound and the extended Kalman filter. Evaluating tradeoffs and highlighting synergies emphasizes the system-level viewpoint, resulting in a method to make better design decisions for emerging applications. This abstract consideration becomes concrete through the application of the methods and metrics to the survey design for USS Monitor, a proof-of-concept case-study.

Hypothesis grids, the second part of the story, is both a representation and an algorithm for navigating in an instrumented environment. Archaeological missions require the fixed-reference precise navigation achievable with acoustic range measurements. Functioning autonomously in such an environment, with multipath errors and spurious measurements, strains current techniques. The hypothesis grid method models the instrumented environment. Three components summarize the algorithm: a mixed-distribution model of range observations, a algorithm for concurrently char-

acterizing multipath range measurements and identifying a geometric model, and a coarse grid capturing the spatial dependency of the sensor behavior. Based on the estimated location, a hypothesis grid produces a probabilistic belief that subsequent range observations will be associated with direct-path, multipath, or spurious sources. This sensor-based map is intended to be a suitable representation for active motion control and higher level autonomous decision making. The algorithm is not an alternative to standard Bayesian probabilistic navigation methods; it is a complimentary layer to increase the performance of such techniques and expand the capabilities of autonomous navigation.

Autonomous precision navigation unifies the design methods and algorithm development, each motivated by the application to deep-sea archaeology. Figure 1-2 illustrates how these two themes relate to application of the technology. Both parts of the story start general, becoming particular through examples and applications. Application to USS Monitor survey specification brings both stories together.

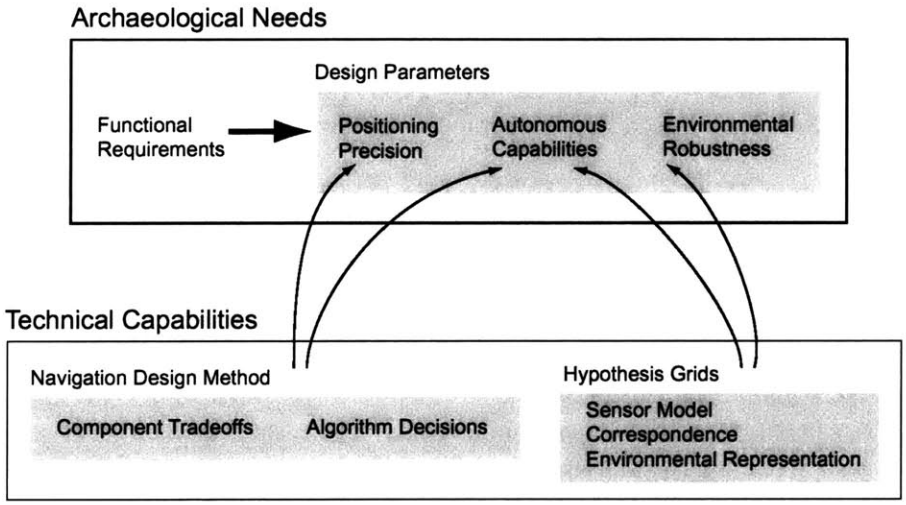

Figure 1-2: Illustration of how the two portions of the thesis, the design method and hypothesis grids, contribute to the overall goal of applying AUV technology to archaeology.

1.2 General Background

This work has a wide base, and the background material is vast. To avoid an overwhelmingly large single treatment of what has come before, this section outlines the references that motivate the work and provide a broad background. The next chapter takes the treatment to greater depth concentrating on the fundamental underpinnings. Each of chapters 3 and 4 contains a review of work specifically related to the design and algorithm stories respectively.

The convergence of the science and engineering motivates this work. The excitement of deep-sea exploration is captured in Broad's history of deep-sea exploration [Broad, 1998]. The technology of recovery is highlighted in the tale of the *SS Central America* [Kinder, 1999], and [Herdendorf and Meserve, 1995] illustrates the opportunity to perform concurrent multi-disciplinary science during

such an expedition. For a history of underwater archaeology, Delgado's encyclopedia [Delgado, 1997] and Bass's early book [Bass, 1966] cover the key concepts, technologies, and explorations. Bascom's book presents the deep ocean as a preservative environment for archaeology [Bascomb, 1976]. The investigation of submerged cultural resources is an endeavor that continues to be intertwined with technology.

The development of the enabling technologies is a tale more challenging to tell. Bellingham's original concept of small autonomous vehicles for oceanography is critical [Bellingham, 1997]. At the same time the idea of precision navigation was being developed as a key capability by researchers at the Wood's Hole Oceanographic Institute [Whitcomb et al., 1999a, Yoerger and Mindell, 1992]. The gap between the requirements of science and the engineering capabilities has been recognized as a topic for continued research by the DeepSea Archaeology Research Group at MIT [Mindell and Bingham, 2001, Foley and Mindell, 2002].

Reliable, repeatable navigation is a basic human challenge. Celestial navigation and astronomy have their roots in antiquity. Many of the great advances in science are consequences of the quest for answers to this challenge. Bowditch continues to be the definitive reference for navigation as both art and science [Bowditch, 2002]. Human and animal navigation is the basis for many concepts and developments in robot navigation, imitating the successes of evolution. Study of Polynesian cultures exposes the complex perception in human navigators [Lewis, 1972]. Animals employ an even greater variety of methods and sensor modalities [Waterman, 1989]. The goal of this thesis, to enable precision autonomous underwater navigation, amplifies the fundamental navigation challenge. Autonomy[3] and localization are closely coupled: "mobility as a necessary basis for the development of true intelligence" [Brooks, 1990]. Navigation is also fundamental to working in the sensor-limited deep-ocean, "precision underwater navigation remains the principal obstacle to improved vehicle control" [Whitcomb et al., 1999a].

This thesis sits at the intersection of deep-sea archaeology and underwater navigation. The challenge is to narrow the gap between the requirements of science and the capabilities of technology.

1.3 Contributions

This dissertation contributes a design method and a navigation algorithm. The following list, categorized based on the two major components of the work, articulates the central contributions.

Design

- A method and metrics for evaluating the precision performance of navigation system configurations based on the Cramér Rao lower bound.
- An articulation of key design choices and their impact on precision: number of acoustic beacons, beacon placement, Doppler velocity log integration, depth sensor integration, active beacon selection, heading observation through acoustic ranging, etc.

[3] Autonomy is a subjective term, but Brooks's offers explanation of autonomous systems in general [Brooks, 1991b, Brooks, 1997]

- A specification for precision, translating image quality requirements to navigation precision parameters
- A classification of AUV missions based on the goals, environment, and platform
- An application of the general navigation design method to the imaging survey of the USS Monitor

Autonomous Navigation

- Hypothtesis grids - a representation of the anticipated quality of acoustic range observation as a function of the current observer's position within the environment.
- A algorithm for creating the hypothesis grid representation.
- A mixed-distribution model for acoustic range observations
- An application of expectation-maximization (EM) to classify and identify multipath returns in acoustic range observations
- The feasiblitly of representing probabilisitc association of a long baseline environment with a coarse rectangular hypothesis grid.

1.4 Document Road-map

The background for this work is distributed. This chapter presents a short overview of some references on the history of deep-sea archaeology and technology. The main contributing components are discussed in chapter 2 to fit this thesis into the fields from which it draws. Chapter 2 provides a brief introduction to underwater archaeology to explain the functional requirements. The closely related work, the literature with direct similarities, is treated in subsequent chapters on design and hypothesis grids (3 and 4).

Chapter 2: Autonomous Survey in the Deep-Sea: Building Archaeological Maps :
This chapter provides the general background and summarizes the assumptions. Definitions explain key concepts and remove ambiguity from the discussions that follows. The chapter concludes with justification for the overarching assumptions of an instrumented homogenous acoustic environment.

Chapter 3: System Design: Autonomous Navigation for Deep-Sea Archaeology :
Starting with the specification for precision, this chapter develops the design methods and metrics. The Cramér Rao lower bound articulates tradeoffs in particular navigation sensor configurations. The extended Kalman filter illustrates the analysis of an active beacon selection algorithm.

Chapter 4: Hypothesis Grids: Mapping Uncertainty in Autonomous Survey :

Hypothesis grid is both a representation and an algorithm. The representation models an acoustic ranging environment and the algorithm describes the method of creating the representation using empirical evidence. The treatment concentrates on developing the fundamental aspects of the algorithm and illustrates the application through an example using data from the autonomous benthic explorer (ABE).

Chapter 5: Proof of Concept: Imaging Survey of the USS Monitor :

This chapter delivers a concrete example of the abstract design notions. A proposed mission to survey the USS Monitor is considered using the design tools from chapter 3 and a plan for implementing the hypothesis grid algorithm from chapter 4.

Chapter 6: Conclusion :

The conclusion draws the disparate contributions together and looks forward to ongoing and future work.

Chapter 2

Autonomous Survey in the Deep-Sea: Building Archaeological Maps

> Navigation is the process of directing the movements of a ship or aircraft form one point to another. Both art and science are involved in conducting a ship safely to its destination. Art is involved in the proficient use of all available aids and methods and the interpretation of data with judgment to determine position and the ship's course. The science of navigation includes the computation of solutions for various navigational problems, and the design and development of instruments, methods, tables, and almanacs intended to facilitate the work of the navigator and to increase the accuracy of the results he may obtain.
> -Dutton's Navigation and Piloting[1]

The motivation, background, and assumptions are critical to this story. This chapter builds on the motivation from chapter 1 by detailing the gap between the needs of science and the capabilities of current technology. The background illustrates the convergence of deep-sea archaeology and autonomous underwater survey, forming a basis in fundamentals for the development in the following chapters and exposing an opportunity for extending the capabilities of the technology. The definitions of section 2.2 clarify the terminology so the meanings and concepts can be used without ambiguity. These technical underpinnings argue to the importance of the contributions and the novelty of their consideration. The chapter culminates with a point-of-departure, an explanation of the key assumptions permeating the analysis which follows and a conception of the convergence of science and technology.

[1] G. D. Dunlap and H. H. Shufeldt, ed., *Dutton's Navigation and Piloting*, 12th ed. (1969).

Chapter Goals

- Contributing Background: Present the state-of-the-art in autonomous underwater navigation technology to locate the contributions of this report within that field, introduce deep-ocean archaeological science, and discuss the convergence technology and archaeology.

- Definitions: Explain the key terms and concepts as they are used in this dissertation.

- Point of Departure: Explain the key assumption - an instrumented survey environment - and motivate the chapters to follow.

2.1 Contributing Background

This thesis is about convergence: the convergence of the technology of autonomous underwater vehicles and the science of maritime archaeology; the convergence of signal processing, control, and estimation for navigation; and the convergence of vehicle, sensor, and navigation techniques for precision underwater navigation. In addition to demonstrating the foundation's breadth, this background highlights the elements missing in the state-of-the-art, the synergies and opportunities exposed at the intersection of scientific needs and engineering capabilities.

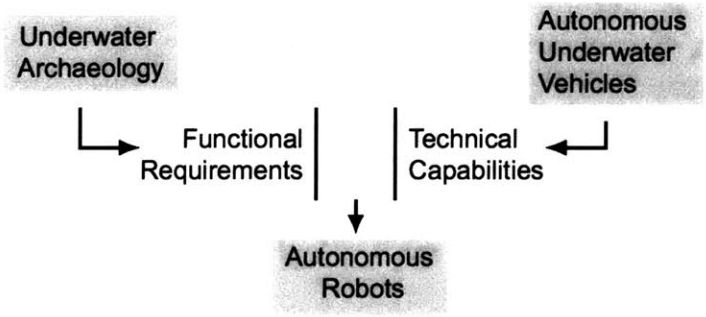

Figure 2-1: Outline of the contributing background: the science of underwater archaeology , AUV technology, and autonomous robot theory.

The motivating argument of this thesis is that a gap exists between the demands of underwater archaeological survey and the capabilities of current autonomous underwater vehicles. Figure 2-1 illustrates this argument. Underwater archaeology contributes the motivating functional requirements for precision navigation, so a brief overview of the science of and methods is presented in the next section. To explain the state of the art in autonomous survey this chapter explores the background on AUV technologies - the systems, sensors, and navigation methods. The goal of presenting these two contributing components is to arrive at a clear concept of the gap between the requirements and capabilities. The last section of background summarizes the techniques in the vast literature on autonomous robots in general, i.e., for land, space, and sea applications, showing what techniques from field robotics might contribute to new solutions for the particular application.

2.1.1 Underwater Archaeology

What is deep-sea archaeology and why is this section included in an engineering dissertation? The background on underwater archaeology is a context for the archaeological requirements quantified in the next chapter. Understanding the application is necessary to approach the questions of design. As the story moves to the current state-of-the-art, a concept of the role of AUVs for archaeology emerges. This role depends on the methods of deep-sea archaeology. This section is included as a brief introduction to the first stage of the design approach - understanding the problem.

The history of underwater archaeology is intertwined with the technologies for ocean exploration. This section follows the relationship between the methods and accomplishments of underwater archaeology and the technology that enables such explorations. At each step the archaeological standard and the technical capabilities have been reciprocal and it is not clear which is the driving force - does the requirements of precision push the technology or do the capabilities determine the standard? The following section makes the current requirements of deep-sea archaeological survey explicit by examining deep-sea archaeology as a method of investigation. A framework is proposed, based on the convergence of capabilities and requirements, and the role of AUVs within that deep-sea archaeology is discussed.

Origins

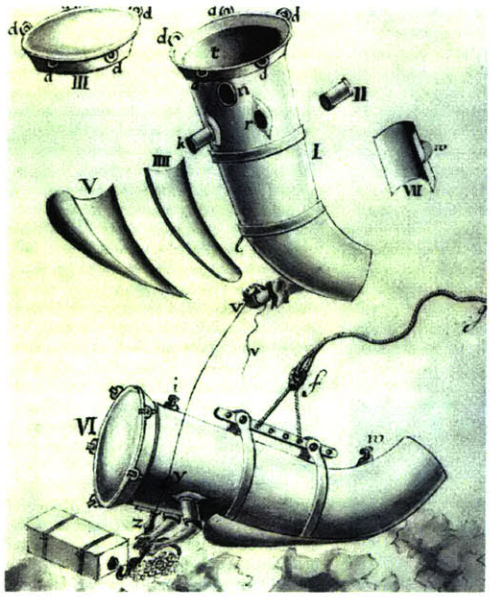

Figure 2-2: Captain Jacob Rowe's patented diving engine, used to recover Adelaar's treasure in 1728. (copyright National Maritime Museum Picture Library) [Delgado, 1997] p20.
qualitative

It is difficult to determine exactly when humans began to use artificial means to explore the underwater world. Watson cites the legend of Gilgamesh to push the date back to the third millennium B.C. [Watson, 1983]. Bascom presents the origin of marine archaeology in 1900 with the

Antikythera project [Bascomb, 1976]. Regardless of the chosen origin, humans have used a variety of technologies to aid in their perception of this remote environment. With the invention of a workable Self-Contained Underwater Breathing Apparatus (SCUBA) by Cousteau in 1946 [Delgado, 1997], explorers could gain access to the upper 50m of the ocean for relatively long times and little expense. By the 1960's the field of underwater archaeology began to emerge as a rigorous academic endeavor through the work of scholars such as George Bass [Bass, 1967]. The evolution of underwater archaeological investigations starts with pioneers such as George Bass, Jacque Cousteau, and Harold 'Doc' Edgerton - archaeologists, explorers, and engineers who personally explored the archaeological record on the sea-floor. A second stage of exploration relying on the deep submergence capability enabled a new kind of explorer to orchestrate the archaeology from the surface using an array of remote sensing technologies. The third stage in this evolution is underway as autonomous survey platforms allow scientists to operate another step removed from the environment.

Imaging and Survey Underwater

The science of underwater archaeology depends on documentation. Careful and complete documentation is necessary for current and future interpretation. In shallow water, this usually involves divers and tape measures, using specially constructed grids and manually recording of large numbers of points for subsequent computer aided triangulation [Delgado, 1997].

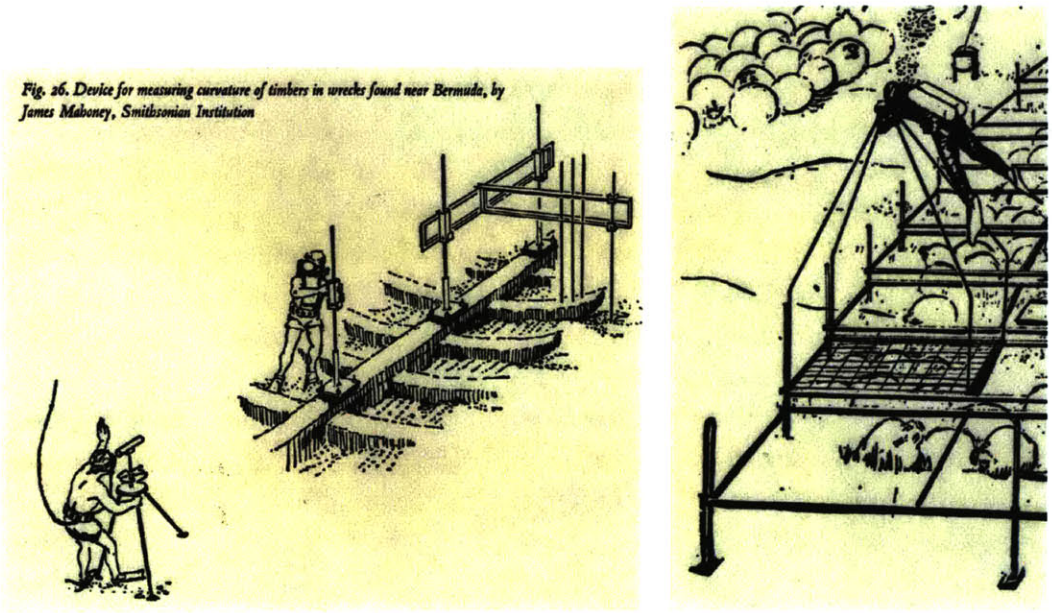

a b

Figure 2-3: Divers surveying. a) Shows terrestrial survey methods being used to measure the shape of the ship's hull. b) Shows the manual method of making a well navigated photomosaic. (Both images from [Bass, 1966].)

The methods and practices underwater imaging are indicative of the technical capabilities and state of scientific practice. A seminal work in underwater archaeology is the Cape Gelidonya

wreck. Divers, swimming slowly at a fixed height, imaged the site for documentation [Delgado, 1997]. These photomosaics provide a view of the site, but to attain a quantifiable result a site-plan must be produced. For shallow-water sites this incorporates painstaking measurements integrated into the overall plan. In deep water the ROV Jason has proven to be adept at the precision navigation and control required to produce high quality photo mosaics and microbathymetry for scientific interpretation [Ballard et al., 2000]. A host of AUV platforms promise a similar capability, but have yet to prove capable of similar precision [Mindell and Bingham, 2001].

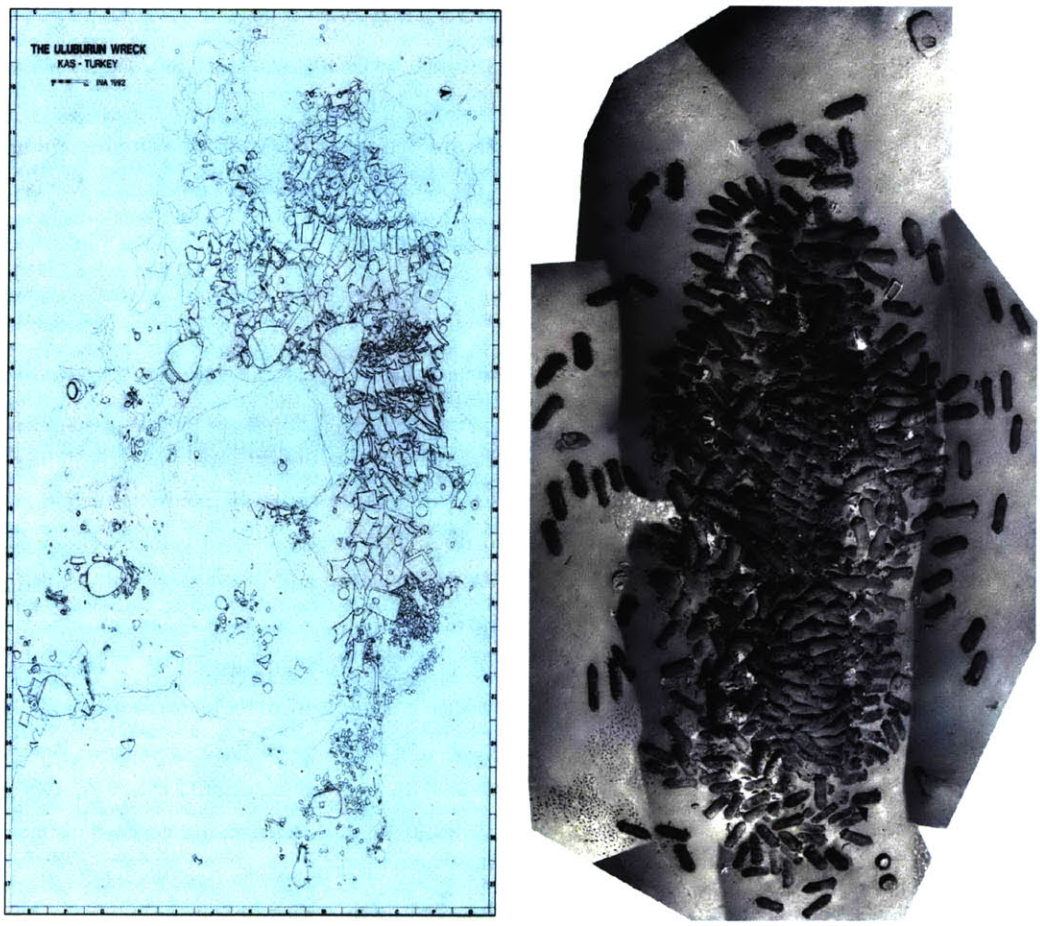

a b

Figure 2-4: Uluburun site plan (from [Delgado, 1997] copyright INA) and Tanit photomosaic (courtesy H. Singh and J. Howland copyright WHOI, IFE, Ashkelon Excavation)

Remote Archaeology in the Deep-Sea

Only a small fraction of the world's oceans are accessible to SCUBA divers. After World War II, the strategic importance of dominating the underwater world led to great advancements in deep submergence technology [Broad, 1998]. SCUBA expanded archaeological investigations from the land to the sea; deep submergence technology allows scientists to tap into the archaeological record

of the deep-ocean. Submerged cultural resources in the deep-sea are now accessible through robotic, navigation, and sensing technologies [Foley and Mindell, 2002]. For archaeologists, the deep-ocean not only increases the space to search, but offers a unique preserving environment [Bascomb, 1976]. The technology for exploring this environment does not replace scientists, but challenges them to adopt new concepts and interpretation methods.

Today a major product of deep-sea archaeology is an image - an important distinction from environments where the archaeologist has direct exposure to the site.

> Archaeology in deep water must conform to the same professional standards as followed on land and in shallow water. This entails generating accurate site plans before touching a single artifact, with measurement precision at least equal to that registered on traditional sites. If a few selected objects are recovered for dating and provenance studies, their positions must be recorded as accurately as possible. [Foley and Mindell, 2002]

Two consequences emerge: precision underwater navigation is critical and the nature of exploration, and explorers, is fundamentally changed.

A new kind of archaeology emerges. The science is intimately connected with the engineering, enabling new investigations and using novel methods. For deep water sites, the JASON ROV (a 6,000 meter rated vehicle system requiring a dynamically-positioned surface vessel) has proven the ability to record this data automatically, under-closed loop control, to high precision. Recent projects at Skerki Bank in the Tyrrenhian Sea, off of Ashkelon (Israel), and in the Black Sea have demonstrated that archaeology can be accomplished with remote and human-occupied submersibles [McAnn and Freed, 1994, Ballard et al., 2000, Ballard, 2001].

Figure 2-5 illustrates the process of deep-sea archaeology using an ROV. The image shows the Jason ROV surveying a shipwreck site using navigation information form the two acoustic transponders. The key concept is that the precise navigation enables high-resolution imaging and that the fixed reference, achieved through instrumenting the environment, enables co-registered data - fusing different remote sensing modalities to build images from multiple data sources. This particular example shows how a measurement from the pencil-beam sonar, receiving and echo off the 3-D structure of the site, is places within the context of the photomosaic (optical sensing) through the navigation solution. This goal of precise repeatable imaging is the focus of deep-sea archaeology.

Deep-Sea Archaeology and Autonomous Vehicles

Archaeology in the deep-sea is a particular method generally applicable to archaeological investigation - not an application of generic methods to a specific environment. Four problems, or stages of investigation, are central to this method [Mindell and Bingham, 2001]:

- Sonar Search / Broad-Area Survey
- Target Identification

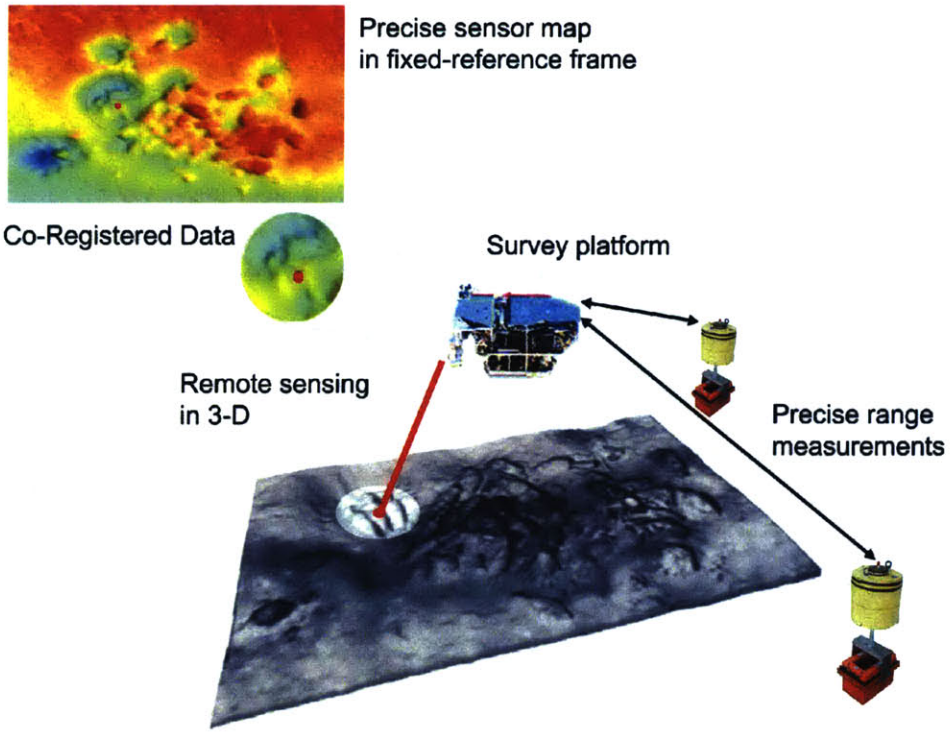

Figure 2-5: The ROV Jason performing a precision survey, collecting still photos and scanning-sonar data.

- Precision Survey
- Remote Excavation

Some important observations distinguish the critical characteristics of this general method. Deep-sea archaeology is remote and reliant on technology for perception. This challenges the technology to accurately represent the environment through a variety of sensing modalities while challenging the scientists to incorporate the new methods. Precision navigation and guidance is fundamental to delivering remote sensing with the quality necessary for interpretation and documentation. These qualities of archaeology in deep water push the engineering in new and beneficial directions.

Small, inexpensive AUVs bring in a new phase in deep water archaeology. Free from the expensive tether and dynamic positioning of towed and remotely operated vehicles, autonomous vehicles are a complimentary capability to the technologies of perception of an extreme environment [Bellingham, 1997]. In addition to decreasing the operational cost of current capabilities, autonomous platforms offer new capabilities that cannot be achieved through towed or tethered systems [Mindell and Bingham, 2001]. This technology enables a broad community of scientists, further opening deep water to archaeological investigations[2]

[2]An good example is the U-166 project done by C and C Technologies [Church et al., 2002] 'The entire investigation survey took less than 9 hours to complete using the AUV, a fraction of the 80 or more hours a conventional deep-towed system would have required.' 'The oil companies' willingness to explore potentially significant archaeological resources led to one of the most intriguing historical finds in the Gulf of Mexico in recent years.'

Precision survey and navigation is still the critical requirement. The ROV Jason has exhibited the capability to perform precise, close-loop surveys of small-area sites, and autonomous platforms have demonstrated the ability to navigate on larger scales, but truly precise navigation has not been realized by autonomous platforms. This convergence is the topic of this work - the capabilities of autonomous underwater vehicles and the stringent requirements of underwater archaeology.

Summary: The Requirements of Underwater Archaeology

This section follows two threads: the expansion of archaeological investigations into the deep ocean and the rise of autonomous vehicles for underwater survey. AUVs are one component in an expanding array of tools for deep-sea investigations. The critical technical challenge to applying AUVs to archaeology is the challenge of precision navigation. The navigation solution requirements come from the needs of scientists to interpret remote sites using images of the complex 3-D structure of the work-site. The next section summarizes the broader field of AUV technologies and shows how current capabilities fall short of these requirements for extreme precision.

2.1.2 Autonomous Underwater Vehicles

Autonomous underwater vehicles (AUVs) are a combination of underwater vehicle technology, mobile robot navigating techniques, and underwater sensors. Each of these three fields is large, so this section concentrates on the portions of each applicable to AUVs.

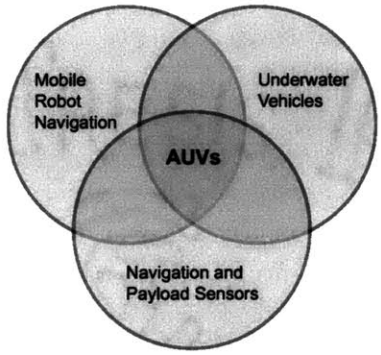

Figure 2-6: Autonomous underwater vehicles (AUVs) as the convergence of vehicles, sensors, and navigation.

In the past decade, autonomous underwater vehicles have matured and become operational assets, useful for a variety of oceanographic and military applications. Small, high-performance vehicles have proven adept at a variety of undersea survey, mapping, and measurement tasks. The ability to operate free from tethers, from expensive dynamically-positioned vessels, and without human intervention during the dive sequence has great potential for replacing traditional towed-systems and remotely operated vehicles. More important, it has also become clear that AUVs have unique capabilities such as close-in terrain following, multiple vehicle operations, and extremely

long endurance. [Mindell and Bingham, 2001]

Underwater Vehicles

As AUV technology continues to evolve, two characteristics emerge: the missions are increasingly disparate and the platforms must be considered within the broader sampling system. One of the first implementations of small cost effective survey vehicles is the *Odyssey* vehicles developed at MIT and commercialized by Bluefin Robotics [Bellingham et al., 1994,Bellingham, 1997]. This class of vehicle, focusing on extreme-duration survey, is the standard of AUV technology. The *Hugin* vehicle has proven the technology's ability for industrial survey [Vestgard et al., 1999]. For military missions, platforms such as the *REMUS* class of vehicles has focused on reconnaissance and mine counter measures [Allen et al., 1997,Purcell et al., 2000]. For scientific and engineering research, vehicles such as ABE [Yoerger et al., 1992], SeaBED, and OTTER [H.Wang et al., 2996] serve to advance the vehicle technology while providing new methods for scientific exploration. Each of these implementations shares an emphasis on long-duration and large range survey. Analysis of vehicle performance focuses on the efficiency of the solution [Singh et al., 1997]. As applications of the technology expand, AUVs are being used for new types of missions. No single solution exists and new designs are necessary for new missions.

Autonomous underwater vehicle capabilities come at a cost. AUVs are limited in their ability to adapt to unknown unstructured environments, are constrained by the amount of energy on-board, and have little or no feedback from the operators. Exploratory missions demanding real-time data interpretation such as video survey and excavation present a challenge to current autonomous means. For these reasons, AUVs must be considered as part of a portfolio of solutions for ocean exploration. Expeditions make use of the strengths of manned, remote, and autonomous systems. Nascent underwater networks promise to expand this holistic view of underwater sampling and the role of autonomous vehicles within these greater systems - [Curtin et al., 1993,McElroy et al., 2001,Delaney et al., 2001].

Navigation Sensors

Navigation underwater presents a distinct challenge. The extreme environment of the deep-sea is sensor-limited. Much of the techniques for terrestrial navigation are based sensors that operate in the electromagnetic spectrum. Sea-water attenuates these signals, necessitating the use different modalities and the development complimentary techniques. In contrast acoustic signals travel large distances, making acoustic fundamental to perception underwater. Figure 2-7 shows the attenuation as a function of range and frequency. Temperature, salinity, and pressure affect the speed of sound in known ways leading to a multitude of transmission paths at these scales.

There are many excellent books on the fundamentals of ocean acoustics [Urick, 1983,Brekhovskikh and Lysanov, 1991,Jensen et al., 2000]. For large-scales and low-frequencies (10's of km and 100's of Hz) ray bending, wave guides, scattering, etc. are all important considerations. Much basic research has focused on developing these models because of the strategic military importance. Tomography is a dual problem - by observing the channel the properties of the transmitting media are

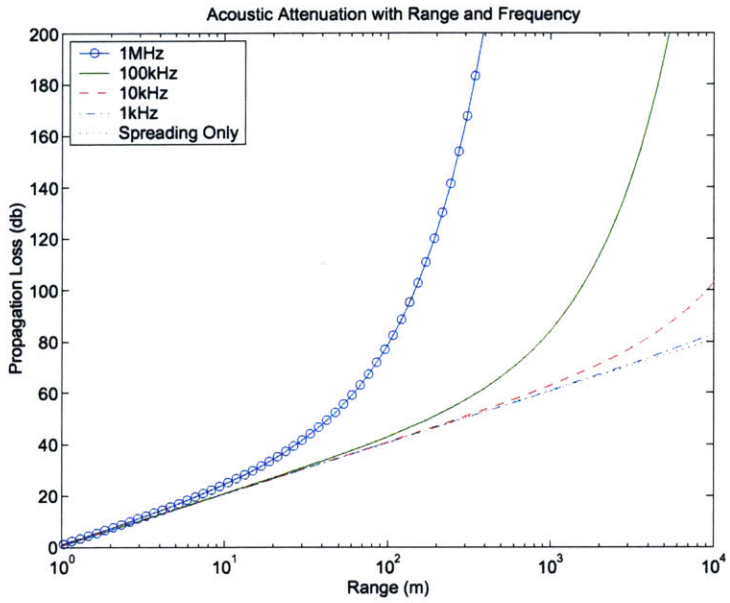

Figure 2-7: Attenuation in seawater as a function of range and frequency

determined [Spindel and Worcester, 1990]. Characterization of the acoustic channel is important for acoustic communication. Increasing the information transmission rate requires an understanding of the fading inherent in the acoustic channel [Loubet and Jourdain, 1993, Green and Blackmon, 2001]. The properties of the ocean environment demand particular sensors and techniques for their use.

Underwater navigation makes use of an ever increasing number of proprioperceptive sensors. To avoid a full recount of all the possibilities a few summaries will be referenced, followed by a discussion of the sensors particularly prominent in this story. Acoustic positioning is a fundamental method of navigating underwater. Milne presents an overview of the basics of long baseline (LBL), short baseline (SLBL) and ultra-short baseline (USBL) techniques [Milne, 1983]; a similar summary is given by Vickery [Vickery, 1998]. Positioning techniques are complimented with a variety of standard sensing modalities: inertial navigation techniques, GPS, Doppler velocity logs, etc. Again a overview is left to the literature [Tuohy, 1993, Leonard et al., 1998].

Categorizing the sensing modalities is more important than simply listing their capabilities. One delineation categorizes the uncertainty in the position estimate from a single sensor as bounded or unbounded. Acoustic position, like GPS, has a bounded uncertainty. Odometry sensors and inertial navigation systems (INS) have accumulated error in the position estimate - unbounded error - because uncertainty in the measurement of velocity or acceleration is integrated to estimate position. For underwater sensors Whitcomb, et al. summarize the possible sensing modalities and illustrate how they can be integrated [Whitcomb et al., 1999a]. Redundant sensors can be combined to remove errors in the observations. Larsen presents an example for underwater navigation that examines the integration of INS and Doppler velocity log (DVL) sensors [Larsen, 2000a]. Whitcomb,

et al. examine the benefits of combining LBL and DVL techniques [Whitcomb et al., 1999b, Whitcomb et al., 1998]. Navigation observations can be delineated as internally or externally referenced, but it is critical to understand the type of inherent uncertainty in the measurement. Systems exhibiting bounded error, such as acoustic positioning and GPS, are compared with those with unbounded error accumulation by Whitcomb, et al. [Whitcomb et al., 1999a].

Another critical consideration is matching the precision of the navigation to the precision of the remote sensors used for survey [Singh et al., 2000a].

> Geo-physicists, geologists, archaeologists, marine biologists, and physical oceanographers share the need for high precision acoustic bathymetric surveys. Of particular interest are sites ranging from hydrothermal vents to shipwrecks, whose overall dimensions may be from 10^1 to 10^3 meters, yet possessing details of interest as small as 10^-1 to 10^-3 meters. There is a mismatch between the high intrinsic sensor resolution and comparatively low navigation accuracy which has precluded the building of maps to the limits of sensor resolution. [Singh et al., 2000a].

Mobile Robot Navigation Techniques for AUVs

The general field of autonomous robot navigation will be explored in a following section, but this section summarizes some particular techniques used for navigating AUVs. The ocean environment presents unique challenges to the navigation system and only a subset of research on terrestrial autonomous robots has proven useful underwater.

Navigation is key to AUV missions [Romeo and Lester, 2001] and solutions bridge the gap between the simplifications of theoretical robotics and the complexity of the ocean environment. The field of autonomous robot navigation was divided into reactive and planning components. Few AUV applications make use of reactive architectures. The layered used in the Odyssey class vehicles seems to be modeled on Brooks's subsumption architecture [Bellingham et al., 1990], but contains many state-based techniques and elements which are decidedly planning-based. Feature-based techniques, CML and SLAM, are applied to navigation in acoustic beacon networks [Bennett and Leonard, 1999,Smith et al., 1998]. For range only measurements where the beacon locations are unknown, Newman and Leonard use the bundle adjustment to estimate both the beacon locations and vehicle positions. Motivated by the operational cost of surveying acoustic beacons and the instrument cost of inertial and DVL sensors, this method solves a large scale non-linear optimization incorporating only range observations. The approach assumes the beacon depth to be known and uses an off-line optimization for creating a map after the dive is complete, but gives no aid to guiding or performing the survey in real-time. The resulting solution is ambiguous in both translation and rotation - i.e., the map from this algorithm is self consistent, but not placed in the world - an expected result since the transponders are never surveyed. The algorithm addresses the popular problem of surveying an unstructured environment.

Acoustic transponders bound the error accumulation while a vehicle is submerged. Many techniques decrease or eliminate the costly deployment of acoustic beacons. Synthetic long baseline navigation uses only one beacon to estimate position by integrating relative position information

[Larsen, 2000b, Larsen, 2002]. Researchers working with the REMUS vehicle have developed similar techniques for dealing with acoustic range measurements [Stokey and Austin, 1999]. Huster and Rock use vision to identify features on the seafloor and eliminate the need for beacons [Huster et al., 1998, Huster and Rock, 2001]. Navigation can also be done using prior maps. Navigating based on *a priori* maps has been transitioned from terrestrial applications such as cruise missile navigation to AUVs. The approach uses cellular representations of bathymetric, magnetic, or gravitational maps to localize the vehicle [Tuohy, 1993, Tuohy et al., 1996].

These approaches reflect the dominant paradigm of AUV research - expanding the capability of autonomous survey platforms to operate in the unstructured ocean. This thesis takes another view examining methods for enhancing the performance of navigation systems. The methods discussed so far lack precision and do not pursue precise navigation on the scales necessary for archaeology. Without surveying the acoustic beacons or by using only one transponder, the navigation solution is ambiguous in translation, rotation or both. The methods diminish the navigation system's reliance on costly acoustic beacons, but do not achieve the precision necessary for archaeology. As discussed below, the documentation of an archaeological site requires mosaicing the data from not only the observations in a single dive, but over many dives separated in time. The uncertainty in overlapping successive surveys is determined by the GPS fix after the dive is complete. This level of precision does not satisfy the requirements of the application.

The requisite precision has been achieved, but not autonomously. Research at the Woods Hole Oceanographic Institution has concentrated on enabling navigation with unprecedented precision by integrating multiple sensors [Whitcomb et al., 1999a, Whitcomb, 2000, Whitcomb et al., 1998, Yoerger and Mindell, 1992]. The sensors and techniques are not specific to autonomous navigation. The ability to navigate without operator feedback requires methods that are more robust to the sensor errors and environmental characteristics.

Specific techniques have been developed for navigating with sonar measurements. Acoustic positioning is an important element in the design and development which follows. Outliers, or spurious measurements, are common in acoustic ranging and can make localization difficult. In general this is a problem suitable for techniques from the tracking literature surveyed previously, but techniques such as median filtering and range gating must be applied carefully to acoustic time-of-flight observations [Vaganay et al., 1996, Yoerger and Mindell, 1992]. Median filters, a standard method of off-line, batch outlier rejection, rely on consensus between chronological measurements [Newman and Leonard, 2002]. Multiple hypothesis tracking addresses the data-association challenge for dealing with sonar observations [Leonard et al., 1995, Smith and Leonard, 1997]. Range measurements are also cluttered by multipath errors arising from multiple acoustic paths between the source an receiver. With a known geometric model of the environment, the model determines the acoustic travel times for various travel paths. By predicting the arrival times and matching the predictions to measured acoustic arrival-times, the multipath returns can be used in the navigation solution [Deffenbaugh et al., 1996b]. Similarly the depth and range can be estimated based on the relative delays between paths [Friedlander, 1988]. Another technique measures not only the range but the arrival angle to help resolve the environmental model and fold the multipath range

information into the navigation scheme [Zielinski and Wu, 1989].

2.1.3 Autonomous Robots

The control architecture classifies autonomous robots according to the structure of the control system and the design of the robot operation. This section offers a simplified decomposition of the fundamental approaches in the literature to situate this thesis within the field.

Two extreme control types bound the continuum of approaches to autonomous robot navigation: *reactive* and *planning* strategies. These contrasting philosophies differ in the resulting operation and capabilities, but also in how the machines are designed. The central issue is the efficacy of an environment's representation.

Reactive	**Planning**
Mapping stimulus-response	Centralized world representation
Descriptive	Normative / Prescriptive
Behavioral	Axiomatic
Inductive design	Deductive design
Experimental analysis	Analytic analysis
Simple behavior in complex environments	Complex behavior in simple environments
Divergent problems	Convergent problems

Table 2.1: Characteristics of autonomous robot control strategies

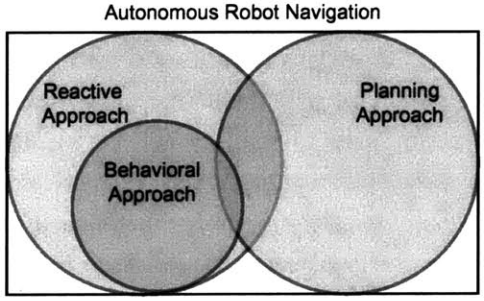

Figure 2-8: The two extremes of autonomous robot control architectures: reactive and planning. The behavioral approach is considered as a subset of the reactive approach.

Reactive Approach

> Can there be a theoretical analysis to decide whether one organization for intelligence [traditional or behavior-based AI] is better than another? Perhaps, but I think we are so far away from understanding the correct way of formalizing the dynamics of interaction with the environment that no such theoretical results will be forthcoming in the near term. [Brooks, 1990]

> *The environment is its own best model.* [Brooks, 1991a]

> Incremental design, punctuated by testing and debugging, produces the desired side effects in a controlled fashion. [Mataric, 1992b]

The reactive approach to mobile robotics is founded on the belief that a representation of the environment is insufficient for control, design, or both. Brooks argues for a purely reactive controls strategy, relying on combinations of simple stimulus-response mapping resulting in globally satisfactory behavior [Brooks, 1991b]. Similarly, behavior-based approaches build complex goal-seeking from simple behavioral components [3]. Simple structures, such as Brooks's subsumption [Brooks, 1989, Bellingham et al., 1990] or Materic's behaviors [Mataric, 1992a], are combined, resulting in complex emergent operations.

Mapping the low-level behavior to the resulting global operation is the critical challenge. Given a desired global operation, there is no simple method for synthesizing the component behaviors - no design method. Given a set of component behaviors, there is no simple method for determining the aggregate performance - no analysis method. The empirical strategy of design-and-test relies on inductive reasoning, using experimental evidence to arrive at general conclusions about the global stability or performance of the system. Like a scientific theory, the performance or stability can never be proven in the affirmative, only disproven when the system looses stability or performs poorly.

Planning Approach

Planning control relies on a sufficient representation of the environment. Based on this abstraction, engineers synthesize control strategies to achieve desired global behavior. In contrast with reactive approaches, planner-based control is deductive and prescriptive. Control system analysis, made possible by the abstraction, leads to stability and performance guarantees. System design synthesizes a controller with specified global behaviors. Predictive models of both the environment and platform enable application of engineering design methods. Examples of planning approaches to robot navigation are given in the following section on field robot navigation.

The Middle Way : The Engineering Approach

Neither the reactive approach or the planning approach to mobile robot design is sufficient. The reactive approach relies on iterative experiments in the environment to refine the autonomous behavior - an expensive proposition for underwater work requiring costly support to reach the environment. Conversely the complexity and variety of underwater environments precludes the planning approach because a high fidelity model of the environment is not available. The engineering approach builds a planning control strategy, but realizes the limits of abstraction. To design and operate a complex machine in a harsh and varied environment with a variety of goals requires utilizing the strengths of both approaches to the problem. Using models aids the designers intuition

[3] For the purpose of this discussion behavior-based methods are classified as reactive. This is an over simplification ([Mataric, 1992b, Mataric, 1997] provide a more complete treatment), but at this coarse level behavior-based control strategies have similar attributes to the reactive strategies.

saving time and expense, but the final goal requires building a system that operates in a real-world environment.

2.1.4 Field Robot Navigation

Field robot navigation is a label for approaches to robot navigation that rely primarily on planner-based control architectures to perform defined goals within real-world environments. This class of problems combines the fundamentals of the autonomous robot navigation with the constraints of implementation. This section discusses a subset of the large variety of techniques in the literature, examining the portions of the background applicable to autonomous precision underwater survey.

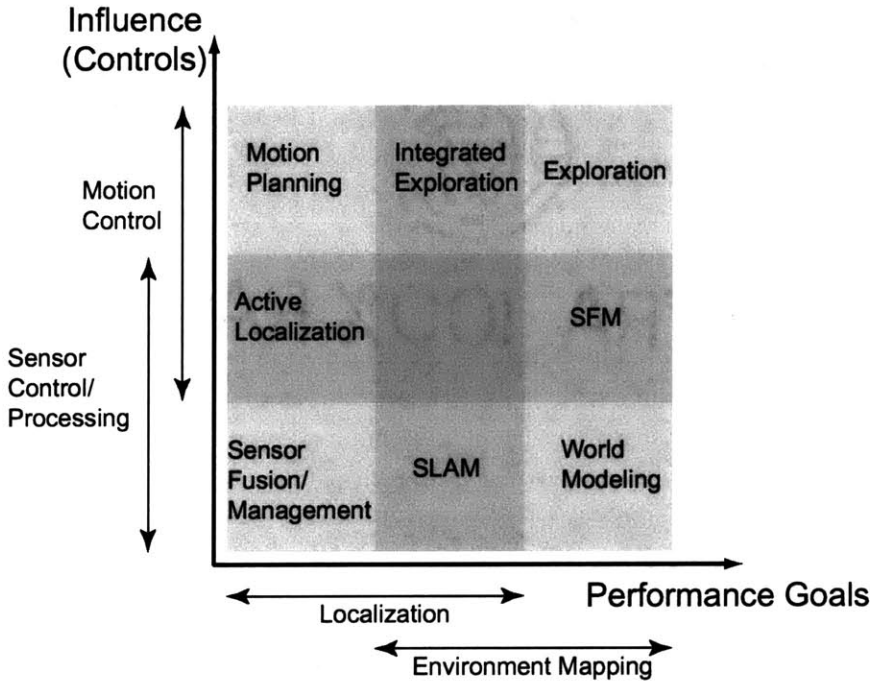

Figure 2-9: Approaches to field robot navigation. SLAM = Simultaneous localization and mapping, SFM = Structure from motion.

Locating itself is a fundamental cognitive capability of a mobile robot. Figure 2-9 presents a decomposition of the literature on field mobile robots. The overall performance of the system is measured by the attainment of the performance goals- the output - and the control effort required - the input. This is analogous to optimal control where the cost function expresses tradeoffs between performance and cost - both expressed as functions of the system's state. Two dimensions of navigation performance are measured by how well the system estimate their location and the quality of information gathered the environment, e.g., the pose and the feature-map in feature-based methods. Two dimensions of influence are exerted to achieve this performance: sensor processing and motion control.

$$\text{Cost Function} = \text{Performance Measure} + \text{Control Cost}$$

$$= \{\text{Localization, Mapping}\} + \{\text{Motion Control, Sensor Processing}\}$$

The particular combination of performance and control differentiates the approaches to field robot navigation. Figure 2-9 illustrates the possible combinations. The following sub-sections discuss the relevant work in each of these areas.

Sensor Fusion

The lower left corner of the grid in figure 2-9 represents the oldest and most basic approach to robot navigation - techniques that estimate location based on processing or controlling sensors. Kalman filtering techniques have been applied to a staggering variety of problems. The seminal work by Rudolph Kalman [Kalman, 1960] is reprinted along with a history of the development and applications of Kalman filtering [Sorenson, 1985]. Dozens of textbooks provide background in designing Kalman filters along with the prerequisite background on probability and stochastic processes - a few general references are provided [Brown and Hwang, 1996, Bar-Shalom et al., 2001, Gelb, 1974]. More specific references address the application to robot navigation [Bar-Shalom et al., 2001, Manyika and Durrant-Whyte, 1994, Smith et al., 1990].

Data association, or correspondence, is a critical component of autonomous navigation. Techniques are often brittle with respect to correspondence - errors in determining the source of a particular observation. Thrun's summary article provides an overview of this facet of robot navigation [Thrun, 2002]. Tracking problems are a useful analogy; determining correspondence plays a critical role in distinguishing observations from multiple targets, clutter, and noise [Bar-Shalom and Li, 1998]. Multiple hypothesis tracking (MHT) is one method [Reid, 1979]. MHT applies to both generic robotic navigation [Cox and Leonard, 1994] and AUV navigation [Leonard et al., 1995, Smith and Leonard, 1997]. Other approaches extend the Kalman filtering approach to deal with uncertain correspondence through geometric constraints [Neira and Tardos, 2001] or by adding memory to discern consistency [Leonard and Rikoski, 2001].

World Modeling

A dual of the sensor fusion approach ignores localization and focuses on estimating environmental parameters from observations. This approach considers localization as external to the map-building process. A canonical approach represents the environment as a set of features. A state vector contains the feature locations - an approach that leads directly to combining the robot and feature states into a single vector of parameters [Smith et al., 1990]. Another method is occupancy grids [Elfes, 1989] [Thrun, 2001, Moravec, 1988]. The environment is decomposed into a multidimensional grid. The binary probability of the cell being occupied or free is maintained through Bayesian inference and repeated observations. Dempster-Shafer grids [Pagac et al., 1996, Ribo and Pinz, 2001] extend this model by using the method of evidence [Shafer, 1976] to avoid Bayesian difficulties with representing ignorance and prior probabilities.

SLAM/CML

Concurrently considering the environment and the robot's location in the environment is a large component of field mobile robotics literature. Based on the concept of location and environment features combined into a single state vector [Smith et al., 1990], concurrent mapping and localization (CML) or simultaneous localization and mapping (SLAM) bring probabilistic tools to bear on the problem. Thrun gives a comprehensive overview of the challenges and approaches [Thrun, 2002, Thrun, 2000]. Research initiatives by Leonard and Durrant-Whyte apply Kalman filtering techniques to various implementations of the problem [Leonard and Durrant-Whyte, 1992, Leonard, 1990, Leonard and Durrant-Whyte, 1991]. Thrun uses Bayesian (particle) filters and expectation-maximization to solve the same problem [Thrun et al., 1998a, Doucet et al., 2001]. The advantage of Thrun's approach is in relaxing the linear-Gaussian restrictions on the Kalman filter, but the complexity cost can be prohibitively high.

Motion Planning and Active Localization

Sensor processing and control are used to influence performance. Methods from the top row of figure 2-9 approach localization and mapping by considering the influence of motion control on performance. Motion planning looks specifically at how to reduce uncertainty through movement [Latombe, 1991]. This is rarely accomplished without also considering the sensor processing as part of the problem - active localization. Kalman filtering and information metrics are combined in Manyika and Durrant-Whyte's book with examples of active perception and sensor management [Manyika and Durrant-Whyte, 1994, Grocholsky et al., 2003]. In the context of occupancy grids, Elfes provides many references on active perception [Elfes, 1992] for mobile robots. Optimization algorithms can be used to solve for the path through an instrumented environment that minimizes the uncertainty - path-planning for precision [Deffenbaugh, 1997]. Research in sensor management and active perception for mobile robots uses metrics (normative methods) to build rules for controlling both sensors and their platforms. Many of these techniques are based on information theory; Shannon's seminal work [Shannon, 1948] is summarized by many books - [Pierce, 1980] is a good introduction to the fundamentals of information theory.

Exploration

Robot exploration, in the upper right corner of figure 2-9, determines motion to increase the robot's knowledge about the environment. Both planning and behavior-based approaches apply to this problem. The former are typically classified as exploration while the latter are often labeled action selection [Newman et al., 2003]. Many methods use occupancy (evidence) grids and the frontier-based approach to determining paths of exploration [Yamauchi, 1997]. Makarenko proposes the term *integrated exploration* to distinguish techniques that consider navigation and world-modeling concurrently [Makarenko et al., 2002]. These methods build on extensions of mobile robot navigation maximize the feature-map information while maintaining quality position estimates [Feder et al., 1999, Newman et al., 2003, Schultz et al., 1999].

Structure from Motion

Machine vision research solves similar navigation problems, but the sensing modality demands unique methods. The central challenge of vision is the perception and not the navigation. Structure from motion reconstructs a 3-D scene, a model of the environment, based on repeated measurements from a set of known locations. The focus of this approach is on the model, but the uncertainty of the navigation is considered simultaneously [Soatto et al., 1996, Dellaert et al., 2003, Dellaert et al., 2000]. A related challenge is to determine optimal motion, gathering the most information about the scene. These canonical problems, coupling vision and navigation, are summarized by Faugeras [Faugera, 1993, Ayache and Faugeras, 1989]. Probabilistic robot navigation and vision based navigation share common aspects and similar solution methods. Navigation underwater presents unique challenges to vision based methods - separate solutions are necessary.

Summary: Autonomous Robot Navigation

The previous section uses decomposition of figure 2-9 to divide the vast literature on field mobile robot navigation. Taken as a whole the trend is towards increasing the integration - moving towards the center of the grid where motion and sensor control are both used to reduce uncertainty about the environment and location. Hypothesis grids, presented in chapter 4 are a continuation of this trajectory. The algorithm builds a representation of the acoustic positioning environment specifically for increasing the navigation capability. This sensor-based map is a product of observation processing, but is intended to be particularly suitable for active motion control and higher level autonomous decision making.

requirements

2.1.5 Summary: Navigation Capabilities for Precision Survey

The literature shows a wide base of fundamentals. Research on mobile land robots leads to open questions and a variety of standard solutions. The techniques for mobile robots are often not directly applicable because of the sensor-limited nature of the ocean environment. Conversely, much of the work on underwater navigation does not directly address the challenges of autonomous operation. Autonomous precision underwater navigation is a distinct and challenging problem that demands considering the particular constraints of working underwater to develop new methods based on the fundamentals of autonomous robot navigation. So far only human operated vehicles have illustrated the ability to navigate precisely - with centimetric precision. This dissertation brings these pieces together toward a system capable of achieving precise navigation autonomously. The design methods and algorithm development that follows is based on these fundamentals, but extends them in a new directions.

2.2 A Taxonomy for Autonomous Underwater Survey

> Taxonomy, n. - (1)The classification of organisms in an ordered system that indicates natural relationships. (2) The science, laws, or principles of classification; systematics. (3) Division into ordered groups or categories. [4]

It is important to be specific about some key terms used throughout this work. Many of the terms have come to represent so many concepts that they communicate none. The following definitions organize these key concepts.

Mission Classification

A mission, defined by its *goals*, *environment*, and *platform*, refers to the operation of an autonomous underwater vehicle over an entire investigation. A mission - a single dive or multiple deployments - focuses on a single set of goals. For archaeology a precise survey is the general goal driving the functional . The environment is both the physical attributes of the survey site and the operational environment. The physical artifact performing the mission is the platform. Platforms have a variety of capabilities and limitations; understanding these aspects influence the mission design decisions. The mission is the fundamental unit of work for underwater exploration.

Survey: Maps and Images

In the sensor-limited ocean, remote sensors are transported over and through the area of interest. Navigation information enables mosaicing these observations into a overall view of the environment. The platform performs a *survey* specified by the target trajectory - the locations and speed of the vehicle. The product of a survey is a *map* or an *image* - remote sensing data correlated with navigation estimates. For underwater science a fundamental task it to map a phenomena using the right sensors, in the right place, at the right time. The result is a spatial image of the sensor data. We need to be explicit with this terminology because in the field robotics literature (see section 2.1.4) a map often refers to the estimated feature locations within the environment. This concept will be explicitly referred to as a *feature-map*.

Navigation, Localization, Guidance, and Control

> Navigation - From the Latin navigatus, past participle of the verb navigere.
> Navigere: navis=ship; agere=to direct or move.[5]

Navigation is the central concept of this work, referring to the determination of location and direction of movement - the convergence of estimation and control. *Localization* and *positioning* are synonymous for estimating of the Cartesian position with respect to a particular reference frame. *Guidance* refers to process of commanding actuation to achieve desired location. Guidance

[4] www.dictionary.com
[5] Dutton's Navigation and Piloting, 12th ed., ed. by G.D. Dunlap and H.H. Shufeldt, 1969.

to achieve a target state is *control*. Guidance to achieve a target uncertainty requires *path-planning*, a more complex form of feedback. Navigation encompasses both localization and guidance.

In addition to the spatial decomposition of navigation, the concept can be characterized temporally. Navigation is causal estimation using only past and current observation. In contrast re-navigation batch processes all the observations (past, current, and future) off-line to estimate the state. This distinction between *real-time* and *off-line* navigation is an important determinant of the navigation system operation.

The Instrumented Environment

Placing acoustic *beacons* (*transponders*) and surveying their location produces an *instrumented environment*. Multiple *hosts* move within an instrumented space, the *acoustic network*, measuring the round trip time-of-flight range between the mobile and fixed components. Trilateration estimates the position from the range estimates - the localization solution. There are many uses for an instrumented environment, and the ability to measure range to fixed, known locations is independent of the localization method.

Uncertainty in Navigation

Navigation performance is quantified by the precision of the position and attitude estimate - the degree to which uncertainty has been eliminated through estimation and control. For navigation, especially underwater, the frame of reference is supremely important. *Precision* is defined by the navigation solution error relative to a local, fixed coordinate frame. *Accuracy* is error in the navigation solution in a world coordinate frame. This work is concerned with advancing the precision of underwater navigation. Precision is indicative of the ability to build fine-resolution images and maps and is a less stringent requirement than accuracy. Consider a precise survey and an accurate survey with equivalent uncertainty specified in terms of precision and accuracy respectively. Both surveys will yield the same image quality, but the accurate survey will also place the image within the environment with little uncertainty. For a more detailed discussion on the pertinent issues in handling uncertainty see appendix B.5.

Autonomy and Underwater Vehicles

In the underwater vehicle vernacular autonomy is synonymous with untethered. From the operator's point of view, the level of abstraction, where the human-machine interface divides the functions controlled by the operator and the functions controlled by feedback, is the measure of autonomy.

> As we shall see, automatic control does not set machines free as autonomous agents, but rather brings them under the purview of human intention. ...Whether the operation of an individual device, the piloting of a vehicle, or the command of a large system, control involves a complex exchange of function and responsibility between operator and machine, traversing the boundary between human and artificial. [Mindell, 1996]

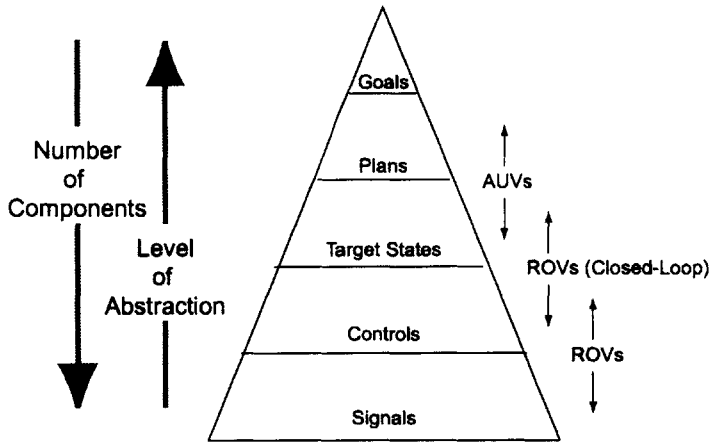

Figure 2-10: Illustration of functional components of a controlled system. The role of human and machine is specified by the location, at boundaries between functions, of underwater robotics.

Figure 2-10 shows the abstract functions of a controlled system, for example, a robot for underwater survey. At lower levels of abstraction the functions have many components; thousands or millions of serial communications and actuation signals are necessary to accomplish a single survey goal. The autonomy of three classes of underwater robots are evaluated using this conception. The operator of an ROV specifies the control functions; the machine translates the commands into the appropriate signals. Under closed-loop control the operator specifies targets, locations for the vehicle to move to, which are translated into control commands and then the appropriate signals. An AUV operates at the next level, generating target states from mission plans.

This analysis follows Sheridan's work in explicitly considering the human-machine boundary for supervisory control [Sheridan, 1987,Sheridan, 1992]. While the classification from in figure 2-10 focuses on the action side of control a similar characterization considers the human-machine boundary in the feedback loop, considering sensing and actuation. Methods for coping with complexity are also an important foundation. These methods include modularity, abstraction, hierarchy, and level abstraction [Saltzer, 1985].

As AUVs evolve, the operators will operate at higher levels of abstraction. By recognizing the role of the autonomous system and the human operator as an interconnected whole, the design of the systems can be approached from stronger footing.

2.3 Point of Departure

The preceding background provides a fundamental base for analysis and exposes an opportunity to extend the current capabilities. Analysis of this background frames the question in terms key considerations not addressed in the previous work. To launch the following chapters the conclusions and key assumptions are presented explicitly.

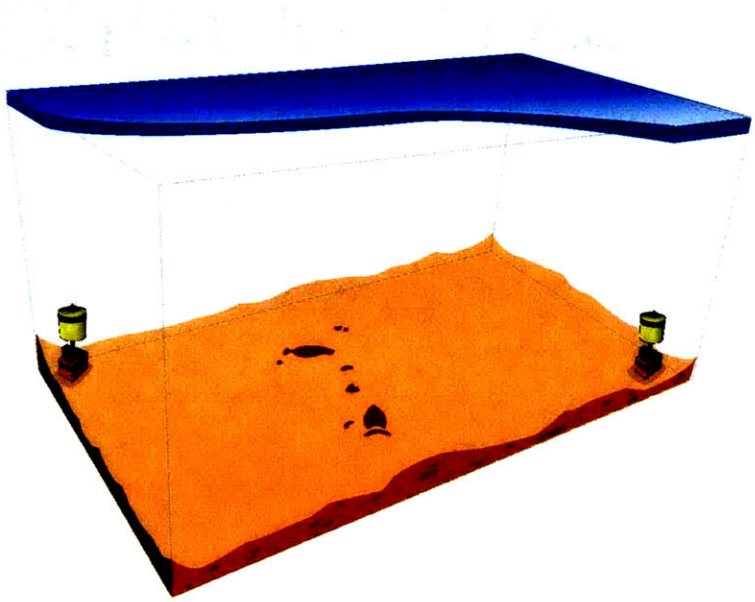

Figure 2-11: Illustration of the instrumented environment. Two fixed acoustic beacons are shown inside the 100m discrete environment.

2.3.1 Key Assumption: Instrumented Homogenous Environment

The design and development which follow assume the presence of an homogenous instrumented environment, i.e., acoustic beacons placed at known locations within an acoustically uniform environment. The distinctive goals and requirements of archaeological survey justify this common environment: the need for precision and repeatability and the small discrete size of typical sites. This environment is illustrated in figure 2-11.

The extreme precision and need for repeatability require acoustic beacons. Precise navigation is the defining characteristic that differentiates archaeology from salvage through the ability to do thorough documentation. Achieving the requisite precision requires a fixed reference. Because of the small survey area, high-frequency precision acoustic beacons are capable of instrumenting the environment and providing a high quality reference, e.g., the EXACT system [Yoerger and Mindell, 1999]. The methods of deep-sea archaeology involve multiple visits to a site [Mindell and Bingham, 2001]. Co-registering the data from multiple dives using a variety of sensing platforms requires an independent and external reference. A fixed reference frame enables comparing surveys separated by hours, days, or years.

Because of the limited size of typical archaeological sites (100's of m compared to ocean basins that are 1000's of km) the acoustics are considered homogeneous. At larger scales attributes such as variation in the speed of sound, the air-water interface, and the sea-floor boundary result in a complex acoustic environment; diffraction, ray-bending, and reflections create dense multipaths and wave-guides. The development that follows considers acoustic signals to follow straight ray paths between source and receiver.

Much work has gone into diminishing the reliance on fixed acoustic beacons because of their high logistical cost; deploying and surveying the transponders can require large amounts of valuable

operation time. Currently this method of navigation is necessary to satisfy the requirements of archaeological survey, but this work continues the trend to continually diminish the reliance on fixed transponders.

2.3.2 Conclusion

- A gap exists between the requirements of archaeology and the capabilities of AUVs.
  - Archaeological survey demands precision navigation within small-scale environments.
  - AUVs have cost and capability advantages over other methods of operating in the deep ocean.
- A new navigation solution demands concurrent consideration of the application, sensors, and integration.
- The technological components for autonomous precision navigation exist in disparate fields (ocean engineering, acoustics, signal processing, estimation, communication, etc.). Bringing these key techniques together demands a new treatment of the navigation problem.
- A consideration of the problem of AUV navigation which focuses on autonomous precision is distinct from past work.

This chapter argues the fundamental nature of navigation in general and the critical role of navigation for autonomous vehicles in particular. Navigation lies at the intersection of the technology of AUVs and the science of deep-sea archaeology. The background illustrates a gap between precision required for archaeological survey and the localization capabilities of AUVs. Narrowing this gap is the focus of what follows. The importance of this problem goes beyond the application to a single mission type; new industrial, military, and other science missions are enabled by the ability to autonomously navigate precisely. The following designs and analysis are based on these fundamentals while extending the capabilities in a novel direction.

Chapter 3

System Design: Autonomous Navigation for Deep-Sea Archaeology

> It is the organization of components, and not their physical properties, that largely determines behavior.
> - Herbert A. Simon[1]

The goal of this chapter is to present a method for making decisions about the design of autonomous underwater navigation systems. Design is a divergent problem for which a solution employs both art and science; designs are not general and the solutions are not cumulative. In contrast convergent problems, a invention of engineering analysis, are the subject of rational consideration and can be solved definitively. The answers to convergent problems are built upon, generating a cumulative process that appears as technological progress. This report contributes to the accumulation of knowledge for building and using autonomous underwater vehicles (AUVs) by developing a general method, based on engineering science, for quantifying design tradeoffs and leaves the required judgments to particular applications. This thesis presents abstractions useful for a navigation system designer, but it is the metis[2] of the the human designer which combines the abstract analysis with intuition and experience to arrive at a solution.

Chapter Goals

- Discuss closely related work to highlight the contribution of the methods and metrics presented.
- Present a precision specification connecting archaeological requirements with navigation parameters.
- Develop metrics to quantify design decisions and methods for analyzing candidate solutions.
- Articulate the critical design tradeoffs

[1] [Simon, 1996] p 21.

[2] Metis (Greek): cunning, many-sided intelligence, prudence.
Metis was the wisest of all gods and mortals alike - the mother of Athena.

- Match classes of missions to particular designs
- Identify leverage points where sensor capabilities will greatly improve navigation performance

What follows applies a systems approaches to the problem of designing precision underwater navigation systems, i.e., the integration of multiple aspects of navigation (sensing, control, signal processing, autonomy, etc) are considered concurrently to develop synergies not apparent at the component level. Building on the key assumptions of section 2.3.1, this analysis considers designing a system to inhabit an acoustically instrumented environment. Navigation is considered an estimation problem; the designer determines sensory, processing, and spatial aspects of the solution to estimate position and attitude. The potential of autonomous systems, where the vehicle is an active and adaptive participant in the environment, are only realized through an increased understanding of the design decisions.

3.1 Closely Related Work

This chapter is about approaching autonomous underwater navigation as a design problem, focusing on the unique challenges of precision, so this section discusses the relevant literature on the design of AUVs and their navigation systems. It also presents research on navigation systems specifically intended for precision.

Autonomous Systems

Designing autonomous systems is an open research question. The field of complex systems offers some general guidance to techniques for dealing with the design. Simon offers a concept of designing artificial systems based on their functions, environments, and adaptations [Simon, 1996] - an abstraction used in developing this design approach. Simon also offers a succinct trajectory of the evolution of complex systems [Simon, 2000] beginning with the rejection of reductionism, through general systems theory and cybernetics, to the applicability of complex systems methods to disparate fields.

Focusing on Design

Section 2.1.2 presents a brief overview of current AUV technology. This literature is replete with accomplishment-style reports describing a particular vehicle - a point in the design space. The research presents vehicle capabilities to accomplish the goals of particular missions, but the tradeoffs and candidate designs are not included [Bellingham et al., 1994, Bellingham, 1997, Yoerger et al., 1992, Allen et al., 1997]. Singh, et al. deviate from this formula and present a set of clear design rules for understanding the energy budget of an autonomous platform [Singh et al., 1997]. The report articulates the tradeoff between vehicle speed and distance covered, and presents the concept of hotel load - the fixed power required to run the computation and sensors of an AUV.

Focusing on Precision

Current work focuses on survey-class AUVS; precision applications demand new designs. Much of the work on AUVs concentrates on addressing the limited on-board energy. This binding constraint focuses the design decisions on issues of mission duration and survey range. The resulting vehicle designs reflect their mission, to survey increasingly large areas of the sea-floor. For archaeology, and a variety of emerging applications, other constraints dominate new designs [Mindell and Bingham, 2001]. This trend towards integrated design and integrated navigation demands a holistic approach.

The deep submergence laboratory at the Woods Hole Oceanographic Institution has focused on precision navigation. This work is the direct predecessor to the treatment that follows and highlights the technologies that make precision navigation possible: long baseline navigation, EX-ACT precision long baseline, Doppler velocity odometry and inertial navigation. Whitcomb and Yoerger compare navigation sensor technology and present a clear summary [Whitcomb et al., 1998, Whitcomb et al., 1999a, Yoerger and Mindell, 1992]. The integration of long baseline and Doppler velocity log (DVL) techniques is highlighted in a similar report [Whitcomb et al., 1999b]. By measuring the velocity over the bottom, DVLs provide accurate and reliable position estimates, but with unbounded error. This literature addresses the navigation requirements of remote sensing surveys. In contrast, this chapter emphasizes the creation of a system for autonomous rather than remotely operated guidance and navigation - a decisive divergence.

Evaluating the precision of candidate designs is rarely presented. The results of navigation research can be experimental verification, theoretical results, or ideally both. The references above primarily present experimental results. Deffenbaugh presents theoretical results of using the Cramér Rao lower bound to quantify the effect of timing uncertainty in positioning using acoustic beacons [Deffenbaugh, 1997, Deffenbaugh et al., 1996a]. In particular he shows the common spherical navigation is a special case of the more general hyperbolic navigation with uncertainty in the time synchronization. Larsen develops synthetic long baseline (SLBL) navigation system as part of the MARPOS navigation system [Larsen, 2000b, Larsen, 2002]. An extended Kalman filter predicts the navigation performance, but the tradeoffs between SLBL and other navigation techniques are not clear.

Although not useful underwater, the global positioning system (GPS) provides an analogy for LBL navigation. The error contributions from various sources are often combined into error budgets for various configurations [Kaplan, 1996]. The uncertainty due to the geometry is termed the geometric dilution of precision (GDOP)[3].

Summary

Research treating the general methods of AUV design is sparse, and the specific tradeoffs made in arriving at design decisions are rarely explicit. The previous work illuminates points in the design space where particular performance is achieved at specific costs. This dissertation focuses on the design decisions to fill the design space so that future tradeoffs can be made with better information.

[3] A useful conception of this is the Unit Vector Volume - The volume of the shape described by the unit-vectors from the receiver to the beacons is inversely proportional to GDOP.

The methods and metrics that follow concentrate on the precision dimension of performance where survey range and longevity are secondary considerations. Building on the work in human-operated precise navigation, this change in priorities yields new designs for autonomous navigation systems.

3.2 Specification for Precision Navigation

This section illustrates the development of an engineering specification for an underwater autonomous navigation system - the quantitative performance goals for a system to accomplish a particular task. The first sub-section characterizes autonomous vehicle missions and draws the navigation system limits, highlighting what is included and more importantly what is not. These abstractions are made concrete by considering the functional requirements and design parameters for archaeological imaging - the first step in developing a specification. A common characteristic is proposed for considering the dimensions of navigation performance. Finally a specification for the precision relates the requirements of image quality to the navigation sensor capabilities. This specification guides the analysis of this chapter and the case-study of chapter 5.

3.2.1 Problem Characteristics

Mission classification is the first step in defining the design challenge. The following three aspects of an autonomous vehicle mission characterize the application:

Goals: The motivation for the autonomous mission, e.g., imaging a deep-sea archaeological site. Goals drive the functional requirements that specify the design solution necessary to accomplish the goals.

Environment: The physical properties of the location where the mission is executed, e.g., a discrete shipwreck site in the deep-ocean. Environmental challenges have a strong influence on the system design.

Platform: The autonomous vehicle and its capabilities. The platform is considered external to the navigation system to focus the design and analysis on the navigation in general rather than on a particular vehicle solution.

System Boundaries

Whether an artifact is a system or a component is a matter of perspective. Figure 3-1 illustrates the functions within the scope of the autonomous navigation system. Information about the environment enters the system through the navigation (proprioperceptive) sensors. The distinction between the navigation and payload sensors is often not clear, but this coarse decomposition highlights the fact that not all sensing is used for navigation. The control block interprets the navigation output to produce AUV actuation commands. The environment couples the vehicle's output back to its input, i.e., actuation influences the sensory observations through the environment. Environmental influence is exercised through both sensed and unsensed pathways - modeled and unmodeled

dynamics. Figure 3-1 highlights the important boundary between the vehicle and the navigation. The ability to consider the navigation problem in general, without reference to a particular platform or environment, is an important theme of this work.

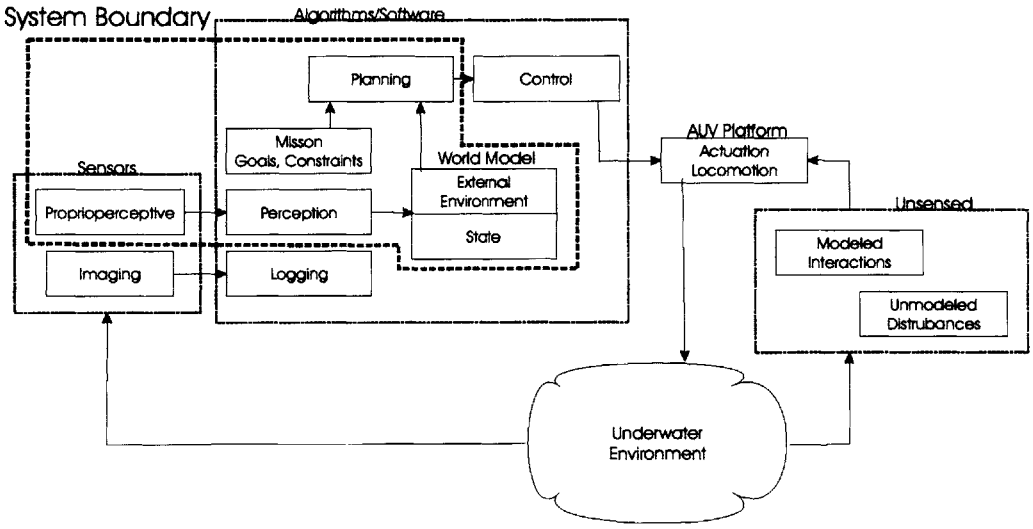

Figure 3-1: A functional description of an underwater imaging system. The system boundary (the dashed blue line) shows what functions are included in the autonomous navigation system.

3.2.2 Design for Imaging

A quantifiable specification is developed following a method-based engineering design approach where *customer needs* are translated into *functional requirements* and then *design parameters* [Otto and Wood, 2001]. This sub-section presents the specific requirements associated with the goal of high-resolution imaging. The functional requirements specify "what" the system is to accomplish and the design parameters specify "how" the requirements are to be met. Functional requirements are qualitative and design parameters are quantitative. The three elements correspond to three design domains: customer, functional, and physical. The customer in this design is the scientist - the archaeologist who must interpret information from the site. The background in chapter 2 presents some of these needs.

Functional Requirements

The overarching technical goal of archaeology in the deep-sea is high-quality imaging. Requirements for navigation performance follow directly from this emphasis on resolution and, when mapped to design parameters, lead directly to the need for precision. From the point-of-view of the navigation system, the following general functions are imperative:

- Deliver navigation and guidance in real-time suitable for executing precision survey including the following functions:
  - Locate the survey site.

- Survey the site with sufficient coverage (sensor overlap).
- Control the vehicle to minimize uncertainty (path planning).

- Make navigation observations for post-processing suitable for producing high-quality images from on-board sensors.
  - Record proprioperceptive observations.
  - Transform observations to vehicle coordinates.
  - Transform vehicle coordinates to world coordinates.
  - Produce image through mosaicing observations.

These requirements are general; each project has particular mission goals and uses specific imaging sensors that dictate the exact requirements. Section 3.7.1 at the conclusion of this chapter illustrates a set of example missions and possible solutions and a case-study is presented chapter 5. The next challenge is to translate these qualitative requirements into quantitative design parameters.

Design Parameters

Design parameters are the physical attributes that specify the design. The specification translates the functional domain into the physical domain, building a connection between archaeological imaging and precision navigation. Figure 3-2 illustrates the dependencies between requirements in the function domain and parameters in the design domain.

Two decompositions of the design parameters separate the navigation parameters into real-time versus off-line navigation and fixed-reference versus relative navigation. In the functional domain only the first dichotomy is obvious. The block diagonal form of figure 3-2, highlighted by the dashed lines, shows that the real-time functions and design parameters are tightly coupled, and the off-line functions and parameters are coupled, but the real-time and off-line requirements are decoupled. This decomposition is important because it allows the designer to consider each aspect of the mission and navigation independently.

Common Characterization for Comparison

Precision is of primary importance in this design study, but other dimensions of the system performance are also important. The following factors capture the dimensions for comparing designs. Some of these dimensions compete for scarce resources, e.g., the acoustic beacons can add precision but add logistical cost, and some dimensions are complimentary, e.g., autonomous navigation algorithms ideally increase both precision and robustness. The precision dimension is most amenable to quantification, but each dimension contributes to the overall fitness of the design. System-level decisions are made for a variety of reasons, not all of which are listed here. All the influencing factors can never be predicted, but the methods for making decisions that follow are one component of the design process.

Dimensions of Design Characterization:

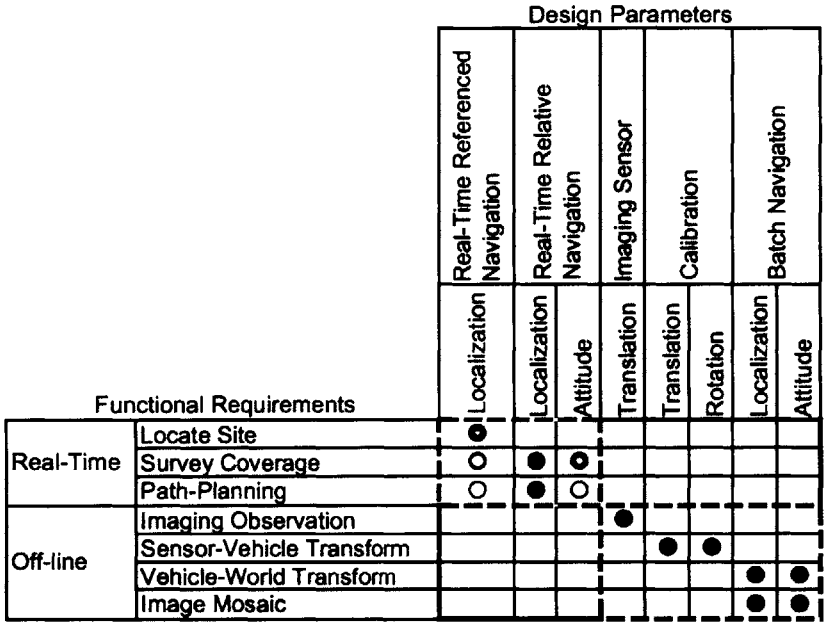

Figure 3-2: Matrix of functional requirements and design parameters. The markers indicate the dependence strength between the appropriate functional (row) and parameter(column) - darker, filled markers indicate stronger dependencies.

- Localization Precision: This chapter focuses on evaluating this metric as a function of the design options.
- Logistical Cost: The operational overhead of a particular navigation solution varies. Operational complexity is a function of the type of support equipment, necessary site preparation, and required time on site. For the spherical positioning example, additional transponders increase the precision, but the cost of deploying and surveying these elements is important. The high cost of ship time provides a strong incentive for minimizing the logistical cost through increased autonomous capabilities.
- Component Cost: Navigation sensors cost money (ranging from $\$10^2$-$10^6$) and increase the size and weight of the platform. Missions differ in sensitivity to these costs.
- Algorithmic Complexity: Algorithms increase the necessary computational capability of the host platform. The complexity of these algorithms can adversely affect the robustness of the final solution; testing complex algorithms is difficult and inexact.
- Robustness and Reliability: Systems vary in their sensitivity to particular events. Managing this sensitivity is challenging because the events are not always predictable or quantifiable.

3.2.3 Precision: Understanding, Quantifying, and Classifying Uncertainty

Estimating position and attitude is always inexact. The resolution of the image product is a function of this uncertainty. A represtative model and a concrete quantification of uncertainty

allow a thorough consideration of the relationship between the navigation uncertainty and the image resolution.

A Representative Abstraction

Three general categories of remote sensors are typical in underwater survey:

- Point sensors (1-D) measure a range and bearing, eg., scanning sonar.
- Swath sensors (2-D) measure a set of ranges and bearings on line, eg., side-scan sonar.
- Patch sensors (3-D) make a set of measurements over a 2-D area, eg., still camera.

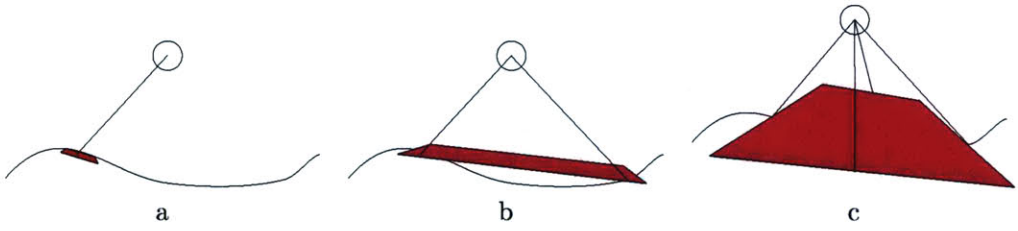

Figure 3-3: Three sensor abstractions: a) Point, b) Swath, and c) Patch

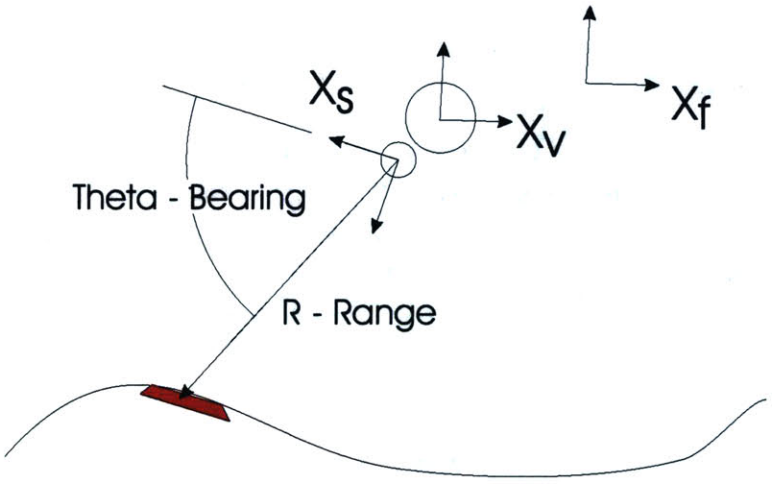

Figure 3-4: Coordinate frames in a simplified point sensor representation. X_s - sensor frame, X_v vehicle frame, and X_f fixed frame.

For considering the overall survey precision, the point-sensor shown in figure 3-3a is a useful abstraction. *Pointing precision* implies precision for the remaining remote sensing modalities. The three reference frames shown in figure 3-4, the sensor, vehicle, and fixed frames, decompose the global uncertainty into contributing errors.

Two coordinate transformations transform the sensor observations to an image. Measruement occurs as an observation is made in the local, or sensor, coordinate frame, X_s. Calibration is the transformation from sensor to vehicle coordinates, X_v. Navigation transfroms the observation from

vehicle coordinates to a fixed frame , X_f (this may be true 'world' coordinates or relative to a known fixed point). The aggregate uncertainty in the measurement transformed into this fixed coordinate frome is the quality of the image product, therefore the quality of the image is directly related to the coordinate transfromations: measurement, calibration, and navigation.

Calibration Transform:

$$X_v = T_{sv} + R_{sv}X_s \tag{3.1}$$

Navigation Transform:

$$X_f = T_{vf} + R_{vf}X_v = T_{vf} + R_{vf}[T_{sv} + R_{sv}X_s] \tag{3.2}$$

Uncertainty Propagation

The sensor measurement, calibration transform, and navigation transform are each uncertain. The uncertainty in the map, the figure-of-merit, is a function of these contributing factors. The translation variables are the Cartesian coordinates x, y, and z. The rotation variables are pitch (ϕ - rotation about x), roll (θ - rotation about y), and heading (φ - rotation about z).

Uncertainty Source	Uncertainty Variables	Description
Sensor	$\epsilon_{X_s} = \{\epsilon_x, \epsilon_y, \epsilon_z\}$	Uncertainty in the remote measurement.
Calibration	$\epsilon_{T_{sv}} = \{\epsilon_{x_c}, \epsilon_{y_c}, \epsilon_{z_c}\}$ $\epsilon_{R_{sv}} = \{\epsilon_{\phi_c}, \epsilon_{\theta_c}, \epsilon_{\varphi_c}\}$	Uncertainty in transforming from the sensor coordinates to the vehicle coordinates as a result of uncertain measurements between the vehicles navigation center and sensor position and alignment.
Navigation	$\epsilon_{T_{vf}} = \{\epsilon_x, \epsilon_y, \epsilon_z\}$ $\epsilon_{R_{vf}} = \{\epsilon_\phi, \epsilon_\theta, \epsilon_\varphi\}$	Uncertainty in the position and attitude estimates used to transformation from the vehicle to fixed coordinate frame.

Table 3.1: Navigation System Uncertainties

Applying *general uncertainty analysis* quantifies how uncertainty accumulates in a dependent variable as a function of the uncertainty in the independent variables [Rabinovich, 2000]. Consider a derived quantity r that is functionally dependent on a set of variables x_i.

$$r = f(x_1, \ldots, x_n)$$

The variance in r, ϵ_r^2, is the sum of product of the partial derivatives of the the function and the individual variances, $\epsilon_{x_i}^2$.

$$\epsilon_r^2 = \sum_{i=1}^{n} \frac{\partial r}{\partial x_i}^2 \epsilon_i^2 \tag{3.3}$$

Equation 3.3, applied to the navigation compounded coordinate transform of equation 3.2, yields an expression for the uncertainty in the image, ϵ_{X_f}, as a function of the sensor, calibration, and

navigation uncertainties.

$$\epsilon_{X_f} = \epsilon_{T_{vf}} + R_{vf}\epsilon_{T_{sv}} + (T_{sv} + R_{sv}X_s)\epsilon_{R_{vf}} + R_{vf}X_s\epsilon_{R_{sv}} + R_{vf}R_{sv}\epsilon_{X_s} \tag{3.4}$$

Two observations simplify this expression. First, because the magnitude of the uncertainty is the important quantity, the rotations are ignored when evaluating uncertainty[4]. Second, because the platform is small relative to the sensor measurement range, that calibration translation is neglected. The calibration translation, T_{sv}, is the difference between the sensor location and the navigation center. Assuming the magnitude of the sensor measurement is larger than this translation value, i.e., $T_{sv} << X_s$, simplifies the expression. Under these two restrictions the image uncertainty from equation 3.4 becomes,

$$\epsilon_{X_f} = [\epsilon_{T_{vf}} + \epsilon_{T_{sv}} + \epsilon_{X_s}] + (\epsilon_{R_{vf}} + \epsilon_{R_{sv}})X_s \tag{3.5}$$

The translation errors, from the sensor, the calibration and navigation localization, add directly to the image uncertainty. The rotational (angular) errors multiplied by the amplitude of the sensor measurement also add to the image error. Equation 3.5 is similar to an error budget and specifies how the various components of uncertainty are related to the figure-of-merit, the image resolution. Table 3.2 names and categorizes these sources of uncertainty.

Source	Translation Error	Rotation Error
Sensor measurement	Measurement - ϵ_{X_s}	n/a
Navigation	Positioning - $\epsilon_{T_{vf}}$	Attitude - $\epsilon_{R_{vf}}$
Calibration	Translation - $\epsilon_{T_{sv}}$	Rotation - $\epsilon_{R_{sv}}$

Table 3.2: Precision Survey Specification - Sources of Imaging Error

3.2.4 Summary

The previous sections present a specification for autonomous underwater navigation connecting the driving functional requirement, image quality, with the design parameters specifying navigation precision. Since real-time and off-line navigation are independent for the purposes of remote imaging, each requirement can be addressed separately using the uncertainty propagation model. Analysis of the uncertainties, using the pointing precision abstraction, leads to a succinct expression of the error budget for precision were measurement, calibration, and navigation uncertainty each contribute to the overall performance.

3.3 Estimation Tools for Navigation Design

The design tradeoffs articulated in the following section use the Cramér Rao lower bound (CRLB) and the extended Kalman filter (EKF) to explore the design space. These tools enable design studies

[4]The 2-norm of the uncertainty vectors is invariant with rotation. For example, the rotational transform $X_2 = R_{12}X_1$ is used to calculate the norm $X_2^T X_2 = X_1^T R_{12}^T R_{12} X_1$. $R12^T R12 = I$ where I is the identity matrix.

but require an introduction; this section explicitly treats their capabilities, their limitations, and the relationship between the two methods.

3.3.1 The Cramér Rao Lower Bound

Navigation is an estimation problem; a set of unknown parameters, location and attitude, are estimated from a set of observations. The CRLB is a standard tool for determining the uncertainty in the estimate based on uncertainty in the observations and a model relating the observed and estimated quantities. For navigation, the bound relates the sensor uncertainty to the navigation precision.

Consider the estimation of an unknown parameter vector $\mathbf{x}$ from a set of observations $\mathbf{z}$ with known probability density $p_z(z;x)$. When it exists, the Cramér Rao lower bound (CRLB) gives the lower bound on the variance of *any* valid unbiased estimator $\hat{\mathbf{x}}()$ for $\mathbf{x}$ [Willsky et al., 1997, Bar-Shalom et al., 2001, Spiegel et al., 2000]. The *Fisher information*, $\mathbf{I_z(x)}$, is the information about the parameters, $\mathbf{x}$, contained in the observations, $\mathbf{z}$.

$$\mathbf{I_z(x)} = \mathbf{E}\left[\left(\frac{\partial}{\partial \mathbf{x}} \ln \mathbf{p_z(z;x)}\right)^{\mathbf{2}}\right] = \mathbf{E}\left[\frac{\partial^{\mathbf{2}}}{\partial \mathbf{x^2}} \ln \mathbf{p_z(z;x)}\right]$$

The Cramér Rao lower bound, $\lambda_{\hat{\mathbf{x}}}(\mathbf{x})$, is the inverse of the Fisher information.

$$\lambda_{\hat{\mathbf{x}}}(\mathbf{x}) \geq [\mathbf{I_z(x)}]^{-\mathbf{1}}$$

The CRLB is the minimum uncertainty achievable by an unknown optimal estimator. An estimator that approaches this bound is *efficient*, but the bound does not guarantee that an efficient estimator exists or that one can be found. Efficiency amounts to the extracted information being equal to the existing information [Bar-Shalom et al., 2001]. The references give enlightened discussions of the general properties of the CRLB. Section 3.4.1 applies the method to spherical positioning and discusses the non-dimensional results and performance metrics.

3.3.2 The Extended Kalman Filter

In addition to the CRLB, the extended Kalman filter (EKF)[5] is a tool for evaluating design tradeoffs. The Kalman filter is the workhorse of estimation filters and has been used for a vast variety of applications. The seminal work by Rudolph Kalman [Kalman, 1960] is reprinted along with a history of the development and applications of Kalman filtering [Sorenson, 1985]. Dozens of textbooks provide background in designing Kalman filters along with the prerequisite background on probability and stochastic processes - a few general references are [Brown and Hwang, 1996, Bar-Shalom et al., 2001, Gelb, 1974]. For robotic navigation a few more specific references address the application to the specific challenges [Bar-Shalom et al., 2001, Manyika and Durrant-Whyte, 1994, Smith et al., 1990]. The well-known filter equations are presented in appendix B.2 for completeness.

[5]The addition of the modifier 'extended' indicates that equations used in the algorithm are linearized forms of the non-linear system and/or observation models.

The EKF builds on the theoretical elegance of the Kalman filter. The Kalman filter is the optimal estimator, in the mean-square sense, under the linear-Gaussian assumption; it is the best possible estimator (linear or non-linear); it is efficient estimator, achieving the CRLB and extracting all the possible information from the observations. Adaptations of the Kalman filter extend the fundamental recursive method: *predict* the state, covariance, and observations, *observe* the measurable quantities related to the state, and *update* the predictions using the calculated gain. The state and covariance estimates contain all the information available and necessary at each time-step - a consequence of the Gaussian, Markov, and measurement assumptions. The result is a recursive algorithm that maintains computational simplicity. The Kalman filter is rarely applied to scenarios that fit these restrictive assumptions. For non-linear models, the EKF simply linearizes the models about the state estimate at each time-step. The strong guarantees of the Kalman filter do not hold for this case; the performance and even stability of the algorithm must be empirically verified. Despite the difficulty in analyzing the application to non-linear processes, the EKF is a widely used estimation method.

The Kalman filter is a representative navigation algorithm. The method is often used for navigation and guidance, but even in cases where it performs poorly as a navigation solution, it is a useful design tool. Kalman filter estimation, as a representative navigation algorithm, enables exploring the design space. The assumptions, dynamic models and types of uncertainty, are simplistic. The section on active beacon selection illustrates this approach through an example.

3.3.3 Information, the CRLB, and the EKF

The Cramér Rao lower bound and extended Kalman filter have important similarities and differences. The CRLB represents the precision performance of a static estimator - an estimator that incorporates the observations and the measurement model to approximate the hidden parameters of interest. An extended Kalman filter is a dynamic estimator, connecting sequential observations through a dynamic model of the system. A vehicle moves both smoothly and moderately; large changes in position are not physically reasonable, and this fact is incorporated into the estimation.

For design considerations the CRLB gives a definitive answer while the EKF yields a solution dependent on random sampling. The theoretical bound is a function of the probability density function and the observation model. The bound is calculated deterministically and fully characterizes the uncertainty limits. EKF simulations are based on ensembles of random data, generated from the assumed density functions. Each random simulation gives a different result, a sample of all the possible outcomes, and the simulations must be repeated in Monte-Carlo fashion to derive general and conclusive results. For design the CRLB is like deduction, deriving a particular instance from a general characterization of uncertainty. In contrast, the EKF is like induction, drawing general performance conclusions from a set of particular simulation results.

The application of both methods to the same spherical positioning scenario is a concrete example of the comparisons and contrasts. Appendix B.3 contains the details, but the results are quickly summarized. For a simple survey the CRLB is shown to be a conservative estimate of the precision performance, i.e., it overestimates the uncertainty. The example illustrates how both

methods produce the same answer for a case where the EKF has no knowledge of the platform dynamics. Adding the platform dynamics with increasing certainty provides a better estimate taking advantage of the dynamic constraints. The example illustrates the similar treatment of uncertainty and the two methods for arriving at the estimator performance. The CRLB is a conservative estimate of the performance corresponding to complete ignorance of the vehicle dynamics, i.e., no continuity constraints are present between observations.

Information is the opposite of uncertainty; the Fisher information matrix is the inverse of the state-covariance. The Kalman filter algorithm specified as an information filter (see appendix B.2) explicitly represents the information accumulation through observation. The information is updated through the following expression.

$$\mathbf{P}^{-1}(k \mid k) = \mathbf{P}^{-1}(k \mid k-1) + \mathbf{H}^T(k)\mathbf{R}^{-1}(k)\mathbf{H}(k) \tag{3.6}$$

The state prediction information matrix, $\mathbf{P}^{-1}(k \mid k-1)$, expresses the information carried forward in time by the dynamics. When the process noise filter design parameter is high, the information in the prediction is low - the limiting case described above where the state covariance is equivalent to the CRLB of a static observation of the measurements. The second term in equation 3.6 is the Fisher information matrix for a linear Gaussian observation. The information from the dynamics adds to the information from the observations.

Summary

This section introduces the tools used in the sequel to quantify the precision of navigation solutions. The CRLB is shown to be a conservative estimate of positioning performance and the fundamentals of its application are laid out. The EKF is also presented as a design tool for the situations where the CRLB is not applicable. The methods are connected through an example to explicitly illustrate the relationship between the two (appendix B.3).

Both these methods are simplifications of reality. The noise and dynamic models are simplified, typically linear and Gaussian (LG). This simplification enables the prediction necessary for design, but also restricts the application of the results. It is important to keep these fundamentals in focus when applying the methods.

3.4 Articulating Component Tradeoffs

Examining particular tradeoffs illustrates the general design methods and metrics while exploring the design space. In accordance with the approach proposed in the introduction of this chapter, thorough analysis. Table 3.3 summarizes the key component decisions treated in this thesis. The design study considers the configuration of the acoustic beacon network and the integration of a Dopper velocity log (DVL) by analyzing the resulting performance predicted by the CRLB. As part of the example, applying the performance metrics, the precision factor and multiplier of precision, generalizes the results. Evaluating the performance of an algorithm for active beacon selection

illustrates the application of EKF simulations for predicting performance.

Factor	Levels	Level Descriptions	Where?
Odometry Sensor	2	{Yes, No} DVL	Section 3.4.2
Number of Beacons	4	{4, 3, 2, 1} beacons	Sections 3.4.3
Beacon Placement	Continuous		Section 3.4.1 and Appendix C.4
Host Configuration	2	{1, 2} beacons	Section 5.3.1
Depth Sensor	2	{Yes, No} depth sensor	Appendix C.2
Heterogeneous Network	2	{Yes, No} heterogeneous	Appendix C.3

Table 3.3: Factors and levels for component tradeoffs

The following are the key arguments of this chapter:

1. The estimation methods, the CRLB and EKF, are powerful tools for making design decisions about autonomous navigation systems.

2. The additional performance (precision and reliability) of precise odometry, heading reference, and depth sensors makes the inclusion of these sensors prerequisite for archaeological survey.

3. Attitude sensing (with the exception of heading) can be considered independent of the positioning solution. Therefore, the attitude sensor is selected independent of the other navigation components.

4. The number of beacons in a network using two or more elements has a direct and measurable effect on performance.

5. A system using only one beacon is definitively different, sacrificing precision and robustness for a modest decrease in logistical cost.

3.4.1 Configuration Baseline: Spherical Positioning

For navigation within an acoustic network, the CRLB predicts the quality of the solution as a function of the beacon placement, range observation uncertainty, and position within the instrumented environment. This section develops the method for analyzing the precision performance. The method uses non-dimensional metrics for positioning performance and scale-free environments to draw general conclusions. The baseline configuration is three acoustic beacons with equivalent range measurement uncertainty placed in an equilateral triangle. Different configurations and the addition of other sensors, presented as other tradeoffs, are compared with this baseline. An example with non-ideal geometry is also analyzed to illustrate the effect of beacon placement on the navigation precision and the ability of the CRLB to quantify the erosion of performance.

The Value of a Depth Sensor

Adding a depth sensor has a significant positive influence on position estimation. The analysis that follows assumes a depth measurement. The comparative analysis of long baseline positioning

with and without the added depth measurement included in appendix C.2 quantifies the reasons for measuring depth. Low-cost, robust, accurate pressure sensors measure depth, providing a level of redundancy to range-only positioning. Integrating a depth measurement decreases the sensitivity of the position estimate to the geometry, specifically to the separation between the estimator and the plane of the acoustic beacons. Decreasing this sensitivity also extends the portion of the environment available for survey or reducing the range necessary to achieve a particular precision. Measuring depth transforms the positioning problem from three-dimensions to two. This simplification enables conceptual intuition and eases the analysis of the performance. Lastly, depth is often an important oceanographic measurement independent of its utility for navigation.

Spherical Positioning

The CRLB for spherical positioning quantifies the effect of geometry on the navigation solution. Appendix A.1 presents the linearized spherical positioning model assuming Gaussian range uncertainty. The linearized model, including additive Gaussian noise, is

$$\mathbf{z}(k) = \begin{Bmatrix} r_1(k) \\ \vdots \\ r_N(k) \end{Bmatrix} = \mathbf{C}(k)\mathbf{x}(k) + \mathbf{w_r}(k) = \mathbf{C}(k) \begin{Bmatrix} x(k) \\ y(k) \\ z(k) \end{Bmatrix} + \mathbf{w_r}(k) \tag{3.7}$$

$$\mathbf{w_r}(k) \sim N(0, R) \tag{3.8}$$

$$E[\mathbf{w_r}(k)\mathbf{w_r}^T(k)] = \mathbf{R}$$

where $\mathbf{z}(k)$ is the range observation vector, $\mathbf{x}(k)$ is the estimator location vector, $\mathbf{C}(k)$ is the Jacobian of the nonlinear measurement equations, $\mathbf{w_r}(k)$ is the unbiased Gaussian sensor noise vector with covariance matrix $\mathbf{R}$, and k is the time index. This linearization is a function of the location of the estimator and the geometry of the beacon network. The CRLB, calculated from the linearized model, is also dependent on the network configuration and estimator location at time k.

$$\lambda_{\hat{\mathbf{x}}}(\hat{\mathbf{x}}) \geq \left[\mathbf{C}(\hat{\mathbf{x}})^{\mathbf{T}}\mathbf{R}^{-1}\mathbf{C}(\hat{\mathbf{x}})\right]^{-1} \tag{3.9}$$

The contour plot in figure 3-5 shows the results of evaluating the CRLB at a set of discrete positions within the 2-D environment. Both the independent geometry parameters and the resulting uncertainty values are non-dimensionalized to keep the conclusions general. Figure 3-6 illustrates how the design tool can be used to evaluate particular geometries.

- The two-dimensional area shown is normalized by the *baselines*, the characteristic distance between known beacon locations, so that the results are independent of the scale of the beacon network.

- The contour lines represent a constant *precision factor*, a scalar measure of position estimate uncertainty relative to the range observation uncertainty. The results are independent of the system's range precision.

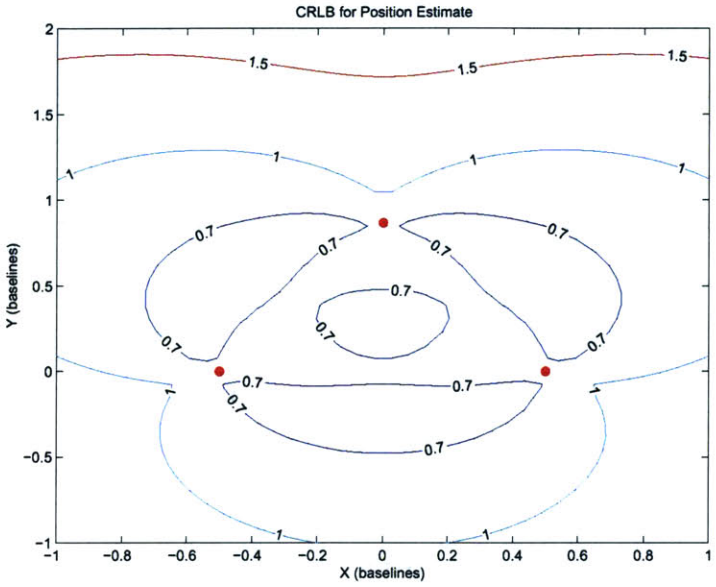

Figure 3-5: Baseline for the Cramér Rao lower bound analysis of long baseline spherical positioning. The beacons arranged in an equilateral triangle - the ideal geometry for 3 beacons.

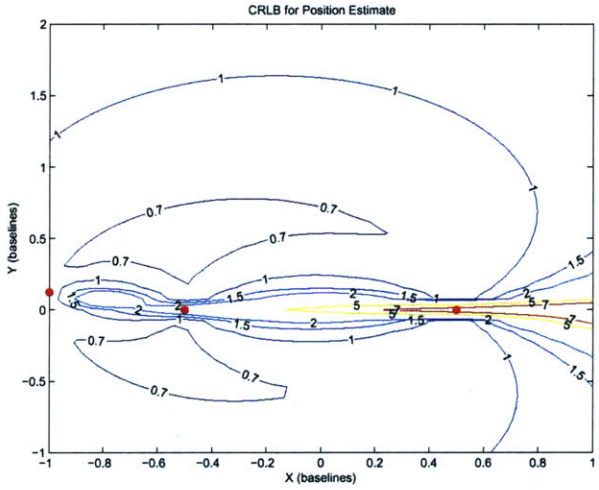

Figure 3-6: Example of the Cramér Rao lower bound illustrating the decrease in GDOP and the ability to analyse the effect of geometry with the CRLB

Precision Factor:

The CRLB in equation 3.9 is the covariance matrix of the position estimate. The determinant of this matrix is proportional to the area of the n-dimension uncertainty ellipsoid[6]. The range measurement

[6]This treatment of uncertainty is treated more fully in appendix B.5

variance raised to the n-th power normalizes the determinant of the covariance matrix.[7]

$$\text{Precision Factor} = \epsilon^2_{CRLB} = \frac{|\lambda_{\hat{\mathbf{x}}}(\mathbf{x})|}{(\sigma_r^2)^n}$$

Put simply, the precision factor (PF) is the ratio of the final position precision to the uncertainty in the actual range measurement[8]. Since precision is the inverse of uncertainty, the inverse of the precision factor is a measure of the increase in positioning precision relative to the range measurement precision - the multiplier of precision (MOP).

$$\sigma_{position} = (\sigma_{range})(PF) \tag{3.10}$$

$$\frac{1}{\sigma_{position}} = \left(\frac{1}{\sigma_{range}}\right)(MOP) \tag{3.11}$$

The non-dimensionalized results in figure 3-5 present the design space in a way that is generally applicable to a variety of navigation design problems. The results in figure 3-5a show a precision factor of approximately 0.7 within the acoustic network. Table 3.4 deduces the positioning uncertainty of two different positioning systems from the single non-dimensional results.

System	Range Uncertainty (m)	Baseline (m)	**Positioning Uncertainty (m)**
EXACT	0.02	100	0.014
12 kHz LBL	1	2000	0.7

Table 3.4: Positioning uncertainty prediction for two acoustic positioning systems based on the CRLB analysis of figure 3-5. The uncertainty is reported as the standard deviation.

Considering a simple embodiment of a spherical positioning system using the CRLB is a baseline for what follows. The next section repeats and extends these methods and metrics to include a DVL odometry sensor.

3.4.2 Integrated DVL and LBL Positioning

Considering the integration of a Doppler velocity log (DVL) and an acoustic positioning system quantifies the added value of the DVL and illustrates operation of the two sensing modalities. A DVLs has a tremendous impact on underwater navigation by accurately and reliably measuring velocity over the bottom, but the uncertainty in the position estimate from uncertain velocity measurements accumulates over time. An integrated solution combines the precise, high-bandwidth,

[7]The scalar ϵ^2_{CRLB} can be interpreted two ways. If we consider the uncertainty to be equivalent in each direction then the parameter is the variance in the position normalized by the variance in the range. Considering each direction separately the equivalent interpretation considers the scalar as the product of the standard deviations in each direction normalized by the standard deviation in the range for each direction. $\epsilon^2_{CRLB} \approx \frac{\sigma_x}{\sigma_r}\frac{\sigma_y}{\sigma_r} = \frac{\sigma^2_{(x,y)}}{\sigma^2_r}$.

[8]This measure is similar to the geometric dilution of precision (GDOP), a concept from the literature on the global positioning system (GPS). Contributions to GDOP are categorized as horizontal (HDOP) and vertical (VDOP). Unit Vector Volume - The volume of the shape described by the unit-vectors from the receiver to the space vehicles used in a position fix is inversely proportional to GDOP.

reliable DVL odometry with the small, fixed uncertainty of spherical navigation - an important synergy.

This section extends the CRLB analysis, applying the method to an integrated navigation system using both LBL and DVL information. The section begins with a simple 1-D analysis of the problem that represents the most important characteristics of the problem. To consider a set of range observations and differential distance measurements requires modifying the CRLB equations. The result is a quantified assessment of the value of a DVL for precision navigation. Three assumptions are made to simplify the analysis.

Gaussian Range Error: The range observations are assumed corrupted by noise with a normal distribution. Range measurements are not Gaussian - a fact that erodes the reliability many navigation estimators. This simplified model is appropriate for modeling the precision performance of the solution, but ignores the issue of robustness.

Random Walk Model: Uncertainty in position estimation from velocity measurements is assumed to accumulate according to the random walk model for stochastic processes: $\sigma_{position} = \sigma_{velocity}\sqrt{t}$.

Neglect Heading Error: Position estimation uncertainty accumulates linearly with distance travelled and the error in heading: $\sigma_{position} = (\text{Distance})\sigma_{heading}$. This analysis assumes the distance traveled between range measurements is relatively small; therefore, the uncertainty contribution from heading errors for the relative displacement measurement is small.

Simple Example Problem: One-Dimensional Positioning

Estimating position in one-dimension illustrates the most important considerations, builds design intuition, and acts as a check for the more complex application. In one-dimension the position is completely observable from a single range measurement. Measuring odometry between multiple positions enables a more precise estimate of position by adding information. The CRLB for a set of observation, both range and incremental distance, quantifies this intuition.

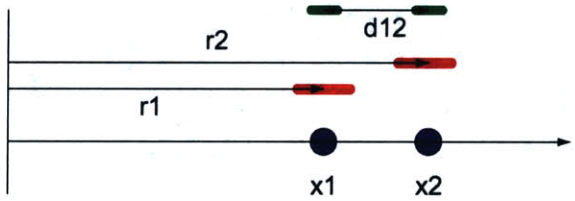

Figure 3-7: Illustration of the simple 1-D range and odometry example. The (blue) circles indicate two positions, x1 and x2. The lines with arrows indicate the corresponding range measurements, r1 and r2, and the relative distance (odometry) measurement, d12. The colored bars above each arrow indicate the uncertainty in the measurements.

Figure 3-7 illustrates the 1-D example problem. Considering a set of n range observations and $n-1$ incremental distance observations concurrently, the CRLB is found for the estimated position from the $2n-1$ measurements. The error in the incremental distance estimate, the odometry

uncertainty, is a function of both the uncertainty in the velocity observation and the time between observations ($\sigma_{distance} = \sigma_{velocity} * \sqrt{t}$). Figure 3-8 shows the results for a variety of sensor precision values. The vertical axis in the figure shows the ratio of the position estimate to the range error - the

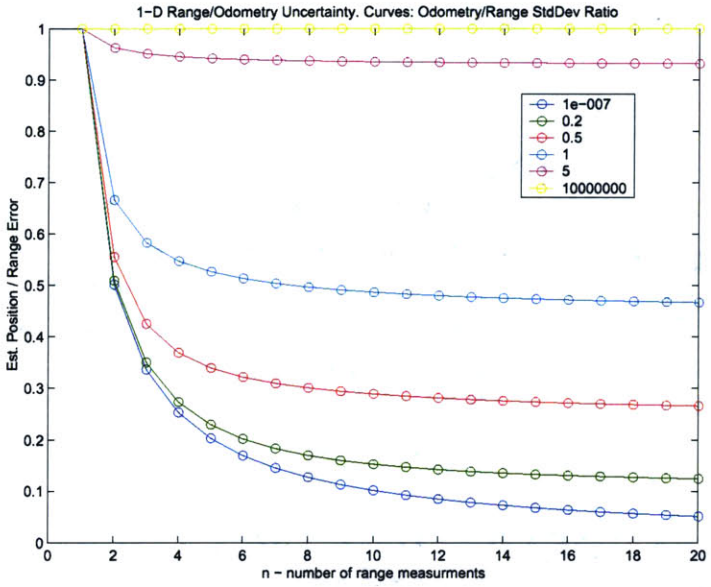

Figure 3-8: One-dimension range/odometry curves. The relationship between the position uncertainty, normalized by the range uncertainty, and the number of measurements is shown for a set of odometry vs. range ratios.

precision factor (PF). Each curve in the figure is for a different relative range/odometry uncertainty, measured by the ratio of the odometry standard deviation to the range standard deviation.

Two limiting cases are illustrative. As the odometry uncertainty approaches zero the estimator has perfect information about the separation between locations where the ranges are measured. Since the relative location between observations is known exactly this is equivalent to averaging observations and the random uncertainty should approach zero.

$$\sigma_{position} = \frac{\sigma_{range}}{\sqrt{n}}$$

This case is shown by the lowest curve (blue line) in the figure. The opposite case, as the inter-range uncertainty grows toward infinity, illustrates the limit of having no information about the relative position between measurements. In this case the covariance matrix of the positions is uncorrelated (diagonal) and the position estimate uncertainty is equivalent to the range uncertainty. This case is shown as the upper curve (the gold curve) where the uncertainty ratio is 1.0.

Considering this simple one-dimensional example highlights the effect of combining range and odometry measurements. This example is simple to understand, providing a clear design rule for integrating spherical positioning and DVL odometry. The extension to multiple dimensions, presented in the next section, shows that this simple case illustrates the important considerations;

it is as simple as possible, but not too simple[9].

The CRLB for Integrated LBL/DVL

Expanding the measurement model extends the CRLB from the spherical positioning baseline presented in section 3.4.1 to analyze integrated range and odometry navigation. This section presents the extension of the CRLB equations and the results of the analysis. The results quantify the value of the added DVL sensor and illustrate how the two modalities can be operated in concert.

The CRLB is a quantitative measure of the quality of the estimation performed using multiple range and odometry observations. Following the 1-D example of the previous section, a set of n locations are considered. At each location, range observations are made to the fixed acoustic beacons. Between these locations, $n-1$ distance measurements are made based on the odometry observations. The CRLB is developed by extending the linearized-Gaussian observation model from equation 3.7. At each of the n locations an independent noisy observation of the ranges is made.

$$\mathbf{z}_i(k) = \left\{ \begin{array}{c} r_1(k) \\ \vdots \\ r_N(k) \end{array} \right\}_i = \mathbf{C}_i(k)\mathbf{x}_i(k) + \mathbf{w_r}(k) \tag{3.12}$$

$$= \mathbf{C}_i(k) \left\{ \begin{array}{c} x(k) \\ y(k) \\ z(k) \end{array} \right\}_i + \mathbf{w}_r(k) \tag{3.13}$$

$$\mathbf{w_r}(k) \sim \mathbf{N}(\mathbf{0}, \mathbf{R})$$

where $i = 1, \ldots, n$ is the position index, $\mathbf{C}_i(k)$ is the linearized spherical positioning model at location i and time k, and $\mathbf{x}_i(k)$ is the position state to be estimated. The covariance in the range measurements is constant for each set of observations. Integrating the velocity information measures the relative displacement between range updates. The odometry observation model uses the unknown position states from two successive locations.

$$\begin{aligned} \mathbf{y}_i(k) &= \left[\begin{array}{cccccc} -1 & 0 & 0 & 1 & 0 & 0 \\ 0 & -1 & 0 & 0 & 1 & 0 \\ 0 & 0 & -1 & 0 & 0 & 1 \end{array} \right] \left\{ \begin{array}{c} \mathbf{x}_i(k) \\ \mathbf{x}_{i-1}(k) \end{array} \right\} + \mathbf{w}_o \\ &= \left[\begin{array}{cc} -\mathbf{I}_{3x3} & \mathbf{I}_{3x3} \end{array} \right] \left\{ \begin{array}{c} \mathbf{x}_i(k) \\ \mathbf{x}_{i-1}(k) \end{array} \right\} + \mathbf{w}_o \\ &= \mathbf{H}_i \left\{ \begin{array}{c} \mathbf{x}_i(k) \\ \mathbf{x}_{i-1}(k) \end{array} \right\} + \mathbf{w}_o \end{aligned}$$

$$\mathbf{w}_o \sim N(\mathbf{0}, \mathbf{R}_o$$

$$\mathbf{R}_o = \sigma_o^2 \, \mathbf{I}_{3x3}$$

[9] "Everything should be made as simple as possible, but not simpler." Albert Einstein

where the variance in the distance measurements σ_o is modeled as random walk uncertainty accumulation. These observations can be lumped together to create the linearized-Gaussian observation equations for the CRLB.

$$\begin{Bmatrix} \mathbf{z}_1(k) \\ \mathbf{y}_1(k) \\ \vdots \\ \mathbf{y}_n(k) \\ \mathbf{z}_n(k) \end{Bmatrix} = \begin{bmatrix} \mathbf{C}_1(k) & \begin{bmatrix} 0 & 0 \end{bmatrix} & \dots & \begin{bmatrix} 0 & 0 \end{bmatrix} & 0 \\ 0 & \mathbf{H}_2 & \dots & \begin{bmatrix} 0 & 0 \end{bmatrix} & 0 \\ & & \ddots & & \\ 0 & \begin{bmatrix} 0 & 0 \end{bmatrix} & \dots & \mathbf{H}_n & 0 \\ 0 & \begin{bmatrix} 0 & 0 \end{bmatrix} & \dots & \begin{bmatrix} 0 & 0 \end{bmatrix} & \mathbf{C}_n(k) \end{bmatrix} \begin{Bmatrix} \mathbf{x}_1(k) \\ \mathbf{x}_2(k) \\ \vdots \\ \mathbf{x}_{n-1}(k) \\ \mathbf{x}_n(k) \end{Bmatrix} + \begin{Bmatrix} \mathbf{w}_r \\ \mathbf{w}_o \\ \vdots \\ \mathbf{w}_o \\ \mathbf{w}_r \end{Bmatrix}$$

$$\mathbf{Z}_N(k) = \mathbf{C}_N(k)\mathbf{x}_N(k) + \mathbf{w}_N$$

Because of the independence of the measurements the covariance matrix for the total observation vector is diagonal.

$$\mathbf{w}_N \sim N(\mathbf{0}, \mathbf{R}_N)$$

$$\mathbf{R}_N = \begin{bmatrix} \mathbf{R} & 0 & \dots & 0 & 0 \\ 0 & \mathbf{R}_o & \dots & 0 & 0 \\ & & \ddots & & \\ 0 & 0 & \dots & \mathbf{R}_o & 0 \\ 0 & 0 & \dots & 0 & \mathbf{R} \end{bmatrix}$$

Appending the the observation model in this way enables the CRLB to be expressed in a familiar form.

$$\lambda_{\hat{\mathbf{x}}_N(k)}(k) \geq \left[\mathbf{C}_N^T(k)\mathbf{R}_N^{-1}\mathbf{C}_N(k)\right]^{-1}$$

In this case the CRLB is the minimum variance of an estimate of the unobserved states of the system $\mathbf{x}_N$. This state vector composed of many unknown sequential positions concatenated into a single vector. The bound is an approximation of the quality of an estimate of all these positions given a set of ranges at n locations with $n-1$ relative distance measurements between those locations - batch processing the positioning.

To arrive at a contour map comparable to the baseline case, these $2n-1$ measurements must be associated with a particular location. Consider these n points to lie on a circle or radius r. The center of that circle assumes an estimated uncertainty value equal to the average of the uncertainties at each point on the circle. Based on a nominal vehicle speed of 1m/s, aggregating ranges from $n = 10$ locations, and an update rate of 1Hz, a circle of radius $r = 1.56$ defines a cluster of equally spaced locations. Evaluating the CRLB for this cluster of 10 locations around each point in the map creates the contour map. Figure 3-9 illustrates this procedure. Each of the locations represented by 'o' markers in the figure is considered simultaneously in the CRLB calculation to arrive at an average position uncertainty. The center point of these locations is then associated with this average when assembling the contour map.

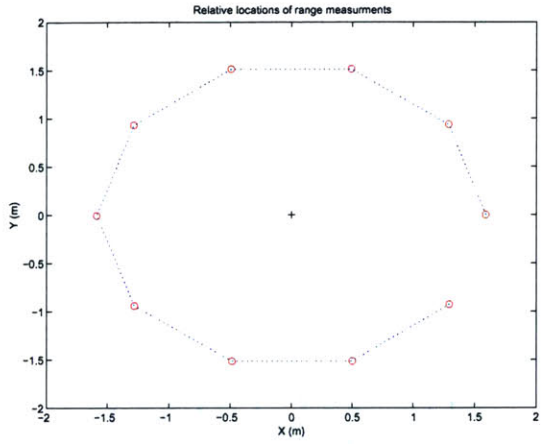

Figure 3-9: Illustrates the 10 locations for measuring acoustic ranges (the red circles) and the relative position measurements from odometry (the blue dotted lines).

Results

Comparing the positioning position with and without accurate odometry quantifies the effect of integrating a DVL sensor an LBL network. Figure 3-10b illustrates the positioning accuracy for a

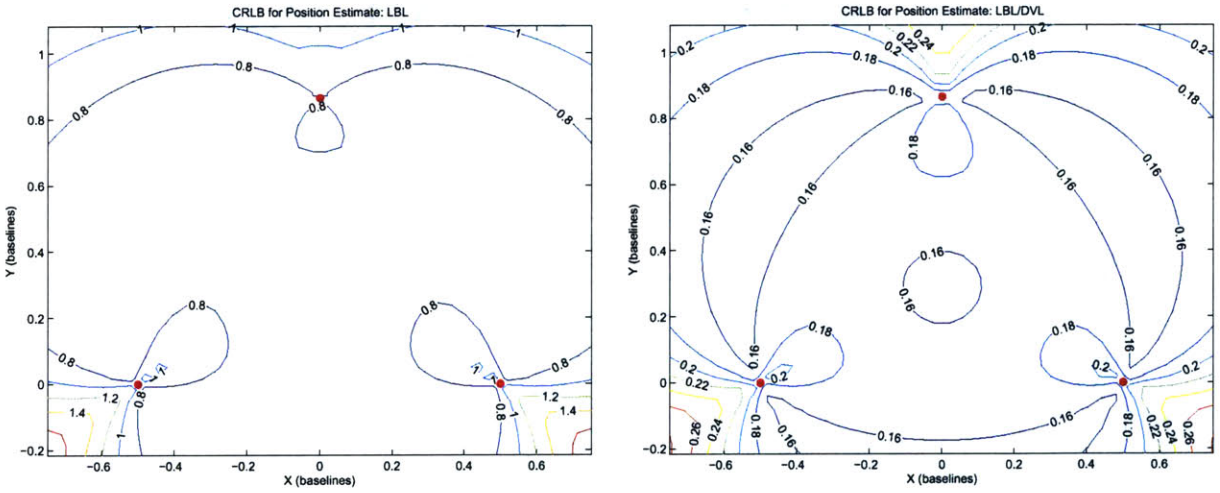

a b

Figure 3-10: Uncertainty contours for LBL/DVL position estimation. a) Shows the baseline case where the analysis method is the same, but the DVL error is increased so so that the estimate is only based on LBL observations - compare this to the spherical positioning baseline in figure C-1. b) The velocity uncertainty is 0.003 m/s (standard deviation).

system integrating accurate DVL odometry and acoustic range localization. The ratio of range to relative displacement uncertainty, the precision factor, is 0.3. Comparing this case with the baseline shown in figure 3-10a we can estimate an increase in precision by a factor of approximately 4.5. The sensor parameter values used in this example correspond with the performance of the EXACT precision LBL system (standard deviation 0.01m, update 1Hz) combined with an RDI DVL

(standard deviation 0.003 m/s).

The case in figure 3-10a is similar to the baseline case presented in section 3.4.1, but the beacon-only navigation is analyzed by considering the case were the odometry error is very large ensuring a fair comparison. Comparison of figure 3-10a and figure 3-5 show little difference and verify the conclusion. The small difference between the figures is a consequence of the LBL/DVL analysis use of mean uncertainty for a set of locations while a single location is used in the LBL-only scenario.

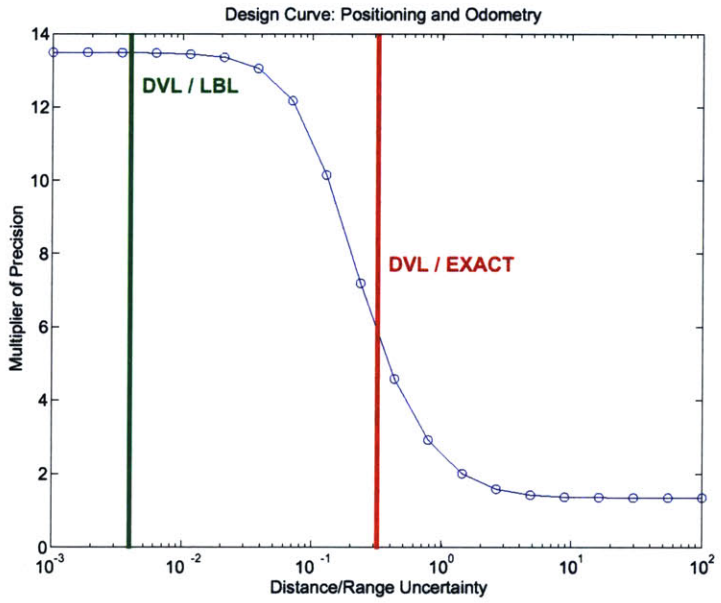

Figure 3-11: Uncertainty contours for localization with 3 acoustic beacons. The 'DVL/LBL' line (green) shows where the measurement uncertainty ratio for an RDI 300 kHz DVL integrated with 12kHz LBL (0.003/1). The 'DVL/EXACT' line (red) illustrates the integration of an RDI DVL with the EXACT precision LBL system (0.003/0.01).

Considering a variety of sensor configurations results in a general design rule. The design curve in figure 3-11 summarizes contour maps similar to those in figure 3-10 for a variety of odometry uncertainty values. This curve illustrates how the relative odometry uncertainty contributes to the position estimate quality. The multiplier of precision (MOP) on the vertical axis is the inverse of the precision factor. The MOP is the ratio of the range uncertainty to the uncertainty in the position estimate, i.e., it is the factor of improvement in the precision of the positioning relative to the precision in the range information. When the DVL is exceedingly precise relative to the range uncertainty, the performance gain in precision is almost an order of magnitude, i.e., the left-hand side of the 's-curve' has an asymptote at approximately 13.5 while the right-hand asymptote is approximately 1.35. Even when the odometry position estimate has equivalent uncertainty to the uncertainty in the range-based position estimate, by combining the two modalities the system precision can be increased by a factor of 2. Two particular designs are shown on the curve, an RDI DVL with both the standard 12kHz LBL solution and the precision EXACT solution.

The Value of a DVL

The preceding analysis quantifies the added performance in terms of precision for integrating a Doppler velocity log into a long baseline navigation system. Figure 3-11 illustrates an example of this quantification that achieves its succinctness based on simplifying assumptions. The conclusion is that odometry measurements of modest precision contribute strongly to the precision of the overall system.

This analysis, using the CRLB, does not account for a model of the dynamics of the platform (for a discussion of this aspect of the CRLB see the section 3.3.1 which discusses the relationship between the bound and the EKF dynamic estimator). Inclusion of accurate odometry is analogous to an accurate dynamic model in the way it improves the performance of the system. The following points summarize the conclusions of the preceding analysis:

- The CRLB quantifies the increase in precision for adding accurate odometry observations, such as those from a DVL. Articulated in general form the tradeoff becomes clear as a design decision.
- For traditional LBL positioning (12kHz, 1m range uncertainty) the increase in precision is approximately an order of magnitude.
- For precise LBL positioning (300 kHz, 2cm range uncertainty) the precision is increased by almost a factor of 5. Incorporating the same odometry sensor into a precise LBL system does not increase the quality of the solution as much as adding the same sensor to a less precise LBL system.
- A DVL provides a redundant and complimentary observation. The redundant measurement of position increases the robustness of the system and the complimentary measurement of relative displacement increases the precision of the solution.
- The combination of DVL and LBL sensors provides a more precise and robust solution than either sensor alone.

3.4.3 Number of Beacons

The number of beacons used for long baseline positioning has a strong and quantifiable effect on the performance of the navigation solution. No single solution is best for all cases. The goals and environment of the particular mission weight the costs and benefits of various solutions. This chapter develops a method for deciding how to trade the costs associated with deploying and surveying beacons with the precision and reliability of adding transponders to the network.

This analysis extends the Cramér Rao lower bound analysis of the previous sections and builds on those results. To develop a fair comparison between each of the potential solutions, the candidate designs use range, depth, and velocity measurements. Choosing a common navigation architecture and varying the number of beacons enables comparing the relative performance of candidate designs. The previous section argues that a DVL is an essential part of a precision navigation system, so

a DVL is included in the common architecture used in the comparisons to follow. Analysis of the single-beacon scenario, synthetic long baseline (SLBL), requires a complimentary measurement of relative position. To compare the single-beacon case with two, three, and four beacon situations they all must be analyzed with a DVL included. But this analysis is not constrained to navigation solutions that include a DVL sensor. Although the absolute measures of performance may change, the relative performance of the multi-beacon solutions is still valid.

The following analysis requires some prior component decisions. The uncertainties of the three navigation sensors impact the positioning performance. The analysis remains general with respect to the particular range precision by specifying the relative performance of the other two sensors. The depth is known precisely, i.e., with an uncertainty less than the range uncertainty. Following the analysis of the previous section, integrating a velocity measurement estimates the incremental distance between acoustic range observations. The range to distance uncertainty ratio is 0.3; a value corresponding to a range standard deviation of 1cm updated at 1Hz and a velocity standard deviation of 3mm/s. This example represents the EXACT precision positioning system integrated with an RDI 300kHz DVL and operating in a limited (100m) environment. The results, however, are not particular to that situation. The focus is on articulating the sensitivity of performance with respect to the number of beacons. Relative comparisons between the scenarios presented describe this dependence.

Four Beacons

An acoustic network employing four beacons provides precision, redundancy, and flexibility. The analysis evaluates the CRLB as described in the previous section on integrated LBL/DVL navigation. Figure 3-12 illustrates the resulting precision bound for estimating the location from four ranging beacons, depth observation, and accurate odometry. The important result is the precision factor within the acoustic network - 0.14 - indicating a position estimate 7 times as precise as the range estimate. Using four beacons provides a redundancy since only two are required for producing a fix. This redundancy increases the robustness with respect to spurious range measurements. Appendix A.3 presents an example of doing outlier rejection with least squares positioning. Using a large network also allows for increasing the survey area for a given acoustic range capability.

Three Beacons

An acoustic network employing three beacons provides precision and redundancy, but less flexibility. Figure 3-13 shows the CRLB for the three beacon case. Compared with the previous four beacon configuration, the precision is only slightly less - a precision factor of 0.16 compared with 0.14 - and the area covered by the acoustic network is decreased. Three beacons also provide a level of redundancy which can identify range outliers.

These results reiterate the conclusions from the LBL/DVL integration from section 3.4.2. The LBL/DVL design curve in figure 3-11 shows the multiplier of precision as a function of the ratio of distance to range uncertainty. For the parameters of this example the positioning estimate is approximately 6 times more precise than the range estimate. The same information is shown in

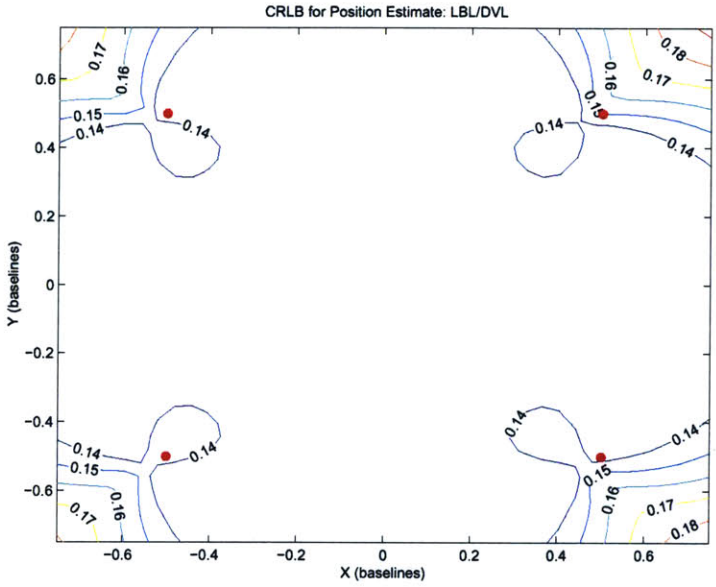

Figure 3-12: The CRLB contours for four beacon acoustic positioning including a DVL and depth sensors. The contours are the ratio of position uncertainty to range uncertainty - the precision factor. The four beacons are shown as red marks.

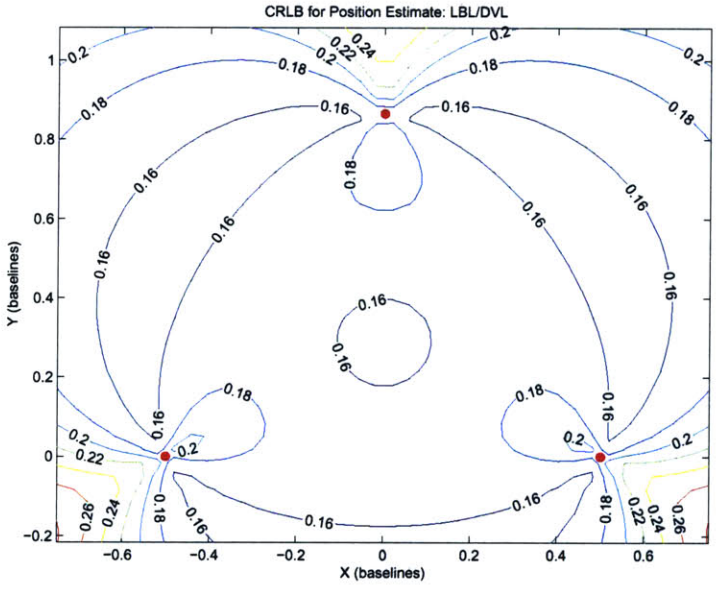

Figure 3-13: Precision factor contours for three beacon positioning including DVL and depth measurements.

the contour plot of figure 3-13 where the precision factor is 0.16 within the network. The contour plot is general to the range precision. Combined with the design curve the results are general for a variety of range and odometry precision parameters.

Two Beacons

The two beacon acoustic network provides precision comparable to networks with more elements, but without redundancy and with less flexibility. Figure 3-14 illustrates the configuration where

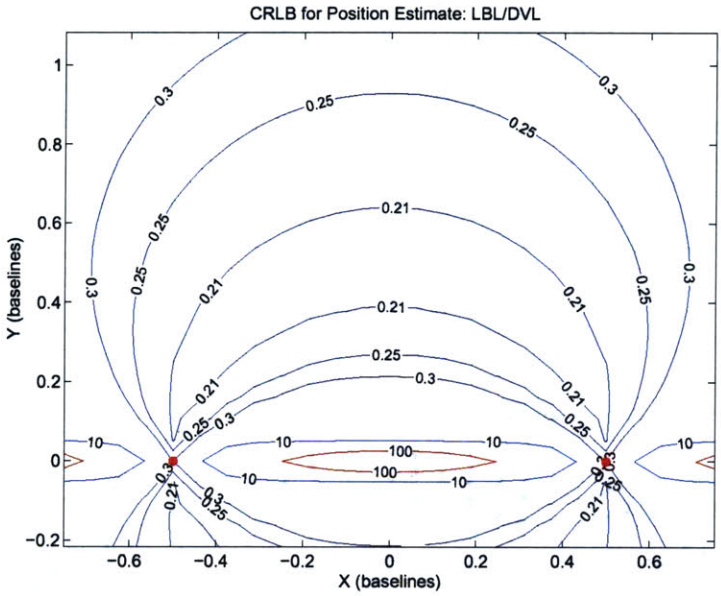

Figure 3-14:

only two beacons are used. For an appropriately configured survey, the overall precision factor for this scenario is approximately 0.25 - the multiplier of precision is roughly 4.0. This is a 50% decrease in precision compared to the three beacon configuration. Using just two beacons and a depth sensor is a minimal configuration for traditional acoustic positioning, requiring that both beacons be observable at all times and precluding the ability to do outlier rejection using redundant range measurements for an individual fix. The sharply increasing uncertainty near the baseline (the line connecting the two beacons) highlights and important tradeoff; the survey area is constrained by the necessity to avoid areas near the baseline. This configuration demands a more capable ranging system for a given survey because the area covered is reduced. It also demands a guidance algorithm capable of representing relationship between the positioning precision and the location with in the network to avoid baseline crossings while executing the survey.

One Beacon

Localization with a single fixed beacon is distinctively different from multi-beacon positioning, but a fair comparison can be made between this configuration and the previous case-studies. Quantifying the positioning uncertainty requires extending the CRLB analysis. Synthetic long baseline (SLBL) uses a single beacon to estimate position. The fundamental idea is to use the ability of precise odometry sensors, e.g., a DVL, to provide information between successive range observations. Using

the set of relative distance measurements from the odometry and range measurements to a single beacon taken at various locations, an estimate of position is made.

Applied directly, the method developed in the previous case-studies over-estimates the uncertainty. The CRLB calculation considers a batch of range and odometry observations. The previous configurations consider ten locations around a small circle (1.56m radius) where the ranges are observed. The geometry of these locations determine the size of the synthetic baseline. This small baseline gives little information - the position is barely observable - and the resulting uncertainty is two orders of magnitude higher than for the multi-beacon case.

A more accurate estimate of the precision of an SLBL system is delivered by expanding the observations considered when calculating the CRLB - using a large synthetic baseline. The preceding analysis used a cluster of 10 locations in a circle with radius of 1.56m to formulate the CRLB estimation problem. The average position estimate uncertainty is then associated with the center of this cluster when creating the contour maps of precision. To represent SLBL each location in the contour map is associated with circular cluster of locations. The radius of this circle is 50m and it includes 314 range observations and 313 odometry measurements. Figure 3-

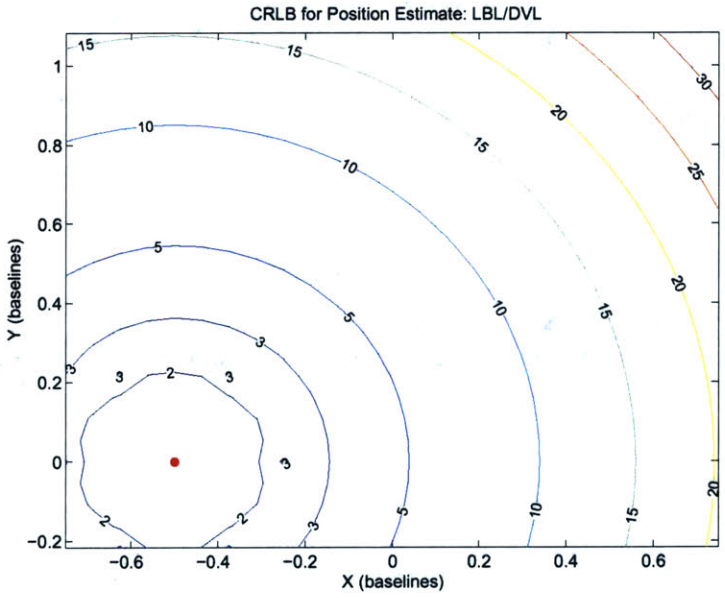

Figure 3-15: Contour plot of CRLB for positioning uncertainty with only one beacon. The cluster radius = 50m

15 shows precision factor contours for the single-beacon positioning case. This figure is directly comparable to the preceding multi-beacon configurations. Because of the rotational symmetry, the same information can be condensed into a relationship between the precision and the distance from the single beacon. Figure 3-16 shows the decrease in precision with distance from the beacon. The baseline of the previous analyses is 200m. The discontinuity at 50m is caused by the coincidence of the cluster circle radius and the distance from the beacon. For this scenario some of the estimator locations are close to the beacon location and yield little additional information.

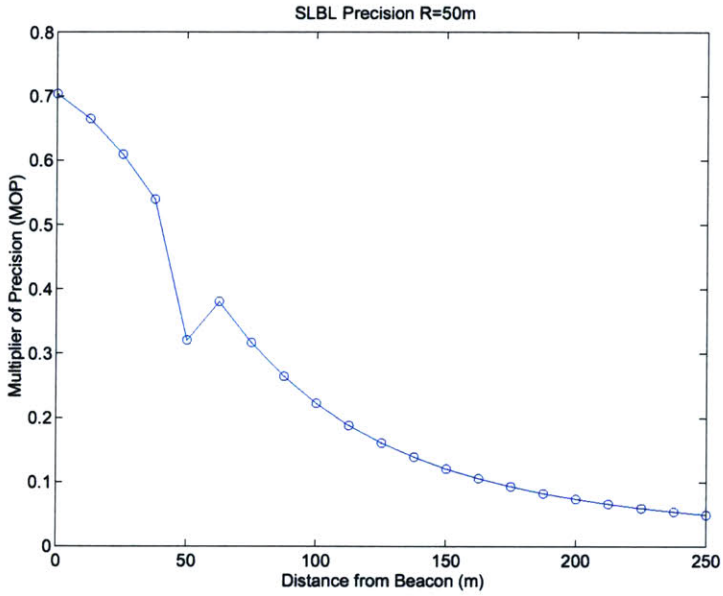

Figure 3-16: CRLB for positioning uncertainty with only one beacon as a function of the distance from the beacon.

The single-beacon case trades precision and redundancy for logistical cost. The precision of the localization is much worse than any of the multi-beacon configurations. Using a single beacon also challenges the algorithms to robustly reject spurious data without any redundant measurements. An occluded region or poorly performing beacon would quickly erode the navigation quality. The solution does achieve reduced logistical cost since only one beacon needs to be located at the site.

Robustness and Redundancy

For traditional acoustic positioning, acoustic networks with more than two beacons have redundancy that can be used to reject spurious returns. Considering the probability of a systematic error as the value p_s, the probability of a range measurement that is not line-of-sight, quantifies the reliability tradeoff. For the two beacon scenario, calculating a position fix from two ranges cannot simultaneously recognize spurious data. An incorrect position fix will occur with probability $p = p_s$. When three beacons are employed, a false observation is recognized by inconsistency between the three ranges. Receiving two false returns will yield a bad position fix. The probability of that event is $p = p_s^2$. If the redundancy is increased by adding a fourth beacon the probability of a spurious fix is further reduced to $p = p_s^3$.

Precision Summary

We can now summarize a comparison of the results from above. The table below shows the best-case precision bound for systems with different numbers of acoustic beacons. The numbers are unit-less

and are ratios of the localization precision to the range precision (an amplification factor due to integrating a DVL). These results must be used cautiously. Assumptions about the geometry and

Number of Beacons	4	3	2	1
Precision Factor	0.14	0.16	0.25	3
Multiplier of Precision	7.1	6.25	4	0.3

Table 3.5: Precision and Number of Beacons

operation of the system limit the applicability of this analysis, but it is useful to a system designer to quantify the tradeoffs that must be made in configuring the navigation system

Localization Precision	Three beacons achieves twice as much precision as two beacons and only a little less than four beacons. One beacon is much less precise than multiple beacon solutions (see Table 3.5).
Logistical Cost	At least one beacon is assumed so the logistical cost should be proportional to the number of beacons deployed, i.e., the logistical cost is linear with the number of beacons deployed. The process of surveying the beacons is also non-trivial.
Classification Reliability	Greater than three beacons gives us redundancy that lessens the reliance on algorithms and an opportunity to decrease the algorithmic complexity and the resulting robustness cost.
Algorithmic Complexity	One beacon requires sophisticated path planning (this will be treated again in the following section on controlling uncertainty). Therefore a single beacon solution requires a very capable platform.
Component Capabilities	A two beacon configuration requires more range because the site must be separate from the baseline between the beacons.

Table 3.6: The dimensions of system performance and the influence of beacon number.

3.4.4 Component Configuration Summary

- The addition of an accurate depth sensor adds to the flexibility of long baseline positioning, enables simpler acoustic networks (fewer beacons), and reduces the 3-D positioning to a 2-D problem.
- Accurate odometry, enabled by the addition of a DVL, has a large effect on the precision of the positioning solution. The precision improvement, dependent on the operating parameters of the sensors, is quantified using the CRLB.
- A decision about the number of acoustic beacons to employ for a particular situation is dependent on trading off the logistical cost of deployment and the requirement for precision.

Table 3.5 summarizes the precision.

- The type (heterogeneous networks) and placement of transponders has an infinite variety of design options. The preceding work illustrates, through representative examples, using CRLB analysis of particular scenarios to develop quantitative comparisons.

3.5 Articulating Algorithm Tradeoffs

Quantifying design tradeoffs includes considering the impact of decisions about the navigation components and the way they are interconnected. Algorithms, the software on an AUV, make the interconnections between the navigation elements, controlling both the motion and sensors based on feedback from the environment. Algorithms enable autonomous and adaptable behavior. The preceding section concentrates on hardware decisions - physical attributes of the system. This section focuses on the impact of algorithms on the system's performance using a method for analyzing the design decision while articulating the effect of a particular algorithm on the navigation performance. Active beacon selection for long baseline navigation illustrates the EKF.

3.5.1 Algorithm Simulation: Active Beacon Selection

The beacons of an acoustic network are often queried in series. Actively choosing the range to observe at each time-step can improve the positioning precision. This section proposes an algorithm that manages the range sensor by choosing the beacon in the network to query, minimizing the predicted uncertainty in the position estimate.

Beacon Selection: A Fisher Information Metric

By maximizing a information metric, the algorithm selects the beacon to query minimizing the position uncertainty. The Fisher information is the inverse of the covariance[10], $\mathbf{P}_i^{-1}(k \mid k)$, where i is the beacon index and k is the time index. The objective of the algorithm is to maximize the Fisher information by choosing the beacon i from a set of possibilities $\mathbf{J}$.

$$i(i) = \max_{i \in \mathbf{J}} \{\mathbf{P}_i^{-1}(k \mid k)\} \tag{3.14}$$

The range observations are independent. Evaluating the information potential from each possible measurement solves the optimization in equation 3.14. Following the Kalman filter notation in appendix B.2, the measurement information accumulates according to the update equation,

$$\mathbf{P}_i^{-1}(k \mid k) = \mathbf{P}^{-1}(k \mid k-1) + \mathbf{I}_i(k)$$

$$\mathbf{I}_i(k) \triangleq \mathbf{h}_i^T(k)\mathbf{r}_i^{-1}(k)\mathbf{h}_i(k)$$

[10]The state vector contains both the velocity and position states, but to keep the presentation simple $\mathbf{P}(k \mid k)$ is considered the covariance of the position.

where $\mathbf{P}^{-1}(k \mid k-1)$ is the predicted position information and the information in the single range observation is $\mathbf{I}_i(k)$. The observation vectors, $\mathbf{h}_i(k)$, are dependent on the estimated position because of the way the linearization is done. The optimization is now,

$$i(k) = \max_{j \in \mathbf{J}} \left\{ |\mathbf{P}^{-1}(k \mid k-1) + \mathbf{I}_j(k)| \right\} \tag{3.15}$$

The determinant of the information matrix is the area of the information ellipse. The information has both magnitude and direction. If this were not the case, the algorithm would ignore the predicted state information term, $\mathbf{P}^{-1}(k \mid k-1)$, and simply maximize the information available at each location, i.e., the sensor choice effects the magnitude and direction of the predicted state information term. Without direction the solution could be calculated off-line for all locations within the network, $\mathbf{I}_i$. At each time-step equation 3.15 guides the beacon choice based on maximizing the most potential information about the position given the current estimated position and state of uncertainty.

Representative Survey

The performance of the active beacon selection algorithm is assessed by implementing a representative survey simulation. The simulation is based on the simple vehicle dynamics described in appendix B.1 and uses an extended Kalman filter to estimate the location from simulated range measurements. Feeding back the estimated position and velocity from the EKF generates the control inputs based on the target trajectory. The scenario is similar to the baseline spherical positioning setup.

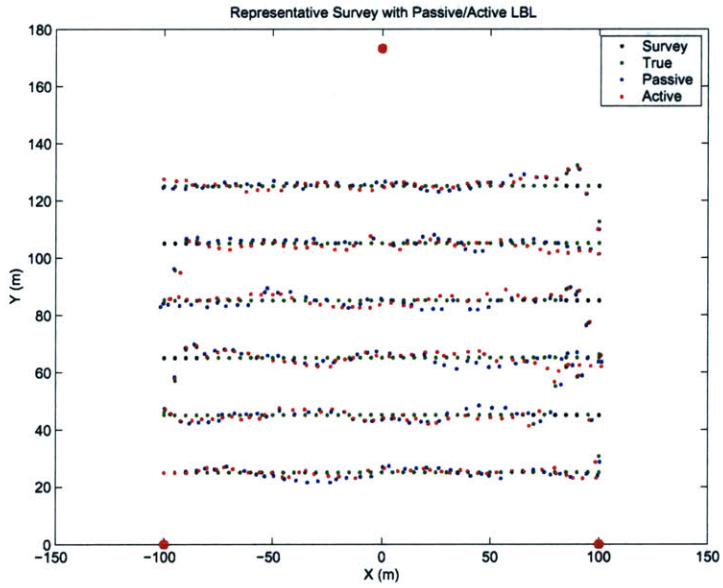

Figure 3-17: Illustrates a representative survey used to evaluate the potential of active LBL. The 3 beacons are represented by the large red dots and the data points show the target survey locations, the 'true' track, and two localization estimates (passive and active).

Two separate EKF estimators are implemented concurrently. The *passive* EKF sequentially queries each beacon. The *active* EKF manages the network to maximize the information at each time-step by evaluation equation 3.15. Figure 3-17 shows this representative survey. The dimensions and parameters are chosen to give reasonable coverage of the acoustic network. The figure shows the 'true' position states of the survey and the estimated position states from the two estimators.

3.5.2 Evaluating Performance

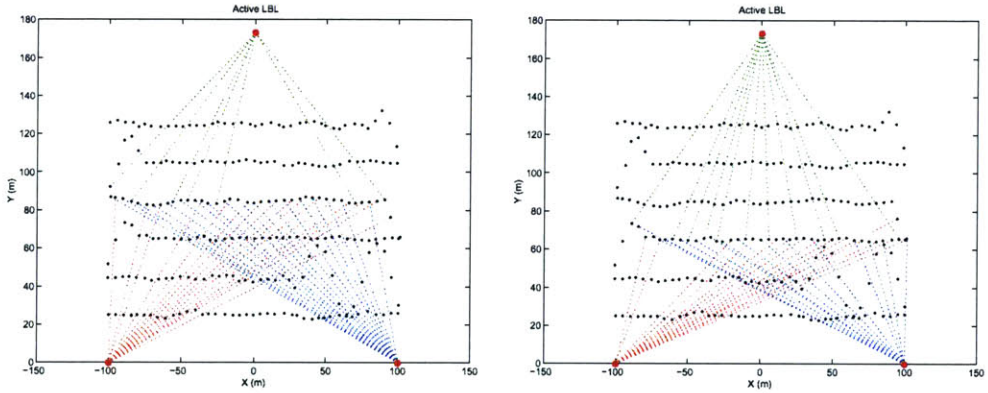

a b

Figure 3-18: Two transects of the same survey. The dotted lines show the beacon choices.

A single simulation illustrates the operation of the algorithm. Figure 3-18 shows the decisions of active long baseline interrogation for the representative survey. For clarity the figure shows two transects of the survey separately. Distinctive behaviors are evident in each instance. These results offer some preliminary conclusions, but because of randomness in the simulation, Monte-Carlo methods are necessary to ascertain the overall behavior and performance. Running many instances of the random EKF simulation illustrates aspects of using EKF estimators for designs. First, the consistency of the estimators must be verified, i.e., the estimator must be shown to converge to the 'true' state of the system. Second, since there is randomness in the individual simulation runs, it is important to consider many cases before generalizing the behavior of an algorithm or the results. Finally, considering multiple runs of the survey simulation is necessary to quantify the performance of the active management algorithm.

Consistency of an estimator is analogous to stability of a controller. The consistency of an estimator must be verified as a first step in analyzing a potential design. The Normalized Estimation Error Squared (NEES) is an important metric for inferring the consistency of an estimator [Bar-Shalom et al., 2001]. Figure 3-19 illustrates the NEES calculation for each run of the simulation . Since the average NEES is less than the dimension of the state vector (4), the estimators are shown to be consistent.

Two metrics quantify the performance of the algorithm design. Figure 3-20 shows the number of non-sequential queries for each simulation - an indication of how often the active decision deviates form the passive decision. A similar metric (not-shown) is relative frequency for each beacon. These

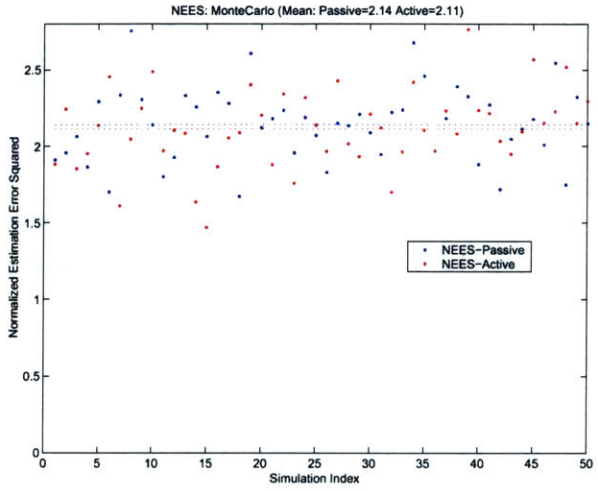

Figure 3-19: the normalized estimation error squared for 50 Monte Carlo runs of the survey. Since the average is below the number of degrees of freedom (4), the consistency of the estimators is inferred.

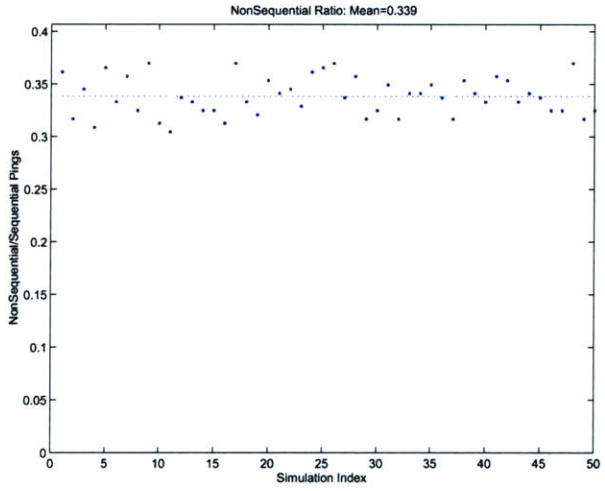

Figure 3-20: Approximately 1/3 of the time the active LBL system chooses to ping a beacon that is not the sequential choice.

two metrics measure the activity of the algorithm, but not the impact on performance.

Minimizing the position uncertainty in the survey is the purpose of the algorithm; the achievement of this goal is measured by the position variance. Figure 3-21 shows the variance in the survey. The estimated variance is the diagonal terms of the covariance matrix ($\mathbf{P}(k \mid k)$) corresponding to the x and y location states. The measured variance is measured by the squared error between the estimate and the 'true' position of the simulation. The upper axes of figure 3-21 show the variance estimates for active and passive LBL. The lower axes present the fractional reduction in the variance - a useful performance metric. The mean measured and estimated variance reduction are similar with values slightly greater than 10%, but the variation between individual simulations

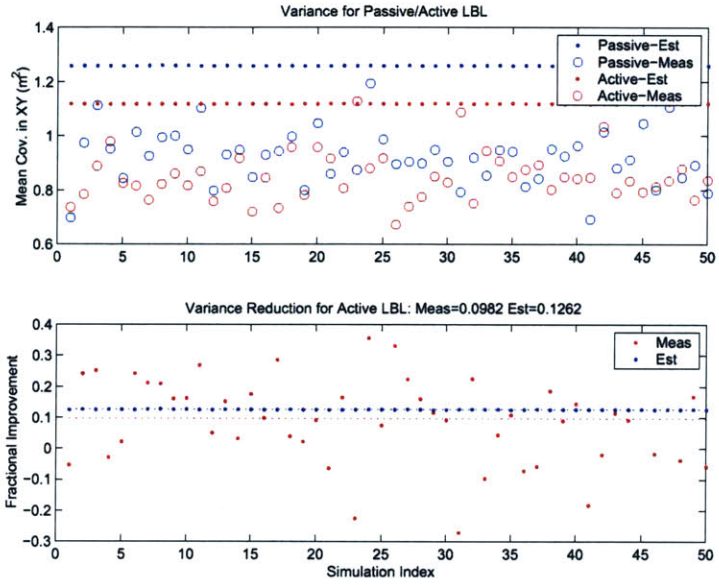

Figure 3-21: Performance of multiple instances of the active-beacon selection simulation.

is important. A few of the individual data points in the lower axes of figure 3-21 fall below zero, indicating that for these cases the active beacons selection decreased performance. This result highlights the importance of considering multiple runs to quantify the randomness in EKF simulations for design.

Sensitivities

Sensitivity analysis illustrates the effect of two geometric aspects on the general performance conclusions. As the size of the vehicle survey increases relative to the beacon network the performance gain for using active beacons selection increases. Similarly as the geometry of the network deviates from the optimal configuration, i.e., the GDOP increases, the active algorithm increases the performance.

Figure 3-22 illustrates the sensitivity of the two performance metrics to changes in the survey size. The variance reduction increases with the survey size, and the ratio of non-sequential beacon choice decreases. As the survey size increases a greater proportion of the queries are chosen sequentially, i.e., in the passive, 1-2-3, ordering, indicating less activity. Nevertheless, the variance reduction shows that although fewer queries are made 'out-of-order', it is increasingly important to do so.

A single example illustrates the sensitivity of the results to the geometric dilution of precision (GDOP). Beacon #3 is moved lower and to the left. Figure 3-23 illustrates how the beacon management occurs in this situation. A generalization is that motion along the radial line connecting a beacon and a particular location does not add information to the system [11]. Comparing figure 3-24

[11] Appendix B.4 illustrates the connection between the geometry and the information from sequential range observations. The optimal trajectory is to move tangent to the line connecting the current location the acoustic beacon to maximize the incremental information.

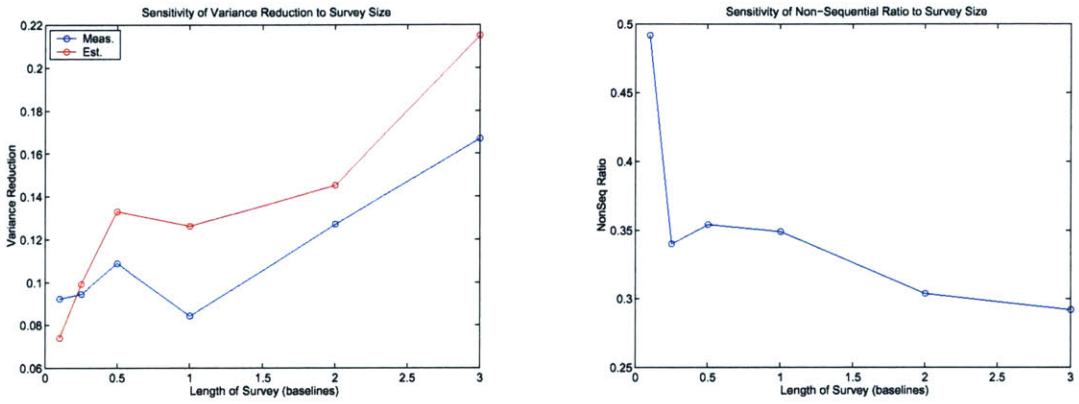

a b

Figure 3-22: The relationship between survey size, parameterized by the relative length of the survey in the x-direction, and the results of the active LBL Monte Carlo analysis. For each data point a 50 iteration MC simulation was run and the performance recorded.

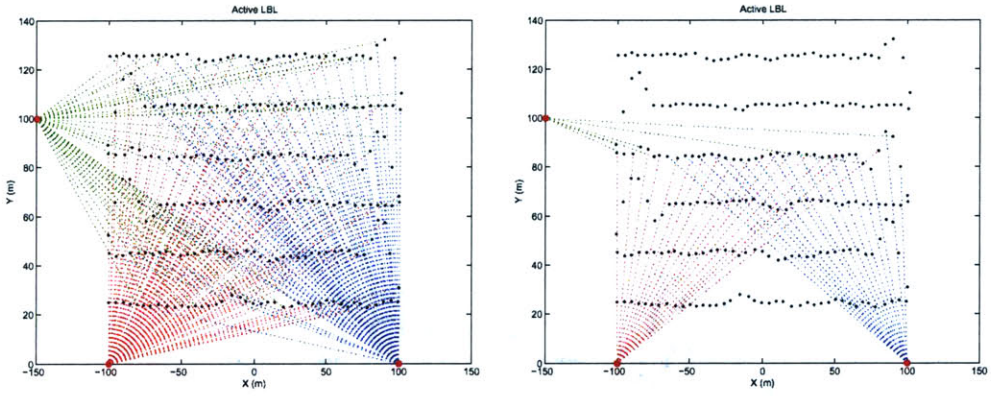

a b

Figure 3-23: a) The full survey is shown. The colored lines indicate the beacons that are 'pinged' at each location. The data points are the estimated locations. For this case the geometry dictates that beacon #3 (upper left) is used only 40% as often as beacons 1 and 2. b) A single transect of the survey is shown to highlight the roll of the active beacon management algorithm. Because the motion is collinear with the location-beacon line for beacon #3 the system does not query that beacon during the transect, but relies on the other portions of the system. For the points where there is appreciable motion tangent to this line-of-sight the system chooses to query the beacon.

with figure 3-21 illustrates the performance gain as the network geometry degrades. The variance reduction is summarized in table 3.7

GDOP	Variance Reduction	
	Measured	Estimated
Good	0.01	0.16
Poor	0.13	0.18

Table 3.7: The relationship between variance reduction for active beacon selection and geometric dilution of precision

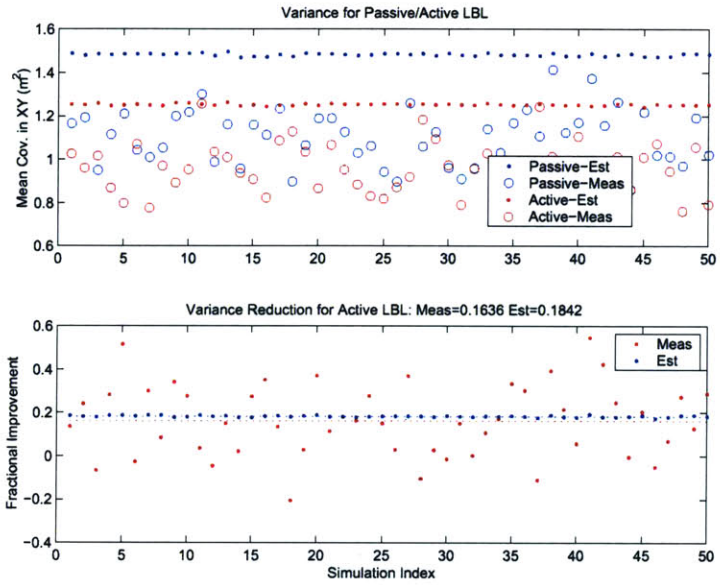

Figure 3-24: Illustrates the improved performance of the active LBL method for the case of increased GDOP.

In general these two cases of examining the sensitivity show that the geometry of the system is an important determinant of the performance increase with active beacon selection. More importantly this section illustrates the importance of considering sensitivity analysis when employing the EKF for design.

Summary: EKF and Active Beacon Selection

The active beacon selection case-study illustrates both the performance of the specific algorithm and the application of the EKF as a navigation design tool. The Monte-Carlo EKF simulation illustrates the consistency of the estimator and quantifies the precision performance gains through specific metrics, and sensitivity analysis explores the relationship between the acoustic network GDOP and the relative performance improvement. Networks with poor geometry have the largest potential for improved precision through active beacon selection. The cost of this approach compared with the passive solution is qualitative; the algorithm increases the computational complexity which could adversely affect the navigation robustness.

These results generalize along two dimensions. This particular algorithm is founded on information metrics used for making sensor decisions. These metrics are useful in making a variety of decisions autonomously, particularly for sensor-management and path-planning. Chapter 4 presents an environmental model that is formulated to quantify information especially helpful in making such autonomous decisions. Secondly, this case-study illustrates a method for using the EKF for design including Monte-Carlo techniques, performance metrics, and sensitivity analysis. The case illustrates the importance of Monte-Carlo simulations for drawing general conclusions from simulations with random variables. Metrics quantify the performance and enable definitive design decisions.

Sensitivity analysis verifies the conclusions and identifies leverage points.

3.6 Conclusion

The method of design is as important as results of the analysis. This chapter presents the design of autonomous navigation systems in general by developing a specification, articulating design tradeoffs, and presenting methods for quantifying performance.

The precision specification connects the functional requirements and design parameters. Precision navigation is the defining element of deep-sea archaeological imaging. In the functional domain the goal of the mission is expressed as the resolution of the remote sensing image. In the physical domain this translates to navigation sensor performance, in real-time for guidance and off-line for re-navigation.

Examples illustrate the design methods and metrics. Instead of presenting the capabilities of a single design solution, the methods articulate the design tradeoffs, illuminating the design space. Combining the CRLB with non-dimensional metrics of precision, the precision factor and multiplier of precision, enables investigation of sensor component tradeoffs. The increased precision of adding an accurate velocity sensor, a DVL, to an LBL network is quantified and case-studies also show the effect of beacon configuration, number and placement, on the navigation solution. Simulations of EKF navigation quantify the performance of active beacon selection. The example not only articulates the performance of the candidate design algorithm, but develops the important considerations of using an EKF for design - performance metrics, consistency , Monte-Carlo simulations, and sensitivity analysis.

Methods generalize and designs do not. This chapter proposes general design methods and metrics, and articulates the key tradeoffs for precision navigation in an instrumented environment. This approach does not neglect the more quantitative considerations, such as cost and reliability, but arms the designer with tools to make informed decisions in the quantitative dimensions of design performance.

3.7 Future Work

The preceding analysis concentrates on the particular challenge of navigating precisely. This is primarily due to the importance of precision in the high-resolution imaging and partially because of the quantifiable nature of precision. Extending this method-based approach to the qualitative aspects of navigation design would benefit future designs. Of particular importance are the design of autonomous systems, the challenge of making them robust, and the relationship between autonomy and robustness.

The following offers two types of extensions: a plan for applying the methods of this chapter and a look at the important technologies that will affect future designs.

3.7.1 Applications: Matching Designs and Requirements

The functional requirements of archaeological imaging drive the functional requirements of this chapter's design studies, but the methods and metrics are applicable to other missions. This section matches some of the particular missions with possible designs. The following descriptions touch on the goals, environment, and platform that characterize each mission, but concentrate on the unique facet of these missions and how those requirements translate to unique design features.

Deep-Sea Archaeology

The need for extreme precision,a benign deep-water environment, and a static, long-term deployment characterize the deep-sea archaeology mission. The sites are often visited multiple times, evolve over time, and are spatially discrete. This necessitates fixed referenced navigation and makes the logistical cost of beacon deployment worthwhile. A canonical solution would likely involve two or more beacons placed carefully around the site.

Military Survey

The sensitivity to logistic cost, the capability of the platform, and the relaxed precision constraint characterize the military survey mission. This is the type of mission that may be able to implement a single beacon solution. Many military applications specify quick over-the-horizon deployment making beacon placement extremely costly. Synthetic baseline applications and self-calibrating networks are attractive. For mine counter measures (MCM) there must be a global reference to revisit the site. Current detection and perception are inadequate and targets are identified and dealt with by follow up missions.

Shallow Reverberant Deployment

The challenging acoustic environment and the relatively low logistic cost characterize the shallow reverberant deployment. An enclosed tank or a constrained ocean environment (e.g., a dock, hull-inspection, etc.) is such a distinct mission. The noisy environment and dense multipath structure presents a classification/correspondence challenge that might be addressed with redundant beacons (≥ 3). The ease of beacon deployment reduces the cost of deploying multiple beacons.

Tiny Hovering AUV

The need to minimize the platform size and cost and the need to provide precise localization for station keeping characterize the hovering AUV mission. Hovering requires an absolute reference which would require more than one beacon. Redundant beacons, multiple host transponders, or both might limit the size and cost of the vehicle. Such a dense acoustic network might eliminate the need for extra sensors. A single small acoustic transponder could give complete localization information without the need for depth and odometry sensors which add cost, complexity, and size to the platform.

3.7.2 Future Designs

This chapter has examined many options for the design of autonomous navigation systems, but there are an infinite number of other design possibilities. The challenge is to identify two things: the leverage points where new capabilities could lead to the largest performance gains and key technologies that are being developed to increase navigation precision.

Spread Spectrum

Spread spectrum, using coded signals for detection, has potential benefits for the capability of precision navigation systems [Austin, 1994]. The main functional benefit of using spread spectrum techniques is in allowing increased range and resolution. The results of this chapter have been presented as general to the operating range and precision of the acoustic ranging system implemented. Therefore, this aspect of the technology will improve performance, but the methods and metrics discussed previously retain their validity.

There are other benefits of using spread spectrum signal processing that are not as obvious as the range/resolution improvement. Distinct codes allow multiple users to use the same channel without interference. This would allow many platforms to use the same positioning system and/or faster updates by multiple interlacing queries and having simultaneously pinging multiple beacons. The ability to operate in high noise environments enables positioning in high noise environments or clandestine operation. Spread spectrum essentially offers a new set of design decisions and new dimensions of operation that can be exploited to increase the precision performance, add robustness, and expand the capabilities. There are many new design parameters in spread spectrum signaling; signal processing, control, and estimation will continue to converge, leading to increasingly integrated designs.

Communication

Reliable, high bit-rate communication underwater continues to be a challenge. Integrating these systems into autonomous surveying systems will provide increased navigation performance in multiple dimensions. Communication is a fundamental enabling technology for the next generation of autonomous platforms.

For navigation, just a few bits of information can make a tremendous operational difference. As mentioned in the previous section on spread spectrum (using different codes is one way to transmit small amounts of information), communication allows for a new level of adaptability for navigation systems. We envision communication as another dimension of the integration of AUV design. Vehicles capable of relaying information acoustically and reacting to this information can use the signals for navigation and communication concurrently. The challenge is to determine how this will impact the design of the navigation system.

Multiple Vehicles

Using multiple AUVs in concert has been the driving force of many research efforts but has yet to be realized in practice. The integration theme continues and now the challenge is to coordinate multiple elements operating in a single environment - to design their communication, navigation, motion, and planning. Research into how multiple inhabitants of a single environment will communicate has important implications on network topologies for navigation [Stojanovic et al., 2002].

Chapter 4

Hypothesis Grids: Mapping Uncertainty in Autonomous Survey

> Behold! human beings living in a underground den, which has a mouth open towards the light and reaching all along the den; here they have been from their childhood, and have their legs and necks chained so that they cannot move, and can only see before them, being prevented by the chains from turning round their heads. Above and behind them a fire is blazing at a distance, and between the fire and the prisoners there is a raised way; and you will see, if you look, a low wall built along the way, like the screen which marionette players have in front of them, over which they show the puppets.
> -Plato[1]

Perception, limited by sensory input, is a tenuous connection to reality. This chapter presents a grid-based representation of the acoustically instrumented underwater environment for navigation - hypothesis grids (Hgrids) - and a method for creating the representation from past observations - the Hgrid algorithm. Hgrids increase the localization precision and expand the autonomous capabilities and are comprised of three components: a mixed-distribution sensor model, a classification-identification algorithm, and a representation. The fundamental premise is that the quality of an acoustic range measurement depends upon the location of the measurement. The quality captured by the Hgrid representation is the prior association probability, the belief in the particular source of subsequent range observations[2].

By modeling prior probabilities, Hgrids contribute to the performance of standard probabilistic navigation techniques. Methods of navigation based on Bayesian inference use an estimate of the prior probability in their formulation. The numeric value of this term is often assumed, estimated, or specified to contain no information. Hgrids provide a value for this belief through an explicit representation of the environment, a value that can then be used in the navigation algorithm of choice, e.g., multiple hypothesis tracking (MHT), Bayesian filters, particle filters, or Kalman filtering techniques (see section 2.1.4 for background on probabilistic navigation).

[1] Plato, "The Simile of the Cave," in *The Republic*, 2nd ed., Desmond Lee, trans. (Viking Press, 1955).
[2] Prior probability and *a priori* probability are used interchangeably.

Uncertainty in acoustic range measurements is not Gaussian. Acoustic multipaths cause consistently erroneous range observations, whales and outboard motors cause storms of false data, transponders refuse to reply, and measurements are often just wrong. Capturing all the possible sources of error in range measurement is not possible - there is always a new type of failure. This chapter argues that by modeling range sensors as mixtures of simple distributions and using evidence to approximate how the probabilistic characteristics of the sensors change with location, autonomous systems can realize more performance and new capabilities when operating in instrumented environments.

Chapter Goals

- Present a clear, succinct problem statement and summary of the approach
- Discuss the closely related work
- Develop hypothesis grids using data from an AUV expedition
  - Propose a mixed-distribution model for acoustic range measurement, including an empirical ray-traced multipath model
  - Apply the expectation-maximization algorithm to simultaneously classify the data and identify the sensor model
  - Represent the dependency between location and probabilistic classification using a 2-D grid of the environment
- Provide concrete conclusions and directions for future investigations

4.1 Hypothesis Grid Overview

As an overview this section presents a succinct problem statement and addresses the approach to that problem. Three key aspects summarize the approach: a mixed Gaussian and uniform distribution sensor mode, observation classification using expectation-maximization, and a grid representation based on localization.

Problem Statement

Given an autonomous platform operating in an instrumented, discrete acoustic environment, what determines the probability that any range observation is associated with the direct-path measurement and not from some other source?

Three statements focus this general problem on the problem of autonomous underwater navigation using acoustic range observations:

- A mixture of simple distributions models the operation of acoustic range transponders. Three distributions, representing the type or source of the observations, combine in the model: direct-path (DP), multipath (MP), or outlier (OL)

- Prior association probabilities, $P(\theta_i)$, are an important sensor characteristic for implementing a variety of estimation techniques. The association hypotheses, θ_i, are exhaustive and mutually exclusive: $\theta_i = \{DP, MP, OL\}$ and $\sum_{i=1}^{3} P(\theta_i)) = 1.0$
- The prior probabilities are spatially dependent: $P(\theta_i) = f(x)$.

These statements focus the problem statement:

Given range observations and position estimates, approximate the dependence between the prior probabilities and the estimated location, i.e., approximate the function, $f(\hat{x}$, in the relationship $P(\theta_i) = f(\hat{x})$.

4.1.1 Approach

Mixed-Distribution Model: Prior Probabilities

Observations, $z(k)$, are a time-varying function, $h()$, of the state vector, $x(k)$.

$$z(k) = h(x(k)) + \nu$$

where k is the time index, and additive noise, ν, models uncertainty in the measurement. A popular model assumes ν to be normally distributed, an assumption that allows powerful analytical results, but restricts the application to sensors with such behavior. To model more complex observations, either the random variable distribution or the functional dependence is expanded. A distribution that captures the rich uncertainty of acoustic range measurements would be analytically and computationally challenging. Exploiting the structure of the sensor allows shifting the complexity to the functional representation, preserving of the simple distributions. A mixed-model captures the three hypotheses used to characterize the source of range measurements: {DP, MP, or OL}.

$$z(k) = \begin{cases} h_{DP}(\hat{x}(k)) + \nu_{DP} & P_{DP} \equiv P(\theta(k) = DP) \\ h_{MP}(\hat{x}(k)) + \nu_{MP} & P_{MP} \equiv P(\theta(k) = MP) \\ h_{OL}(\hat{x}(k)) + \nu_{OL} & P_{OL} \equiv P(\theta(k) = OL) \end{cases} \tag{4.1}$$

From observations, a set of mutually exclusive probabilities captures the chance of or belief in an individual measurement's source (based on the frequency of the event, not the prior belief).

$$P_{DP} + P_{MP} + P_{OL} = 1$$

The mixed-distribution of equation 4.1 and illustrated in figure 4-1 captures the observed behavior of active acoustic range sensors.

Range Classification: Direct Path, Multipath, and Outliers

Individual range observation are classified based on the source of the measurement. The association probability values, $\{P_{DP}, P_{MP}, P_{OL}\}$, constitute classifying an observation. Given a model

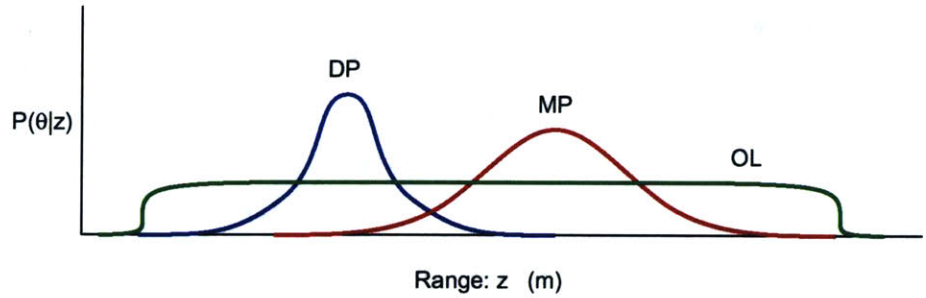

Figure 4-1: Probability density functions for the three associations. DP=direct-path, MP=multipath, OL=outlier

and measurements, probabilistic classification is a straight forward calculation based on Bayesian inference, but the model parameters are not known. A method must simultaneously determine the model based on the data and classify the data based on the model.

The direct-path model is known. The line-of-site distance and the variance in the observation parameterize this component of the mixed-distribution model (see appendix A.3) and spurious data is assumed uniformly distributed. The remaining unknowns in the sensor model are the multipath ray-model parameters. The challenge is to concurrently identify the unknown multipath parameters and classify each observation's source. The expectation-maximization algorithm solves this simultaneous identification and classification problem.

Grid Representation

Hgrids combine individual observation classifications into a spatially dependent representation, making a map of the sensed environment. The association step yields a classification of each observation. The representation captures important aspects of the sensed environment: a particular dead-zone where spurious returns are likely, a sweet-spot where the ranges are direct and repeatable, or a corner of the survey where multipath measurements are prevalent. Building hypothesis grids is a model fitting problem; the model is a grid representation of the survey site and the classification data is fit to the grid.

A representation of the data should be compact, allow for efficient interrogation, accurately model the data, and quantify uncertainty [Tuohy, 1993]. To capture the location dependence of the prior probabilities this chapter proposes a cellular decomposition. Figure 4-2 illustrates the basics of this representation. The cells are shown as a 3-by-3 Cartesian grid in 2 dimensions, but these cells could be multidimensional, have an alternative shape, or have changing size.

4.1.2 Summary: Increased Capabilities

Hypothesis grids are based on the characteristics of acoustic range measurements. The flowchart in figure 4-3 is an overview of the algorithm. Associating range observations with direct-path, multipath or outlier sources, is a task that human operators are quite good at, but a challenge that can break brittle autonomous estimators. The algorithm generates an empirical map of the sensed

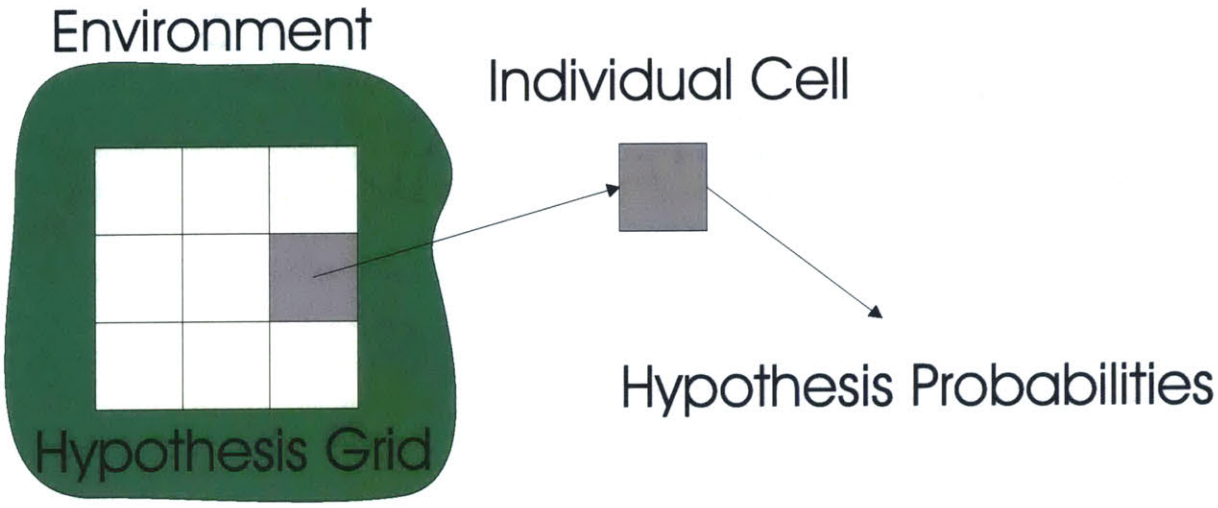

Figure 4-2: Representation: Capturing the spatial dependencies

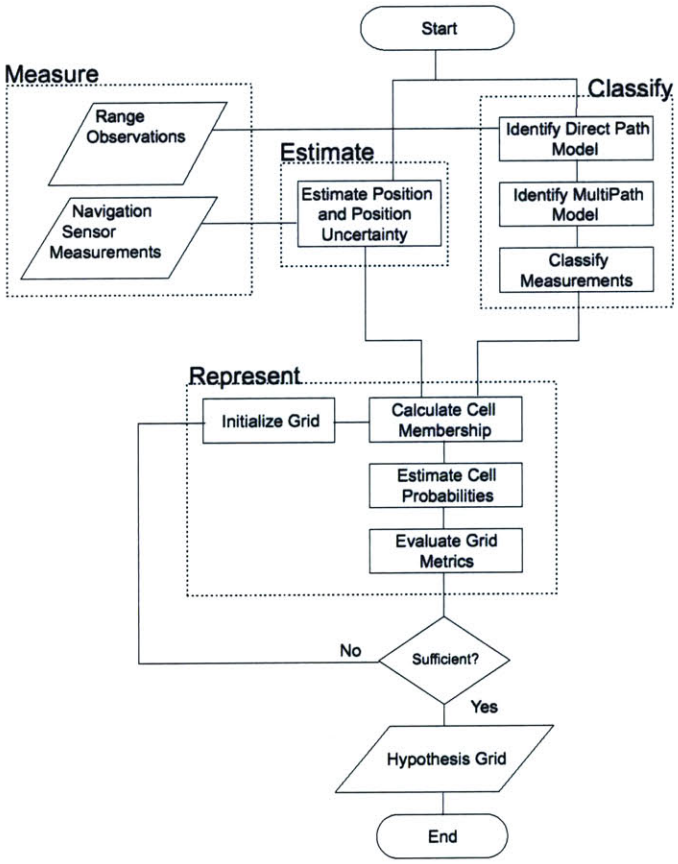

Figure 4-3: Algorithm flowchart for building hypothesis grids

environment, increasing the performance and expanding the capabilities of autonomous systems. The remainder of this chapter develops the method and its impact on the precision, robustness, and autonomous capabilities of the navigation solution.

4.2 Closely Related Work

Hypothesis grids connect with fundamental Bayesian estimation techniques for navigation and focus on a unique application. The genesis of the approach comes from three main sources sources: Deffenbaugh's work using multipath range data for navigation [Deffenbaugh et al., 1996b], Leonard's application of multiple hypothesis tracking to underwater navigation [Leonard et al., 1995], and Blimes' basics of the expectation-maximization algorithm [Bilmes, 1997]. These disparate references each contributed to the idea of generating a hypothesis grid of an underwater environment, but the approach draws upon other work in probabilistic navigation, data-association, navigation, tracking, and imaging. A few current navigation techniques (occupancy grids and map-based navigation) share aspects of hypothesis grids, but are distinctively different in application and formulation.

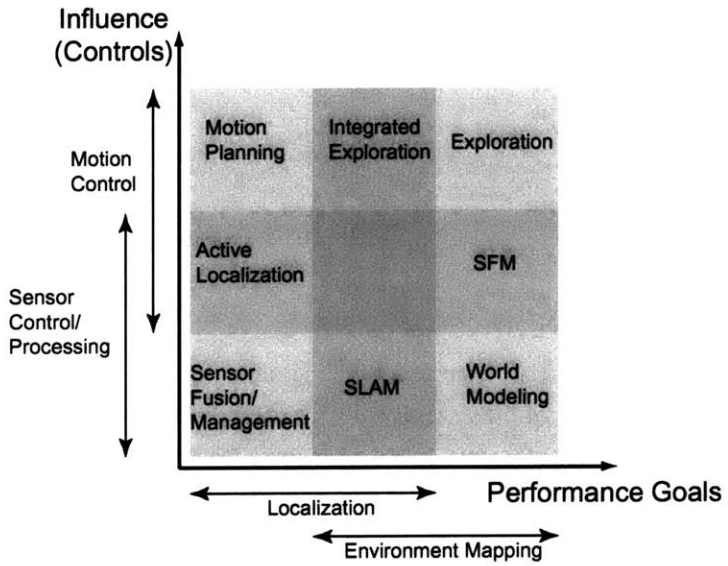

Figure 4-4: Approaches to field robot navigation. SLAM = Simultaneous localization and mapping, SFM = Structure from motion.

This section presents the fundamentals important in the development of hypothesis grids. A broader treatment of the background is given in chapter 2. Section 2.1.4 presents a classification of field mobile robotics based on the performance targets - localization, mapping, or both - and the control means - motion control, sensor processing, or both. The decomposition of the field is summarized by figure 2-9, repeated as figure 4-4 for convenience. The hypothesis grid algorithm focuses on using measurements to create an empirical representation of the sensed environment. This places Hgrids in the lower row of the grid in figure 4-4 where sensor processing is used for localization and environmental mapping.

4.2.1 Probabilistic Navigation

Probability and Inference

Bayesian techniques are the basis for many estimation techniques [Papoulis, 2002, Willsky et al., 1997, Spiegel et al., 2000]. Bayes filters, occupancy grids, Kalman filters, etc. are all based on Bayesian inference. Thrun's summary develops the techniques from the fundamentals and draws connections between the disparate approaches [Thrun, 2002]. The shortcomings of the Bayesian approach are discussed by Jeffreys [Jeffreys, 1961] and an alternative, evidence reasoning, is proposed by Shafer [Shafer, 1976]. Bayesian techniques depend on prior beliefs, a fundamental criticism of the approach. Hypothesis grids operate in concert with Bayesian estimation techniques. By explicitly modeling a prior probabilities, the algorithm forms a foundation for other navigation techniques and supplies an informed estimate of values that are typically approximated heuristically.

Navigation Techniques

In addition to the general techniques for mobile robot navigation summarized in section 2.1.4, the relationship between related techniques and hypothesis grids deserves highlighting.

Occupancy or inference grids are similar to hypothesis grids; they share a rectangular representation of a sensor environment [Elfes, 1989, Thrun, 2001, Moravec, 1988]. This approach splits the environment into small cells and uses the information from sensor readings (typically laser-line-scanners) to estimate whether or not each cell contains an object or is unoccupied. The differences are greater than the similarities. Hgrids model the probability of association; occupancy grids capture the physical geometry of the environment. Hgrids consider multiple (≥ 3) possibilities; occupancy grids use only two possibilities, simplifying the inference. Simple Hgrids, dividing the space into modest number of cells, are shown to capture the critical sensor behavior; dense occupancy grids, requiring complex computation, are necessary to model even simple environments

The failure of the Bayesian techniques of occupancy grids to represent ignorance is addressed by Dempster-Shafer grids by using an evidence model to build similar environment representations [Pagac et al., 1996]. Ribo makes a comparison of three methods for computing occupancy probabilities [Ribo and Pinz, 2001]. The Hgrid addresses this challenge using observation, eliminating the need to represent ignorance.

Navigation with some prior known map of the environment is a well studied problem. Tuohy develops a technique for navigating an AUV based on a prior map and examines the related techniques [Tuohy, 1993]. Two basic types of maps are typical in mobile robot navigation, metric and topological maps. Thrun marries these two and provides an informative overview of both approaches [Thrun, 1998, Thrun et al., 1998b]. Building a hypothesis grid for a particular installation yields a map for navigation where the tools of map-based navigation can be applied. This chapter develops the algorithm for making the map and leaves the question of effectively using the map for future work.

Classification, Association, and Correspondence

A fundamental challenge of this chapter is the association of range observations with their individual sources. Using a mixed-distribution sensor model the probability that each observation is a measurement of the direct-path (line-of-sight), a multipath, or an outlier is calculated as the probabilistic association. This approach follows the probabilistic association techniques in radar tracking were measurements are classified based on the multiple sources of a particular return [Bar-Shalom and Fortmann, 1988,Bar-Shalom and Li, 1998]. This challenge is also related to the correspondence problems in robot mapping and machine vision. Correspondence in robot mapping seeks to match features across disparate sensor scans, i.e., to find a feature known from a previous measurement in the current observation [Thrun, 2002]. In machine vision the difficulty is finding the same portions within multiple images - correspondence. A similar challenge in image processing is to classify segments an single image to match the physical properties of the scene [Anderberg, 1973].

4.2.2 Multipath Identification

Multipath Modeling

A general model of the acoustic communication channel is an open research question. At the coarsest level there are two basic multipath models: a probabilistic reflector model prevalent in applications to electromagnetic wave communications ([Proakis, 1989, Tourrilhes, 2000], and a deterministic ray-tracing model typical in the ocean acoustics community [Jensen et al., 2000,Brekhovskikh and Lysanov, 1991].

Equalization techniques from electromagnetic communications are amenable to the acoustic channel. The dynamics of the equalizer implementation are substantially different because of the physics of the channel, but the fundamental concept of a probabilistic, time-varying model of the multipath propagation is the same [Freitag et al., 2000,Freitag et al., 1998, Johnson et al., 1995].

Alternatively, ocean acoustics models are based on an understanding of the large scale propagation of acoustic signals and have grown from military sonar research. Deterministic techniques, such as ray-tracing, yield models that are based on the geometry and properties of the medium. This approach is applied to navigation with a known model of the acoustic environment [Deffenbaugh, 1997]. If the environment is not known system identification techniques are necessary to learn the parameters of the model based on observation; a sparse presentation of such an approach is given by Caimi, et al. [Caimi et al., 1998]. Because of the homogenous acoustic environment assumption (section 2.3.1), a simple geometric multipath model applies to the ranging scenario. This model assumes a static multipath with a geometry empirically identified using past range observations.

The EM Algorithm

> The EM algorithm is a general method for finding the maximum likelihood estimate of the parameters of an underlying distribution from a given data set when the data is incomplete or has missing values. [Bilmes, 1997]

Background on expectation-maximization (EM) ranges from mathematical fundamentals [Bilmes, 1997, Dempster et al., 1977] to applications, such as simultaneous localization and mapping [Thrun et al., 1998a] and image segmentation [Saeed, 1997, Tadjudin and Landgrebe, 2000].

The key characteristics of the EM for application to multipath identification are the batch approach, iterative solution, and the application to mixed density models. The algorithm processes all the data at once, precluding its use in a real-time scenario. Two steps are repeated to iteratively solve the classification and identification. The *e-step* classifies the data based on the current model, followed by the *m-step* which identifies the model based on the classification. The applications of the algorithm, referred to above, have shown the utility of EM for mixed-distribution models similar to the model proposed for range observations. This thesis applies the EM algorithm to a new topic, acoustic range observations, and a new model, a mixed model of Gaussian and uniform distributions.

4.3 Application Overview: Building Hypothesis grids for ABE58

The following example, using data from the autonomous benthic explorer (ABE) [Yoerger et al., 1992, Yoerger et al., 1999, Yoerger et al., 1997], develops a concrete implementation of the fundamental concepts for building hypothesis grids shown in figure 4-3: localization, classification, and representation. This presentation follows these steps:

- Application Overview: ABE58 Data and Measurement Model
- EM Development for Multipath Classification
- Application of EM/MP Algorithm to ABE58 Data
- Hgrid Representation Example
- Sensitivities and Results

Two assumptions simplify the implementation: batch processing and independent localization estimates. The following hypothesis grid is built after the dive is complete using past range measurements, i.e., batch processed rather than considered in real-time. And for the representation step, where the the observations are associated with regions in the spatial map, an position estimate and position uncertainty estimate are generated from an independent estimator. The classification step does not rely on this estimation, but for clarity and brevity the localization is considered independent of the representation. Figure 4-3 illustrates the functional steps in the algorithm.

4.3.1 The ABE58 Survey

The navigation data used to illustrate the process and test the feasibility of the representation come from ABE dive number 58 (figure 4-5a) - ABE58. From November 5 to December 4 of 2001 a research team studied mid-ocean ridge geology to understand the fundamental processes involved in the creation of new ocean crust through h high-resolution mapping of the near-bottom

magnetic field. To study the section of the East Pacific Rise shown in figure 4-5b, the team used a towed system (DSL-120A), a manned submersible (Alvin), and an autonomous vehicle (ABE). ABE surveyed a total of 14.3 km^2 of the seafloor over 11 individual dives at two separate locations. At an altitude of 20-30m the vehicle performed parallel tracklines, 40-60 m apart, with a magnetometer, a 675 kHz Imagenex pencil beam sonar, a digital still camera, and a CTD, producing high-resolution maps of the phenomena [Schouten et al., 2002].

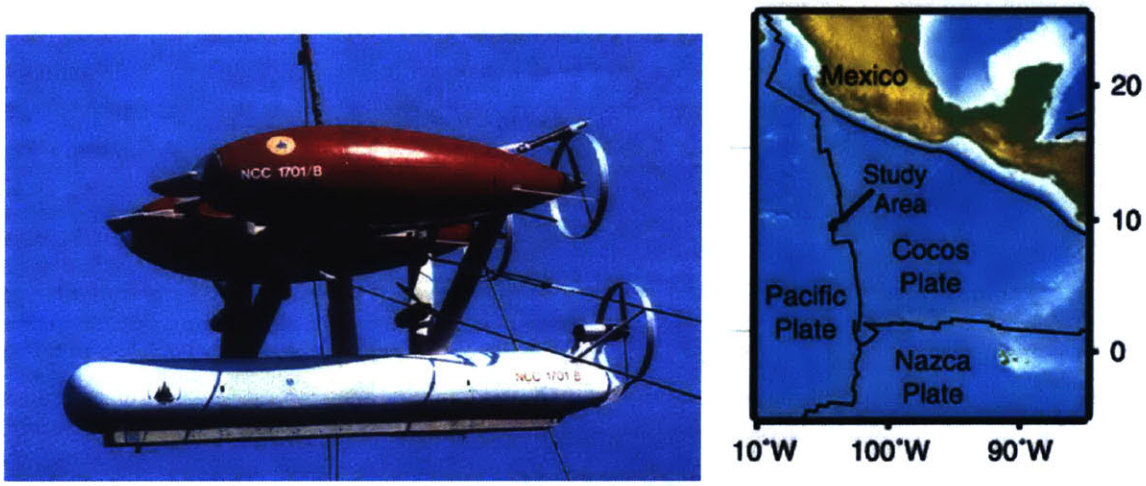

a b

Figure 4-5: a) The Autonomous Benthic Explorer (ABE) vehicle. b) Location of the ABE58 dive off the Pacific coast of Mexico.

Long Baseline Data Overview

The long baseline positioning data from ABE58 is ideal for illustrating and evaluating the hypothesis grid algorithm. The vehicle made range measurements to 4 beacons at known locations using standard 12kHz acoustic transponders. Figure 4-6 illustrates the ABE58 survey by plotting the estimated positions of the vehicle projected into the x-y plane and the long baseline transponder locations.

Figure 4-7 illustrates the raw range information including direct-path, multipath, outliers and null returns. The ranges from the third beacon, shown in red, illustrate the multiple sources of particular range observations. The direct-path is evident in the sawtooth pattern of first return ranges oscillating between 700 and 2200m. Another sawtooth pattern indicates the multipath with a similar sawtooth pattern for ranges between 3000 and 4000m. A weaker second multipath is evident at at about 5100m. Returns corresponding to neither of these three paths clutter the data. The clutter is especially strong at two particular times - around 2000 and 3500 on the data index axis. Lastly ranges with a value of zero are null returns that should not be used in localization. This qualitative examination exposes four general classes of acoustic range from each transponder: a consistent direct-path, consistent multipaths, inconsistent spurious returns, and null ranges. While the human eye is adept at this classification, autonomously classifying and identifying this type of

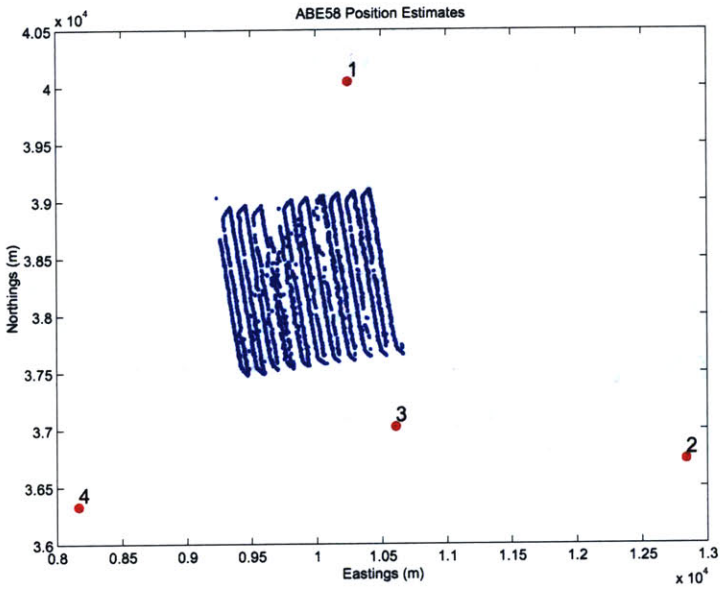

Figure 4-6: ABE58 survey in the X-Y plane. Approximately 5,000 data points are plotted from the survey. The 12 kHz LBL beacon locations are shown as labeled red markers

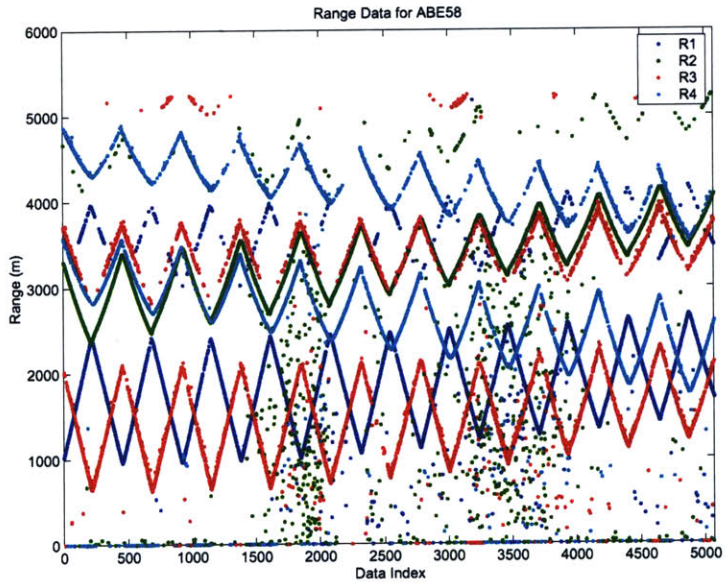

Figure 4-7: ABE58 12kHz LBL range data. Time-of-flight is reported as range in meters for successive observations.

data is difficult.

4.3.2 Measurement Model

The measurement model combines three possible sources for each observation. For each measurement, indexed in time (k), a hypothesis ($\theta_i(k)$) represents association of the observation with each

of three possible sources: a direct-path (DP) range, a multipath (MP) range, or an outlier (OL)[3]. The mixed-density measurement model combines these sources.

$$z(k) = \begin{cases} |\hat{\mathbf{x}}(k) - \mathbf{x_0}(k)(|^2 + \nu_{DP} & \nu_{DP} \sim N(\nu_{DP}; 0, \sigma_{DP}) & P_{DP} \\ f_{MP}(\hat{\mathbf{x}}(k), \mathbf{x_0}(k), \mathbf{\Phi}) + \nu_{MP} & \nu_{MP} \sim N(\nu_{MP}; 0, \sigma_{MP}) & P_{MP} \\ \nu_{OL} & \nu_{OL} \sim Uniform & P_{OL} \end{cases}$$

The direct-path measurement is simply the Cartesian distance metric between the observer's estimated position, $\hat{\mathbf{x}}(k)$, and the known survey location, $\mathbf{x_0}(k)$, with a zero-mean Gaussian noise. The multipath observation is a function of the observer location, the beacon location, and the environment geometry. The geometry of the multipath model is contained in the parameter vector Φ. The outlier observations are modeled as uniformly distributed over a specified range. Figure 4-1 illustrates this combination of probability density functions and how the model captures the quantitative aspects of the data in figure 4-7. The prior probability of a particular association is the belief, before observation, that a measurement will be from one of the three sources. For example, a value of $P_{MP} = 0.25$ relates a prediction that a subsequent measurement will be an observation of the multipath range with a probability of 25%.

Measurements corresponding to the direct-path range, the line-of-site between the host and transponder, are modeled with Gaussian uncertainty. Since a Gaussian distribution is fully characterized by just the first and second moments, the standard deviation of the direct-path range observations is sufficient to identify the model. In appendix A.3 this property is estimated from the ABE58 range data using least-squares model-fitting. From this analysis the standard deviation of the direct-path range measurement is **3.97m** for the 12kHz LBL observations.

Multipath Model

The range observations in figure 4-7 illustrate a strong multipath component. The proposed ray-trace model captures the main characteristics of the data with a minimal complexity. This geometric model may not be appropriate for larger scale environments where variation in the speed of sound and the resulting ray bending lead to a variety of sound paths, but this homogeneous assumption simplifies the investigation for small-scale environments.

An acoustic reflector creates an alternate path for the sonar signal. For specular reflections the length of this path is a function of the relative heights of the source, receiver, and reflecting plane. Figure 4-8 illustrates this geometry in a vertical plane containing the host and the beacon. The multipath range (S_{MP}) is a function of the two-dimensional horizontal plane and the depth.

$$S_{MP} = \frac{d_0 + \hat{d}}{\sin\left(\arctan\left(\frac{d_0 + d_b}{|x_0 + \hat{x}|}\right)\right)} \tag{4.2}$$

$$= f_{MP}(x_0, d_0, \hat{x}, \hat{d}) \tag{4.3}$$

[3]Time-of-flight is actually measured, and the range is estimated based on this measurement and an uncertain estimate of the speed of sound.

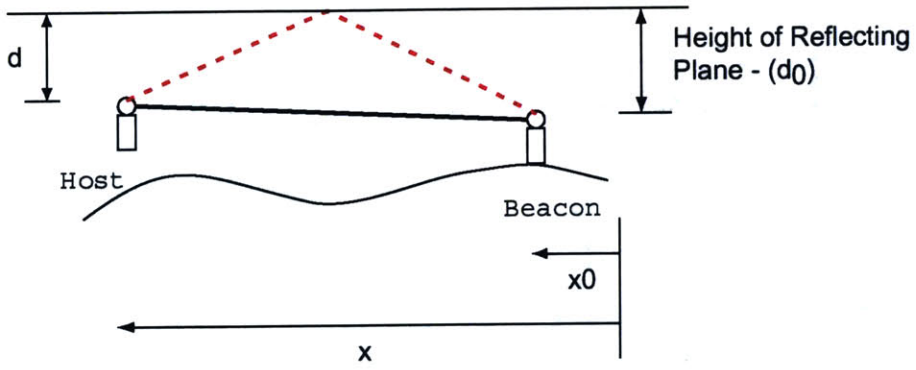

Figure 4-8: The geometry of the multipath model. The model is parameterized by the height of the reflecting plan. The dashed (red) line shows the multipath trace while the solid (black) line shows the direct path. Since the range estimated from the round trip travel time the path may consist of both the slant range (line-of-sight) and the specular reflection - the triangle path.

where d_0, x_0 and $\hat{d}, \hat{x}$ are the depth and horizontal locations for the beacon and host respectively. Depth is used here as the relative vertical distance to the reflecting plane - the *height of the reflecting plane* (HRP= d_0).

$$d_0 = \frac{1}{2}\left[(d_0 - \hat{d}) + |\hat{x} - x_0| \tan\left(\arccos\left(\frac{|\hat{x} - x_0|}{S_{MP}}\right)\right)\right]$$

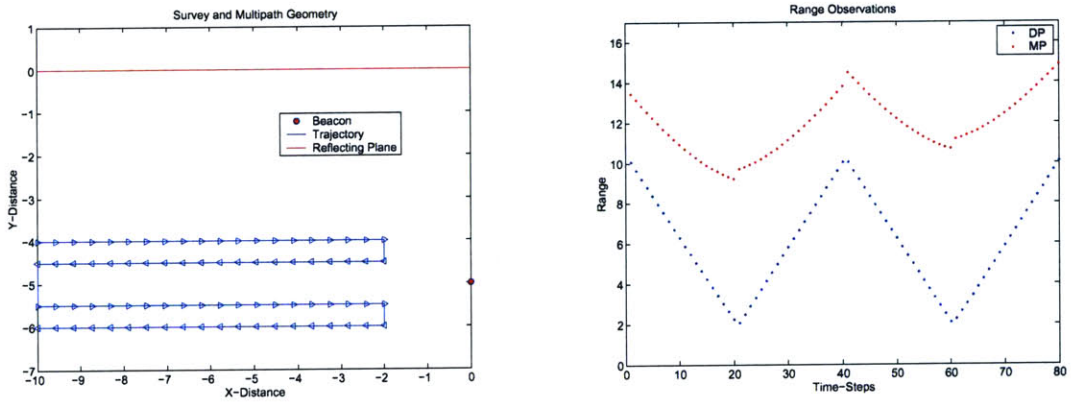

a b

Figure 4-9: Multipath illustration. a) The geometry of a simple ray-model for reflected path. The range is observed along the trajectory shown in blue. The triangle markers indicate the direction of travel. b) The resulting range observations using the simple geometrical model and a constant reflecting plane height.

A simple simulated survey illustrates this geometric model. The survey specifies a set of locations where the direct-path and multipath ranges are measured - see figure 4-9a. The reflecting plane is at a known locations so the geometry leads directly to direct-path and multipath range measurements shown in figure 4-9b. This illustration highlights archetypes observed in the actual

range data, reinforcing the geometric model. The characteristic sawtooth patterns in the direct-path ranges of figure 4-9b are evident in the ABE58 data. The multipath trace shows a similar pattern, but the slope of the range measures is less - a characteristic also evident in the ABE58 data. This simple model captures the main aspects of the multipath returns observed in practice. The multipath geometry is dependent on the known beacon location, the host position estimate, and the relative height of the reflecting plane. Using only few parameters simplifies the classification step.

4.4 Expectation-Maximization for Multipath Modeling

If every range observation were normally distributed about the true line-of-sight range to a fixed, known location, long baseline positioning would be just simple trilateration. The resulting position uncertainty would be predictable, and autonomous operation would be reliable and robust. A glance at the range data in figure 4-7 is evidence that this simple concept is not realized in application. The EM method, extended to the mixed-distribution model, simultaneously identifies and classifies the range observations. Concurrently identifying the model *and* classifying the observations presents a particular challenge. Given a model, classifying the observations is a straight forward estimation problem with various solution methods. Given the classification, estimating the parameters of the model is a also straight forward. Taken together the challenge is a *chicken and egg problem*[4]. The EM algorithm presents an iterative solution.

This section begins with the development of an EM algorithm for range observations incorporating the mixed-distribution model. The following sub-section applies the algorithm to the range data from one beacon in the ABE58 survey. This section concludes with the results of classifying the data from all four range beacons and identifying four multipath models.

4.4.1 EM Development for Multipath Classification

Application of the EM algorithm to range observations requires developing a parameterized data model, a classification criteria, and a parameter estimation technique. The combination of these three steps, presented below, illustrates how the algorithm applies to the acoustic range measurements.

Data Model

Equations 4.3.2 and 4.2 capture the geometry and uncertainty in the mixed-distribution range measurement model. The EM algorithm alternatively classifies the data probabilistically by estimating the prior probabilities ($P(\theta_i(k))$, $\theta_i(k) = \{DP, MP, OL\}$) and identifies the multipath model by estimating the model parameters ($\Phi = \{d_0, \sigma_{MP}\}$).

[4] "Thus, the general problem of map building is an example of a chicken-and-egg problem: To determine the location of the entities-of-interest, the robot needs to know where it is. To determine where it is, the robot needs to know the locations of the entities-of-interest." [Thrun et al., 1998a]

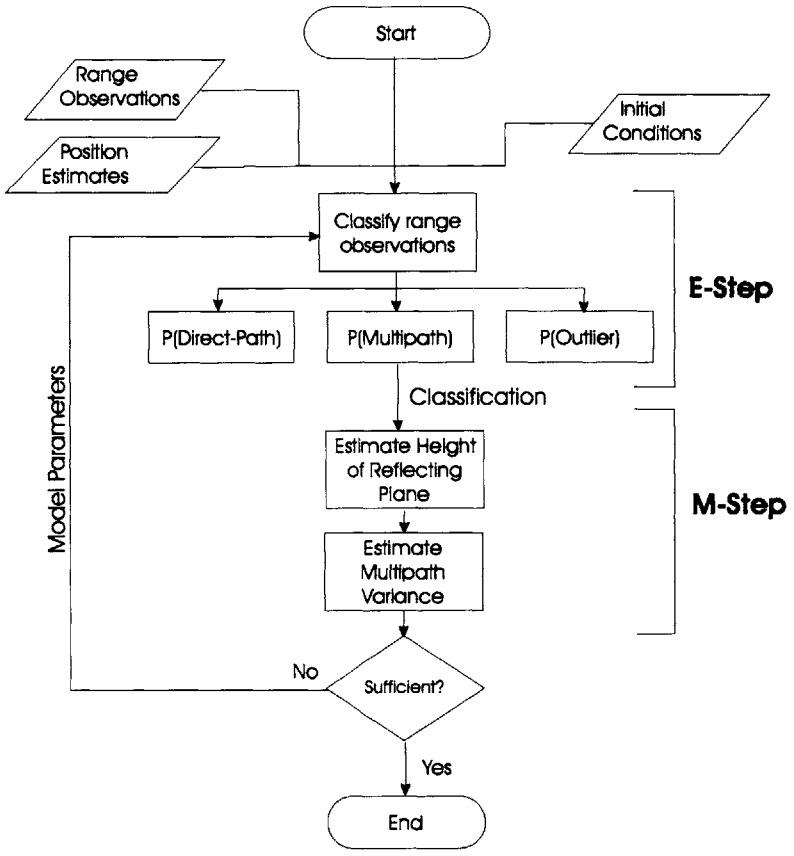

Figure 4-10: Flowchart of the EM algorithm applied to range association.

E-Step: Classification

Given a set of model parameters, the estimation step (e-step) classifies the observations. The model parameters, Φ, are 'known' from the previous iteration or from initial conditions, and the algorithm proceeds based on this model. For each data point the association probabilities are calculated in the Bayesian sense.

$$\gamma_j(k) = P(\theta(k) = j|z(k), \Phi) = \frac{P(z(k)|\theta(k) = j, \Phi)P(\theta(k) = j|\Phi)}{\sum_{j=1}^{M} P(z(k)|\theta(k) = i, \Phi)P(\theta(k) = i|\Phi)}$$

- Time index: $k = 1, \ldots, N$ for N data points

- Class index: $j = 1, \ldots, M$ for M hypotheses

The algorithm calculates the generative term for a particular observation based on the probability density function of the particular classification. For DP and MP associations, the distributions are Gaussian, characterized by estimated mean and variance values. Calculating the following values determines the posterior probability:

Bayesian Term	Notation	Description
Posterior	$P(\theta \mid z, \Phi)$	Probability of the association given the data
Generative	$P(z \mid \theta, \Phi)$	Probability of the measurement given the hypothesized association
Prior	$P(\theta \mid \Phi)$	Probability of the association without the measurement evidence
Normalization	$\sum_{i=1}^{M} P(z \mid \theta = i, \Phi) P(\theta = i \mid \Phi)$	Sum of the probabilities to enforce the mutual exclusive constraint

Table 4.1: Bayesian terminology and notation for equation 4.4.1

$\hat{z}_{j=DP}(k)$ Estimated range under the direct-path hypothesis from the current position estimate and the known beacon location.

σ^2_{DP} Variance in the direct-path range estimate - a characteristic of the sensor.

$\hat{z}_{j=MP}(k)$ Estimated range under the multipath hypothesis from the current position estimate, known beacon location, and current iteration of the multipath model parameters.

σ^2_{MP} Variance in the multipath range estimate - a parameter of the current iteration of the multipath model.

The conditional probabilities are calculated using the cumulative distribution functions for a chi-squared distribution.

$$P(z(k) \mid \theta = j, \Phi) = 1 - \int_0^u \chi^2(x) dx$$

$$u = \frac{(z(k) - \hat{z}_j(k))^2}{\sigma_j^2}$$

The conditional probability of a spurious measurement is constant.

$$P(z(k) \mid \theta = OL, \Phi) = P_{OL}$$

The conditional probabilities on the right hand side of equation 4.4.1 infer the posterior probabilities on the left hand side. The prior probabilities, $P(\theta_i = j \mid \Phi)$, are equivalent and can be left out of the calculation because of the normalization. This important detail is discussed more in the implementation and as a topic of future work.

M-Step: Model Parameter Estimation

The maximization step (m-step) estimates the model parameters (Φ) based on the probabilistic classification from the preceding e-step. The challenge is to find the maximum likelihood estimate of the parameters, given the range observations and their classifications. Since the data model

assumes a mixture of Gaussians and a uniform distribution (which can be viewed as a Gaussian with a large variation), the least-squares merit function is appropriate as the likelihood function; see appendix A.1 for a discussion of least-squares model fitting.

$$\chi^2 = \sum_{k=1}^{N} \left[\sum_{j=1}^{M} \left[\frac{(z(k) - \hat{z}_j(k))^2 \gamma_j(k)}{\sigma_j^2} \right] \right]$$

The estimation is choosing model parameters to minimize the residuals, χ^2, in equation 4.4.1. Using the classification probability ($\gamma_j(k)$) as a weighting function reinforces the clustering necessary for the algorithm to converge. The data classified as multipath has a larger impact on the resulting model parameters. Eliminating the non-multipath contributions to the residuals and assuming the measurement variance constant all observations simplifies the objective function.

$$\chi^2 = \frac{1}{\sigma_{MP}} \sum_{k=1}^{N} \left[(z(k) - \hat{z}_{j=MP}(k))^2 \gamma_{j=MP}(k) \right]$$

Because the variance is constant, the HRP ($\hat{d}_0(i)$) is calculated for each observation. These individual estimates are combined by a weighted average using the MP classification probabilities from the e-step.

$$\hat{d}_b = \frac{\sum_{k=1}^{N} \left[\hat{d}_0(i) \gamma_{j=MP}(k) \right]}{\sum_{k=1}^{N} \left[\gamma_{j=MP}(k) \right]}$$

The maximum likelihood estimate of the variance in these measurements is a similarly weighted average of the residuals.

$$\hat{\sigma}_{MP} = \frac{\sum_{k=1}^{N} \left[(z(k) - \hat{z}_{j=MP}(k)) \gamma_{j=MP}(k) \right]}{\sum_{k=1}^{N} \left[\gamma_{j=MP}(k) \right]}$$

The measurement estimates $\hat{z}_{j=MP}(k)$ are calculated using the estimated height from equation 4.4.1.

This section has detailed the EM algorithm for identifying the multipath model and classifying the range observations from range data. The next section implements this algorithm to arrive at a probabilistic association of each data point and a solution for both the HRP and the multipath variance.

4.4.2 Application of EM/MP Algorithm to ABE58 Data

Applying EM to the ABE58 range data illustrates the operation of the algorithm as it converges on a classification and model identification. The process treats each of the four beacons used in the survey separately. The results present the analysis from all four beacons, but observations from beacon #4 are used in this detailed example. Figure 4-11 presents a selection of the range data. The direct-path (DP) is the first consistent return ranging from approximately 2500 to 3500 meters. A strong second return, the multipath (MP), is evident from the ranges with values between 4000

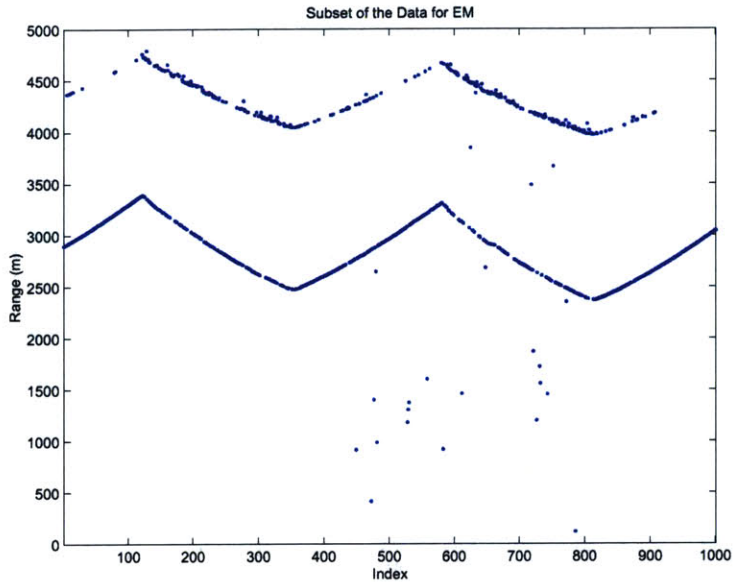

Figure 4-11: A selection of 1000 ranges from the ABE58 dataset.

to 5000 meters. And spurious returns, outliers (OL), are distributed from 0 to 5000 meters.

The observations in figure 4-11 are ranges in meters, but the acoustic measurements are round-trip travel time in seconds. The one-way range estimate is determined by subtracting the known turn-around-time (the delay between the remote transponder receiving the query and replying), converting the travel time to distance using the speed of sound, and dividing the range by one half. The multipath data is the responses that travel along the multipath in one direction and along the direct-path in the opposite direction - a triangle path (see figure 4-8). This geometry is important for achieving physically meaningful results and is easily incorporated into the EM algorithm.

Initial Conditions

The initial parameter vector $\Phi(0)$ is the starting point for the method. It is important to verify that the results, the final values of the algorithm, are insensitive to these initial values. The uncertainty in the multipath observations is initialized at a very high value - $\sigma^2_{MP}(0) \approx 10^7 m^2$. Using a large value is important because it causes the first classification to associate many of the observations as multipath returns. Since the variance is large, the actual value of the height of the reflecting plane parameter does not effect the first classification and this value can also be chosen very large - 4,000 m for this example.

The first e-step, shown in figure 4-12, classifies the measurements based on these initial parameters. Since the direct-path variance is already 'known', the figure shows accurate classification of the direct-path, shown as blue markers in the figure. Because of the very large initial multipath variance, the initial classification considers many of the outliers as possible multipath measurements (red markers in the figure); the algorithm begins with a conservative guess, erring on the side of caution and not throwing away 'good data'. The classification keeps the probability of any of the

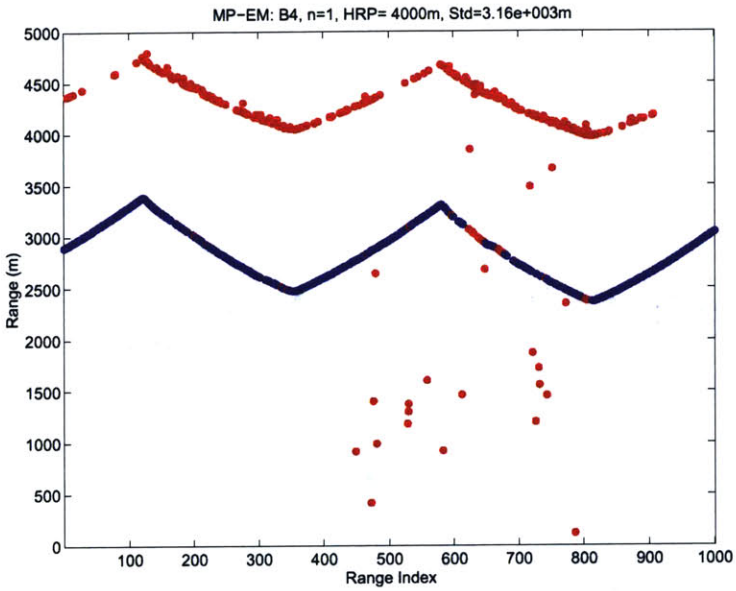

Figure 4-12: Classification plot for the first iteration of the EM algorithm. The probabilistic classifications are mapped to blue, red, and green for direct-path, multipath, and outliers (see figure 4-13).

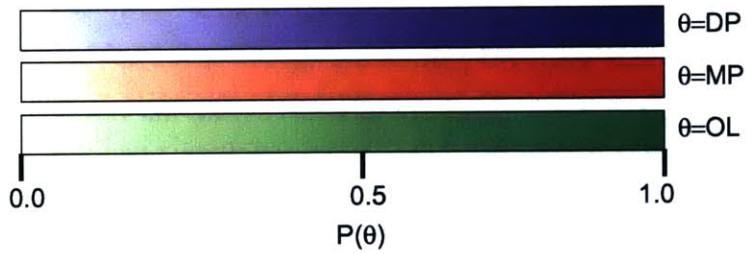

Figure 4-13: Three-value colormap for visualizing the probabilistic associations. The probabilistic classifications are mapped to blue, red, and green for direct-path, multipath, and outliers.

ranges being outliers very low, as evident by the lack of green markers.

Iteration

Following this first classification, the algorithm calculates the parameters of the multipath model based on the least-squares criteria in equation 4.4.1. These two parameters are the height of the reflecting plane and the measurement variance - both determine in the m-step. The parameters are a function of the system's geometry and the probabilistic association of the preceding e-step. A convergence factor (α) controls the rate of convergence of the algorithm. The m-step calculates a new estimate of the HRP - $\hat{d}_b$ of equation 4.4.1. Blending this new value with the old value ($d_0(k)$) estimates the HRP for the next iteration ($d_0(k+1)$.

$$d_0(k+1) = (1-\alpha)d_0(k) + (\alpha)\hat{d}_0$$

Once the new reflecting plane height is available, the algorithm calculates the uncertainty in the multipath using the new plane height and equation 4.4.1.

Final Classification and Identification

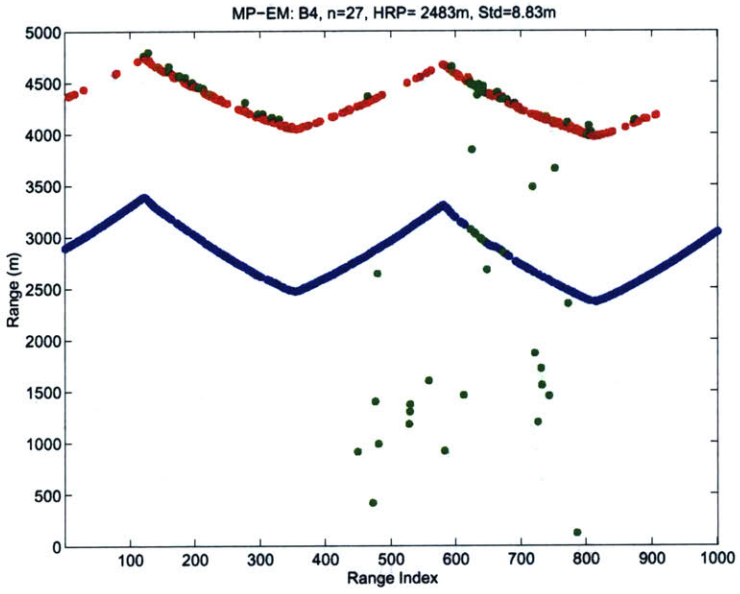

Figure 4-14: Classification plot for the last iteration of the EM algorithm. The probabilistic classifications are mapped to blue, red, and green for direct-path, multipath, and outliers

The algorithm terminates when the change in multipath parameters is sufficiently small. Figure 4-14 shows the final . In contrast to the initial classification in figure 4-12, the decreased multipath range variance identifies the consistent multipath data and excludes the outliers. Figure 4-15 illustrates the convergence of the algorithm by showing the sequence of parameter values. As the reflecting plane height decreases, the variance shrinks, creating increasingly conservative bounds on the observations associated with the multipath range. For this example the final values for the multipath model parameters are a reflecting plane height (d_0) of 2483m and a standard deviation (σ_{MP}) of 8.83 m - twice the standard deviation in the direct-path.

Normalizing and Incorporating a Uniform Distribution

This implementation of the EM algorithm is unique from the related work because of the application and because of the data model. In addition to the typical mixture of Gaussian distributions, the outlier portion of the model adds a uniform distribution to the model. This extension requires special attention to the normalization in Bayes rule. By examining the sensitivity to the normalization, this section explores the effect of adding the uniform distribution to the mixture-model identified through EM.

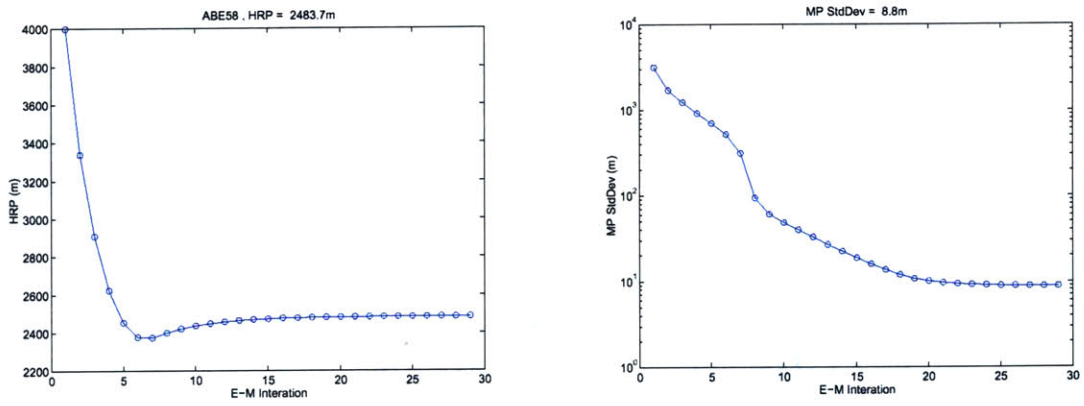

a b

Figure 4-15: Convergence of the model parameters.

A common criticism of Bayesian inference is the requirement of knowing the prior probabilities[5]. For application of the EM algorithm the prior probability of any observation being spurious is challenging to estimate without evidence. One solution is assumes the association probabilities to be mutually exclusive, $P(z|DP) + P(z|MP) + P(z|OL) = 1$. This is true when the algorithm converges, but the beginning stages of the algorithm must deal with ignorance. In the beginning stages, where model parameters are intentionally far from the 'true' values, the calculated probability of a measurement given this erroneous model ($P(z|MP)$ is falsely high. Enforcing the mutual exclusive constraint pushes the outlier association to zero. This low association leads to false confidence and the algorithm does not reliably converge. The challenge is to determine a value for $P(z|OL)$ that satisfies the need for a mutually exclusive final answer while encouraging convergence at intermediate stages.

A threshold, Pol, is introduced in the normalization of the probabilities. At each iteration and for each observation the following steps are taken:

- Calculate $P(z|DP)$ and $P(z|MP)$ for the current model.
- If $1 - P(z|DP) - P(z|MP) < Pol$, let $P(z|OL) = 1 - P(z|DP) - P(z|MP)$.
- If $1 - P(z|DP) - P(z|MP) > Pol$, use the threshold $P(z|OL) = Pol$.

Selecting this maximum value for the prior Pol is important. The normalization is key to the classification of the e-step and hence the identification of the m-step. This threshold is not related to the the empirical probability of an outlier, but is instead a parameter of the algorithm.

Figure 4-16 shows the influence of the threshold Pol on the operation and results of the EM algorithm. The upper axes, a and b, show how the final solution is affected by the parameter's value. The solution for the height of the reflecting plane is relatively unchanged; this physical value is

[5]This complication is subtle but powerful. There is a strong debate about the difference between the probability of belief and the probability of chance (frequency based) and the inference based on these notions of probability. See Dempster-Shafer [Shafer, 1976] and Jeffreys [Jeffreys, 1961].

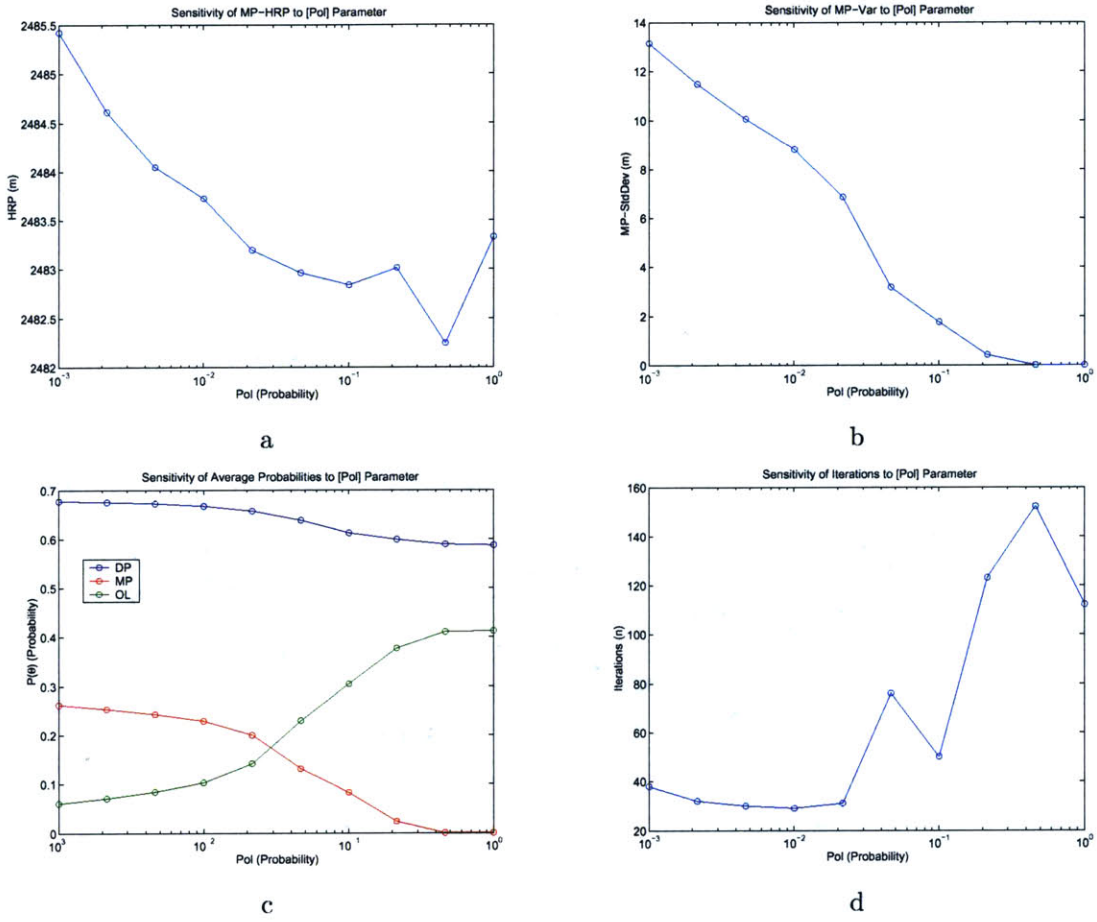

Figure 4-16: Sensitivity of algorithm results to the Pol parameter.

insensitive to changes in the arbitrary algorithm parameter. The variance in the multipath decreases as *Pol* increases because the more observations are considered outliers, fewer are considered to belong to the multipath, and the resulting classification yields multipath data that is more closely centered around the mean. Axis c in the figure shows how the average probabilities resulting for the algorithm are affected. As *Pol* is increased the algorithm tends to associate more data as outliers and less as direct-path and multipath. Finally the plot in axis d shows that as *Pol* increases the number of iterations required for the parameters to converge increases. When *Pol* exceeds 0.02 more iterations are necessary; below this threshold the number of iterations is consistent around 40. This indicates a discontinuity in the associations and a possible threshold for *Pol*. Below $Pol = 0.02$ the results are less sensitive to the actual value, indicating a stronger result, invariant to the parameter choice.

4.4.3 Multipath Identification Results

The previous example illustrates the EM algorithm applied to a limited subset of the measurements from one beacon used in ABE58. The same algorithm is applied to the whole 5,000 point dataset

from each of the four transponders. The results, summarized in table 4.2 and shown graphically in figure 4-17, specify the four multipath models by determining the height of the reflecting plane (HRP) relative to each beacon and the variance in the acoustic measurements. The final row of the table lists the recorded beacon depths which agree with the HRP determined by the EM algorithm. These results shows that the multipath data is the result of the acoustic signal reflecting off the air-water interface on either the outgoing or incoming path and traveling the line-of-sight path in the other direction - the triangle path in figure 4-8.

Beacon #	1	2	3	4
HRP (m)	2392	2500	2404	2486
$\hat{\sigma}_{MP}$ (m)	4.2	10.5	14.0	6.9
Beacon Depth(m)	2392	2491	2395	2472

Table 4.2: Multipath Model

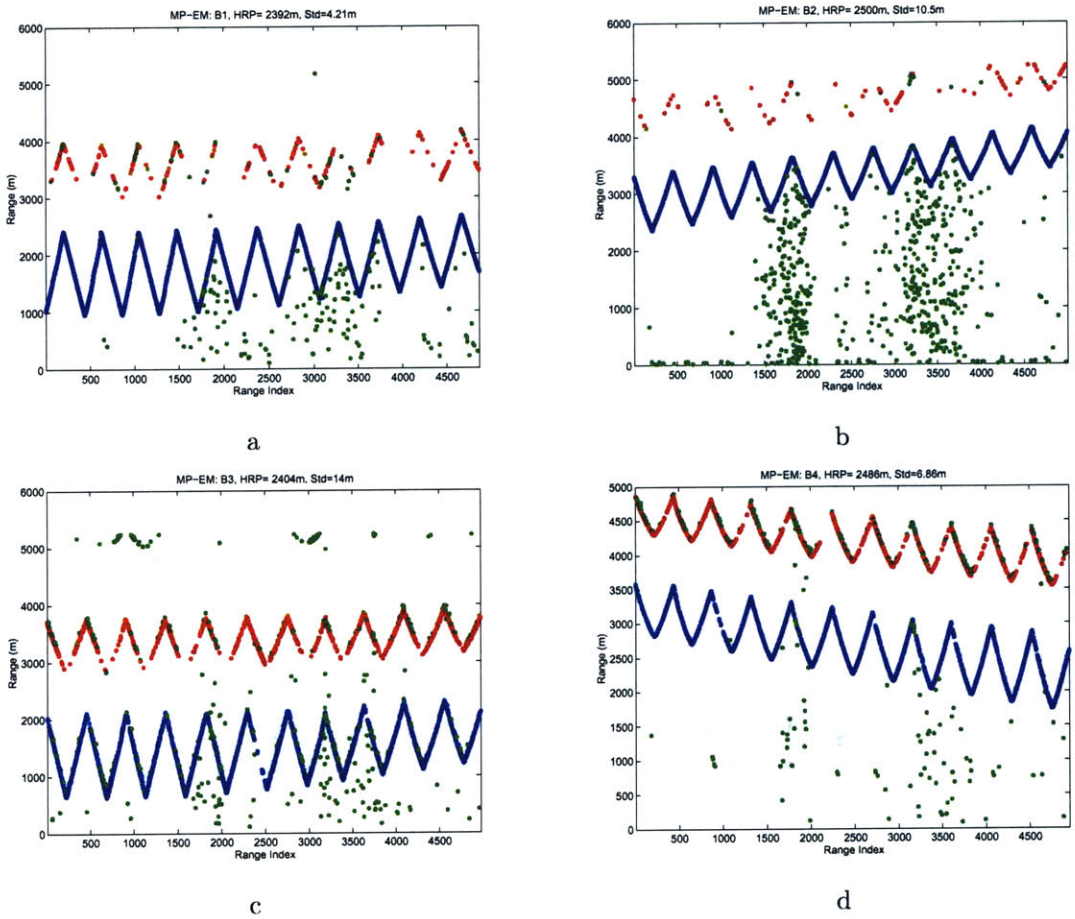

Figure 4-17: Results of multipath identification using expectation-maximization. The parameter values of the classification are summarized in table 4.2 and the colormap is illustrated in figure 4-13.

Summary: MP with EM

This application of the EM algorithm has some important restrictions. Since the implementation is batch, the entire dataset is treated at once rather than in real-time. The measurement model is a combination of two Gaussians and one uniform distribution - a fundamental assumption. The model also assumes a stable multipath environment amenable to the proposed ray-tracing model. A more complex model, capturing the physics of larger scale acoustic ranges, could be integrated into the EM algorithm. The new formulation would have a different vector of model parameters to change in the identification step (m-step). Finally, the algorithm is dependent on an independent estimated location associated with each range observation.

The product of the EM algorithm, the classification results, becomes the hypothesis grids of the next section. This technique is a system identification approach to dealing with acoustic multipath, i.e., physical parameters are identified. The alternative is to use an equalization approach where non-physical parameters, e.g., filter coefficients, are adapted to match the model to the data. This application extends the EM algorithm to a new domain and to a new type of problem by incorporating a uniform distribution. The multipath model and observation characterization are crucial to the ability to build a representation of the sensed environment- a hypothesis grid.

4.5 Representation: From Classification to Hypothesis Grids

The expectation-maximization algorithm yields an identification of the sensor model and a classification of the individual observations as summarized in the preceding section. To generate a compact environmental representation, the classifications are grouped based on their spatial location. For this example that grouping is based on a regular two-dimensional rectangular grid of the survey area. The observations are grouped into cells within the grid and the probabilistic associations are averaged for the members of the individual cells.

The individual measurement classification is shown in figure 4-18 where the reflecting plan heights are from the preceding section and a standard deviation of 20m is used for each of the three beacons. Using the same standard deviation is done for consistency and to adjust the amount of data classified as direct-path, multipath, or outliers. Continuing with the example, this section presents the steps in building the hypothesis grid for one beacon of the ABE58 survey. The grid is initialized based for a 5-by-5 mesh[6] containing the survey area. The classifications from the EM algorithm are associated with each cell in the grid to synthesize the three grids for beacon #3 - one for each hypothesis (DP, MP, OL). Evaluation of the proposed grid metrics justify the chosen grid spacing and illustrate the sensitivity of the results to this decision. This section concludes with the results of the 12 hypothesis grids for 4 beacons and 3 hypotheses.

Grid Initialization and Association

The grid representation sections the survey into rectangular regions. In two-dimensions this grid structure is a regularly spaced mesh in Cartesian coordinates. Figure 4-19 shows the particular grid

[6] A 5-by-5 mesh is a regular rectangular mesh with 5 cells on a side - 25 total cells.

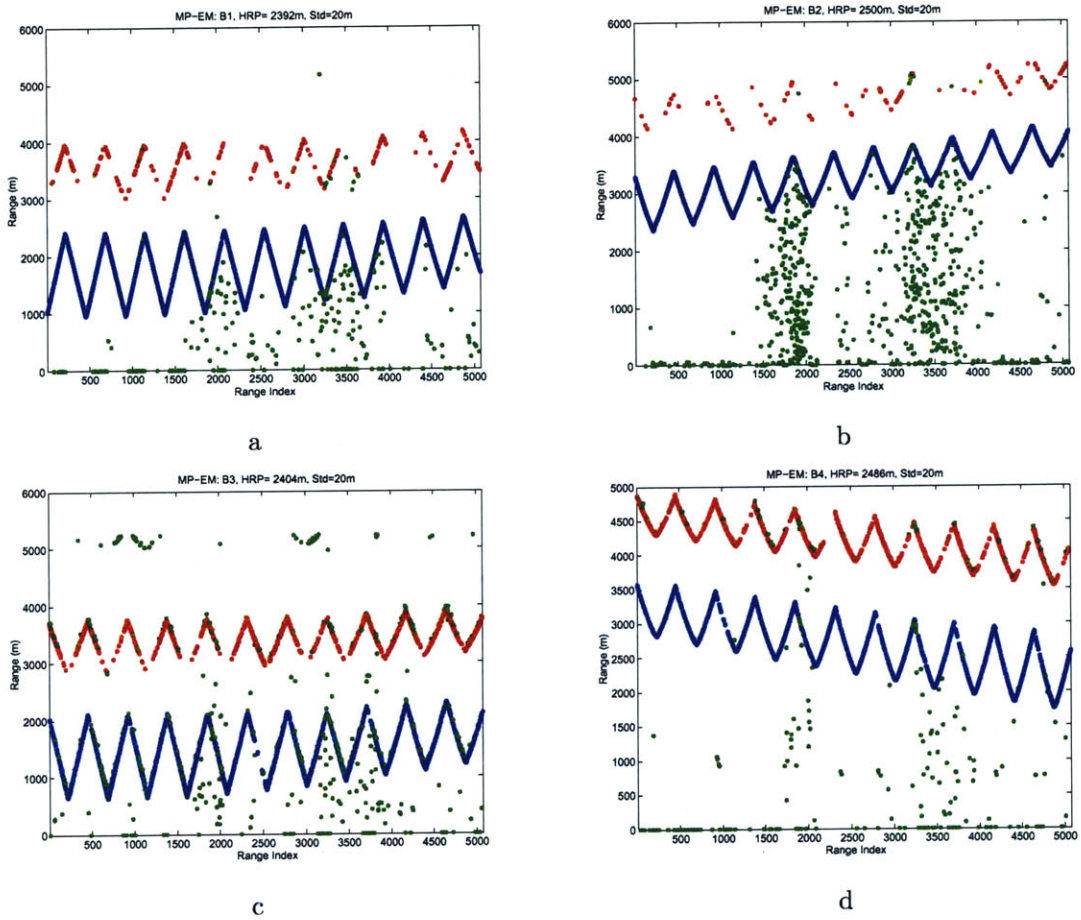

Figure 4-18: Results of multipath identification using expectation-maximization. Standard deviation in multipath is adjusted to 20m for all four beacons.

used for the ABE58 survey. The 5-by-5 representation is chosen, based on the metrics discussed below, to balance the consistency of the information within each cell. In addition to the grid mesh, initializing sets the grid boundaries. The ABE58 survey is roughy north-south so the grid is chosen to align with the cardinal directions: 9.2-10.7km east-west and 37.4-39.2km north-south.

For this example, the localization and classification are considered independent. This *does not* assume perfect navigation, but an uncertainty estimate of position and the estimate covariance. Each range observation is associated with a position estimate, connecting the observation with a particular cell in the grid. The algorithm sorts the observations into the cells of the hypothesis grid based on the uncertain position estimates. This is a simplified version of the cell membership.

4.5.1 Hypothesis Grids for ABE58 Survey, Beacon 3

Figures 4-20 and 4-21 are two visualizations of the hypothesis grid for beacon number 3 in ABE58. Mapping the probabilities to the blue-red-green from figure 4-13 illustrates the entire hypothesis grid in one plot. For this particular beacon the disparity between the northwest corner and the

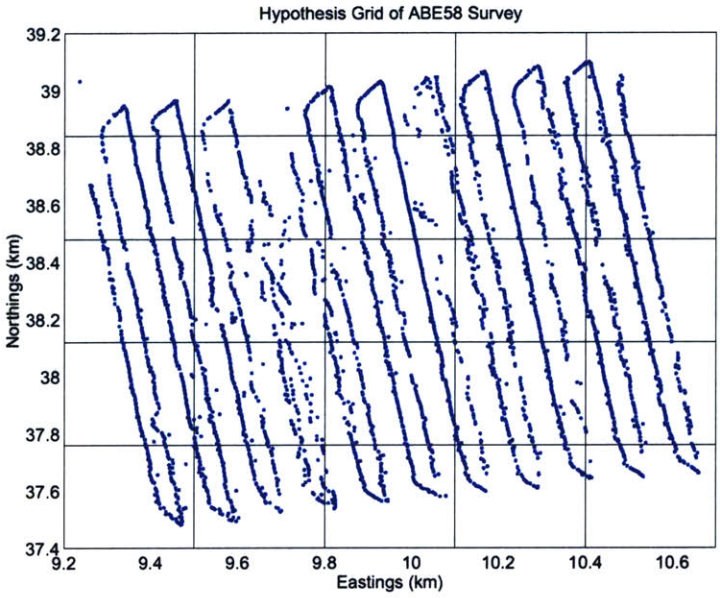

Figure 4-19: The hypothesis grid with the ABE58 survey positions.

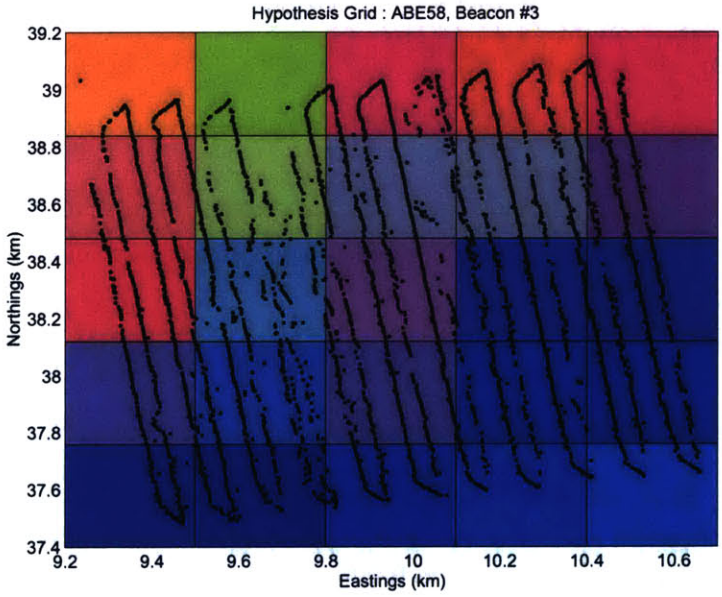

Figure 4-20: The hypothesis grid for beacon 3 with the ABE58 survey positions. The probabilistic associations are mapped into blue, red, and green for direct-path, multipath, and outlier. The small black markers indicate the post processed vehicle positions for reference.

southeast corner illustrates a satisfying spatial characterization of the sensed environment. In the southeast corner and along the southern row of the grid the blue color dominates indicating that most of the observations are associated with direct-path measurements. Figure 4-6 shows the placement of the beacon #3, in the south and east of the survey, and leads to the conclusion that

near the beacon the direct-path is more reliably available. In the northwest corner of the grid and along the north-most row the red colors dominate indicating an increased probability of observing a multipath return. Also in the north-most row is a grid cell that is particularly green indicating an increase probability of observing an outlier. The same hypothesis grid is illustrated numerically in figure 4-21; the actual probability values for each cell are listed. The same figures are presented for the other three beacons of ABE48 in appendix D.

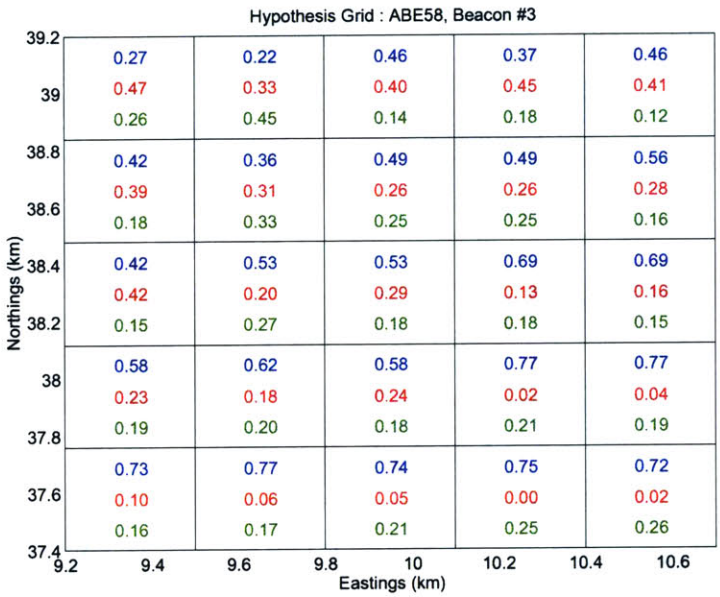

Figure 4-21: The hypothesis grid values for beacon 3. The numbers in each cell are the association probabilities for direct path (blue), multipath (red), and outlier (green).

4.5.2 Representation Evaluation: Grid Metrics

How many cells should there be in the grid representation and where should the grid-lines be drawn? For this example, the grid is assumed rectangular and evenly distributed. Using too fine a mesh reduces the number of observations associated with each cell - reducing the confidence in the resulting probability estimate. Using too course a mesh reduces the information by averaging properties of the environment. The tradeoff is articulated by considering the following metrics:

- Cell Count: The number of range measurements associated with each cell. A high cell count indicates a statistically significant result.
- Cell Variance: The disparity in association probabilities within a cell. A small variance indicates consistency in the estimate.
- Grid Variance or Grid Spread: The disparity in cell probabilities between the cells within the grid. A large disparity indicates a significant variation in the sensor characteristic with

estimator position across the survey area and the existence of an important determinant of sensor performance.

For the cell and grid variance metrics, the disparity is quantified by the standard deviation[7]. The standard deviation of the cell probabilities is calculated using a weighted variance where the cell count is used as a weighting, eliminating the under-sampled cells. The grid spread is the range between the maximum and minimum cell probabilities. A threshold is used to make sure that the spread is calculated with cells that contain a sufficient number of observations, because as the cells in the grid become smaller some, especially in the corners, contain very few data points.

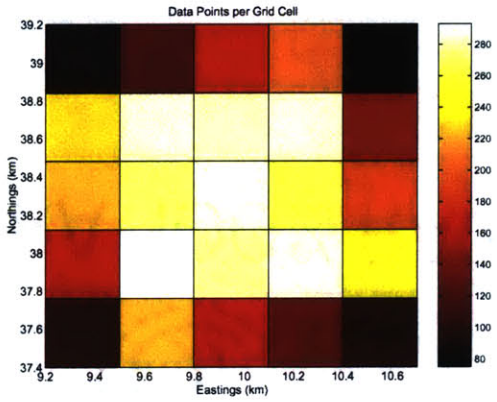

Figure 4-22: Illustration of the membership of the cells in the 2-D hypothesis grids. The values and the colormap range from 75-293.

The finest grid would only contain one measurement and there would be no disparity between data-points - the cell variance and grid variance metrics would indicate a satisfactory grid resolution; however, fewer data points are included, causing less confidence in the resulting answer. The three metrics are used to quantify the tradeoff between significance and information content. Figure 4-22 shows the distribution of cell count for the ABE58 5-by-5 grid. Figure 4-23a shows the exponential decrease in the observations per cell metric as the number of cells increases. With finer resolution the consistency within cells increases, as measured by the cell probability standard deviation. The tradeoff is to decrease the grid resolution to achieve consistency, but to maintain cells large enough to be significant. Figure 4-23b shows how the variance within the cell decreases with the number of cells. The dependency is not strong, the consistency of the clustering is fairly insensitive to increasing the resolution.

Another metric for evaluating the cellular representation is the variation in the cell values across the grid - shown in figure 4-24. A map containing cells of all the same value relays no information, i.e., the probabilities are spatially invariant. A map with a large disparity between regions conveys important information. The disparity between the cells within the Hgrid is measured two ways: by the variance in the probabilities and by the difference between the minimum and maximum values across the grid - the spread.

[7]The variance is measured as the maximum likelihood estimator for a normal distribution. There is no reason to expect a normal distribution, but the results are not dependent on that restriction

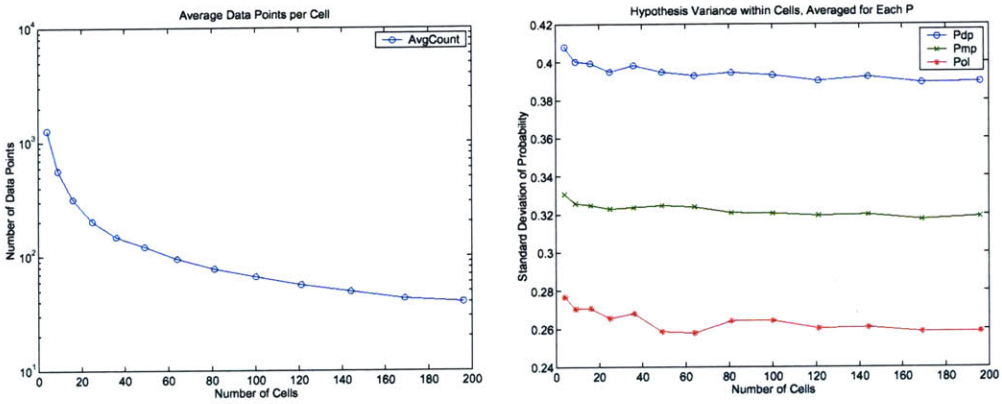

Figure 4-23: a) Shows the reduction in data points per cell as the grid resolution is increased. b) Shows the variety in individual cells, averaged for the grid.

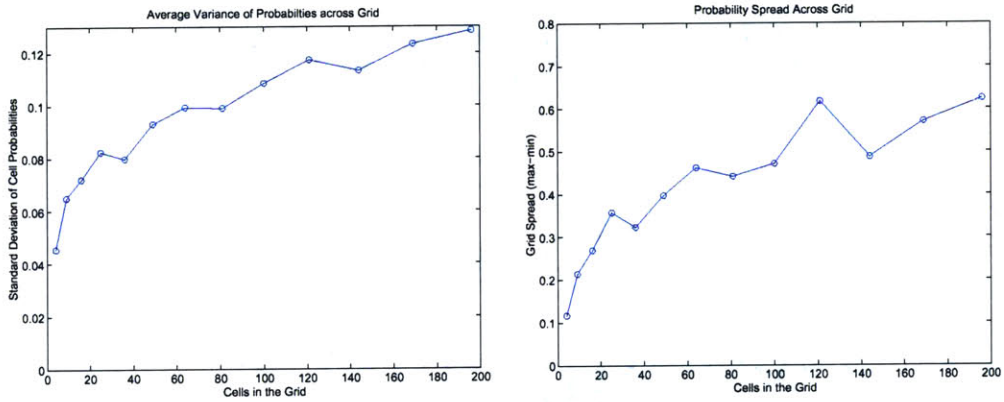

Figure 4-24: Two ways of looking at the variation in cell values

These metrics are the basis for choosing the 25 cell, 5-by-5 grid of this example. Other, more detailed, plots of these metrics are included in appendix D.1 for completeness.

4.5.3 Summary and Results

The boxplots of figure 4-25 summarize the prior probability values across the four beacons and for each of the three association hypotheses. The grid-based representations for each beacon are available in appendix D.2. Examining these results, one can imagine how a human operator would make use of the information - minimizing time spent in particular regions were direct-path information is scarce or using multipath information were the maps indicate a tendency for multipath returns. Hypothesis grids provide a representation for an autonomous platform to use this information for managing sensing and control.

This section illustrates how the observation classification is combined with position estimates to represent the acoustic ranging environment. The results illustrate the application and the feasi-

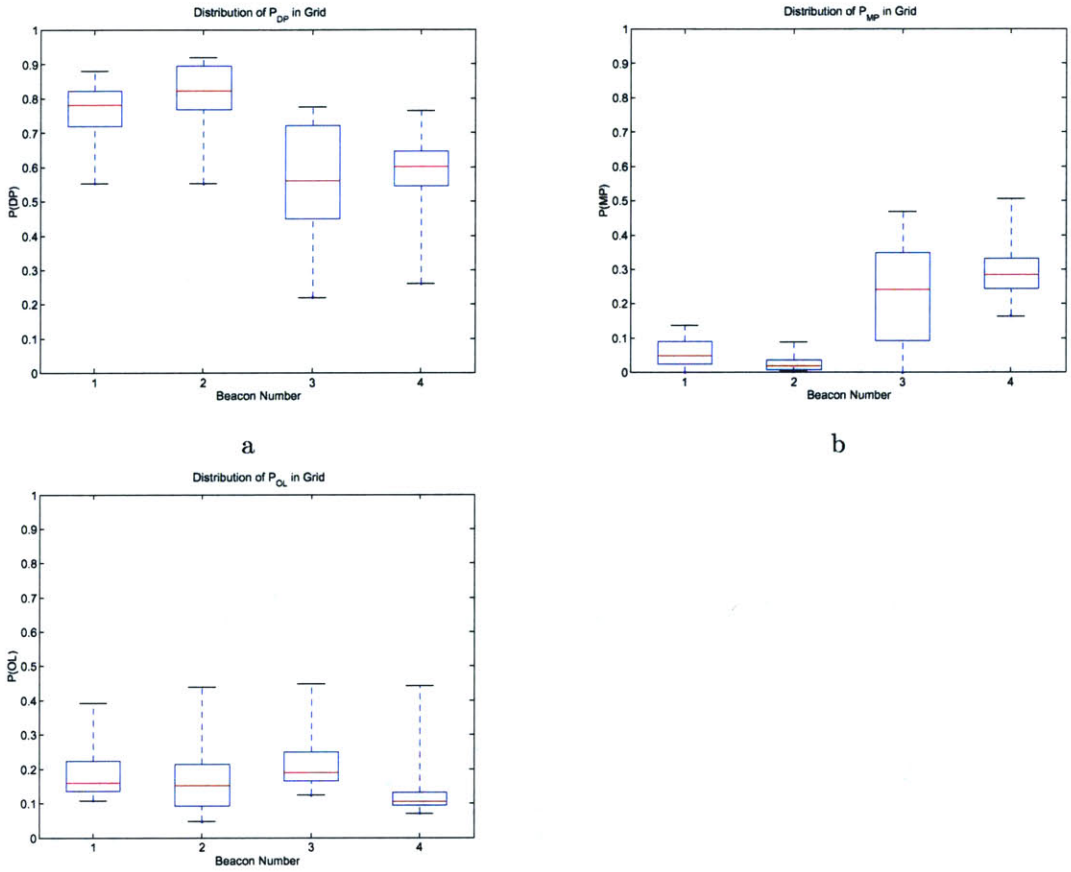

Figure 4-25: Boxplots summarizing the hypothesis grids for each of the 4 beacons and for the 3 hypotheses. The box has lines at the lower quartile, the median, and the upper quartile values of prior probability assigned to the cells in the respective grids. The whiskers, lines extending form each end of the box, show the extent of the rest of the data.

bility for one particular case - the ABE58 LBL survey.

4.6 Conclusion: Feasibility, Utility, and Future Work

Hypothesis grids capture one aspect of range sensor operation and provide a representation of the sensed environment appropriate for autonomous navigation. This chapter develops the concept of hypothesis grid representation and provides an illustrative example of the technique. Simplifications employed to limit the scope of the development focus the treatment on the key contributions: mixed-distribution model of range measurements, classification and identification using expectation-maximization, and representation of an instrumented acoustic environment.

Feasibility

Hypothesis grids are predicated on the spatial dependence of range sensing - that there are regions in a survey area that exhibit particular behaviors, and this relationship can be quantified probabilistically. Empirical evidence supports the notion that there are positions where ranges are reported reliably and other locations where observations are in large part spurious, sections of the survey where the observations measure the line-of-sight path and regions dominated by multipath returns. This chapter illustrates the feasibility of quantifying this intuition in a form appropriate for autonomous operation.

The hypothesis grids for the ABE58 survey illustrate two dimensions of the feasibility. Primarily they illustrate a method for modeling, classification, and representation that captures the sensor's spatial dependency. It is important to challenge the simplifications employed in the example, the batch-processing and independent localization, but the method illustrates the potential of capturing the sensor behavior with a coarse grid representation. The feasibility is also dependent on the presence of a spatial dependency. For this particular case, the grid metrics in section 4.5.2 and hypothesis grid representation show sufficient disparity between locations to prove the importance of capturing the dependence.

Utility

Hypothesis grids are also predicated on the concept of prior probabilities and their importance for probabilistic navigation methods. Bayesian techniques employ prior probabilities that are typically difficult to estimate and lead to complications. By explicitly modeling the prior probabilities, hypothesis grids operate along-side estimation and navigation techniques, forming a base layer of information for higher level algorithms. For example, multiple hypothesis tracking (MHT) uses Bayes rule to maintain many estimators in parallel. Each estimator uses the prior association probabilities in determining correspondence. A more accurate map of these priorities would enable more accurate correspondence and better tracking.

In addition to adding accuracy to general navigation techniques, hypothesis grids extend the capabilities of autonomous survey. Exploration algorithms couple robot motion to the resulting uncertainty. Sensor management employs active sensor control to reduce uncertainty. Hypothesis grids are useful for both types of algorithms because they provide the environmental information to coordinate the survey path or beacon selection (see section 3.5).

Future Work

This investigation has uncovered more questions than it has answered. Four areas categorize the future work: methods for removing the simplifications, extensions of the hypothesis grid concept, building navigation techniques on the capabilities of hypothesis grids, and future investigations into the capabilities of the method.

Examining Simplifications

Simplifying this development focuses the work but restricts the results. Treating localization and association separately limits how and when hypothesis grids can be synthesized. Since the algorithm assumes an estimate of position, associating range observations with possible sources and then aggregating the associations into cells is batch processed off-line. Concurrently estimating position and building a sensor map in real-time is a challenge.

Another approach is to examine the implementation of hypothesis grids into the overall mission profile, making a procedural method out of what this chapter demonstrates. The tradeoff between processing in real-time and off-line needs to be understood as the technique is implemented. One possibility is explored in the USS Monitor survey plan of chapter 5.

Extensions

Investigating the representation and inference methods are useful extensions. The method is not specific to the 2-D rectangular grids used in the preceding example. A third dimension could be added to the spatial representation for surveys where the sensor operation is suspected to be depth dependent. Using the grid structure to sort the observations is a function parameterized by cell dimensions. More general representations might use clustering techniques[8] to segment the space in some optimal way. Other functional approximations such as parameterized basis functions might make better use of the inherent characteristics of range sensors.

Besides expanding the methods for representing the spatial dependence, hypothesis grids can be extended to capture the relationship between sensor behavior and other independent variables. The quality of range observations may be dependent on platform velocity or survey direction, on ocean currents, or a myriad of other possibilities.

The basic premise of the hypothesis grid algorithm is applicable to a variety challenges beyond underwater acoustic range observation. Characterizing the sensed environment based on empirical evidence is useful for applications where robots repeatedly visit the same location. The method of deep-sea archaeology provides the opportunity through repeated investigations of the same site. As autonomous systems become more prevalent they will be used repeatedly in certain environments. Methods for capturing the qualities of those sensed worlds, methods of environmental awareness, will be increasingly useful.

Representing ignorance in the Bayesian formulation of expectation-maximization is a shortcoming. Initial conditions are unknown; this lack of certainty is not accurately represented in Bayesian inference. Dempster-Shafer evidence theory [Shafer, 1976] offers an alternative by explicitly representing ignorance and developing a method of inferring conclusions based on incorporating evidence. This method is an attractive alternative because of its robustness to initial conditions.

[8] For example clustering techniques are used in image processing and dynamic modeling [Anderberg, 1973].

Increasing Navigation Capabilities

In addition to adding accuracy to general navigation techniques, hypothesis grids also provide a representation appropriate for autonomous navigation. Autonomous vehicles are at the convergence of control and navigation. Exploration, optimal survey, sensor management, and active perception algorithms could all utilize the prior sensor map to make autonomous decisions. A map of the sensor characteristics links the spatial domain of control with the probabilistic estimation domain of navigation. Hypothesis grids are a representation that enables making control decisions (where to go next) based on navigation goals (decreasing uncertainty). Conversely, navigation decisions (what sensor to use next) can be made based on the anticipated information gain.

Challenging the Assumptions

The multipath model is fundamental to building the representation. Future work should examine the applicability of the simple geometric ray model for small-scale environments. The model produces consistent results in this example, but the details need dedicated basic experiments. The results from the simple single reflecting plane capture the observed phenomena, but the physical mechanics are not clear. A deeper understanding of this fundamental characterization of the acoustic environment would strengthen a vehicles ability to navigate in complex multipath environments.

The homogenous acoustic medium assumption needs challenging. Experience reinforces this conclusion on sites on the 100m scale, and ocean acoustics shows the assumption to be limited on larger scales, but the transition between small and large scale environments should be illuminated. As the range of precision positioning sensors increases, this limit becomes binding. A general quantification of the acoustic channel for precision positioning is an open and interesting research question.

Chapter 5

Proof of Concept: Imaging Survey of the USS Monitor

> This is logical enough: but real life is bigger than logic.
> - E. F. Schumacher[1]

Planning the autonomous survey of the USS Monitor is an opportunity to illustrate the design methods of this thesis and to build a mission around hypothesis grid navigation. This chapter presents a four step method for creating a survey that draws on the preceding discussions. First, a classification of the mission frames the problem based on the imaging goals, the USS Monitor wreck site environment, and the SeaBED AUV platform. Second, a specification connects the imaging goals with the physical parameters of the navigation and survey design. The proposed AUV mission extends over multiple dives to generate a hypothesis grid representation of the acoustic environment. Third, analysis articulates the key design tradeoffs of real-time guidance, off-line navigation, beacon configuration, and heading measurement. And fourth, the conclusion discusses the sensitivity of these decisions to environmental uncertainties. The chapter is the engineering application of the scientific understanding developed in the previous two chapters.

Chapter Goals

- Classify the proposed USS Monitor survey based on the mission goals, environment, and platform.
- Connect the imaging requirements with a navigation design and survey plan through application of the precision specification.
- Illustrate the key design tradeoffs: beacon configuration, host configuration, real-time versus. off-line processing, etc.
- Propose a mission plan, including multiple dives, to characterize the environment using the hypothesis grid algorithm.

[1] E. F. Shumacher, *Small is Beautiful, Economics As If People Mattered* (Harper Collins, 1989).

5.1 Deep-Sea Archaeology on the USS Monitor

Like all archaeological sites, the resting place of the USS Monitor is evolving under the influence of natural and human forces. For over a century, between her sinking on New Year's Eve 1862 and her discovery in 1973, time has eroded the ship's condition. Since coming to rest on the sandy bottom seventeen miles off Cape Hatteras, the converging ocean currents washed over her exposed hull, corroding the ironclad and threatening her structural stability. Since the identification of the wreck, archaeologists have pursued an accelerated pace of recovery in a race against time to preserve and manage the history. Her anchor was recovered in 1983 and the propeller in 1998. In 2001 an ambitious salvage project raised the Monitor's unique vibrating side-lever steam engine, and in 2002 the famous turret was brought to the surface with the two 11-inch Dahlgren guns.

What is left on the sea-floor is not only an artifact from the civil war, but a history of archaeology as well. The Monitor stands as a symbol of technological change between steam and sail, between shell and shot, and between sailor and seamen. It is appropriate that this site be one of the first to implement a new type of archaeology, a new type of exploration. Explorers operate insulated from the extreme environment and in cooperation with machines to extend their perception in new ways. Scientists challenged to work remotely , satisfying curiosity through a relationship with autonomous machines.

This wreck will eventually decompose completely, but selective preservation and documentation will save the historical information. Researchers began documenting the site shortly after the discovery creating a record of its deterioration from natural and human activities. The site is now protected by NOAA's Monitor National Marine Sanctuary. As part of the management responsibility, an AUV survey is proposed to further document the current state of the USS Monitor.

5.1.1 Mission Classification

The first stage of the proposed method of survey design is to classify the expedition by examining the *goals*, *environment*, and *platform*. The investigation intends to produce both archaeological and engineering results by surveying the USS Monitor wreck site using the SeaBED AUV.

Mission Goals

The science and engineering focus on precise imaging. The mission aims to produce high-resolution imagery of the USS Monitor wreck site and advance the technology for precision navigation. The following specific goals drive the navigation and survey plan:

- Archaeological imaging: Produce a co-registered photographic and microbathymetric survey of the USS Monitor site - the wreck and surrounding debris field.
- Environment characterization: Survey the instrumented environment and model the sensor operation using hypothesis grids.
- Navigation development: Provide a fixed-reference survey data-set for research on image based navigation techniques.

Survey Environment

The environment cannot be completely quantified, but critical aspects of the survey site drive the survey and navigation design. The USS Monitor sits 17 miles off Cape Hatteras, North Carolina, on a sandy bottom 80 meters below the surface. Known as the 'graveyard of the Atlantic', the converging ocean currents and weather patterns are a challenging environment. The following table lists the key aspects of the survey site and the corresponding survey parameters that depend on these qualities.

Environmental Aspect	Survey Parameters
Current strength	Survey plan
Acoustic environment	Beacon configuration and sensor management
Three-dimensional site structure	Guidance requirement
Magnetic signature	Heading reference
Visibility	Optical survey height

Table 5.1: Important environmental for the USS Monitor survey

Autonomous Platform

The SeaBED AUV is designed for precision survey. The vehicle is passively stable in pitch and roll to provide a stable imaging platform, and has actuation in all three cardinal directions for station keeping and performing near zero velocity surveys. The sensor suite, described in figure 5-2 and illustrated in figure 5-1, enable a variety of navigation options. SeaBED's computational capacity and software base make complex algorithms and new hardware integration possible.

5.2 Mission Plan

To combat uncertainties about the operating environment and to build evidence for creating hypothesis grid representations, this section proposes a two stage mission plan. The initial short-duration survey probes the environment, allowing iterative planning and instrumentation deployment. The later surveys record the optical and acoustic data with precision navigation reference to accomplish the mission goals. In both cases, the precision specification outlined in chapter 3 translates the survey requirements to design parameters. Figure 5-3 shows this two stage survey plan.

The first survey is a coarse survey, taking little time to execute, delivering important information about the site. For guidance the AUV relies on DVL position estimates while logging acoustic range observations for off-line re-navigation. To locate the site acoustic ranges must be integrated into the real-time navigation and guidance solution. Because the individual dives are short, the system is adapted to prepare for the fine resolution survey. Probing of the environment will answer uncertainties about the ability of DVL-based guidance, heading error, and the acoustic environment while acquiring preliminary data for photomosaicing.

To accomplish the precision goals, the system is adaptable to information from the initial experiments: the survey orientation can be modified to reduce underwater current effects, the

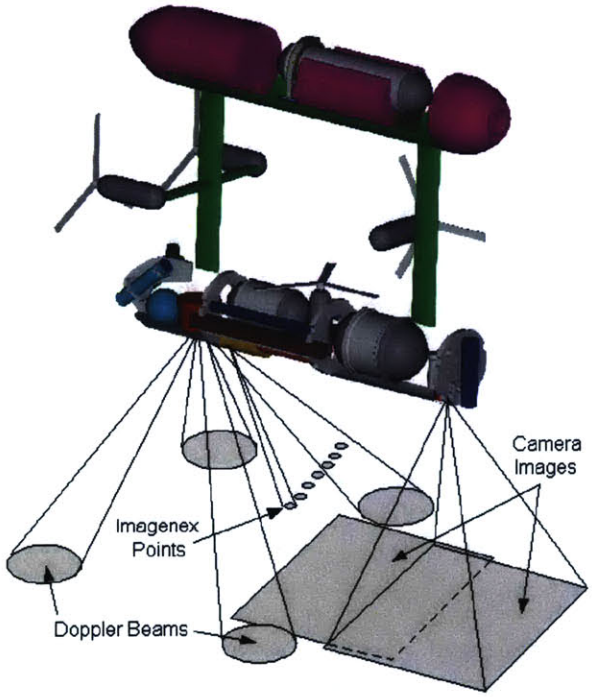

Figure 5-1: The SeaBED imaging AUV (courtesy of DSL/WHOI).

Table 1: SeaBED Vehicle Characteristics

Vehicle	Depth Capability	2000 m
	Size	2.0m(L), 1.5m(H),
	Mass	200 kg in air
	Speed Range	(Typical) 0-1.5m/s (1.0m/s)
	Batteries	2kWh rechargeable Li-ion Pack
	Propulsion	Four DC thrusters Fore 100N Lateral 50N Vertical 50N
Navigation and Attitude	Attitude & Heading Depth Position Altitude	Crossbow AHRS Paroscientific pressure sensor, 0.01% LBL+ 300 kHz RDI navigator, 0.1-1 m RDI navigator, 0.1 m
Optical Imaging	Electronic Camera Lighting Separation	Pixelfly 12bit 1280x1024 bw CCD one 200 Watt-second strobe 1m from Camera to light
Acoustic Imaging	Sidescan sonar	MST 300 kHz (300 m depth capability)
Other Sensors	CTD ADCP	Seabird 37SBI 300 kHz RDI navigator

Figure 5-2: Specification of SeaBED Imaging AUV (courtesy of DSL/WHOI).

beacons locations can be changed, the range observations can be included in the real-time guidance,

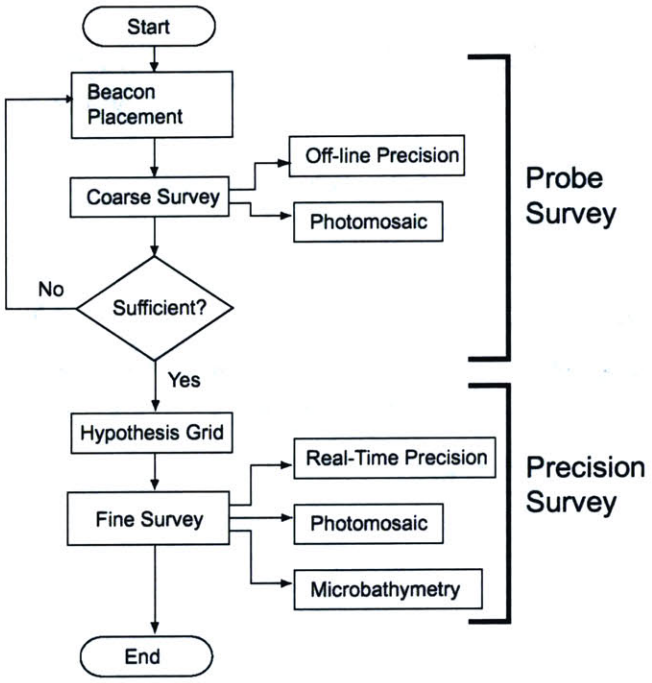

Figure 5-3: Two Stage mission plan

hypothesis grids can be used to enable adaptive and precise survey, and heading sensor options can be implemented. To accomplish the requisite survey coverage, precision range measurements will be fully integrated into the real-time guidance. This survey will be lengthy with little operator feedback during the dive, so acquiring as much information as possible about the site is important. The following sections specify the navigation and survey solutions for both stages of the mission.

5.2.1 Probe Survey Specification

The first surveys will be short dives to explore the sensed environment and to build photomosaic images. The footprint of the still camera determines the 1m trackline spacing and the survey speed of approximately 1 m/s is a reasonable and efficient speed for the vehicle.

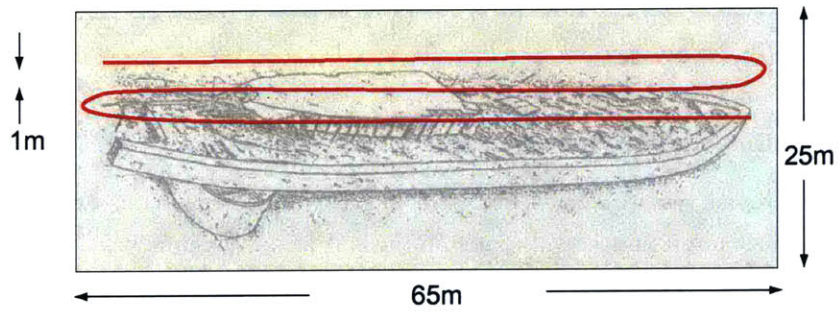

Figure 5-4: Track-lines superimposed on USS Monitor site plan

Figure 5-4 shows three track-lines over the rectangular 65x25m survey area. The vehicle path

shown is along the wreck, from stem to stern, but could also consist of tracks across the site, or a combination of both. The survey height is an important determinant. Still camera operation and vehicle safety dictate a nominal survey height of 2m. SeaBED will maintain this constant height through terrain following behavior as it traverses the wreck. This rough conception of the survey is refined through detailed consideration of the imaging sensors and the goals of the mission.

Still Camera

The SeaBED AUV is equipped with a PixelFly[2] digital still camera for creating photomosaics. The footprint of the camera's image and the desired overlap determine the track-line spacing of the survey. The update rate of the camera is sufficiently fast that the vehicles survey speed is not limited by successive frames.

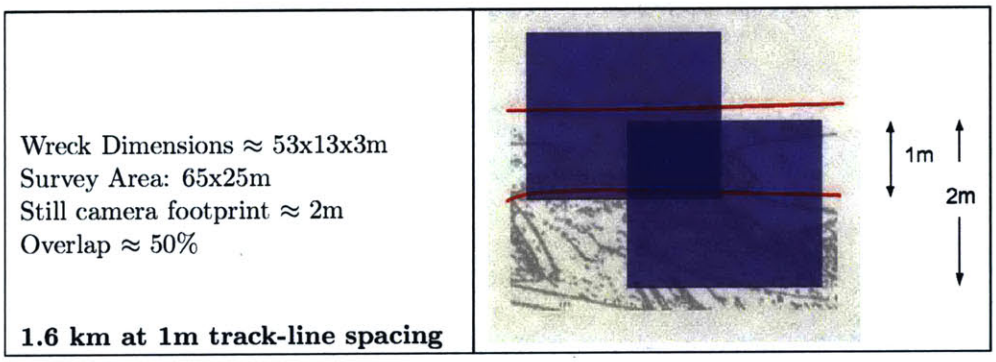

Figure 5-5: Consecutive track-lines over the wreck site. The footprint of the still camera is shown to illustrate the desired overlap for mosaicing.

Specifications	Function of...	Value
Survey area	Environment	65x25m
Track-line spacing	Camera footprint	1m
Vehicle speed	Vehicle	1 m/s
Survey height	Camera, vehicle, visibility	≈ 2m
Total survey length	Area and Spacing	1.6km
Total survey time	Area, spacing, speed	30 minutes

Table 5.2: Probe Survey Specification

5.2.2 Precision Survey Specification

Each of the probe surveys produces 1600 still images, 18,000 range observations[3], and feedback about the navigation and mission solution. At the end of this stage issues about current, heading, acoustic observations, and survey height will be resolved enabling the next stage of the mission - the precision microbathymetric survey.

[2]PixelFly high-resolution digital camera from The Cooke Corporation.

[3]The restricted site dimensions allow a fast update rate - 10 Hz. This will provide acoustic range observations every 20 cm from each of two beacons.

Scanning Sonar

Imagenex Scanning Sonar:
Beam width: 0.03 radians
Footprint: 6cm diameter at 2m
Scanning Speed:

Sector scans: 60°in 1s
Vehicle Velocity = 3.0 cm/s

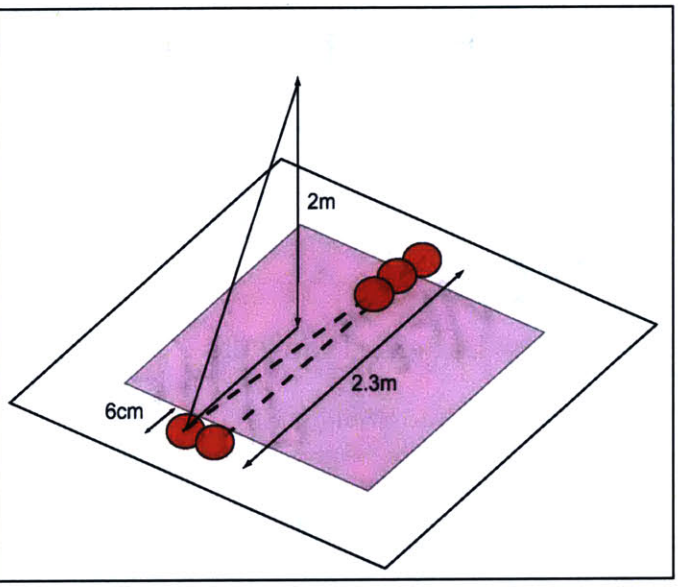

Figure 5-6: Shows the operation of the scanning sonar. The red circles represent the footprint of the acoustic beam. The purple square indicates the footprint of the still camera. To mosaic the acoustic image, individual observations must be overlapped.

The SeaBED AUV is also equipped with an Imagenex 675kHz pencil-beam scanning sonar. The canonical point-sensor model from section 3.2.2 is an appropriate abstraction for this sensor [4]. The mosaicing of the sensor not only drives the vehicle survey speed and real-time guidance requirement. For a 2m survey height the sonar footprint is approximately 6cm. Each sweep of 60°takes approximately 1 second - a back-and-forth scan takes 2 seconds. To achieve the 50% overlap specified for the photo survey, the vehicle would have to move at 1.5 cm/s and the 1.6 km survey would take 30 hours. A more reasonable approach would be to specify full coverage with no overlap between successive scans, a survey that takes 15 hours at 3 cm/s. This duration still exceeds the 10 hour duration of SeaBED. Because of the fixed-reference navigation, the total survey can be spread over two dives, each 8 hours long. Each dive will cover the total site at 6 cm/s and the two dives can be mosaiced together to achieve the desired resolution.

Specifications	Function of...	Value
Survey area	Environment	65x25m
Track-line spacing	Camera	1m
Vehicle speed	Scanning sonar	3 cm/s
Survey height	Camera and vehicle	2m
Total survey length	Area and Spacing	1.6km
Total survey time	Area, spacing, speed	15 hours (two 8 hour dives)

Table 5.3: Precision Survey Specification

[4]Singh et al. models the sonar specifically as a 1.7°cone - 5cm diameter footprint [Singh et al., 2000b]

5.2.3 Conclusion

The survey plan of this section covers multiple days, multiple dives, and multiple configurations. Intentional iteration allows for the solution to deal robustly with uncertainties in the environment and the navigation solution. Because the operation uses fixed, precise, acoustic beacons the data from each dive will be seamless, allowing baseline evaluation and future research on navigation techniques. The variety of sensors, for both navigation and imaging, provides a diverse set of data that will be archaeologically important and useful for continued development in precision navigation development.

5.3 Key Design Tradeoffs

5.3.1 Real-Time Navigation

What precision is necessary to execute the surveys, and what precision is necessary to produce the image product? The answer determines what sensory data is processed in real-time and what data is considered off-line. Incorporating range observations in real-time incurs a time cost; it takes time to integrate and test the vehicle navigation software. Quantifying the precision requirement enables making this tradeoff.

Incorporating range observations in real-time accomplishes two things: it bounds the error accumulation and it enables repeatable site location. Real-time specification demands a dynamic concept of uncertainty - error accumulation due to velocity and heading uncertainties.

$$\sigma_{position} = \sigma_{velocity}\sqrt{t} + \sigma_{heading}(d)$$

The error accumulation model in equation 5.3.1 shows how velocity uncertainty ($\sigma_{velocity}$) and heading uncertainty ($\sigma_{heading}$) contribute to the overall position error. The first term on the right-hand side is the random walk contribution accumulating as velocity is integrated to estimate position. The second term is the contribution from heading error dependent on the distance traveled (d).

The scanning sonar and camera each place a constraint on the error growth. The mosaicing of each sensor demand that the uncertainty between adjacent scans be less than the overlap. This constraint ensures that the real-time guidance achieves the desired overlap. The distance traveled between microbathymetry scans is small ($\approx$ 3cm). Therefore, the binding constraint is that of the camera overlap - images must overlap on successive traverses of the wreck.

Substituting the survey parameters predicts the real-time error accumulated between images. For successful overlap, the vehicle must be capable of estimating its position, relative to the same portion of the previous trackline, with an uncertainty sufficiently low to guarantee image coverage. This analysis assumes the vehicle's control is adequate and does not limit the guidance error. The important survey parameters are the maximum length between mosaiced images (130m for two traverses of the site), the velocity measurement standard deviation (3mm/s), the heading standard deviation (ranging from 0.01 to 0.5°), and the vehicle speed (ranging from 0.005 to 1.0 m/s).

Figure 5-7 illustrates the implementation of equation 5.3.1 using these survey parameters. The

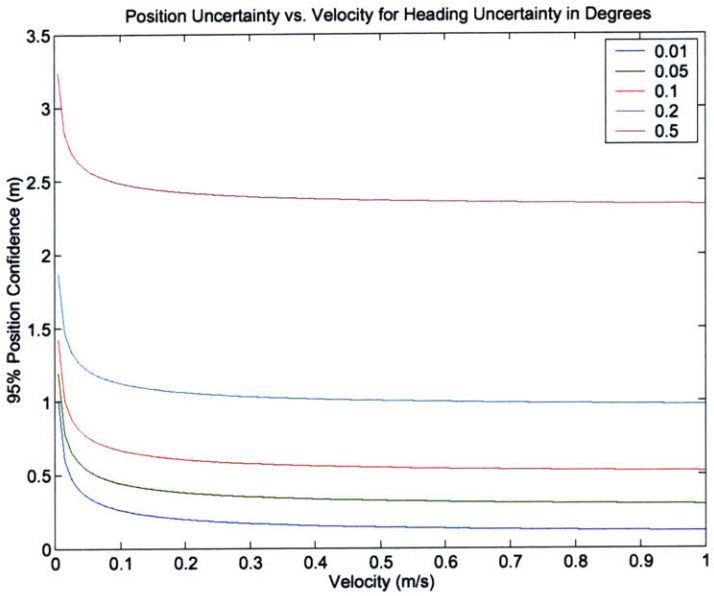

Figure 5-7: The predicted position uncertainty for a range of vehicle velocities and heading uncertainties. Each curve in the plot is for a value of heading uncertainty (standard deviation) listed in the legend in degrees.

position uncertainty metric is the 95% confidence interval - two standard deviations.

The conclusion is that off-line re-navigation is sufficient for the probing surveys, but the requirements of the precise survey require the navigation and guidance to incorporate the range observations in real-time. Assuming an accurate heading reference with 0.1°uncertainty (standard deviation), the red curve in figure 5-7 shows the slow probing survey capable of maintaining its overlap +/-0.5m. For the second phase, a slow precise survey, the uncertainty increases to an unacceptable level of approximately +/-1.0m. The overall mission plan supports this two level approach; the first stage will log precision ranges for off-line re-navigation, and the precision stage will incorporate those measurements into the real-time positioning and guidance.

Beacon Configuration

Figure 5-8 shows proposed beacon configuration and the anticipated positioning uncertainty. The two beacons solution is a compromise between precision, logistical cost, and reliability based on the articulation in section 3.4.3. The precision resulting from using two beacons is not appreciably worse than for the three beacon configuration, but is considerably greater than the singe beacon case. The size of the site is sufficiently small to be adequately covered by just two beacons with 100m range. The data from multiple site surveys must be overlayed, precluding the use of single transponder navigation because of the rotational ambiguity. Using multiple acoustic elements adds redundancy to combat the uncertainty in the acoustic environment.

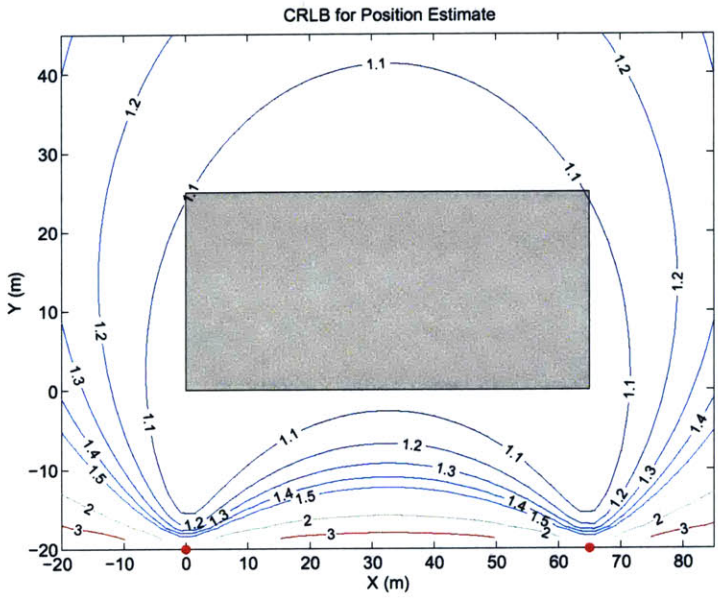

Figure 5-8: CRLB for proposed monitor survey. The survey area (65x25m) is shown as the grey rectangle. The contour lines are the positioning uncertainty bound, standard deviation, in centimeters. Assumes range standard deviation equal to 1cm.

The placement of the acoustic network, relative to the survey site, is also important. The baseline is separated from the wreck so that the tracklines will be executed where the positioning precision is greatest. The site is longer than it is wide (65x25m), so the transponders are placed along the long axis to maximize the length of the baseline (the axes in figure 5-8 are not square so the aspect ratio is distorted). This extends the coverage and leads to geometry that benefits the precision.

Heading

An important consideration for this expedition is determining heading. Because of the amount of iron on the site, the magnetic north seeking heading instruments may require a complimentary heading reference from acoustic range measurements to multiple acoustic antennas on the vehicle. The axes in figure 5-9 illustrates the ability of determining heading from range measurements. By using two host transponders, fore and aft on the 2m vehicle, the difference in range measures the orientation relative to the beacons. Extending the CRLB to understand the capability, the contours in the figure show the heading uncertainty in degrees. In figure 5-9a the heading error for SeaBED moving along the long axis of the site shows this error to be approximately 1°. In figure 5-9b the same analysis yields the uncertainty when the vehicle is oriented north-south, when it is turning between tracklines. Multiple precise range observations from a single platform allows determination of heading, but for the specific case explored in this section, with an on-vehicle baseline of 2 meters, the solutions provides relatively course heading accuracy.

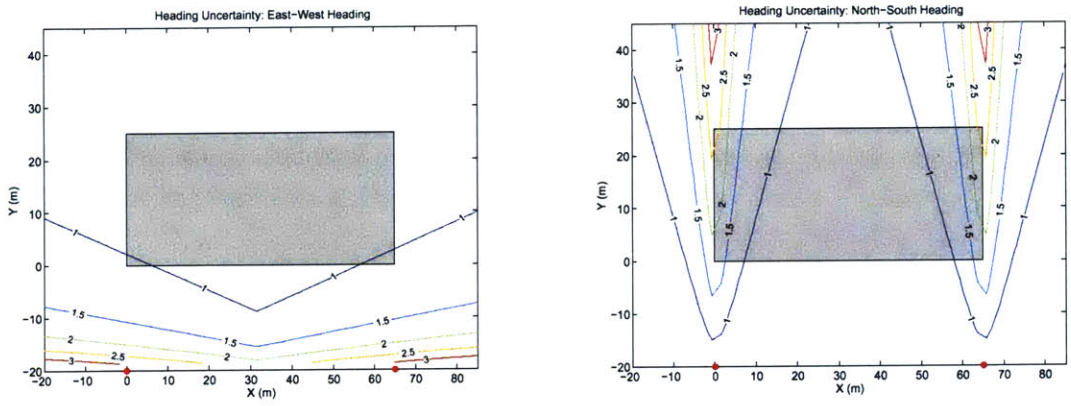

a b

Figure 5-9: Heading uncertainty for proposed monitor survey. Host-Baseline = 2m. Range uncertainty = 1cm. a) Shows the angular uncertainty assuming the vehicle is parallel to the X-axis. b) Shows the angular uncertainty assuming the vehicle is parallel to the Y-axis.

5.4 Conclusion

This chapter presents a mission plan, a survey specification, and a navigation system for archaeology on the USS Monitor. The design follows from mission goals to create precision imaging, microbathymetry. To deal with the environmental uncertainty a two stage survey plan decomposes the mission into 30 minute probing surveys and a 15 hour precision survey. The first stage relies on DVL guidance to quickly explore the environment, collecting range observations for off-line navigation and for hypothesis grid creation. The second stage is a slow precise survey, integrating range measurements and DVL data in real-time to guide the vehicle. For both surveys a two beacon configuration is sufficient to provide the needed reference and redundancy. The beacons are placed parallel to the long-axis of the wreck and 15-20m from the edge of the 65x25m site.

This survey will produce a variety of products: a comprehensive photomosaic of the wreck and debris field, a co-registered microbathymetry map, a baseline for DVL navigation and guidance, a characterization of the finite acoustic environment, and a fine-resolution navigation and imaging dataset for developing future navigation techniques. Precision site-survey on these scales has been accomplished using human operated vehicles, but a mission demanding fine-scale navigation and control has not been done with an AUV.

Chapter 6

Conclusion

> The biologist George Wald once compared his work on an exceedingly specialized subject, the visual pigments of the eye, to a very narrow window through which at a distance one can only see a crack of light. As one comes closer, the view grows wider, until finally through this same narrow window one is looking at the universe.
> -Rachel Carson [1]

> Life can only be understood backwards; but it must be lived forwards.
> - Soren Aabye Kierkegaard

This dissertation contributes a design method and a specialized algorithm to the development of precision autonomous underwater navigation. These two stories are bound by a common goal - to produce high-resolution, quantitative images of deep-sea archaeological sites. Precision navigation is the definitive quality of archaeological survey. Performing such surveys with autonomous underwater vehicles (AUVs) requires navigation systems operating without a human operator and at new levels of performance. As a distinct application, deep-sea archaeology demands revisiting the tradeoffs embodied in survey-class AUVs and their navigation systems - the design portion of the story. Improving the precision and expanding the capabilities of autonomous navigation demands new algorithms for operating within an acoustically instrumented environment - the hypothesis grid portion of the story.

Design: Methods and Tradeoffs for Precision

Design methods build a bridge between the requirements of archaeology and the capabilities of navigation sensors, emphasizing the criticality of precision. Characterizing a mission in terms of goals, environment, and platform defines the functional requirements. The precision specification translates these requirements into design parameters - the necessary navigation precision decomposed into real-time, off-line, fixed-frame, and relative navigation specifications. The result is an uncertainty budget, enabling predictable, repeatable, and quantifiable tradeoffs.

[1] R. Carson. "Through a Narrow Window." *Silent Spring.* [Greenwich:Fawcett, 1970] p. 179, quoting George Wald, 'Life and Light', Scientific American, Oct. 1959 pp 40-42

Considering the navigation system design as a set of quantifiable decisions enables development of engineering methods for analysis and articulation of the key tradeoffs to illuminate the design space. Chapter 3 develops the Cramér Rao lower bound and the extended Kalman filter as design tools for predicting the performance of candidate designs. The analysis in chapter 3 provides definitive conclusions about the impact of beacon placement, number of beacons, combination of ranging and odometry, and active beacon selection on the quality of the solution. Performance metrics, non-dimensional analysis, Monte-Carlo simulations, and sensitivity analysis are important considerations for applying these design methods. Through simple models and analysis tools more insight and certainty is brought to the design decisions for creating autonomous navigation systems.

The general tradeoffs are made particular by considering the USS Monitor case-study of chapter 5. A holistic mission is planned, covering multiple dives, that deals with the environmental uncertainty. The photomosaic and microbathymetry imaging goals determine the requisite navigation precision. Using the CRLB design tool, the chapter presents the site-survey including a two-beacon network to meet the real-time and off-line specifications. The design method follows four steps: characterize the mission to understand the requirements, specify the precision to develop the design parameters, articulate the key tradeoffs to make design decisions, and analyse the sensitivity of the decisions to evaluate the robustness of the solution.

Design decisions are made with more foresight by using methods based on estimation theory for predicting the performance. Taking a system-level view, concurrently considering the impact of various sensors and algorithms, balances the performance and costs, leading to designs that achieve the mission goals in a diverse set of environments with an increasingly varied set of autonomous vehicles.

Hypothesis Grid: Sensor Model for Precise Positioning

Hypothesis grids characterize the instrumented acoustic environment. The algorithm is based on a mixed-distribution sensor model, a simultaneous identification and classification algorithm, and a grid-based representation of the environment. The result is a model of the prior probabilities as a function of position, i.e., an autonomous vehicle has an estimated probability that the next acoustic range will be a direct-path range, a multipath range, or a spurious return based on the platform's current estimated position.

The uncertainty in acoustic range measurements is not Gaussian. A mixed-distribution model captures the behavior of the sensor by hypothesizing three sources for each observation - a direct-path, a multipath, or an outlier. Application to long baseline (LBL) data from the autonomous benthic explorer (ABE) demonstrates feasibility of combining two Gaussian density functions and a uniform density.

The central challenge is to concurrently characterize observations and identify the model. Expectation-maximization iteratively associates the individual ranges with the three possible sources and determines the parameters of the multipath model. The results show the efficacy of a simple ray-tracing multipath model and the ability of the EM algorithm to arrive at a classification of the data and identification of the model.

The grid representation captures the relationship between position and prior association probability - the belief that a subsequent measurement will be from the direct-path, a multipath, or an outlier. Performance metrics and visualizations indicate the feasibility the hypothesis grid representation. For the ABE data, the spatial dependence is a strong determinant of the sensor behavior, and a coarse grid is sufficient to capture the dependence. The grid evaluation metrics articulate the tradeoffs in determining an appropriate resolution.

Archaeological investigation motivates the development because the deep-sea archaeology method calls for multiple site visits; however, the results are not particular to this application. Using hypothesis grids improves navigation precision and expands the capabilities. The prior probability is a common element in Bayesian inference techniques for navigation. By explicitly modeling this characteristic of the sensed environment, standard estimation techniques can realize a solution with more precision. The capabilities are expanded by creating a representation suitable for autonomous decisions. As autonomous methods integrate motion and sensing, a representation of how the quality of the observation depends on position enables autonomous systems greater control over uncertainty. Hypothesis grids formalize the intuition that previous experience, through repeated investigations, should allow better navigation - that navigation should learn from its mistakes.

6.1 Contributions

While this report has focused on the requirements of deep-sea archaeology, the results are applicable to emerging applications requiring precision navigation. The distinctive aspects of archaeological survey are central to both the design and development activities: precise navigation is emphasized in the design tradeoffs, and hypothesis grids enable autonomous operation in a precision environment. Precise survey is a representation of a general class of underwater navigation problems. The contributions of this thesis focus on these challenges.

Design

- A specification connecting the image quality functional requirements to the navigation precision design parameters.
- A classification of AUV missions based on the goals, environment, and platform.
- Design methods, based on the Cramér Rao lower bound and the extended Kalman filter, for making design decisions based on predicting the precision of candidate solutions.
- Articulation of the impact of key design dimensions on precision: number of acoustic beacons, beacon placement, Doppler velocity log integration, depth sensor integration, active beacon selection, heading observation through acoustic ranging, etc.
- Application of the theory and methods to the engineering design of an autonomous survey and navigation system for work on the USS Monitor.

Autonomous Navigation

- The hypothesis grid algorithm for representing the operation of a long baseline navigation environment.
- A mixed-distribution model for representing acoustic range observations using a combination of Gaussian and uniform probability density functions.
- Application of expectation-maximization to simultaneously classify and identify multipath returns in acoustic range observations.
- Feasibility of a ray-traced multipath model using empirical evidence.
- Demonstration of the feasibility of a coarse grid to represent the relationship between prior association probabilities and estimated position.
- A mission plan for producing and utilizing the hypothesis grid algorithm for the precise survey of the USS Monitor.

6.2 Ongoing and Future Work

This thesis satisfies at least one metric for successful research; it creates more questions than it answers. Chapters 3 and 4 contain an explanation of next steps for the extending the design method and hypothesis grids respectively. This section summarizes and adds to those statements. The following organizes the future work by type: ongoing implementation work, challenges to the assumptions, and leverage points where future efforts are best focused.

Implementation

The design methods are general; they apply to applications with varied precision requirements. This work applies the techniques to one application, deep-water archaeological survey, and one example, the USS Monitor survey. Application of these methods to new designs will prove their worth and expose their deficiencies.

Experience will quantify the value of the hypothesis grid algorithm in terms of increased performance and expanded capabilities. Chapter 5 presents a mission plan for creating hypothesis grid representation of the USS Monitor site by exploring the acoustic environment. Executing this plan will strengthen the feasibility of modeling the sensed environment.

Learning requires reinforcement. Quantifiable comparisons are the feedback that praise good decisions and punish shortcomings. Often, for evaluating new precision navigation designs and algorithms there is no baseline for comparison. A surveyed environment only exists in laboratory scenarios, the antithesis of ocean operations. A fundamental challenge for developing underwater navigation is the ability to make quantifiable comparisons - to learn from current designs.

Challenging Assumptions

The small-scale, acoustically homogeneous environment is an assumption. On small scales the physics are simplified and on large scales those simplifications are not valid, but where is the transition from large to small? Classifying the dominant physics for a set of different environments is a fundamental challenge. The solution would clarify the disparity and benefit acoustic navigation and communication.

Characterizing the multipath phenomena is an important component of the challenge of understanding the acoustic channel. The range observations from ABE show a repeatable and stable multipath that agrees with the horizontal reflector ray-tracing model. Implementing the hypothesis grid algorithm will yield more evidence for understanding the multipath environment - its characteristic stability and the efficacy of the empirical model. When creating hypothesis grids, explicitly surveying the sensor environment will generate measurements that shed light on the nature of the multipath phenomena.

The rectangular implementation of hypothesis grids is basic; it is a simple decomposition of the survey area without concern for the particular physics of the sensor operation. The nature of the relationship between sensor operation and spatial location may be more accurately described by other representations: basis functions, adaptive mesh techniques, or clustering. The choice of independent variable, spatial position, is a hypothesis. The strength of this dependency should be compared with other possible dependencies. Other relationships can be represented using hypothesis grids; for example, the vehicle's velocity could be represented in the same way as its position. Other dependencies will require different representation; for example, tidal currents, a temporally periodic factor, would not be amenable to the discrete nature of a grid based solution. Future research will expand our understanding of this sensed environment and yield representations that convey this understanding for autonomous decisions.

Leverage Points

The extensions to this thesis are infinite, but identifying leverage points maximizes the impact of future investigations. The design portion of this thesis focuses on developing the ability to predict performance, specifically the precision. Methods are needed to quantify the other dimensions of the design space. Two extensions of the hypothesis grid algorithm are particularly important: extending how the system uses this information and examining how the system builds the belief.

Robustness is a critical component of an AUV navigation system. Quantifying this concept and developing a predictive capability is an important challenge. Navigation robustness requires insensitivity to sensor failures and environmental changes, often accomplished through adaptation. Unlike measurement uncertainty, environmental uncertainty is difficult to represent quantitatively. A clear, concise concept of this uncertainty would enable robustness predictions the for candidate designs.

There is no general method for analyzing autonomous systems. Currently we lack the vocabulary to discuss the most important traits of autonomous robots, e.g., what does it mean for such a system to be stable or controllable? Designing autonomous systems may be a divergent problem,

without general principles or fundamental underpinnings, but the proven utility of autonomous systems necessitates a deeper understanding.

Current vehicles concentrate on modularity to achieve flexibility, a design principle following the idea that one platform can satisfy all (or most) missions. This thesis argues that new missions demand new designs. From the design considerations of chapter 3 a concept of AUVs as an increasingly integrated and capable unit emerges. How would we design an AUV to inhabit an environment instrumented for navigation, communication and multiple vehicles? This question challenges the component technologies, but the system-level integration is the critical issue. An AUV is a signal processing unit, using mainly acoustic signals to navigation, communicate, and observe the environment. Increasingly integrated designs will continue to extend the utility of this technology.

Hypothesis grids are motivated by, and based upon, Bayesian inference. This probabilistic concept is founded on the notion of probability as chance, or frequency of occurrence. A hypothesis grid is a map of the sensed environment representing the degree of belief that a subsequent observation be from a particular source. Given such a representation, how would a robot manage its sensors and motion optimally? Work on robot exploration and sensor management developed methods for reasoning within feature-based or evidence grid representations. Reasoning within hypothesis grids presents a similar problem, but one that has not be explored.

The dual of the reasoning problem is the representation problem - determining a model appropriate for reasoning. What other information would allow a platform to make autonomous decisions about motion control and perception management? The goal of this approach is to develop autonomous environmental awareness. Human operators fuse disparate and dynamic sources of information to navigate underwater vehicles. The challenge is to find both the right representations and the right methods for reasoning within those abstractions.

Hypothesis grids build a map of beliefs through Bayesian inference. Starting from a state of ignorance, the grid cells build a belief about future observations through past experience. Dempster-Shafer theory offers an alternative to Bayesian inference for building belief. The method is based on the 'theory of evidence' and avoids the difficulties of non-informative prior probabilities for representing ignorance. Applying this theory to the synthesis and application of hypothesis grids would be a fundamental extension.

Appendix A

Long Baseline Navigation and Least-Square Model-Fitting

A.1 Modeling the LBL Environment

The model for long baseline navigation is spherical positioning, the unknown position satisfies the simultaneous quadratic equations for spheres centered at the known beacon locations with radii equal to the observed ranges. The challenge is to fit this representation to the measured data and to quantitatively determine the agreement between observation and model. This is a standard engineering problem and this development follows the general explanation in *Numerical Recipies for C* [Press et al., 1993].

Any procedure for model fitting should provide parameters, error estimates on the parameters, and a statistical measure of the goodness-of-fit. Least squares satisfies these three requirements. The figure-of-merit, the cost function that is minimized by the best-fit parameter selection, measures the agreement between the data and the model. The goodness-of-fit is the statistical standared for measuring the appropriateness of the model. The likelihood of the parameters given the data is the probability of the data given the parameters. Least squares is the maximum likelihood estimate when we assume that the measurement errors are independent and normally distributed.

A.2 Spherical Navigation Using Least Squares

This section outlines the method of least squares for a simple model of spherical localization. The problem is stated explicitly along with the requirements of least squares as the maximum likelihood estimator for the data (measurements). A full treatment of this subject gives insight into how the least squares formulation can be used as a tool in localization particularly for the association and characterization problems treated in the sequel.

Posing the Problem

Least squares is a powerful, flexible technique for fitting empirical data to a theoretical model. The formulation is elegant, intuitive, and analytically satisfying. Presented here is the least squares technique and its application to spherical navigation. The important assumptions and connections are highlighted but many details are omitted; a full treatment is presented in the reference [Press et al., 1993].

Generalized Nonlinear Least Squares

The elegance of least squares data fitting is rooted in the properties of the Gaussian (normal) distribution. Gaussian models are prevalent in statistics for some very good reasons: compactness, linearity, and the central limit theorem. For these same reasons Gaussian models are often overused. It is important to realize the limitations of these models and not abuse the power of the method. The generic model of the data is,

$$\begin{aligned} \hat{z}_i &= \zeta_i(\mathbf{x}) \; \forall \, i = 1, \ldots, N \\ \hat{\mathbf{z}} &= \zeta(\mathbf{x}) \end{aligned}$$

where $\hat{\mathbf{z}}$ is the modeled estimate of the data vector as a function (ζ) of the model parameters $\mathbf{x}$. The figure-of-merit, or merit function, is what measures the agreement between the observed data and the model. The least squares merit function is

$$\chi^2(\mathbf{x}) = \sum_{i=1}^{N} \frac{[z_i - \zeta_i(\mathbf{x})]^2}{\sigma_i^2} = [\mathbf{z} - \hat{\mathbf{z}}]^{\mathbf{T}} \mathbf{R}^{-1} [\mathbf{z} - \hat{\mathbf{z}}] \tag{A.1}$$

where z_i are the individual measurements that make up the measurment vector $\mathbf{z}$, and $\mathbf{R}$ is the covariance matrix of the measurement errors (for independent measurements the covariance is a diagnol matrix with the elements being the inverse of the individual measurement variances). The goal of data fitting is to find a set of parameters resulting in a model that agrees with the data. The merit function quantifies this agreement and maps the problem into an optimization problem. Beyond being intuitively satisfying, the least squares merit function is also the maximum likelihood estimate under the assumption that the errors are normally distributed and independent.

$$z_i = \zeta_i(\mathbf{x}) + \nu_i \quad \nu_i = N(0; \sigma_i^2)$$

Using this Gaussian model of the measurment error and assuming independence of these errors, maximizing the likelihood of the parameters given the data is equivalent to minimizing the least squares merit function.

Remember: Least squares is the maximum likelihood estimate of the parameters given the data when we assume independent, Gaussian error between the measurments and the model. Linearity is not assumed.

Estimating the Parameters

Finding the set of parameters to minimize the least squares merit function is done numerically. The solution presented here is a combination Newton's Method and gradient decent, both of which can be used to approximate where the gradient of the merit function goes to zero.

A first order approximation of the data model is produced by linearizing about the current parameters (x_0).

$$\hat{\mathbf{z}}(\mathbf{x_0} + \delta\mathbf{x}) \approx \zeta(\mathbf{x_0}) + \mathbf{A}\delta\mathbf{x} \quad \mathbf{A}(i,k) = \frac{\partial z_i}{\partial x_k}|_{\mathbf{x_0}}$$

Substituting into the original problem statement and assuming equivalent variances for each measurment

$$\chi^2(\mathbf{x}) = |(\mathbf{z} - \hat{\mathbf{z}}(\mathbf{x_0})) - \mathbf{A}\delta\mathbf{x}|^2$$

This linear least squares problem can be solved using Newton's Method [Strang, 1986] which assumes that the quadratic fit to the model is correct and finds the minimum directly by solving the linear set of equations,

$$\delta\mathbf{x} = (\mathbf{A}'\mathbf{A})^{-1}\mathbf{A}(\mathbf{z} - \hat{\mathbf{z}}(\mathbf{x_0}))$$

$$\mathbf{x_{new}} = \mathbf{x_0} + \delta\mathbf{x}$$

Here the second order terms of the Hessian matrix are neglected for stability reasons thus the solution only uses the gradient of the vector function. Another numerical approach is to simply follow the gradient to find the minimum.

$$\mathbf{x_{new}} = \mathbf{x_0} - \mathbf{constant} * \mathbf{A}$$

These two approaches have complemenatary strengths and weeknesses and can be combined by using the Marquardt method [Press et al., 1993]. For well behaved problems the algorithm basically uses Newton's method by solving the linear equations, but smoothly changes to gradient decent when this approach does not converge.

Least Squares Solution for Spherical Localization

We now apply this method to the problem of spherical localization. The model for the measured ranges from N known locations with M degrees-of-freedom is

$$\hat{r}_i = r(\mathbf{x}) = \left(\sum_{k=1}^{M}(x_k - b_{k,i})^2\right)^{1/2}$$

where

- $\hat{r}_i$ - range estimates. $i = 1, \ldots, N$
- x_k - parameter vector; the cartesian location coordinates. $k = 1, \ldots, M$
- $b_{k,i}$ - beacon locations in cartesian coordinates

Linearizing this equation in vector form

$$\hat{\mathbf{r}} \approx \mathbf{r}(\mathbf{x_0}) + \mathbf{A}\delta\mathbf{x}$$

$$\mathbf{A} = \begin{bmatrix} \frac{(x_0(1)-b_{1,1})}{r_1(\mathbf{x_0})} & \cdots & \frac{(x_0(M)-b_{M,1})}{r_1(\mathbf{x_0})} \\ \cdots & & \cdots \\ \frac{(x_0(1)-b_{1,K})}{r_N(\mathbf{x_0})} & \cdots & \frac{(x_0(M)=b_{M,K})}{r_N(\mathbf{x_0})} \end{bmatrix}$$

The merit function is now

$$\chi^2(\mathbf{x}) = |(\mathbf{r} - \mathbf{r}(\mathbf{x_0})) - \mathbf{A}\delta\mathbf{x}|^2$$

We can now use gradient decent, Newton's method, or Marquardt's method to minimize the merit function. Newton's method ignoring the second order terms in the Hessian leads to iteratively solving the linear system of equations (A.2). Marquardt's algorithm for the spherical positioning problem is presented in the following steps.

- Start with an initial guess of the parameters $\mathbf{x_0}$.
- Calculate the merit function $\chi^2(\mathbf{x})$.
- Choose a starting value for λ, e.g., 0.001.
- † Linearize about $\mathbf{x_0}$ and solve the linear equations

$$\delta\mathbf{x} = (\alpha)^{-1}\mathbf{A}'(\mathbf{r} - \mathbf{r}(\mathbf{x_0}))$$

  where

$$\alpha_{\mathbf{i,j}} = \begin{cases} (\mathbf{A}'\mathbf{A})_{i,j}(1+\lambda) & (i=j) \\ (\mathbf{A}'\mathbf{A})_{i,j} & (i \neq j) \end{cases}$$

- If $\chi^2(\mathbf{x_0} + \delta\mathbf{x}) \geq \chi^2(\mathbf{x_0})$, increase λ by a factor of 10 and return to † (without updating x_0).
- If $\chi^2(\mathbf{x_0} + \delta\mathbf{x}) < \chi^2(\mathbf{x_0})$, decrease λ by a factor of 10, update $\mathbf{x_0} = \mathbf{x_0} + \delta\mathbf{x}$, and return to †.

A.3 Least Squares Estimation Example: Outlier Rejection

To understand the formal presentation of the linearized spherical positioning equations and Marquardt method section A.1, this section presents a concrete example. The method and equations are applied to the same data used in in the hypothesis grid example of section 4.3.1, where the story of the data is explained in detail.

The data contains range information from four beacons located at known locations. Figure A-1 illustrates the raw range information with direct-path, multipath, outliers and null returns. The known locations and the spherical constraints constitute the data-model - the observations are fit to the data by minimizing the least squares performance function through Marquardt optimization.

The algorithm estimates the position at each time-step or observation. Least squares applied directly to the raw range data produces the X-Y scatter plot in figure A-2; the 3-D position estimates

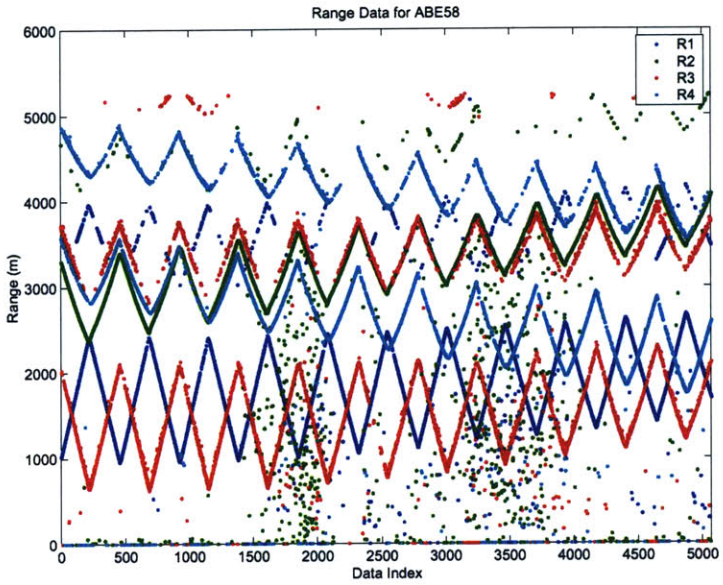

Figure A-1: ABE58 12kHz LBL range data. Time-of-flight is reported as range in meters for successive observations.

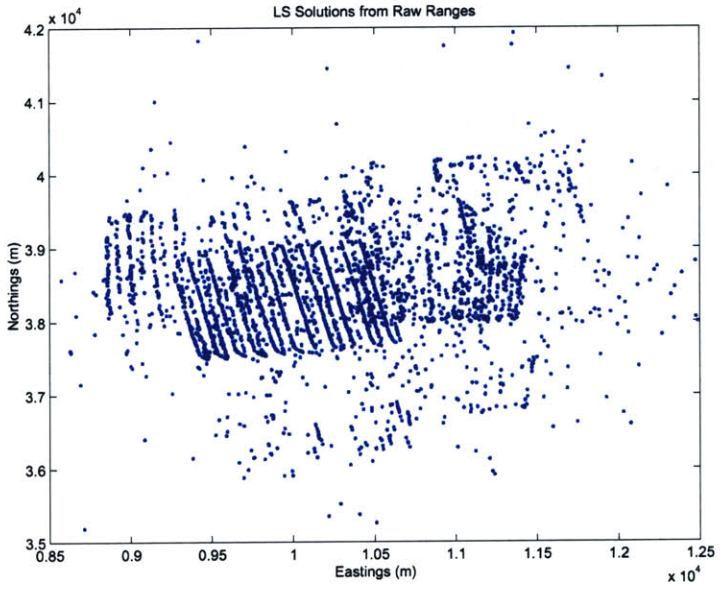

Figure A-2: ABE58 survey in the X-Y plane. Approximately 5,000 datapoints are plotted from the survey. The 12 kHz LBL beacon locations are shown as labeled red markers

are projected into the horizontal plane. These raw fixes obscure the 'true' positions in the data and in the figure shown many of the fixes are off the axes, up to 20 orders of magnitude away (figure A-2 does not show these position fixed where the geometry leads to localization solutions that are extremely far from the survey area). Autonomous estimators are sensitive to these errors that can be the cause for numerical instability. There are many methods to correct the particular

types of errors and the hypothesis grid of chapter 4 is one such technique. The rest of this section explains how the residuals of the least squares solution (equation A.2) can be used as a first step in determining the source of particular observations - direct-path, multipath, or outlier.

Residuals, Uncertainty Measures, and Confidence Intervals

This section shows how the concepts of least squares optimization are useful, not only for theoretical positioning, but for actual long baseline positioning data. The following illustrates how the model estimates the position by fitting a model to the observations and estimates the uncertainty in the observations. By assuming a mixture of distributions for the range measurments, the uncertainty estimates produce a meausure of the variance in the direct-path ranges, an important paramter in the data association of chapter 4

Residuals are the difference between the observations and the model predictions, the merit function of the least squares optimization (see equation A.1). For each time-step in the ABE58 data, a set of four ranges are fit to a spherical positioning model. The difference between these ranges and the ranges predicted, the distance between the beacon and estimated positions, is squared and summed for the ranges to produce the final value of the least squares performance measure.

$$E_r = \sum_{i=1}^{4} r_i - \hat{r}_i(\mathbf{x})$$

An estimate is calculated for each time-step, so each optimization also produces an unbiased estimate of the variance, or standard deviation, in the observations.

$$\hat{\sigma_r}^2 = \frac{\sum_{i=1}^{N}(x - \bar{x})}{N-1} \tag{A.2}$$

$$= \frac{E_r}{3} \tag{A.3}$$

The estimated standard deviations, the error between the measured and predicted range values, for each data point are plotted in the histogram of figure A-3. The errors values vary between $2\text{x}10^{-3}$ and $5\text{x}10^{30}$, but the values shown in the figure are limited for clarity. This plot can be used to infer an estimate of the uncertainty in the direct-path measurement. The data with range errors from 0 to 100m forms the may be classified as direct-path. The spherical positioning data-model assumes direct-path range observations, a restriction not met by the range data in figure 4-7 and highlighted by the error estimates in figure A-3. The challenge is to discern observations that agree with the model, good-data, and those that do not agree, bad-data. A threshold on the estimated standard deviation divides the data into a set where all the ranges are consistent with the model and a set where the observations are deemed inconsistent. This complex tradeoff is condensed to a single scalar.

The range sets that yield an estimated standard deviation below the threshold are classified as direct-path observations. The threshold is chosen based on the information in figure A-4. The

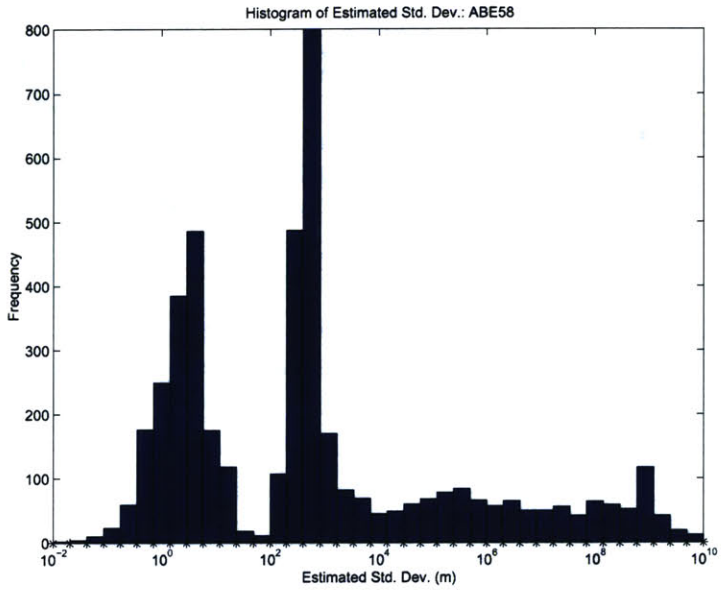

Figure A-3: Histogram of the standard deviation estimates from the least squares positioning estimates.

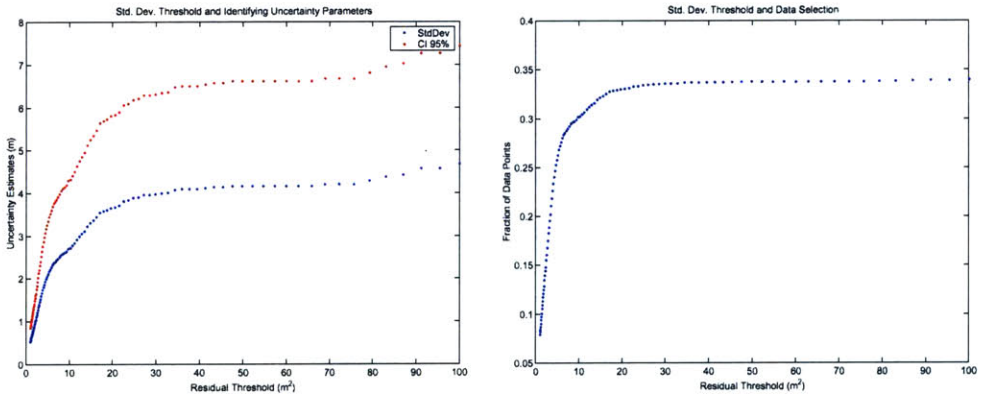

a b

Figure A-4: The relationship between the residual threshold for classifying the range obervations and the resulting statistical metrics for the direct-path acoustic model.

a-axes illustrate how the choice determines the estimate of direct-path uncertainty, an average of the individual standard deviation estimates from the time-steps deemed consistent. The horizontal part of the curves indicate that the uncertainty measures are not sensitive to the choice of threshold value. The b-axes demonstrate another dimension of the tradeoff, the number of time-steps in the set of consistent data and the same insensitivity to threshold value is evident where 35% of the data is kept for threshold values between 20 and 100m. The information in these plots is the same information in the histogram of figure A-3, but these presentations emphasize the insensitivity, important for determining confidence in the scalar value choice.

The average standard deviation determines the confidence interval for range observations

[Spiegel et al., 2000]. For small samples, such as the four ranges, the two sided confidence interval is calculated using a t distribution with $N - 1 = 3$ degrees of freedom.

$$CI_{0.95} = t_{0.95}\frac{\hat{\bar{\sigma}}}{\sqrt{N}} \tag{A.4}$$

$$= 3.18\frac{\hat{\bar{\sigma}}}{2} \tag{A.5}$$

where $\hat{\bar{\sigma}}$ is the average, taken over all the consistent data, of the estimated standard deviation. For the case illustrated in figure A-4a the 95% confidence interval indicates that 95% of the direct-path range observations will be $+/-$ 6.5m of the actual range.

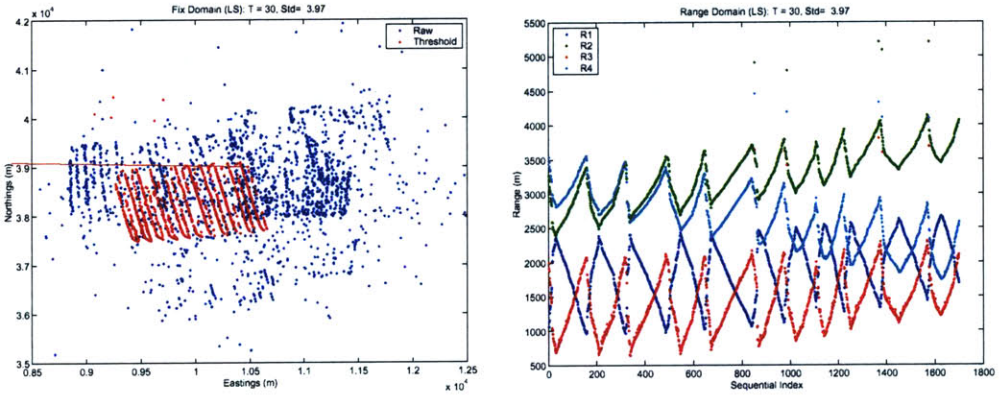

a b

Figure A-5: Fix (a) and range (b) plots for the a subset of the ABE58 LBL data. The threshold value of 30m is used to select this data set. Note the distorted shape of the sawtooth forms in the range plot indicating a directional dependence on the range observations.

Figure A-5 illustrates the data selected by choosing the threshold value of 30m; the standard deviation of the data retained is 3.97m. The data in the fix domain is the same scatter plot from figure 4-6 and the range domain plot presents a subset of the measurements from figure 4-7.

This method relies on consistency to discern the cluster of observations that are classified as direct-path, a metric that achieves intuitively satisfying results. But, data is included that is not direct path returns, illustrating an important caveat. After applying the threshold of 30m, five sets of range observations remain that are consist, but our eye can see that consistency does not capture the full requirement. Both in the fix and range domains these outliers are evident, but the estimated standard deviations are low: 1.1, 26.5, 13.5, 14.7, and 20.8 m. The range domain plot contains an explanation. At each of these points three of the four beacons simultaneously observes a multipath (beacons 2, 3, and 4). This multiplicity of errors yields geometry consistent with the spherical model for the LBL network, and this consistency produces a low residual error and estimated standard deviation. This shortcoming of the consistency metric does not invalidate the intent of the procedure, to estimate the standard deviation in direct-path observations for this LBL scenario, 3.97 m.

The method described above divided the observation sets into time-steps where *all* the ranges

were consistent with the direct-path model and those that at least one observation was erroneous. A more detailed implementation of the method would determine which of the four observations was inconsistent and re-estimate the position based on three ranges, extracting more information from the data. For brevity this is not covered. Another extension of the method is to challenge the assumption that each of the direct path range measurements exhibits the same characteristic uncertainty.

Least squares model-fitting is a standard method for spherical positioning. This section illustrates that solution for the LBL range measurements from the ABE58 survey, and because of the redundancy in localization with four range measurements, the consistency of the observations is measured. The principles of the method yield a classification of the data source, discerning the direct-path observations, and an identification of the parameters of the data model, the direct-path variance. The scalar threshold used to control the classification performs a fundamental tradeoff, compromising between the chance of disregarding good-data and accepting bad-data. This analysis provides an estimate of the direct-path range standard deviation - **3.97 meters**.

Appendix B

Dynamics and Information

B.1 Simulation Dynamics

For the extended Kalman filter examples in section 3.5 and appendix B.3, simple two-dimensional dynamics represent a vehicle motion. The discrete time state-space equations describe the plant model used to generate the 'true' states of the simulation and used for the Kalman filter state transition. The difference being that random process noise is added through the force inputs when generating the state trajectories. The simulation can trivially be extended to three dimensions. The state transition equations are,

$$\begin{aligned} \mathbf{x}(k) &= \mathbf{F}(k-1)\mathbf{x}(k-1) + \mathbf{B}(k-1)\mathbf{u}(k-1) \\ \begin{Bmatrix} \dot{x} \\ x \\ \dot{y} \\ y \end{Bmatrix}(k) &= \begin{bmatrix} 1 & 0 & 0 & 0 \\ \Delta T & 1 & 0 & 0 \\ 0 & 0 & 1 & 0 \\ 0 & 0 & \Delta T & 1 \end{bmatrix} \begin{Bmatrix} \dot{x} \\ x \\ \dot{y} \\ y \end{Bmatrix}(k-1) + \frac{1}{M} \begin{bmatrix} \Delta T & 0 \\ \frac{\Delta T^2}{2} & 0 \\ 0 & \Delta T \\ 0 & \frac{\Delta T^2}{2} \end{bmatrix} \begin{Bmatrix} f_x \\ f_y \end{Bmatrix} \end{aligned}$$

where x and y are the Cartesian position coordinates, ΔT is the sampling period indexed by k, M is the mass of the vehicle, and the force inputs are specified in the two coordinate directions - f_x and f_y.

The range observations, indexed by i, are

$$z_i(k) = \sqrt{(x(k) - x_b)^2 + (y(k) - y_b)^2} + w_i(k)$$

where the known beacon locations are x_b and y_b and the additive gaussian sensor noise, $w_i(k)$, is characterized by the variance.

$$R_{i,i}(k) = E[\omega_i^2(k)] = \sigma_r^2$$

$$\mathbf{R} = \mathbf{R}(k) = E[\mathbf{w}(k)\mathbf{w}^T(k)] = \sigma_r^2 \, [\mathbf{I}]_{nxn}$$

Each range measurement is independent and has the same variance. The measurement covariance, $\mathbf{R}$, is diagonal and constant in time.

B.2 The Kalman Filter Equations

The discrete time Kalman filter equations are important because they relay the discrete time notation used in the thesis. For completeness the notation from [Bar-Shalom et al., 2001] and [Durrant-Whyte and Stevens, 2001] is repeated here.

Kalman Filter Equations

The conventional Kalman filter algorithm generates estimates for the state $\hat{\mathbf{x}}(k \mid k)$ at a time k given all observations up to time k, together with a corresponding estimate covariance $\mathbf{P}(k \mid k)$ as the output of a three-step process: Predict, Calculate Gain, Update.

State Transition Model:

$$\mathbf{x}(k) = \mathbf{F}(k-1)\mathbf{x}(k-1) + \mathbf{B}(k-1)\mathbf{u}(k-1) + \mathbf{G}(k)\mathbf{w}(k)$$

Measurement Model:

$$\mathbf{z}(k) = \mathbf{H}(k)\mathbf{x}(k) + \mathbf{v}(k)$$

Predict:

$$\begin{aligned}
\hat{\mathbf{x}}(k \mid k-1) &= \mathbf{F}(k-1)\hat{\mathbf{x}}(k-1 \mid k-1) + \mathbf{G}(k-1)\mathbf{u}(k-1) \\
\mathbf{P}(k \mid k-1) &= \mathbf{F}(k-1)\mathbf{P}(k-1 \mid k-1)\mathbf{F}^T(k-1) \\
\hat{\mathbf{z}}(k \mid k-1) &= \mathbf{H}(k)\hat{\mathbf{x}}(k \mid k-1)
\end{aligned}$$

Gain:
Measurement Residual:

$$\nu(k) = \mathbf{z}(k) - \hat{\mathbf{z}}(k \mid k-1)$$

Innovation Covariance:

$$\mathbf{S}(k) = \mathbf{R}(k) + \mathbf{H}(k)\mathbf{P}(k \mid k-1)\mathbf{H}^T(k)$$

Filter Gain:

$$\mathbf{W}(k) = \mathbf{P}(k \mid k-1)\mathbf{H}(k)\mathbf{S}^{-1}(k)$$

Update:

$$\begin{aligned}
\hat{\mathbf{x}}(k \mid k) &= \hat{\mathbf{x}}(k \mid k-1) + \mathbf{W}(k)\left[\mathbf{z}(k) + \mathbf{H}(k)\hat{\mathbf{x}}(k \mid k-1)\right] \\
\hat{\mathbf{x}}(k \mid k) &= \hat{\mathbf{x}}(k \mid k-1) + \mathbf{W}(k)\nu(k) \\
\mathbf{P}(k \mid k) &= \mathbf{P}(k \mid k-1) - \mathbf{W}(k)\mathbf{S}(k)\mathbf{W}^T(k)
\end{aligned}$$

$\mathbf{x}(k)$	-	state at time k
$\hat{\mathbf{x}}(k \mid j)$	-	state estimate at time k given observations through time j
$\mathbf{P}(x \mid j)$	-	state covariance estimate at k given observations through time j
$\mathbf{F}(k)$	-	state transition matrix from time $k-1$ to k
$\mathbf{B}(k)$	-	control input matrix
$\mathbf{G}(k)$	-	noise input matrix
$\mathbf{u}(k)$	-	control input
$\mathbf{w}(k)$	-	uncorrelated white process noise $\mathrm{E}\{\mathbf{w}(i)\mathbf{w}^T(j)\} = \delta_{ij}\mathbf{Q}(i)$
$\mathbf{z}(k)$	-	observation vector
$\mathbf{H}(k)$	-	observation model/matrix
$\mathbf{v}(k)$	-	uncorrelated white sensor noise $\mathrm{E}\{\mathbf{v}(i)\mathbf{v}^T(j)\} = \delta_{ij}\mathbf{R}(i)$
$\mathbf{W}(k)$	-	Kalman gain matrix
$\mathbf{S}(k)$	-	innovation matrix

Information Filter

The information form of the Kalman filter highlights the incorporation of measurement information, in the sense of the Cramér Rao lower bound. The Fisher information matrix is the inverse of the covariance matrix and this form concentrates on updating this information matrix explicitly. The important equations are repeated for quantifying the information flow and decentralizing the filter (sequential processing of the Kalman filter algorithm), but for a full treatment see the references [Bar-Shalom et al., 2001].

The information form of the Kalman filter is obtained by transforming the state estimate

$$\hat{\mathbf{y}}(i \mid j) \triangleq \mathbf{P}^{-1}(i \mid j)\hat{\mathbf{x}}(i \mid j)$$

and also the information associated with an observation in the form

$$\mathbf{i}(k) \triangleq \mathbf{H}^T(k)\mathbf{R}^{-1}(k)\mathbf{z}(k), \qquad \mathbf{I}(k) \triangleq \mathbf{H}^T(k)\mathbf{R}^{-1}(k)\mathbf{H}(k)$$

With these definitions, the following summarizes the information filter.

Prediction:

$$\hat{\mathbf{y}}(k \mid k-1) = \left[\mathbf{1} - \mathbf{\Omega}(k)\mathbf{G}^T(k)\right]\mathbf{F}^{-T}(k)\hat{\mathbf{y}}(k-1 \mid k-1) + \mathbf{P}^{-1}(k \mid k-1)\mathbf{B}(k)\mathbf{u}(k) \qquad \text{(B.1)}$$

$$\mathbf{P}^{-1}(k \mid k-1) = \mathbf{M}(k) - \mathbf{\Omega}(k)\mathbf{\Sigma}(k)\mathbf{\Omega}^T(k) \tag{B.2}$$

where

$$\mathbf{M}(k) = \mathbf{F}^{-T}(k)\mathbf{P}^{-1}(k-1 \mid k-1)\mathbf{F}^{-1}(k),$$

$$\mathbf{\Omega}(k) = \mathbf{M}(k)\mathbf{G}(k)\mathbf{\Sigma}^{-1}(k),$$

and

$$\mathbf{\Sigma}(k) = \left[\mathbf{G}^T(k)\mathbf{M}(k)\mathbf{G}(k) + \mathbf{Q}^{-1}(k)\right].$$

Estimate:

$$\hat{\mathbf{y}}(k \mid k) = \hat{\mathbf{y}}(k \mid k-1) + \mathbf{i}(k)$$

$$\mathbf{P}^{-1}(k \mid k) = \mathbf{P}^{-1}(k \mid k-1) + \mathbf{I}(k).$$

The information-filter form has the advantage that the update Equations B.2 and B.2 for the estimator are computationally simpler than the equations for the Kalman Filter, at the cost of increased complexity in prediction.

In multiple sensor problems, explictly representing the information is enlightening.

$$\mathbf{z}_i(k) = \mathbf{H}_i(k)\mathbf{x}(k) + \mathbf{v}_i(k), \qquad i = 1, \cdots, N$$

The estimate can not be constructed from a simple linear combination of contributions from individual sensors

$$\hat{\mathbf{x}}(k \mid k) \neq \hat{\mathbf{x}}(k \mid k-1) + \sum_{i=1}^{N} \mathbf{W}_i(k)\left[\mathbf{z}_i(k) - \mathbf{H}_i(k)\hat{\mathbf{x}}(k \mid k-1)\right],$$

as the innovation $\mathbf{z}_i(k) - \mathbf{H}_i(k)\hat{\mathbf{x}}(k \mid k-1)$ generated from each sensor is correlated because they share common information through the prediction $\hat{\mathbf{x}}(k \mid k-1)$. However, in information form, estimates can be constructed from linear combinations of observation information

$$\hat{\mathbf{y}}(k \mid k) = \hat{\mathbf{y}}(k \mid k-1) + \sum_{i=1}^{N} \mathbf{i}_i(k),$$

as the information terms $\mathbf{i}_i(k)$ from each sensor are uncorrelated. Once the update equations have been written in this simple additive form, it is straight-forward to distribute the data fusion problem (unlike for a Kalman filter); each sensor node simply generates the information terms $\mathbf{i}_i(k)$, and these are summed at the fusion center to produce a global information estimate.

Extending the Kalman Filter

When the state model, the observation model, or both are non-linear the extendend Kalman filter (EKF) uses linearized models in the Kalman filter algorithm. See the reference [Bar-Shalom et al., 2001].

B.3 CRLB, EKF, and Efficiency

This section serves two purposes. First it is an example of implementing an EKF simulation as a design tool and discusses the aspects of that application. Second it illustrates the relationship between the CRLB and the achievable estimator performance.

To use the CRLB as a design tool the capabilities and limitations must be stated explicitly. The CRLB can be used as a design tool if it accurately predicts the performance of the navigation solution. To illustrate that this is indeed the case this section shows that the EKF is an efficient estimator of the spherical positioning solution - indicating that the bound is indicative of achievable performance. It will also show that because the Kalman filter makes use of a dynamic model of the platform the estimation uncertainty can fall below the CRLB - the bound is not a best-case scenario in this case, but a conservative estimate of performance. The CRLB provides a bound on the capability of a static estimate while the EKF illustrates the performance of a dynamic estimate.

Spherical Positioning: An Example

Using a simple example, a clear connection is drawn between the estimator performance and the CRLB as a predictive design tool. Consider the spherical positioning system introduced in section 3.3.1. To illustrate an EKF as a design tool a simple simulation implements two-dimensional dynamics. Operating in the 2-D environment and using range observations from three beacons at known locations, control inputs are synthesized to perform a 'mow-the-lawn survey' of the environment. The dynamic equations are presented in appendix B.1.

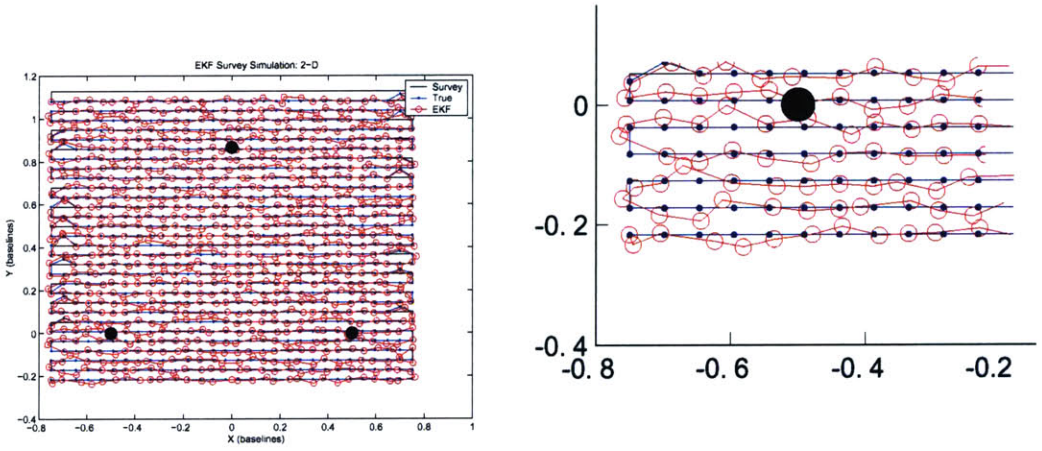

a b

Figure B-1: The planned survey path is shown relative to the beacon location (large black markers). The 'true' state of the simulated dynamics are shown as the hollow circular markers (red) as the simulated vehicle tries to achieve the survey positions indicated by the small markers (blue). The b) axis shows a scaled subset of the the a) axis.

Figure B-1 shows a representative survey. The dynamics are evident from the path which approaches the planned survey. A simple PD controller is implemented to have the dynamics follow

the specified survey trajectory. This simulation allows a clear illustration of the efficiency of the EKF estimator.

Two design parameters are used to control the operation of the Kalman filter. The observation noise is just the variance in the range measurements. The process noise is used in this example to control the bandwidth of the filter or how the filter arbitrates between the dynamic model and the noisy observations. These design parameters correspond to 'true' parameters in the system model, but outside of simulations these parameters are never known with certainty. Intuitively the process noise used in the filter design (distinct from the random process noise introduced in the simulation of the 'true' state) determines the filters reliance on the dynamic model. First the limiting case where the process noise is arbitrarily high is considered. In this case the estimator relies solely on the measurements at each (the filter has no memory and high bandwidth).

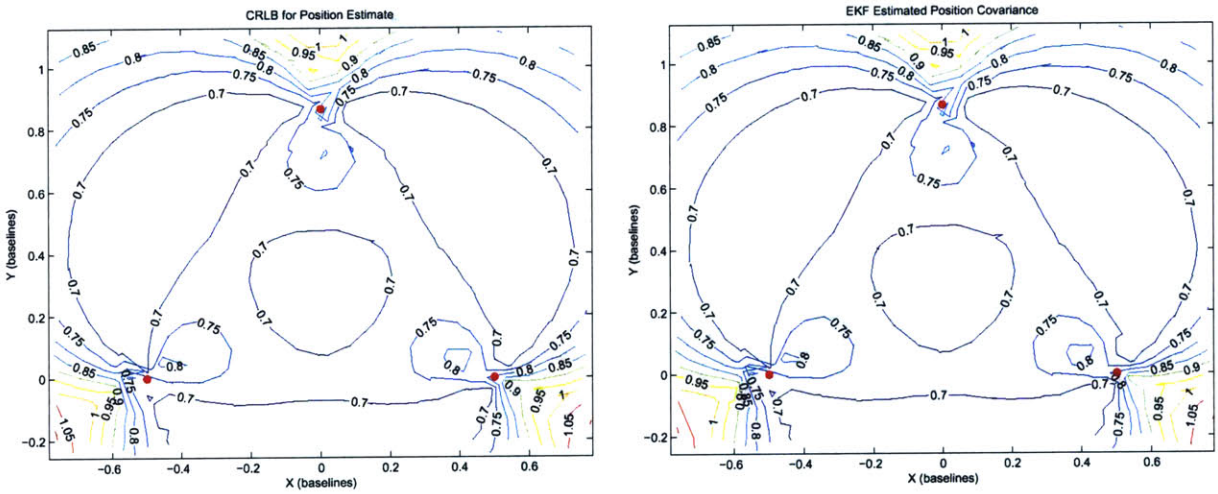

Figure B-2: Contour plots for the position uncertainty estimates from the survey example. a) Shows the CRLB calculated at the vehicle positions. b) Shows the position covariance estimate from the EKF. Both results are normalized by the range uncertainty and represent the Precision Factor.

Figure B-2 illustrates the efficiency of this limiting case. In this scenario the EKF estimator uses only the information in the observations to estimate the state and we can see by the similarity in the two contour plots that the estimator achieves the CRLB, i.e., it is an efficient estimator. This is hardly surprising since for the linear guassian estimation problem the Kalman filter is the optimal estimator, but in this case we have nonlinear measurement equations which are linearized about the estimated position (see appendix A.1 for an explanation of the linearization).

The critical difference between the CRLB and EKF is that the dynamic model used in the formulation of the filter carries information forward in time. Reducing the process noise design parameter results in a filter that takes increasing advantage of this information - in contrast to the previous case. Figure B-3 shows the resulting uncertainty. Plot a in the figure shows the same CRLB for the positions in the survey. Plot b shows the position covariance estimates for the new EKF. The uncertainty, captured in the precision factor contours, has decreased by almost a factor

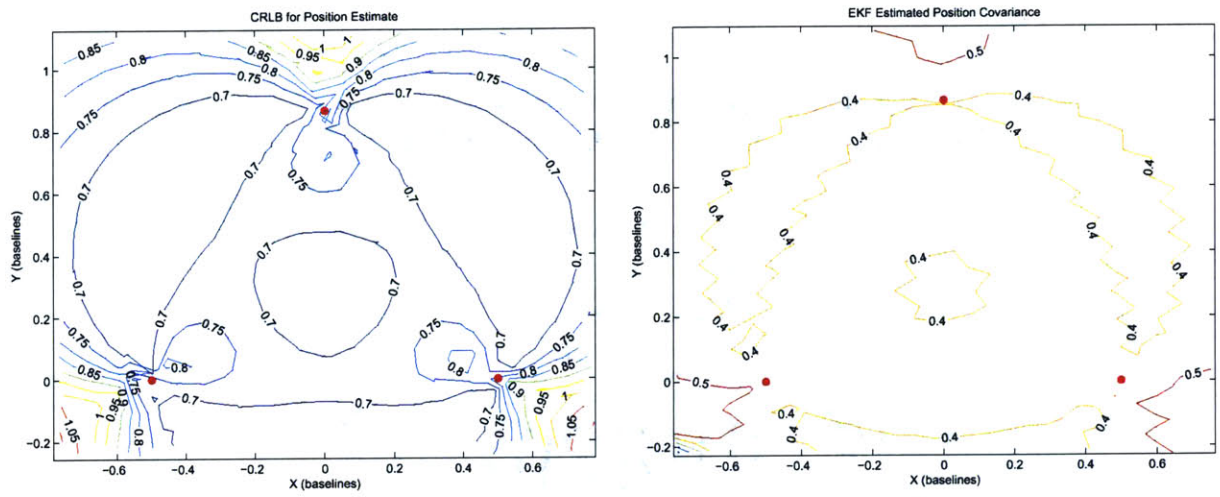

Figure B-3: Similar to the preceding figure but the process noise is reduced

of 2 because the dynamic model has allowed for information about the system to be carried forward in time.

The point is that the CRLB is a useful simplification that enables system-level design decisions. It omits some key considerations by assuming a simple error model (known guassian sensor noise) so care must be taken to address the issues of robustness and reliability to non-guassian or mixed distribution error models. With this caveat the CRLB will be shown to be useful in articulating the complex tradeoffs in designing a system for estimation.

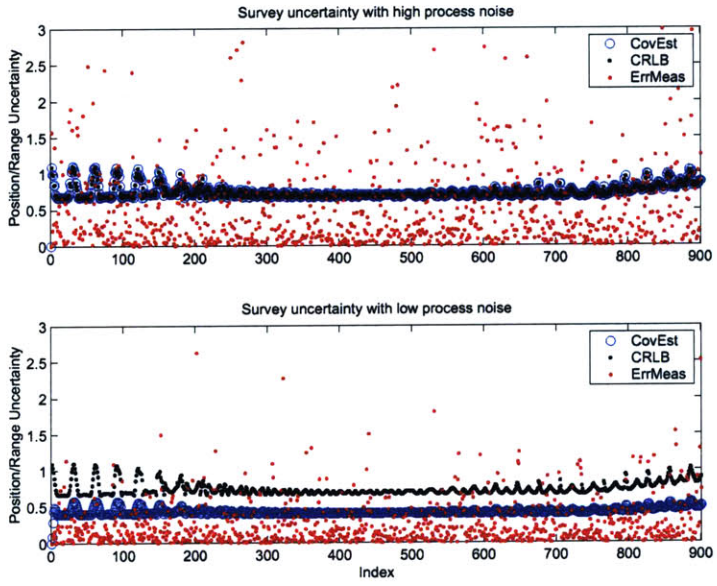

Figure B-4: Illustrates the efficiency of the EKF when there is no model and the performance increase with an accurate dynamic model.

Figure B-4 offers another visualization of the uncertainty. The upper axis shows the first case where high process noise causes the EKF to act as a static estimator. The CRLB and the covariance estimate from the EKF overlap at each point. The second case, where the process noise is decreased, shows how the estimator takes advantage of the dynamic model to produce an estimate with uncertainty below the CRLB. Also the measured error is plotted to make the point that the estimated uncertainty only characterizes the true error in the aggregate.

These examples are for a greatly simplified scenario. Only range sensors are used for positioning, but it would follow directly to incorporate other sensing modalities.

B.4 Geometry and Information

Not sure if this belongs in the section on active beacon selection or on path planning. The intent is to develop a geometric interpretation of the accumulation of information in a long baseline survey.

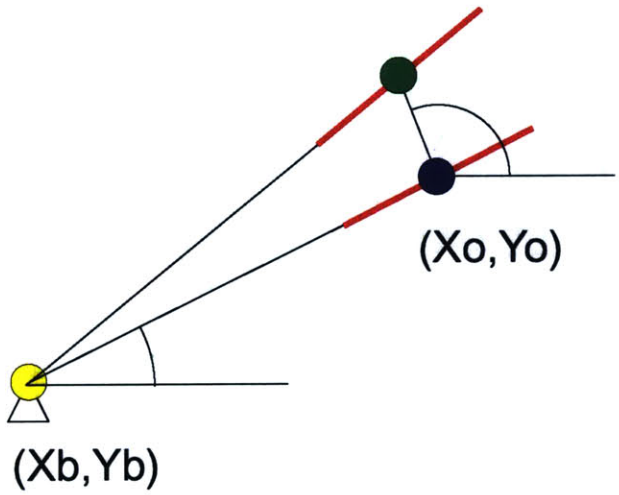

Figure B-5: Illustrates the relationship between the change of position (theta) and the information in a single beacon query.

Figure B-5 is a visualization of the relationship between direction of survey and the information for independent beacon pings. This simplified 2-D single-beacon case scales to multiple dimensions. The geometric interpretation is illuminating for two dual problems: active beacon selection and path-planning. The yellow marker in the figure represents a single fixed beacon at (x_b, y_b). The blue marker is the nominal position of the estimator at (x_o, y_o), and the green marker is the new position of the estimator.

The pertinent question is to find an incremental direction which maximizes the information received from the next ping. Translating this question into information theoretic terms, an angle Θ is found to maximize the information from the linearized observation model.

$$i_j(k) = h_j^T r_{jj}^{-1} h_j$$

For the 2-D case the incremental information matrix is a singular 2x2 matrix - a vector. The eigenvector of the matrix is the direction of the information. The linearization (see appendix A.1) shows that the information lies along the line connecting the estimator and the beacon.

$$h_j(k) = \frac{1}{r} \left\{ \begin{array}{c} x - x_b \\ y - y_b \end{array} \right\} \Bigg|_{x=\hat{x}, y=\hat{y}}$$

$$r = \sqrt{(x - x_b)^2 + (y - y_b)^2}$$

The length of the information vector is determined by the variance in the range measurement, i.e., $r_{jj} = 1/\sigma^2_{range}$.

Since the variance of the range measurement is constant, the magnitude of the information added for each successive ping is constant. The direction of the information becomes the key factor. The change in position is represented by the magnitude Δ and the direction Θ. The magnitude is fixed - the challenge is to determine the angle which minimizes the uncertainty in the system. Moving tangent to the circle centered at the beacon location creates the large change in the direction of the information. Consider two pings, one at the first location (the blue marker) and one at the second (the green marker). Also consider that the uncertainty in each dimension is approximately equivalent (the error ellipse is roughly circular). To shrink the uncertainty the most the estimator would choose Θ such that $\tan\Theta = \frac{1}{\tan\Phi}$. Similarly, given a certain trajectory, the estimator would choose to query the beacon that would yield a similar geometry.

B.5 Uncertainty

The topic of uncertainty or error analysis in measurments is vast and deep. This work uses the simplest of concepts to capture the uncertainty in navigation and hence the image product of a deep-water survey. A few key concepts are presented for completeness and to illustrate how they pertain to the problem at hand, but in the interest of brevity the majority is left in the references. There are specific references dealing with measurment uncertainty and analysis [Coleman and Steele, 1999] and more general references treating the axiomatic fields of probability and statistics [Spiegel et al., 2000], [Drake, 1967], [Papoulis, 2002].

Concepts

The following concepts, and the terms describing them, are so prevalent that they can adopt many meanings. Explanations are given here to clarify exactly how these concepts will be used in the development to follow.

Typically two distinct types of measurment errors are considered - *bias* and *variance*.

- Bias - systematic errors that cause distortion and corruption. Biases do not reduce with more measurments.
- Variance - random errors that reduce the resolution (quality) of the survey.

Variances can be reduced with increasing the number of measurements. Bias and variance are analogous to precision and accuracy. Variance is also used to denote a particular metric relating the diversity in a set of measurements. Standard Deviation is the square root of the variance of a set of measurements (Standard Deviation of the Mean [Taylor, 1982]: $\sigma_{\bar{x}} = \frac{\sigma_x}{\sqrt{N}}$). Ffor large N the estimate of the average approaches the true mean as the sample size increases.

Uncertainty Propagation

How do uncertainties in independent variables contribute to the uncertainty in a functionally dependent variable? *General uncertainty analysis* is a simple method for analyzing the effect [Rabinovich, 2000].

$$r = f(x_1, \ldots, x_n)$$

$$E_r^2 = \sum_{i=1}^{n} \frac{\partial r}{\partial x_i}^2 E_i^2$$

Where E is a common specification for uncertainty (for example, standard deviation, circular probable error (CEP), etc.). General uncertainty analysis does not differentiate between bias (systematic errors) and variance (random errors) and all uncertainty is assumed to be captured by E.

Appendix C

Design Tradeoffs

C.1 Spherical Positioning Precision

Analysis of spherical positioning using only the LBL range sensors is the baseline for what is to follow. The basic concept of quantifying the influence of configuration on precision performance is illustrated through this representative, but not exhaustive, example. The Cramér Rao lower bound as the theoretical limit to the performance of the position estimate presents a general method for articulating the configuration design decisions. Section 3.3.1 introduces the CRLB and the methods and metrics for using it as a design tool. This section begins the process of implementing that tool to consider the system level tradeoffs for precise navigation.

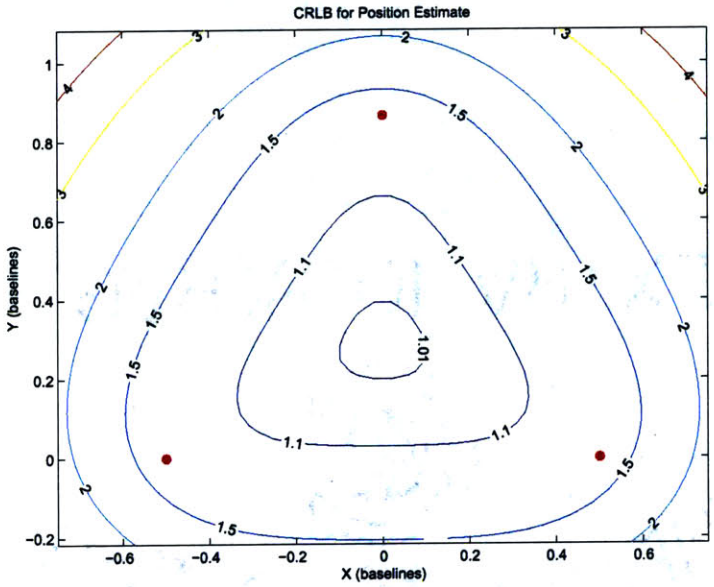

Figure C-1: Spherical positioning with 3 acoustic beacons. The contour values are the ratio of the position estimate uncertainty to the individual range measurement uncertainty as a function of the estimator location relative to the network.

Figure C-1 is the representative configuration case illustrating the method. The configuration

is three transponders with equivalent performance (range uncertainty) arranged in an equilateral triangle pattern. The two-dimensional area in the figure is non-dimensionalized using the network baseline and the contours show the precision factor as discussed in section 3.4.1.

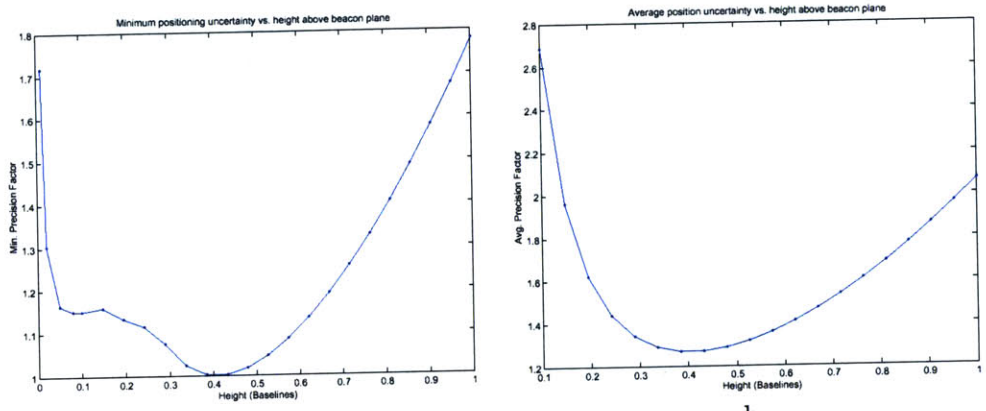

a b

Figure C-2: Optimal height for LBL only survey. a) shows the minimum precision factor as a function of survey height and b) shows the average precision factor for similar survey heights.

The two-dimensional space shown in figure C-1 is a plane parallel to the plane containing the three beacons. Considering just the information from the beacons, without a depth measurement, there is an ambiguity in the Z-plane, i.e., the position solution is consistent if the actual location is above or below the plane containing the transponders. The spherical solution degrades as the location approaches this plane. The results in figure C-1 are for a survey height of 0.4 baselines - where the precision factor is the optimal. Figure C-2 shows how the survey height affects the positioning performance.

For the configuration shown, the precision factor approaches unity in the center of the network indicating that the position estimate will have equivalent uncertainty to the range variance. For example, a precision ranging system might have time-of-flight uncertainty on the order of 1cm (standard deviation of 0.67 ms in seawater). Using three ranges to estimate the three degree-of-freedom position solution would yield equivalent position uncertainty of 1cm in each direction (x, y, and z). Far from the centroid of the acoustic network the position estimates degrades as shown by the increased precision factor.

C.2 Depth Sensor: Reducing the DOF

Depth is measured using low-cost, robust, accurate pressure sensors. The measure provides a level of redundancy to a LBL positioning and is an oceanographic parameter that is useful independent of its navigation utility. For these reasons depth sensors are almost a forgone conclusion when assembling the components of an underwater platform. However, it is worthwhile to consider the impact this additional measurement has on the system performance, especially the precision of the navigation solution. This section will briefly present the value of adding a depth measurement to

the localization estimation problem and illustrate how the CRLB analysis for spherical positioning can be expanded to include an additional measurement.

Extending the CRLB

To extend the CRLB requires appending the observation model from equation 3.7 with a depth measurement.

$$Z = \begin{Bmatrix} Z_r \\ \tilde{z} \end{Bmatrix} = \begin{bmatrix} C \\ \begin{bmatrix} 0 & 0 & 1 \end{bmatrix} \end{bmatrix} \begin{Bmatrix} x \\ y \\ z \end{Bmatrix} + \begin{Bmatrix} w_r \\ w_z \end{Bmatrix} = C_z X + \begin{Bmatrix} w_r \\ w_z \end{Bmatrix}$$

In addition to the range observations an observation of the depth $\tilde{z}$ is included in the observation model. The state vector of the system, the positions, remains the same. The direct observation of the depth and the range measurements are redundant. Recall from equation 3.9 that the Fisher information (the inverse of the CRLB) for our linearized-guassian observation model is expressed as a matrix equation.

$$I_{Z_r}(X) = [C^T R^{-1} C]$$

Since equation C.2 is also linear the Fisher information retains its form.

$$I_{Z_r}(X) = \left[C_z^T \begin{bmatrix} R & 0 \\ 0 & \sigma_z^2 \end{bmatrix}^{-1} C_z \right]$$

Where σ_z^2 is the variance in the depth measurement.

Case: Adding a Depth Sensor to an LBL Network

Section C.1 presents an analysis of the spherical positioning uncertainty for an LBL acoustic ranging system. Extending this analysis we can evaluate the value, in terms of performance, of adding a depth sensor to the localization solution.

Figure C-3 shows how adding a depth measurement affects localization. The scenario is identical to the baseline presented in Figure C-1 so that the results can be directly compared.

Positioning using only beacons was shown to have a strong dependence on the estimator's distance from the plane containing the beacons - the survey height (Figure C-2). With the inclusion of a depth measurement, this dependence is greatly reduced. The precision of the estimate degrades as the survey moves away from the plane, because the overall range to the beacons is increased, but this erosion of the precision is monotonic. The result is that the relative performance is now roughly independent of the survey height.

Figure C-4 is the same scenario shown in Figure C-3, but the locations where the bound is calculated is reduced to almost zero. The resulting reduction in uncertainty, in contrast to increase in uncertainty illustrated without a depth measurement,highlights a contribution to the flexibility of the system.

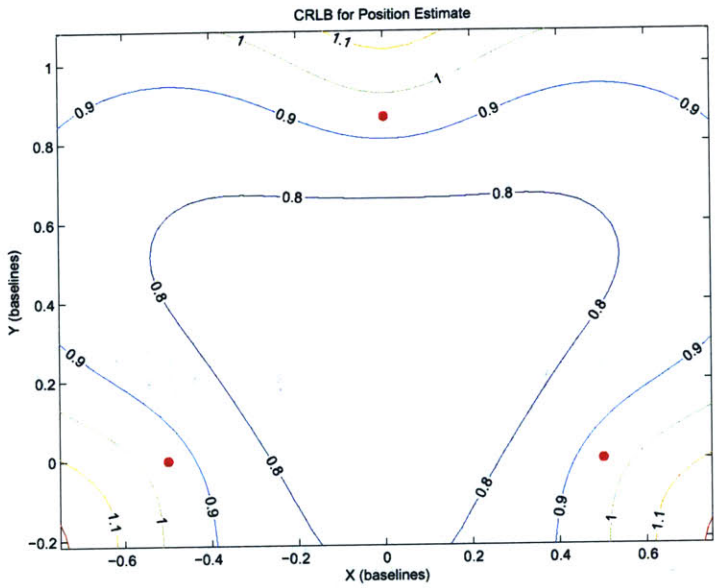

Figure C-3: Using the CRLB to analyze the effect of adding a depth measurement. Height above the plane = 0.4 baselines. Depth uncertainty is equivalent to range uncertainty.

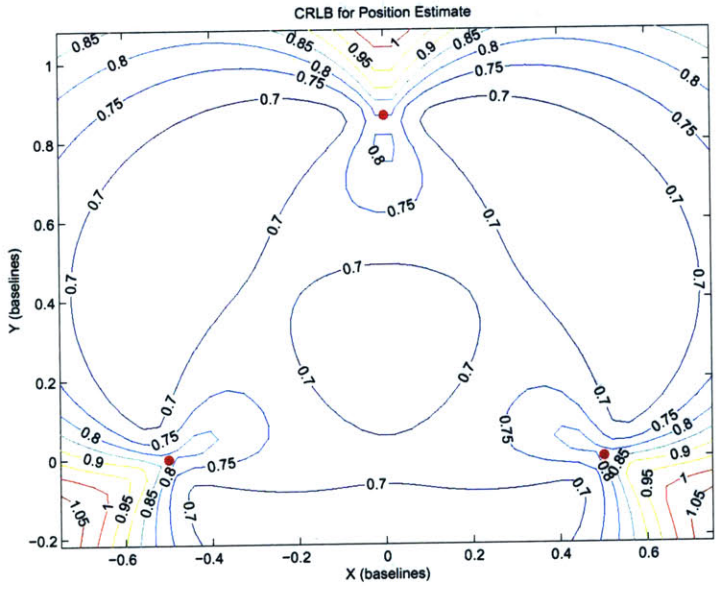

Figure C-4: Reducing the separation between the beacon plane and the survey locations. Height above the plane = 0.05 baselines. Depth uncertainty is equivalent to range uncertainty.

The addition of a depth sensor also contributes to the precision of the solution, but to a small degree. To quantify this comparison a slightly different figure-of-merit is considered. As described in section 3.3.1, the precision factor is the ratio of the volume of the positioning error ellipsoid normalized by the range uncertainty. With the addition of an accurate depth sensor the z-axis of this volume shrinks considerably, but the pertinent question is the effect on the projection of this

volume in the x-y plane.

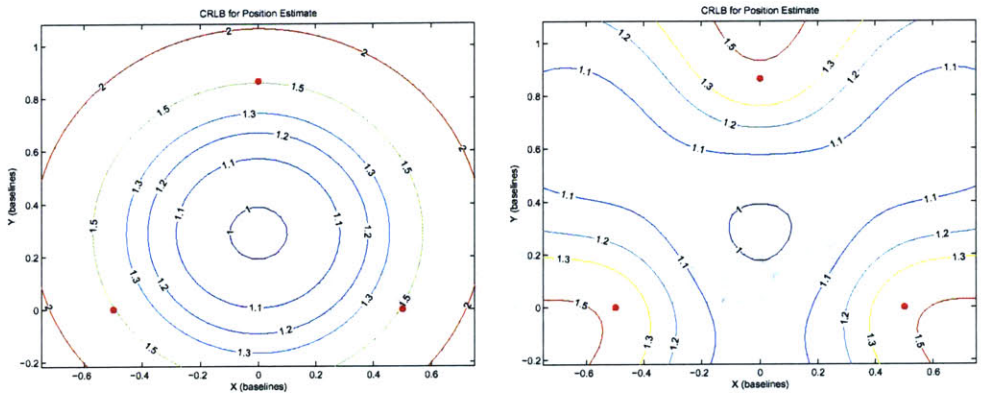

a b

Figure C-5: Contour plots of for the uncertainty with and without a depth sensor. The survey heigh is 0.4 baselines and the 2-d error ellipse in x-y is used in calculating the precision factor. a) Just LBL b) With Depth measurement

Figure C-5 gives a clear comparison which follows from this slight modification of the performance metric. For consistency the results are presented for a case where the survey height is large - 0.4 baselines. The two contour plots show similar magnitudes of precision factor values indicating a minimal increase in horizontal positioning and highlighting the fact that the reason for integrating a depth measurement is the added flexibility and robustness.

To further quantify effect on the horizontal positioning, the relationship between the quality of the depth measurement and the overall improved precision is considered. To present this relation a series of solutions similar to the contour plots from above were calculated over a range of depth sensor measurement qualities. The precision factor is averaged over a rectangular area centered on the beacon layout with characteristic length of 0.75 baselines.

The results in figure C-6 show that the depth measurement has little impact on the horizontal positioning. The *multiplier of precision* (MOP) is plotted on the vertical axis. This metric indicates the multiplicative increase in precision relative to the range uncertainty - the inverse of the precision factor. The lower solid blue curve shows the relationship for the case following from the previous discussion where the survey height is again 0.4 baselines. The upper broken red curve shows the same analysis where the survey height is reduced to 0.05 baselines. For this latter case the value of the depth sensor is illustrated by the increased MOP as the depth sensor uncertainty is reduced. However, even for cases employing precise ranging sensors the depth is *at least* as accurate as the range measurement. This all leads to the conclusion that adding a depth sensor to a long baseline positioning system increases the flexibility of the system by allowing operation close to the depth of the beacons (making it less sensitive to the geometry in the z-dimension), but the relative quality of the depth measurement does not have a strong effect on the overall position estimation.

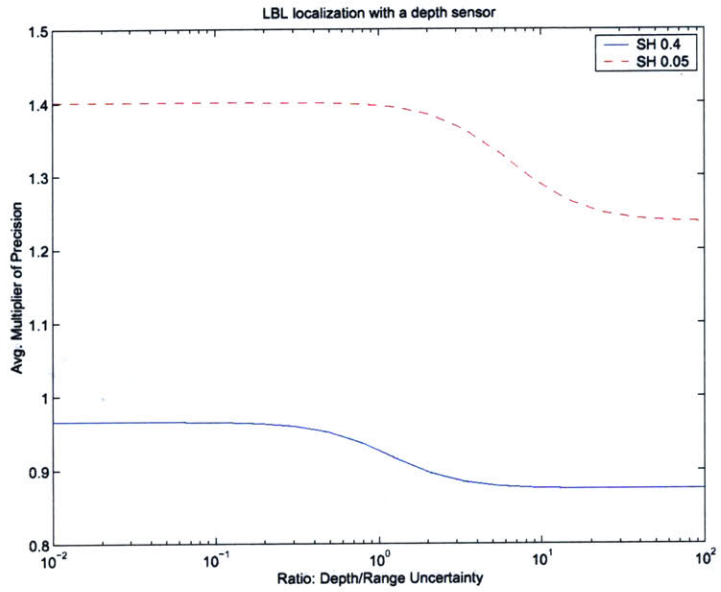

Figure C-6: The relationship between depth uncertainty and positioning precision. Two survey heights (SH) are shown 0.4 baselines and 0.05 baselines

Case: Using Fewer Beacons

The redundancy introduced by adding a depth measurement allows for a position estimate to be attained using fewer beacons. Next we can consider how reducing the number of beacons will affect the precision of a survey and the overall performance of the navigation system.

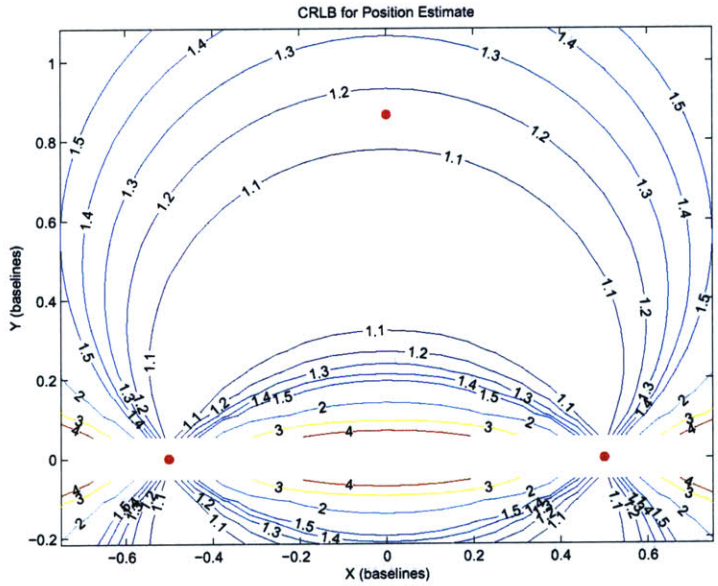

Figure C-7: Eliminating a beacon

Figure C-7 shows the position uncertainty for a scenario where two range measures and

a depth measurement are used to estimate the three degree-of-freedom position. Unsurprisingly the uncertainty is somewhat increased over the case shown in Figure C-4, but is approximately equivalent to the case of three range measurements without a depth measurement.

The Value of a Depth Sensor

Adding a depth sensor has a significant positive influence on position estimation. The following conclusions arise from comparing the long baseline positioning with and without the added depth measurement.

- Integrating a depth measurement decreases the sensitivity of the position estimate to the geometry, specifically to the separation between the estimator and the plane of the acoustic beacons.
- Decreasing this sensitivity also extends the portion of the environment available for survey. Conversely, the range necessary to achieve a particular precision is reduced.
- Measuring depth transforms the positioning problem from three-dimensions to two. This simplification enables intuition and eases the analysis of the performance.
- Baseline crossings must be avoided requiring increased fidelity in the planning and execution of the mission. [active sensing and uncertainty management]

C.3 Network Configuration: Heterogeneous Networks

Another design option is to create a heterogeneous network using beacons of different range/resolution capabilities. This section works through a design example to show another dimension of the flexibility of the method of analysis.

Figure C-8a illustrates a beacon network where the range and uncertainty (standard deviation) are both an order of magnitude higher than the precision beacon. The addition of an accurate odometry sensor in figure C-8b reduces the positioning uncertainty by an order of magnitude - consistent with the results of section 3.4.2. A precision beacon is added in the contour plots shown in figure C-9.

C.4 Network Configuration: Beacon Placement

The previous analysis used ideal geometries for the acoustic transponder networks. The ideal geometry is realized when the distances to the individual beacons is equivalent. Optimal placement is never fully realized and realistic placement is often far from ideal.

The contribution of the beacon placement to the general positioning uncertainty can be quantified by applying the CRLB to the design case. Instead of presenting an exhaustive examination of the possible configuration options, a few illustrative cases are shown to build an intuitive concept for how the geometry of the network affects the solution. This also gives an example of how this

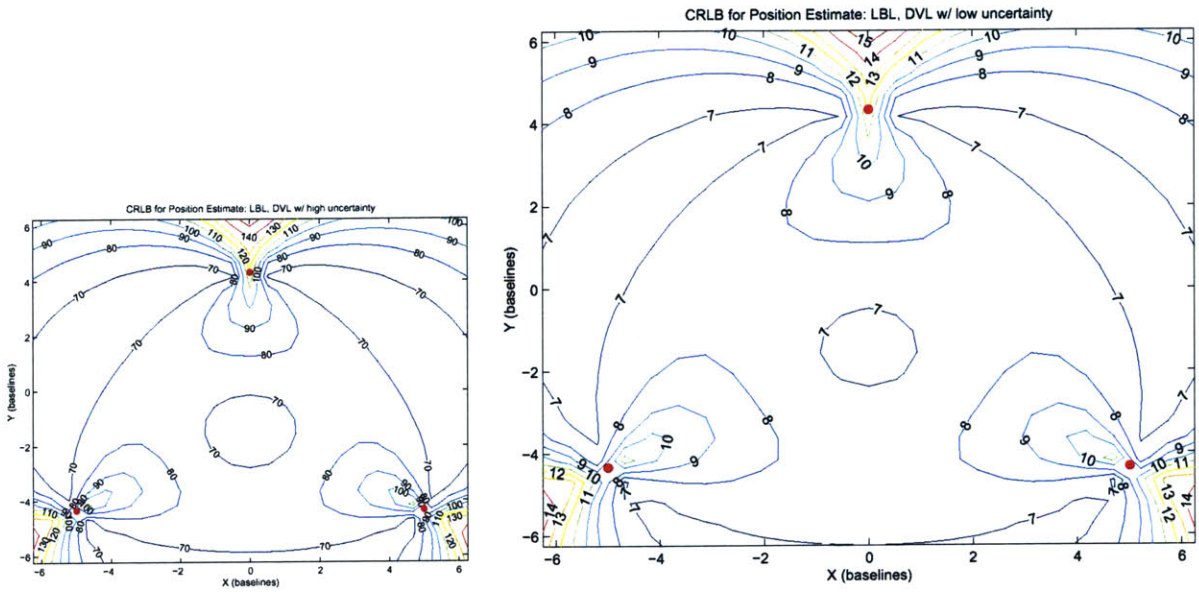

a b

Figure C-8: a) Shows the positioning precision for using acoustic transponders with an inaccurate odometry sensor. b) The same scenario with accurate odometry.

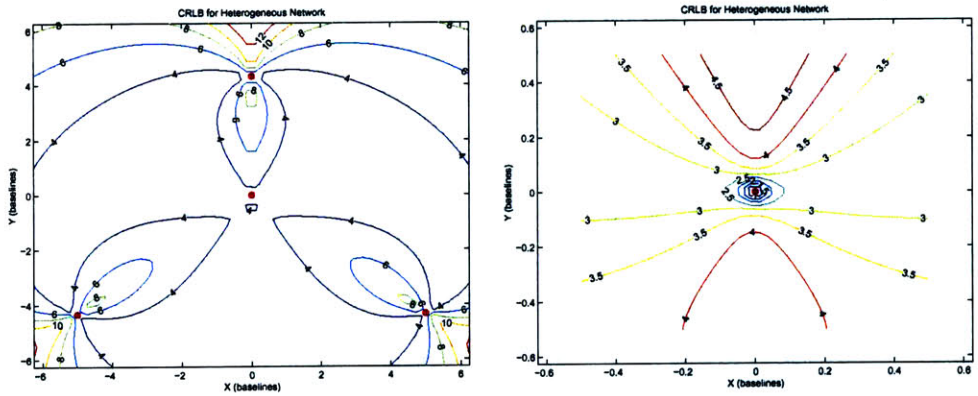

a b

Figure C-9: Adding a precision beacon to an LBL network. a) Shows the entire network and b) is a close up of the contours near the added beacon. All normalization is in terms of the range (baseline) and resolution (uncertainty) of the single precision beacon.

method of considering the layout of survey can be used to design a particular instance and builds towards the concrete example in the following chapter. To make the design choices for a particular instance an engineer could apply the general tool to the particular configurations and geometries of interest.

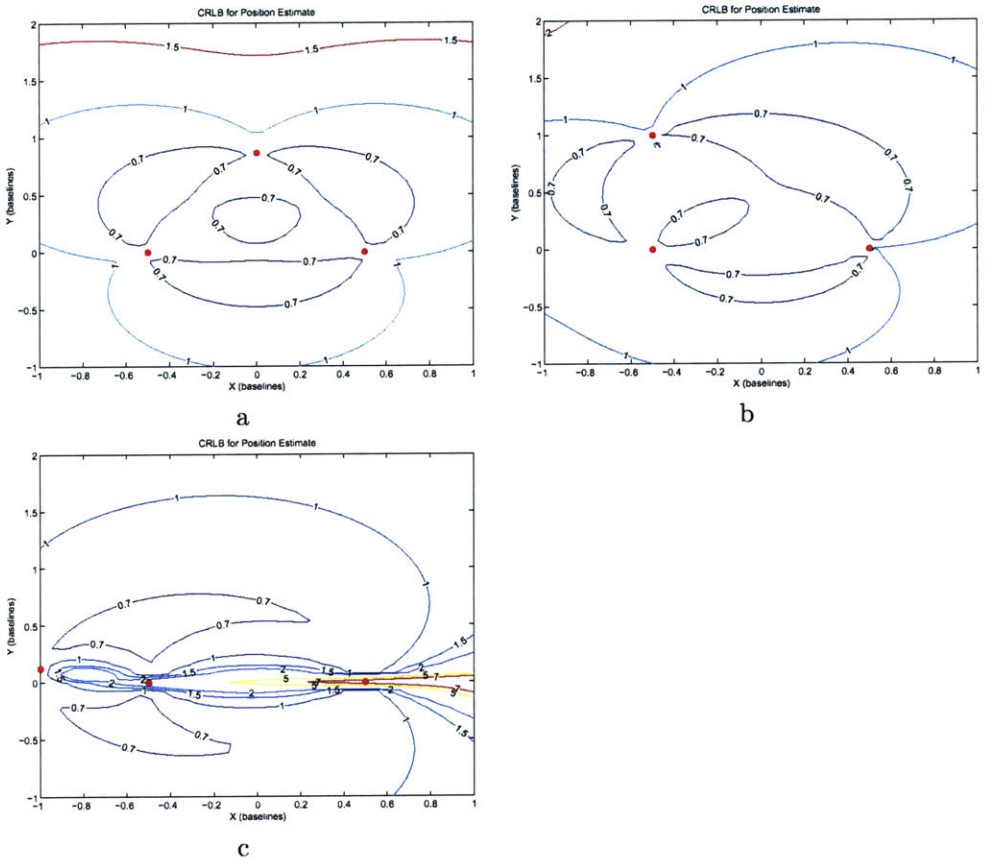

Figure C-10: Illustrating the dependence of precision factor (PF) on the geometry of the acoustic network. Three cases are shown for comparison - each is the 2-D solution using 3 beacons and shown on equivalent axes.

Appendix D

Hypothesis Grid Results

This appendix presents the results of applying the hypothesis grid algorithm to ABE58 as a compliment to section 4.3. The first section of the appendix shows the analysis of grid spacing on the resulting hypothesis grid, justifying the coarse 5x5 grid used for ABE58. The second section shows the hypothesis grid results for beacons 1, 2, and 4 used in ABE58, complimenting the results in chapter 4.

D.1 Metrics for Hypothesis Grid Example

This section explores the metrics for used in the dividing the survey area into a grid structure. As discussed in chapter 4, the challenge is to strike the appropriate tradeoff between accuracy of the representation and the statistical significance of the decomposition. As the number of cells within the grid increases, i.e., the grid becomes more fine, the representation tends to capture more if the information (consider the extreme case were each data point has its own cell within the grid and the grid therefore represents all the information in the classification of the data). But as the cells become smaller, fewer observations are contained within each cell and infering overall characteristics for the cell based on only a few member observations is less significant. The following subsections show how three metrics, *cell variance*, *grid variance*, and *grid spread*, are each affected by the choice of grid resolution.

Cell Variance

The variance within the individual cells is a measure of the accuracy of the representation. The method of building hypothesis grids in chapter 4, assigns the average association probabilities of the members of an individual cell to that cell. The variance (or standard deviation) of this association probabilities about this mean is calculated for a variety of possible grid resolutions. Figure D-1 shows this variance for each of the four hypothesis grids corresponding the the four beacons in the survey and for each of the three hypotheses (DP, MP, and OL). For each set of axes in the figure the variance decreases slightly as the number of cells increases, but remains fairly consisten for representations with more than 16 cells in the grid. The conclusion to be drawn from this metric is that the quality of the representation is insensitive to the grid resolution beyond a certain threshold

and this threshold is low - a 4x4 grid. The figure also shows a slight drop in the variance at 25 (a 5x5 grid) indicating that this may be a good choice for a coarse representation.

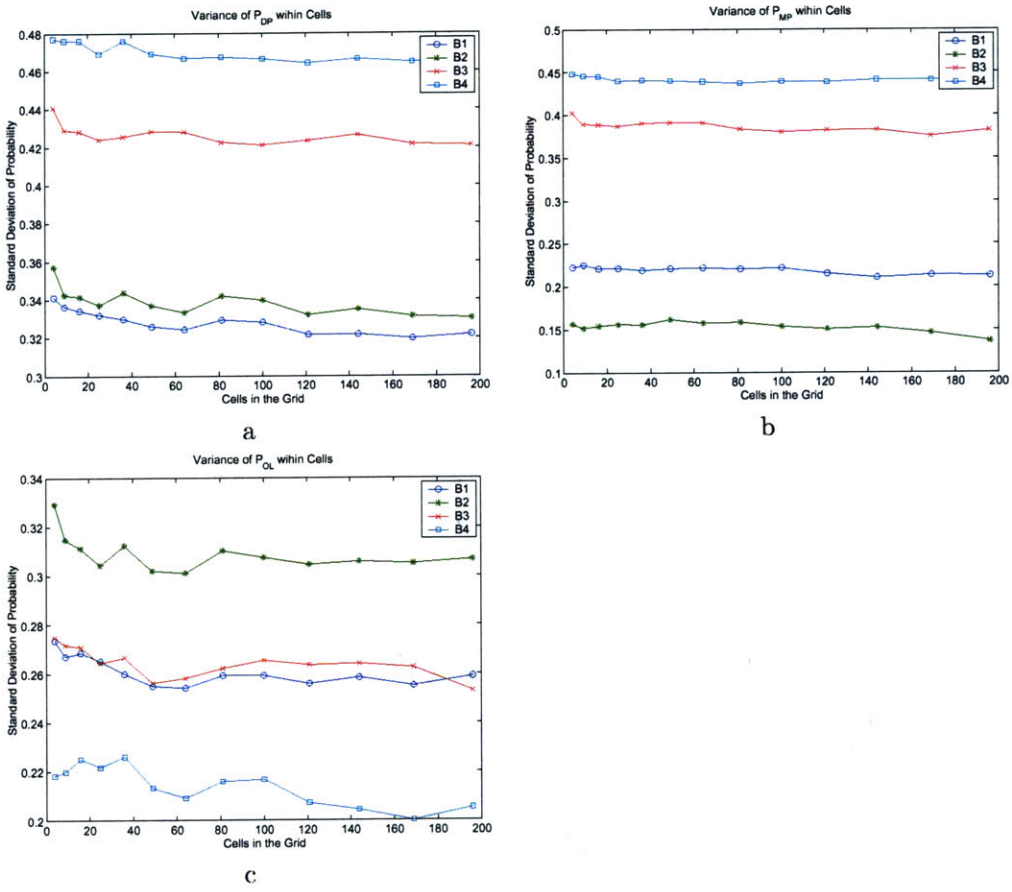

Figure D-1: Shows the variety of probability values within each cell as the grid resolution increases.

Grid Variance

As the number of cells in the grid increases the variance within each cell decreases, but the variance across the grid increases. The grid variance measures the disparity between cells in the grid. A large grid variance indicates that the hypothesis grid contains useful information - that the difference between cells in the grid is large and can be used to benefit the precision and behavior of the survey. Figure D-2 shows the grid variance for all four beacons and the three hypotheses. The trend of of increasing grid variance with increased grid resolution is evident as the curves tend to to have a positive slope. A small peak is evident at 25 cells (a 5x5 grid), especially in axis c of the figure, indicating a good choice for a coarse representation.

D.1.1 Grid Spread

Another method for measureing the disparity of probabilities across the grid is to by calculating the difference between the maximum and minimum association probabilities. This metric captures

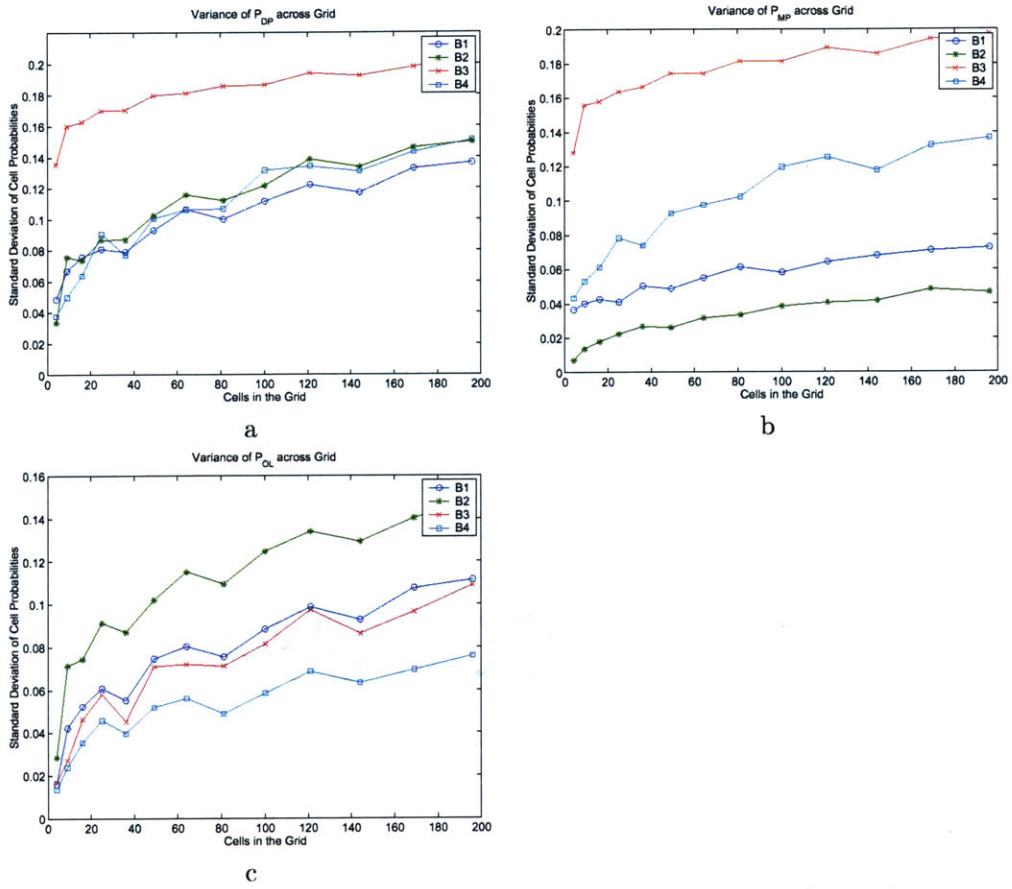

Figure D-2: Shows the growing variety of cell values as grid resolution increases.

the same tradeoff as the grid variance metric, but in a slightly different way. Figure D-3 shows the grid spread as a function of the resolution of the grid. Axis a shows the aveage spread for each of the four hypothesis grids averaged across the probabilities, eg., the curve for beacon #3 is the average spread for P_{DP}, P_{MP}, and P_{OL}. Axis b shows the grid spread for each hypothesis averaged across the four hypothesis grids, eg., the P_{DP} curve shows the average spread for all four beacons. Lastly, axis c shows the average spread, averaged across the threehypotheses and the four beacons. As with the grid variance metric, a small peak is evident at 25 cells (a 5x5 grid) indicating a good choice for a coarse grid.

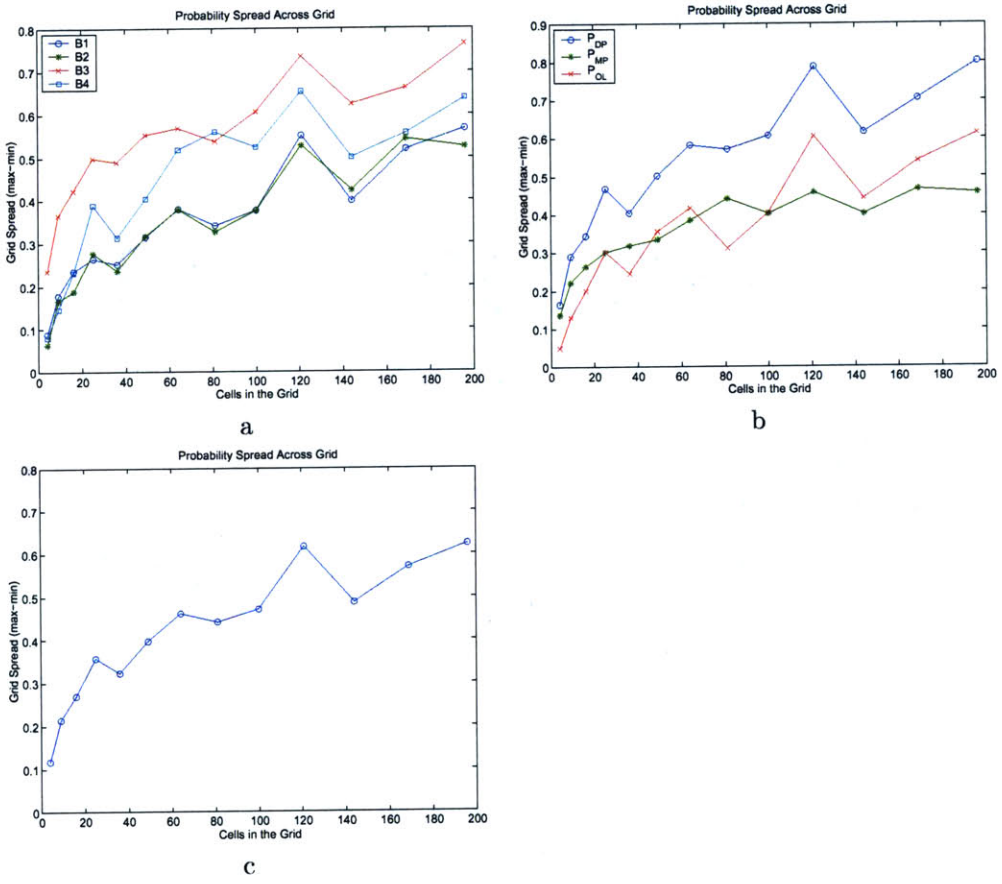

Figure D-3: Different averaging

D.2 Hypothesis grids for ABE58

This section presents the results of the hypothesis grid creation from chapter 4 where only beacon #3 was presented for brevity. The blue, red, and green colormap represents the probability of direct-path, multipath, and outlier as shown in figure 4-13. For each beacon a hypothesis grid is created and visualized by a colored grid and a numeric grid. The black markers ineach of the colored grid plots are the post-processed ABE locations included for spatial reference.

Figure D-4 shows the hypothesis grid for beacon #1 of ABE58. Figure 4-6 shows the X-Y localization estimates of ABE58 and the relative beacon placement. Beacon #1 is north of the survey area and slightly east of the centerline. The predomenantly blue cells in the upper area of the hypothsis grid indicate that direct-path observation is probabable in this region of the survey. The more green cell in the north-most row is consistent across all the beacons where the probability of receiving an outlier is particularly high ($\approx 40\%$). This could be a region of the survey area that is particularly problematic or may indicate a temporal dependence and an particular time that was problematic.

Figure D-5 shows the hypothesis grid for beacon #2 of ABE58. This hypothesis grid exhibits more variation. In addition to the blue areas indicating a probability of direct-path observation green cells indicate areas where outliers are probably and the more red areas those that tend to contain multipath observations.

Figure D-6 shows the hypothesis grid for beacon #4 of ABE58. Beacon #4 is south and west of the survey area. The increased red component of the cells in the southeast corner of the grid indicate that in this corner, far from the beacon, there is an increased probability of observing a multipath return. Again, the green cell in the northern row indicates a problematic area of the survey with and increased probability of observing and outlier.

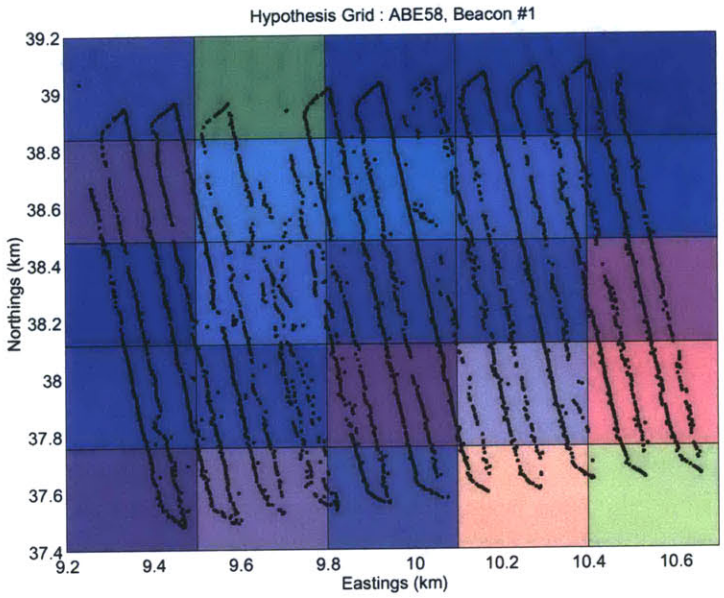

a

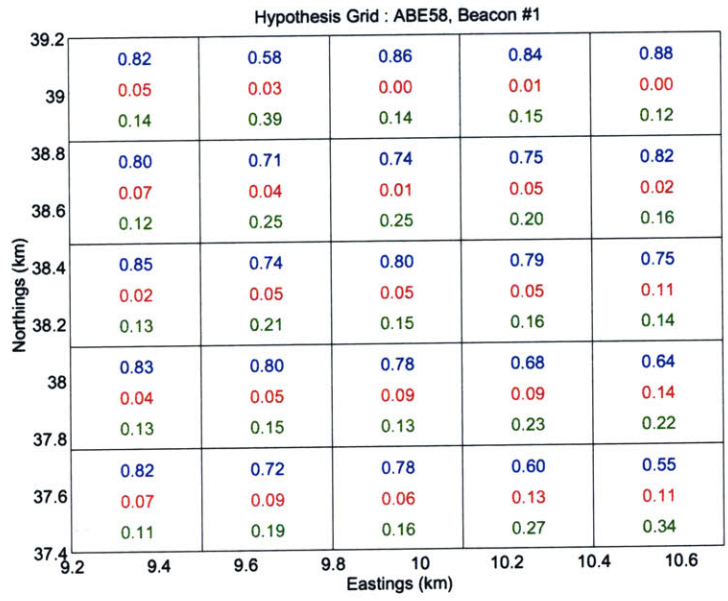

b

Figure D-4: a) The hypothesis grid for beacon 1 with the ABE58 survey positions. b) The hypothesis grid values for beacon 1. The numbers in each cell are the association probabilities for direct path (blue), multipath (red), and oultlier (green).

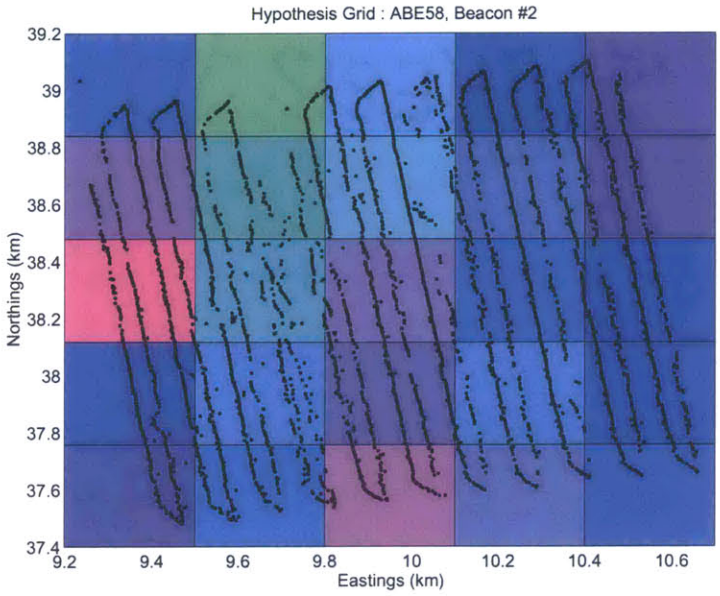

a

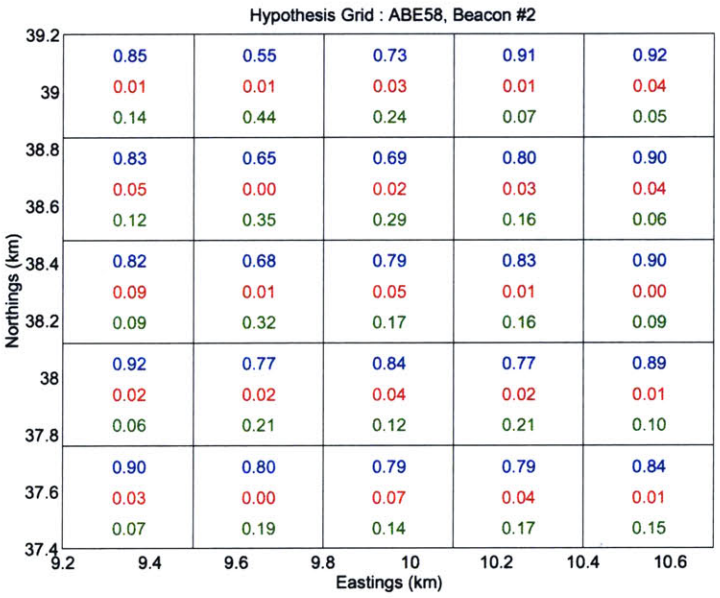

b

Figure D-5: a) The hypothesis grid for beacon 2 with the ABE58 survey positions. b) The hypothesis grid values for beacon 2. The numbers in each cell are the association probabilities for direct path (blue), multipath (red), and oultlier (green).

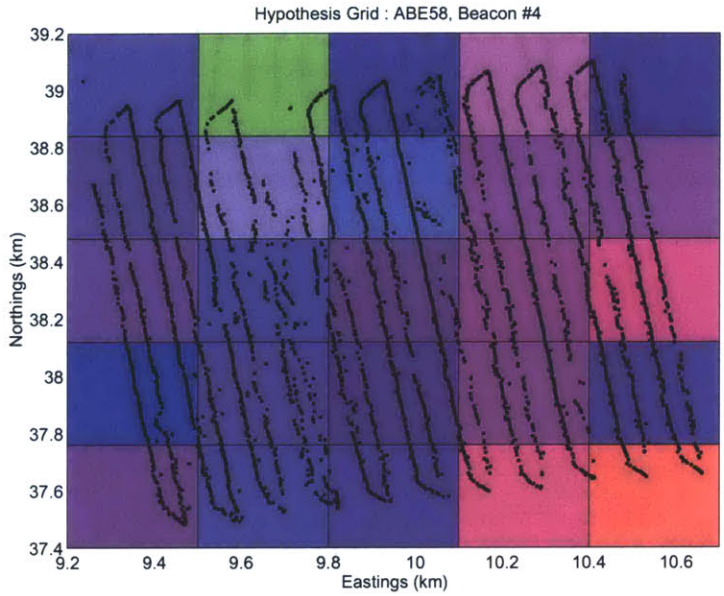

a

Hypothesis Grid : ABE58, Beacon #4

Northings (km) / Eastings (km)

39.2	0.64 0.23 0.13	0.26 0.30 0.44	0.70 0.20 0.10	0.50 0.35 0.15	0.68 0.25 0.07
39 / 38.8	0.63 0.28 0.09	0.53 0.28 0.19	0.59 0.23 0.17	0.55 0.33 0.12	0.55 0.33 0.12
38.6 / 38.4	0.59 0.30 0.10	0.64 0.22 0.13	0.61 0.31 0.08	0.56 0.35 0.10	0.48 0.41 0.10
38.2 / 38	0.76 0.16 0.07	0.62 0.25 0.12	0.64 0.29 0.08	0.56 0.34 0.11	0.65 0.25 0.10
37.8 / 37.6	0.60 0.32 0.08	0.65 0.23 0.12	0.65 0.25 0.10	0.47 0.42 0.12	0.34 0.51 0.15
37.4	9.2	9.4 / 9.6	9.8 / 10	10.2 / 10.4	10.6

b

Figure D-6: a) The hypothesis grid for beacon 4 with the ABE58 survey positions. b) The hypothesis grid values for beacon 4. The numbers in each cell are the association probabilities for direct path (blue), multipath (red), and oultlier (green).

Bibliography

[Allen et al., 1997] Allen, B., Stokey, R., Austin, T., Forrester, N., Goldsborough, R., Purcell, M., and von Alt, C. (1997). REMUS: A small, low cost AUV; system description, field trials and performance results. In *OCEANS'97*, volume 2, pages 994–1000, Halifax, NS. MTS/IEEE.

[Anderberg, 1973] Anderberg, M. R. (1973). *Cluster Analysis for Applications.* Academic Press Inc.

[Austin, 1994] Austin, T. C. (1994). The application of spread spectrum signaling techniques to underwater acoustic navigation. In *Proceedings of the 1994 Symposium on Autonomous Underwater Vehicle Technology*, pages 443–449. IEEE.

[Ayache and Faugeras, 1989] Ayache, N. and Faugeras, O. (1989). Maintaining representations of the environment of a mobile robot. *IEEE Trans. Robotics and Automation*, 5(6):804–819.

[Ballard, 2001] Ballard, R. (2001). Black sea mysteries: Ancient shipwrecks and telltale shells bring to life epics of distant trade and a prehistoric flood. *National Geographic*, pages 52–69.

[Ballard et al., 2000] Ballard, R. D., McCann, A., D.Yoerger, Whitcomb, L., Mindell, D., Oleson, J., Singh, H., Foley, B., Adams, J., and Picheota, D. (2000). The discovery of ancient history in the deep sea using advanced deep submergence technology. *Deep-Sea Research*, 47(9):1591–1620.

[Bar-Shalom and Fortmann, 1988] Bar-Shalom, Y. and Fortmann, T. E. (1988). *Tracking and Data Association.* Academic Press.

[Bar-Shalom and Li, 1998] Bar-Shalom, Y. and Li, X. R. (1998). *Estimation and Tracking: Principles, Techniques, and Software.* Yaakov Bar-Shalom (YBS).

[Bar-Shalom et al., 2001] Bar-Shalom, Y., Li, X.-R., and Kirubarajan, T. (2001). *Estimation with applications to tracking and navigation.* John Wiley and Sons, Inc.

[Bascomb, 1976] Bascomb, W. (1976). *Deep Water, Ancient Ships.* Doubleday and Company, Inc.

[Bass, 1966] Bass, G. (1966). *Archaeology Under Water.* Praeger.

[Bass, 1967] Bass, G. F. (1967). Cape gelidonya: A bronze age shipwreck. *Transactions of the American Philosophical Society*, 57(8).

[Bellingham et al., 1994] Bellingham, J., Goudey, C., Consi, T., Bales, J., Atwood, D., Leonard, J., and Chryssostomidis, C. (1994). A second generation survey AUV. In *Proceedings of the 1994 IEEE Symposium on Autonomous Underwater Vehicle Technology*, pages 148–155, Cambridge.

[Bellingham, 1997] Bellingham, J. G. (1997). New oceanographic uses of autonomous underwater vehicles. *MTS Journal*, 31(3):34–47.

[Bellingham et al., 1990] Bellingham, J. G., Consi, T. R., Beaton, R. M., and Hall, W. (1990). Keeping layered control simple. In *Proceedings of the (1990) Symposium on Autonomous Underwater Vehicle Technology - AUV '90*, pages 3–8.

[Bennett and Leonard, 1999] Bennett, A. A. and Leonard, J. J. (1999). Feature-relative navigation of an autonomous underwater vehicle. In *Int. Symp. on Unmanned Untethered Submersible Technology*, New Hampshire.

[Bilmes, 1997] Bilmes, J. (1997). A gentle tutorial on the EM algorithm and its application to parameter estimation for gaussian mixture and hidden markov models.

[Bowditch, 2002] Bowditch, N. (2002). *The American Practical Navigator: Bowditch.* Paradise Cay Publications. http://www.irbs.com/bowditch/.

[Brekhovskikh and Lysanov, 1991] Brekhovskikh, L. M. and Lysanov, Y. P. (1991). *Fundamentals of Ocean Acoustics.* Springer-Verlag, second edition.

[Broad, 1998] Broad, W. (1998). *The Universe Below.* Touchstone Books.

[Brooks, 1989] Brooks, R. A. (1989). How to build complete creatures rather than isolated cognitive simulators. In VanLehn, K., editor, *Architectures for Intelligence*, pages 225–239, Hillsdale, NJ.

[Brooks, 1990] Brooks, R. A. (1990). Elephants don't play chess. *Robotics and Autonomous Systems*, 6:3–15.

[Brooks, 1991a] Brooks, R. A. (1991a). Intelligence without representation. *Artificial Intelligence*, pages 139–159.

[Brooks, 1991b] Brooks, R. A. (1991b). New approachs to robotics. *Science*, 253(5025):1227–1232.

[Brooks, 1997] Brooks, R. A. (1997). From earwigs to humans. *Robotics and Autonomous Systems*, 20:291–304.

[Brown and Hwang, 1996] Brown, R. G. and Hwang, P. Y. (1996). *Introduction to Random Signals and Applied Kalman Filtering: with MATLAB Exercises and Solutions.* John Wiley & Sons, Inc., 3 edition.

[Caimi et al., 1998] Caimi, F., Tongta, R., Carroll, M., and Murshid, S. (1998). Acoustic impulse response mapping for acoustic communications in shallow water. In *OCEANS '98*, volume 3, pages 1739–1743. IEEE.

[Church et al., 2002] Church, R. A., Warren, D. J., Hill, A. W., and Smith, J. S. (2002). The discovery of u-166: Rewriting history with new technology. In *2002 Offshore Technology Conference Proceedings*, Houston, TX.

[Coleman and Steele, 1999] Coleman, H. W. and Steele, G. W. (1999). *Experimentation and uncertainty analysis for engineers.* John Wiley.

[Cox and Leonard, 1994] Cox, I. J. and Leonard, J. J. (1994). Modeling a dynamic environment using a bayesian multiple hypothesis approach. *Artificial Intelligence*, 66:311–344.

[Curtin et al., 1993] Curtin, T. B., Bellingham, J. G., Catipovic, J., and Webb, D. (1993). Autonomous oceanographic sampling networks. *Oceanography*, 6(3):86–94.

[Deffenbaugh, 1997] Deffenbaugh, M. (1997). *Optimal Ocean Acoustic Tomography and Navigation with Moving Sources.* PhD thesis, MIT WHOI.

[Deffenbaugh et al., 1996a] Deffenbaugh, M., Bellingham, J. G., and Schmidt, H. (1996a). The relationship between spherical and hyperbolic positioning. In *OCEANS 96 MTS/IEEE*, Ft. Lauderdale, Florida.

[Deffenbaugh et al., 1996b] Deffenbaugh, M., Schmidt, H., and Bellingham, J. G. (1996b). Acoustic positioning in a fading multipath environment. In *OCEANS '96, MTS/IEEE*, pages 596–600.

[Delaney et al., 2001] Delaney, J., Chave, A., Heath, G. R., Howe, B., and Beauchamp, P. (2001). Neptune: Real-time, long-term ocean and earth studies at the scale of a tectonic plate. In *OCEANS 2001*, Honolulu, HI.

[Delgado, 1997] Delgado, J., editor (1997). *Encyclopedia of Underwater and Maritime Archaeology.* Yale University Press.

[Dellaert et al., 2000] Dellaert, F., Seitz, S., Thorpe, C., and Thrun, S. (2000). Structure from motion without correspondence. *Conference on Computer Vision and Pattern Recognition.*

[Dellaert et al., 2003] Dellaert, F., Seitz, S. M., Thorpe, C., and Thrun, S. (2003). EM, MCMC, and chain flipping for structure from motion with unknown correspondence. *Machine Learning*, 50(1-2).

[Dempster et al., 1977] Dempster, A., Laird, A., and Rubin, D. (1977). Maximum likelihood from incomplete data via the EM algorithm. *Journal of the Royal Statistical Society.*

[Doucet et al., 2001] Doucet, A., de Freitas, N., and Gordon, N., editors (2001). *Sequential Monte Carlo Methods in Practice.* Statistics for Engineering and Information Science. Springer.

[Drake, 1967] Drake, A. W. (1967). *Fundamentals of applied probability theory.* McGraw-Hill.

[Durrant-Whyte and Stevens, 2001] Durrant-Whyte, H. and Stevens, M. (2001). Data fusion in decentralized sensing networks. In *4th International Conference on Information Fusion 2001*, Montreal, Canada.

[Elfes, 1989] Elfes, A. (1989). Using occupancy grids for mobile robot perception and navigation. *IEEE Computer*, pages 46–57.

[Elfes, 1992] Elfes, A. (1992). Dynamic control of robot perception using multi-property inference grids. In *Proceedings of the 1992 IEEE INternational Conference on Robotics and Automoation*, pages 2561–2567.

[Faugera, 1993] Faugera, O. (1993). *Three-Dimensional Computer Vision*. MIT Press.

[Feder et al., 1999] Feder, H. J. S., Leonard, J. J., and Smith, C. M. (1999). Adaptive mobile robot navigation and mapping. *Int. J. Robotics Research*, 18(7):650–668.

[Foley and Mindell, 2002] Foley, B. and Mindell, D. (2002). Precision survey and archaeological methodology in deep water. *ENALIA The Journal of the Hellenic Institute of Marine Archaeology*, VI:49–56.

[Freitag et al., 2000] Freitag, L., Johnson, M., Stojanovic, M., Nagle, D., and Catipovic, J. (2000). Survey and analysis of underwater acoustic channels for coherent communication in the medium-frequency band. In *OCEANS 2000*, volume 1. MTS/IEEE.

[Freitag et al., 1998] Freitag, L., Stojanovic, M., Singh, S., and Johnson, M. (1998). Analysis of channel effects on direct-sequence and frequency-hopped spread-spectrum acoustic communication. *Oceanic Engineering, IEEE Journal of*, 26(4):586–593.

[Friedlander, 1988] Friedlander, B. (1988). Accuracy of source localization using multipath delays. *IEEE Transactions on Aerospace and Electronic Systems*, 24(4):346–351.

[Gelb, 1974] Gelb, A. (1974). *Applied Optimal Estimation*. MIT Press.

[Green and Blackmon, 2001] Green, D. and Blackmon, F. (2001). Performance of channel-equalized acoustic communications in the surf zone. In *OCEANS 2001, MTS/IEEE Conference*, volume 4, pages 2262–2269.

[Grocholsky et al., 2003] Grocholsky, B., Makarenko, A., and Durrant-Whyte, H. (2003). Information-theoretic coordinated control of multiple sensor platforms. In *IEEE International Conference on Robotics and Automation (ICRA'03)*, Taipei, Taiwan.

[Herdendorf and Meserve, 1995] Herdendorf, C. E. and Meserve, L. A., editors (1995). *Science on a Deep-Ocean Shipwreck*, volume 95. The Ohio Journal of Science. Special Issue.

[Huster et al., 1998] Huster, A., Fleischer, S. D., and Rock, S. M. (1998). Demonstration of a vision-based dead-reckoning system for navigation of an underwater vehicle. In *OCEANS '98*, pages 326–330.

[Huster and Rock, 2001] Huster, A. and Rock, S. M. (2001). Relative position estimation for manipulation tasks by fusing vision and inertial measurements. In *OCEANS 2001, MTS/IEEE Conference and Exhibition*.

[H.Wang et al., 2996] H.Wang, H., Rock, S. M., and Lee, M. J. (2996). OTTER: The design and development of an intelligent underwater robot. *Autonomous Robots*, pages 297–320.

[Jeffreys, 1961] Jeffreys, H. (1961). *Theory of Probability.* Oxford University Press.

[Jensen et al., 2000] Jensen, F. B., Kuperman, W. A., Porter, M. B., and Schmidt, H. (2000). *Computational Ocean Acoustics.* Springer-Verlag, New York, NY.

[Johnson et al., 1995] Johnson, M., Brady, D., and Grund, M. (1995). Reducing the computational reqirements of adaptive equalization in underwateracoustic communications. In *OCEANS '95*, volume 3, pages 1405–1410. MTS/IEEE.

[Kalman, 1960] Kalman, Rudolph, E. (1960). A new approach to linear filtering and prediction problems. *Transactions of the ASME–Journal of Basic Engineering*, 82(Series D):35–45.

[Kaplan, 1996] Kaplan, D. (1996). *Understanding GPS.* Artech House Publisher.

[Kinder, 1999] Kinder, G. (1999). *Ship of Gold in the Deep Blue Sea.* Vintage Books.

[Larsen, 2000a] Larsen, M. B. (2000a). High performance Doppler-inertial navigation - experimental results. In *IEEE OCEANS 2000.*

[Larsen, 2000b] Larsen, M. B. (2000b). Synthetic long baseline navigation of underwater vehicles. In *OCEANS 2000*, volume 3, pages 2043–2050.

[Larsen, 2002] Larsen, M. B. (2002). High performance autonomus underwater navigation. *Hydro International.*

[Latombe, 1991] Latombe, J.-C. (1991). *Robot Motion Planning.* Boston: Kluwer Academic Publishers.

[Leonard, 1990] Leonard, J. J. (1990). *Directed Sonar Sensing for Mobile Robot Navigation.* PhD thesis, University of Oxford.

[Leonard et al., 1998] Leonard, J. J., Bennett, A. A., Smith, C. M., and Feder, H. J. S. (1998). Autonomous underwater vehicle navigation. Technical Report 98-1, Marine Robotics Laboratory.

[Leonard and Durrant-Whyte, 1991] Leonard, J. J. and Durrant-Whyte, H. F. (1991). Simultaneous map building and localisation for an autonomous robot. In *IEEE/RSJ International Workshop on Intelligent Robots and Systems (IROS '91)*, pages 1442–1447.

[Leonard and Durrant-Whyte, 1992] Leonard, J. J. and Durrant-Whyte, H. F. (1992). *Directed Sonar Sensing for Mobile Robot Navigation.* Kluwer Academic Publishers.

[Leonard et al., 1995] Leonard, J. J., Moran, B. A., Cox, I. J., and Miller, M. L. (1995). Underwater sonar data fusion using an efficient multiple hypothesis algorithm. In *Proc. IEEE Int. Conf. Robotics and Automation*, pages 2995–3002.

[Leonard and Rikoski, 2001] Leonard, J. J. and Rikoski, R. J. (2001). Incorporation of delayed decision making into stochastic mapping. In *Experimental Robotics VII*, volume 271 of *Lecture Notes in Control and Information Sciences,*, pages 533–542. Springer-Verlag.

[Lewis, 1972] Lewis, D. (1972). *We, the Navigators: The Ancient Art of Landfinding in the Pacific.* University of Hawaii Press, second edition.

[Loubet and Jourdain, 1993] Loubet, G. and Jourdain, G. (1993). Characterization of the underwater medium as an acoustical horizontal transmission channel. In *IEEE International Conference on Acoustics, Speech, and Signal Processing*, volume 1, pages 329–332.

[Makarenko et al., 2002] Makarenko, A. A., b. Williams, S., Bourgault, F., F., H., and F, H. (2002). An experiment in integrated exploration. In *2002 IEEE/RSJ International Conference on Intelligent Robots and Systems (IROS 2002).*

[Manyika and Durrant-Whyte, 1994] Manyika, J. and Durrant-Whyte, H. (1994). *Data Fusion and Sensor Management: A Decentralized Information-Theoretic Approach.* Ellis Horwood.

[Mataric, 1992a] Mataric, M. (1992a). Designing emergent behaviors: From local interactions to collective intelligence.

[Mataric, 1997] Mataric, M. (1997). Behavior-based control: Examples from navigation.

[Mataric, 1992b] Mataric, M. J. (1992b). Behavior-based systems: Main properties and implications. In *IEEE International Conference on Robotics and Automation, Workshop on Architectures for Intelligent Control Systems*, pages 46–54.

[McAnn and Freed, 1994] McAnn, A. M. and Freed, J. (1994). Deep water archaeology: A late Roman ship from Carthage and an ancient trade route near Skerki Bank off northwest Sicily. *Journal of Roman Archaeology, Supplementary Series*, (13).

[McElroy et al., 2001] McElroy, M. K., Edson, J. B., Austin, T. C., McGillis, W. R., and Purcell, M. J. (2001). Underwater observatories: The challenges and promise of applying off-shore cable technology to long-term environmental studies. In *Proceedings of Under Intervention-2001 MTS/ADC.*

[Milne, 1983] Milne, P. H. (1983). *Underwater Acoustic Positioning Systems.* Gulf Publishing Company, Houston.

[Mindell, 1996] Mindell, D. A. (1996). *Datum for its Own Annihilation: Feedback, Control, and Computing 1916-45.* PhD thesis, Massachusetts Institute of Technology.

[Mindell and Bingham, 2001] Mindell, D. A. and Bingham, B. (2001). New archaeological uses of autonomous undersea vehicles. In *OCEANS '01 - MTS/IEEE Oceans Conference.*

[Moravec, 1988] Moravec, H. P. (1988). Certainty grids for sensor fusion in mobile robots. *AI Magazine*, 9(2):61–77.

[Neira and Tardos, 2001] Neira, J. and Tardos, J. (2001). Data association in stochastic mapping using the joint compatibility test. In *IEEE Trans. Robotics and Automation*, volume 17, pages 890–897.

[Newman et al., 2003] Newman, P. M., Bosse, M., and Leonard, J. J. (2003). Autonomous feature-based exploration. Technical report, MIT Marine Robotics Laboratory Technical memorandum 2002-03. Submitted to the 2003 IEEE International Conference on Robotics and Automation.

[Newman and Leonard, 2002] Newman, P. M. and Leonard, J. J. (2002). Pure range-only sub-sea slam. Technical report, MIT Marine Robotics Laboratory. Submitted to the 2003 IEEE International Conference on Robotics and Automation.

[Otto and Wood, 2001] Otto, K. N. and Wood, K. L. (2001). *Product Design.* Prentice Hall.

[Pagac et al., 1996] Pagac, D., Nebot, E. M., and H., D.-W. (1996). An evidential approach to probabilistic map-building. In *Proceedings. 1996 IEEE International Conference on Robotics and Automation (Cat. No.96CH35857)*, volume 1 of *IEEE. Part*, pages 745–750, New York, NY, USA.

[Papoulis, 2002] Papoulis, A. (2002). *Probability, random varianbles, and stochastic processes.* McGraw-Hill.

[Pierce, 1980] Pierce, J. R. (1980). *An Introduction to Information Theory: Symbols, Signals and Noise.* Dover, second edition.

[Press et al., 1993] Press, W. H., Flannery, B. P., Teukolsky, S. A., and Vetterling, W. T. (1993). *Numerical Recipies in C: The Art of Scientific Computing.* Cambridge University Press, second edition.

[Proakis, 1989] Proakis, J. G. (1989). *Digital Communications.* McGraw-Hill.

[Purcell et al., 2000] Purcell, M., von Alt, C., Allen, B., Austin, T., Forrester, N., Glodsborough, R., and Stokey, R. (2000). New capabilities of the REMUS autonomous underwater vehicle. In *Proceedings Oceans 2000*, Providence, RI.

[Rabinovich, 2000] Rabinovich, S. G. (2000). *Measurement errors and uncertainties: theory and practice.* SIP Press, second edition.

[Reid, 1979] Reid, D. B. (1979). An algorithm for tracking multiple targets. In *IEEE Transactions on Automatic Control*, pages 843–854.

[Ribo and Pinz, 2001] Ribo, M. and Pinz, A. (2001). A comparison of three uncertainty calculi for buildign sonar-based occupancy grids. *Robotics and Autonomous Systems*, 35:201–209.

[Romeo and Lester, 2001] Romeo, J. and Lester, G. (2001). Navigation is key to AUV missions. *Sea Technology.*

[Saeed, 1997] Saeed, M. (1997). Maximum likelihood parameter estimation of mixture models and its applicaiton to image segmentation and restoration. Master's thesis, Massachusetts Institute of Technology.

[Saltzer, 1985] Saltzer, J. H. (1985). Topics in the engineering of computer systems: 6.033 class notes.

[Schouten et al., 2002] Schouten, H., Tivey, M., Fornari, D., Yoerger, D., Bradley, A., Edwards, M., Johnson, P., , Science, S., and Teams, T. (2002). Near-bottom investigation of the central anomaly magnetic high (CAMH) at the east pacific rise 9 25'-57'n. Technical report, R/V Atlantis, Voyage 7, Leg 4. http://www.soest.hawaii.edu/HMRG/EPR/.

[Schultz et al., 1999] Schultz, A. C., Adams, W., Yamauchi, B., and Jones, M. (1999). Unifying exploration, localization, navigation and planning through a common representation. In *Proceedings of the IEEE International Conference on Robotics and Automation*, volume 4, pages 2651–2658.

[Shafer, 1976] Shafer, G. (1976). *A mathematical theory of evidence.* Princeton University Press.

[Shannon, 1948] Shannon, C. (1948). A mathematical theory of communication. *Bell Systems Technical Journal.*

[Sheridan, 1987] Sheridan, T. B. (1987). *Supervisory control*, chapter Handbook of Human Factors, pages 1243–1268. John Wiley.

[Sheridan, 1992] Sheridan, T. B. (1992). *Telerobotics, Automation, and Human Supervisory Control.* MIT Press.

[Simon, 1996] Simon, H. A. (1996). *The Sciences of the Artificial.* MIT Press, third edition.

[Simon, 2000] Simon, H. A. (2000). Can there be a science of complex systems. In Bar-Yam, Y., editor, *Unifying Themes in Complex Systems: Proceedings fo the International Conference on Complex Systems*, pages 3–13. New England Comples Systems Institute, Perseus Books.

[Singh et al., 2000a] Singh, H., Pizarro, O., Whitcomb, L., and Yoerger, D. (2000a). In-situ attitude calibration for high resolution bathymetric surveys with underwater robotic vehicles. In *Proceedings of the 2000 IEEE International Conference on Robotics and Automation*, pages 1767–1774, San Francisco, CA. IEEE.

[Singh et al., 2000b] Singh, H., Whitcomb, L., Yoerger, D., and Pizzaro, O. (2000b). Microbathymetric mapping from underwater vehicles in the deepocean. *Computer Vision and Image Understanding.*

[Singh et al., 1997] Singh, H., Yoerger, D., and Bradley, A. (1997). Issues in AUV design and deployment for oceanographic research. In *Proceedings of the 1997 IEEE International Conference on Robotics and Automation*, pages 1857–1862, Albuquerque, NM.

[Smith et al., 1998] Smith, C. M., Feder, H. J. S., and Leonard, J. J. (1998). Making difficult decisions autonomously: the impact of integrated mapping and navigation. In *Proceedings of IEEE Conference on Autonomous Underwater Vehicles.*

[Smith and Leonard, 1997] Smith, C. M. and Leonard, J. J. (1997). A multiple hypothesis approach to concurrent mapping and localization for autonomous underwater vehicles. In *International Conference on Field and Service Robotics*, Sydney, Australia.

[Smith et al., 1990] Smith, R., Self, M., and Cheeseman, P. (1990). Estimating uncertain spatial relationships in robotics. In Cox, I. and Wilfong, G., editors, *Autonomous Robot Vehicle*, page 167. Springer-Verlag.

[Soatto et al., 1996] Soatto, S., Frezza, R., and Perona, P. (1996). Motion estimation via dynamic vision. *IEEE Trans. on Automatic Control*, 41(3):393–414.

[Sorenson, 1985] Sorenson, H. (1985). *Kalman Filtering: Theory and Application.* IEEE Press.

[Spiegel et al., 2000] Spiegel, M. R., Schiller, J. J., and Srinivasan, R. A. (2000). *Schaum's Outline of Theory and Problems of Probability and Statistics.* McGraw-Hill, second edition.

[Spindel and Worcester, 1990] Spindel, R. C. and Worcester, P. F. (1990). Ocean acoustic tomography. *Scientific American*, pages 94–99.

[Stojanovic et al., 2002] Stojanovic, M., Freitag, L., Leonard, J., and Newman, P. (2002). A network protocol for multiple AUV localization. In *OCEANS 2002, Proceedings MTS/IEEE Oceans 2002 Conference.*

[Stokey and Austin, 1999] Stokey, R. T. and Austin, T. (1999). Sequential, long base line navigation for REMUS, an autonomous underwater vehicle. Technical report, Information Systems for Navy Divers and Autonomous Underwater Vehicles Operating in Very Shallow Water and Surf Zone Regions.

[Strang, 1986] Strang, G. (1986). *Introduction to Applied Mathematics.* Wellesley-Cambridge Press.

[Tadjudin and Landgrebe, 2000] Tadjudin, S. and Landgrebe, D. A. (2000). Robust parameter estimation for mixture model. *IEEE Transactions on Geoscience and Remote Sensing*, 38(1):439–445.

[Taylor, 1982] Taylor, J. R. (1982). *An introduction to error analysis: the study of uncertainties in physical measurements.* University Science Books.

[Thrun, 1998] Thrun, S. (1998). Learning metric-topological maps for indoor mobile robot navigation. *Artificial Intelligence*, 99(1):21–71.

[Thrun, 2000] Thrun, S. (2000). Probabilistic algorithms in robotics. *AI Magazine*, 21(4):93–109.

[Thrun, 2001] Thrun, S. (2001). Learning occupancy grids with forward models. Submitted for publication - 2001:http://www-2.cs.cmu.edu/ thrun/papersall.html.

[Thrun, 2002] Thrun, S. (2002). *Exploring Artificial Intelligence in the New Millenium*, chapter Robotic mapping: a survey. Morgan Kaufmann.

[Thrun et al., 1998a] Thrun, S., Fox, D., and Burgard, W. (1998a). A probabilistic approach to concurrent mapping and localization for mobile robots. *Machine Learning*, 31:29–53.

[Thrun et al., 1998b] Thrun, S., Gutmann, J. S., Fox, D., Bugard, W., and Kuipers, B. J. (1998b). Integrating topological and metric maps for mobile robot navigation: A statistical approach. In *AAAI-98*.

[Tourrilhes, 2000] Tourrilhes, J. (2000). Linux wireless LAN HowTo.

[Tuohy, 1993] Tuohy, S. T. (1993). *Geophysical Map Representation, Abstraction and Interrogation for Autonomous Underwater Vehicle Navigation.* PhD thesis, MIT.

[Tuohy et al., 1996] Tuohy, S. T., Leonard, J. J., Bellingham, J., Patrikalakis, N. M., and Chryssostomidis, C. (1996). Map based navigation for autonomous underwater vehicles. *International Journal of Offshore and Polar Engineering.*

[Urick, 1983] Urick, R. J. (1983). *Principles of underwater sound.* McGraw-Hill.

[Vaganay et al., 1996] Vaganay, J., Leonard, J. J., and Bellingham, J. G. (1996). Outlier rejection for autonomous acoustic navigation. In *Proceedings of the 1996 IEEE International Conference on Robotics and Automation*, pages 2174–2181, Minneapolis, Minnesota. IEEE.

[Vestgard et al., 1999] Vestgard, K., Storkersen, N., and Sortland, J. (1999). Seabed surveying with Hugin AUV. In *Proceedings of the 11th International Symposium on Unmanned Untethered Submersible Technology*, Durham, NH.

[Vickery, 1998] Vickery, K. (1998). Acoustic positioning systems a practical overview of current systems. In *AUV 98*, pages 5–17.

[Waterman, 1989] Waterman, T. H. (1989). *Animal Navigation.* Scientific American Library.

[Watson, 1983] Watson, P. J. (1983). Method and theory in shipwreck archaeology. In Gould, R. A., editor, *Shipwreck Anthropology*, pages 23–36. University of New Mexico Press.

[Whitcomb et al., 1999a] Whitcomb, L., Yoerger, D., Singh, H., and Howland, J. (1999a). Advances in underwater robot vehicles for deep ocean exploration: Navigation, control, and survey operations. In *Robotics Research 9: Proceedings of the Ninth International Symposium of Robotics Research (ISRR '99)*, Snowbird, Utah, USA.

[Whitcomb et al., 1998] Whitcomb, L., Yoerger, D., Singh, H., and Mindell, D. (1998). Towards precision robotic maneuvering, survey, and manipulation in unstructured undersea environments. In Shirai, Y. and Hirose, S., editors, *Robotics Research - The Eighth International Symposium.* Springer-Verlag, London.

[Whitcomb, 2000] Whitcomb, L. L. (2000). Underwater robotics: Out of the research laboratory and into the field. In *Proceedings of the 2000 IEEE International Conference on Robotics and Automation*, pages 709–716, San Francisco, CA. IEEE.

[Whitcomb et al., 1999b] Whitcomb, L. L., Yoerger, D. R., and Singh, H. (1999b). Combined doppler/lbl based navigation of underwater vehicles. In *Proceedings of the International Symposium on Unmanned Untethered Submersible Technology.*

[Willsky et al., 1997] Willsky, A. S., Wornell, G. W., and Shapiro, J. H. (1997). Stochastic processes, detection and estimation: 6.432 course notes. MIT Course Notes.

[Yamauchi, 1997] Yamauchi, B. (1997). A frontier based approach for autonomous exploration. In *IEEE International Symposium on Computation al Intelligence in Robotics and Automation.*

[Yoerger et al., 1997] Yoerger, D., Bradley, A., and Walden, B. (1997). Scientific survey with the Autonomous Benthic Explorer. In *Proc. Int. Symp. on Unmanned Untethered Submersible Technology*, pages 41 49.

[Yoerger et al., 1999] Yoerger, D. R., Bradley, A. M., Cormier, M.-H., Ryan, W. B., and Walden, B. B. (1999). High resolution mapping of a fast spreading mid ocean ridge with the Autonomous Benthic Explorer. In *proceedings of the 11th International Symposium on Unmanned Untethered Submersible Technology*, Durham, NH.

[Yoerger et al., 1992] Yoerger, D. R., Bradley, A. M., and Walden, B. B. (1992). Autonomous benthic explorer, deep ocean scientific AUV for seafloor exploration: Untethered, on station one year without support ship. *Sea Technology*, 33(1):50–54.

[Yoerger and Mindell, 1992] Yoerger, D. R. and Mindell, D. A. (1992). Precise navigation and control of an rov at 2200 meters depth. In *Proceedings of ROV '92*, San Diego, CA.

[Yoerger and Mindell, 1999] Yoerger, D. R. and Mindell, D. A. (1999). Performancd of the EXACT subsea navigation system. Technical report, Woods Hole Oceanographic Institution.

[Zielinski and Wu, 1989] Zielinski, A. and Wu, L. (1989). Underwater acoustics positioning using surface multipath. In *IEEE Pacific Rim Conference on Communications, Computers, and Signal Processing*, pages 553–559.